Phenotypes related to schizophrenia induced by chronic inflammation in the brain resulting from a genetic factor

遺伝的な要因による脳内の慢性炎症によって引き起こされる統合失調症に関連する表現型

髙雄 啓三

TALBE OF CONTENTS

ABSTRACT

Schnurri-2 (Shn-2), a nuclear factor-κB site-binding protein, tightly binds to the enhancers of major histocompatibility complex class I genes and inflammatory cytokines, which have been shown to harbor common variant single-nucleotide polymorphisms associated with schizophrenia. Although genes related to immunity are implicated in schizophrenia, there has been no study showing that their mutation or knockout (KO) results in schizophrenia. Here, I show that Shn-2 KO mice have behavioral abnormalities that resemble those of schizophrenics. The mutant brain demonstrated multiple schizophrenia-related phenotypes, including transcriptome/proteome changes similar to those of postmortem schizophrenia patients, decreased parvalbumin and GAD67 levels, increased theta power on electroencephalograms, and a thinner cortex. Dentate gyrus granule cells failed to mature in mutants, a previously proposed endophenotype of schizophrenia. Shn-2 KO mice also exhibited mild chronic inflammation of the brain, as evidenced by increased inflammation markers (including GFAP and NADH/NADPH oxidase p22 phox), and genome-wide gene expression patterns similar to various inflammatory conditions.

Chronic administration of anti-inflammatory drugs reduced hippocampal GFAP expression, and reversed deficits in working memory and nest-building behaviors in Shn-2 KO mice. These results suggest that genetically induced changes in immune system can be a predisposing factor in schizophrenia.

1. INTRODUCTION

Elucidating the neural and genetic basis of schizophrenia and other psychiatric disorders remains difficult, in part because psychiatric phenotypes in human patients are largely dependent on subjective clinical evaluation criteria that lack quantifiable biological indicators. The biological heterogeneity of schizophrenia patients has particularly hindered the identification of genetic risk factors (Braff et al., 2007). Thus, the development of animal models with homogenous backgrounds is imperative for investigating genetic contributions to schizophrenia. For the past decade, I and colleagues have sought to identify rodent models of neuropsychiatric disorders, including schizophrenia, by analyzing genetically engineered mice with a comprehensive behavioral test battery that covers many distinct behavioral domains, from simple sensorimotor functions to cognition-intensive functions like learning and memory (Figure 1a) (Miyakawa et al., 2003; Powell & Miyakawa, 2006; Takao et al., 2007; Yamasaki et al., 2008). To date, I and colleagues have screened >200 mutant mouse strains using the same protocol and identified several strains with behavioral phenotypes that resemble symptoms in human schizophrenia patients (Takao et al.,

2008; Yamasaki et al., 2008) (Figure 1). Because schizophrenia is a multi-factorial disorder, the effects of many of the individual factors identified in human genetics or epidemiological studies are small. Therefore, even if one of those factors were introduced into mice, the phenotype would be weak, and it would be difficult to make a good mouse model of schizophrenia. In contrast to those etiology-driven research strategies, phenotype-driven research strategies analyze mice without a specific hypothesis and search for mice that resemble schizophrenia. If a new model mouse with a very similar behavioral phenotype, i.e., one with high surface validity, is identified, we can use it to search for and find novel endophenotypes of the brain.

Schnurri-2 (Shn-2; also called major histocompatibility complex (MHC)-binding protein 2 (MBP-2), Hivep2 or Mibp1) was originally identified as a nuclear factor-κB (NF-κB) site-binding protein that tightly binds to the enhancers of MHC genes in the MHC regions of chromosome 6 (Fukuda et al., 2002). Recent genome-wide association studies identified a number of single-nucleotide polymorphisms (SNPs) in the MHC region associated with schizophrenia (Purcell et al., 2009; J. Shi et al., 2009; Stefansson et al., 2009; Yue et al., 2011). MHC class I proteins coded in this region

have been reported to play a critical role in neural development and plasticity (Shatz, 2009). Genes in MHC regions often contain NF-κB-binding sequences in their promoter regions. Shn-2 constitutively binds NF-κB-binding site to suppress NF-κB-dependent gene expression (Kumar et al., 2004), including tumor necrosis factor (TNF)-α, interleukin (IL)-1β, IL-6, cyclin D1, prostaglandin-endoperoxidase synthase 2 (PTGS2, also called COX2), NADH/NADPH oxidase p22 phox, and vimentin. To induce an immune response, Shn-2 detaches from the NF-κB-binding site, allowing the transcription of NF-κB target genes (Kimura et al., 2005, 2007). Accordingly, Shn-2 KO mice demonstrate constitutive NF-κB activation in CD4+ T cells (Kimura et al., 2007). Shn-2 expression is also reported in several brain regions including hippocampus, cortex, and cerebellum (Fukuda et al., 2002). Previously, it is reported that Shn-2 KO mice exhibited hyperactivity (Takagi et al., 2006), suggesting the functional significance of Shn-2 in the brain.

As a course of the large-scale screening to identify animal models of psychiatric disorders, Shn-2 KO mice were subjected to a comprehensive behavioral test battery. Shn-2 KO mice displayed behavioral alterations and cognitive impairments

resembling those of schizophrenia. I observed significant similarities in transcriptome/proteome changes between Shn-2 KO mouse brain and postmortem brains of human schizophrenia patients. Granule cells of the dentate gyrus (DG) also failed to mature in Shn-2 KO mice, a previously proposed candidate endophenotype of the disease observed in at least one additional mouse model of schizophrenia and its related phenotypes (Yamasaki et al., 2008). Finally, Shn-2 KO mice demonstrated mild, widespread brain inflammation characterized by the upregulation of NF-κB-responsive genes and activation of astrocytes. Results of my study demonstrate that Shn-2 KO mice serve as an animal model of schizophrenia with good face and concept validity. The present study also suggests that immune system changes induced by genetic factors may contribute to the pathophysiology of schizophrenia. This doctoral dissertation is mainly based on an original paper "Deficiency of schnurri-2, an MHC enhancer binding protein, induces mild chronic inflammation in the brain and confers molecular, neuronal, and behavioral phenotypes related to schizophrenia", which was previously published in *Neuropsychopharmacology* (Takao et al., 2013). The dissertation also partly based on other original papers published in *Neuroscience Research* (Takao et al.,

2007) and *Proceedings of the National Academy of Sciences of the United States of America* (Takao & Miyakawa, 2015).

2 MATERIALS AND METHODS

2.1 Animals and experimental design

All behavioral tests were carried out with male mice that were at least 9 weeks old at the start of testing. Raw data from the behavioral tests, the date on which each experiment was performed, and the age of the mice at the time of the experiment are shown in the mouse phenotype database (http://www.mouse-phenotype.org/). Mice were group-housed (2–4 mice per cage) in a room with a 12-h light/dark cycle (lights on at 7:00) with access to food and water ad libitum. The room temperature was kept at 23 ± 2°C. Behavioral testing was performed between 9:00 and 19:00. After the tests, all apparatuses were cleaned with diluted sodium hypochlorite solution to prevent a bias due to olfactory cues. Sixteen independent groups of mice were prepared for behavioral tests. One group consisted of equal numbers of Shn-2 KO mice and wild-type control

littermates. All behavioral tests were separated from each other by at least 1 day. All behavioral testing procedures were approved by the Animal Research Committee, Graduate School of Medicine, Kyoto University (MedKyo 09539, MedKyo 10259), Fujita Health University (I0741) and National Institute for Physiological Sciences (15A021).

Shn-2 KO mice

The generation of Shn-2 KO mice has been previously described (Takagi et al., 2001). Shn-2 KO mice were backcrossed with C57BL6/J or Balb/cA for at least 10 generations for each strain. Shn-2 KO mice with an F1 hybrid background were obtained by mating heterozygous C57BL6/J male and heterozygous Balb/cA female mice. The F1 mice on the C57BL/6J and BALB/cA genetic background were used for all experiments, both KO and WT mice as well. The effect of the genetic background is virtually the same for both genotypes. I used F1 mice for the experiments because the number of Shn-2 KO offspring obtained with a single genetic background is very small.

Arc-dVenus mice

Transgenic mice expressing destabilized Venus driven by the Arc gene promoter (Eguchi & Yamaguchi, 2009) were backcrossed with C57BL/6J mice for at least 6 generations. Arc-dVenus mice were crossed with Shn-2 heterozygous KO mice on a C57BL/6J background. Arc-dVenus-expressing Shn-2 KO mice on the F1 hybrid background were obtained by mating Arc-dVenus heterozygote Shn-2 KO male (C57BL/6J) with heterozygote Balb/cA females.

Anti-inflammatory treatment

Mice were treated with rolipram (4 mg/kg, i.p.; Sigma-Aldrich, St. Louis, MO) in saline containing 2% dimethyl sulfide (DMSO) once daily and kept on a ibuprofen (400 ppm; Tokyo Chemical Industry, Tokyo, Japan)-containing chow for 3 to 4 weeks. Control mice were treated with saline containing 2% DMSO and fed an identical diet, but without added ibuprofen.

2.2 Behavioral analysis

Open field test

Locomotor activity was measured using an open field test. Each mouse was placed in one corner of the open field apparatus (40 × 40 × 30 cm; Accuscan Instruments, Columbus, OH). Total distance traveled (in cm), vertical activity (rearing measured by counting the number of photobeam interruptions), time spent in the center, the beam-break counts for stereotyped behaviors, and the number of fecal boli were recorded. Data were collected for 120 min.

Social interaction test in home cage

Social interaction monitoring in the home cage was conducted as previously described (Miyakawa et al., 2003). The system contains a home cage (29 × 18 × 12 cm) and a filtered cage top, separated by a 13-cm-high metal stand containing an infrared video camera, fitted on top of the stand. Two mice of the same inbred strain that had been

housed separately were placed together in a home cage. Their social behavior was then monitored for a week. Outputs from the video cameras were fed into a Macintosh computer. Images from each cage were captured at a rate of one frame per second. Social interaction was measured by counting the number of particles in each frame: two particles indicated the mice were not in contact with each other; and one particle indicated contact between the two mice. I also measured locomotor activity during these experiments by quantifying the number of pixels that changed between each pair of successive frames. Analysis was performed automatically using Image SI software (see 'Image analysis').

Eight-arm radial maze

The eight-arm radial maze test was performed with 21- to 25-week-old male mice in a fully-automated eight-arm radial maze apparatuses (O'Hara & Co., Tokyo, Japan). The floor of the maze was made of white plastic and the wall (25 cm high) consisted of transparent plastic. Each arm (9 × 40 cm) radiated from an octagonal central starting platform (perimeter 12 × 8 cm) like the spokes of a wheel. Identical food wells (1.4 cm

deep and 1.4 cm in diameter) with pellet sensors were placed at the distal end of each arm. The pellets sensors were able to automatically record pellet intake by the mice. The maze was elevated 75 cm above the floor and placed in a dimly lit room with several extra-maze cues. During the experiment, the maze was maintained in a constant orientation.

One week before pretraining, animals were deprived of food until their body weight was reduced to 80-85% of the initial level. Pretraining started on the 8th day. Each mouse was placed in the central starting platform and allowed to explore and consume food pellets scattered over the whole maze for a 30-min period (one session per mouse). After completion of the initial pretraining, mice received further pretraining to take a food pellet from each food well after being placed at the distal end of each arm. A trial was finished after the mouse consumed the pellet. This was repeated eight times, using eight different arms, for each mouse. After these pretraining trials, actual maze acquisition trials were performed. In the spatial working memory task of the eight-arm radial maze, all eight arms were baited with food pellets. Mice were placed on the central platform and allowed to obtain all eight pellets within 25 min. A trial was

terminated immediately after all eight pellets were consumed or after 25 min had elapsed. An “arm visit” was defined as traveling more than 5 cm from the central platform. The mice were confined to the center platform for 5 s after each arm choice. The animals completed one trial per day. For each trial, arm choice, latency to obtain all pellets, distance traveled, number of different arms chosen within the first eight choices, number of arms revisited, and omission errors were automatically recorded. Data acquisition, control of guillotine doors, and data analysis were performed using Image RM software (see “Image analysis”).

T-maze forced alternation task

The forced alternation task was conducted using an automatic T-maze (Shoji et al., 2012). It was constructed of white plastic runways with walls 25 cm high. The maze was partitioned into six areas by sliding doors that opened downwards. The stem of the “T” comprised of area S2 (13 cm × 24 cm), and the arms of “T” comprised of areas A1 and A2 (11.5 cm × 20.5 cm). Areas P1 and P2 were the connecting passageways from the arm (area A1 or A2) to the start compartment (area S1) (Figure 3o). The end of each

arm was equipped with a pellet dispenser that could provide a food reward. The pellet sensors were able to automatically record pellet intake by the mice.

One week before the pre-training, mice were deprived of food until their body weight was reduced to 80–85% of the initial level. Mice were kept on a maintenance diet throughout the course of all the T-maze experiments. Before the first trial, mice were subjected to three 10-min adaptation sessions, during which they were allowed to freely explore the T-maze with all doors open and both arms baited with food. On the day after the adaptation session, mice were subjected to a forced alternation protocol for 16 days (one session consisting of 10 trials per day; cut-off time, 50 min). Mice underwent 10 pairs of training trials per day. On the first (sample) trial of each pair, the mouse was forced to choose one of the arms of the T (area A1 or A2) and received the reward at the end of the arm. Choosing the incorrect arm resulted in no reward and confinement to the arm for 10 s. After the mouse consumed the pellet or the mouse stayed >10 s without consuming the pellet, the door that separated the arm (area A1 or A2) and connecting passageway (area P1 or P2) was opened, and the mouse could return to the starting compartment (area S1) via the connecting passageway. The mouse

was then given a 3-s delay followed by a free choice between both T arms and was rewarded for choosing the arm that was not chosen on the first trial of the pair. The location of the sample arm (left or right) was varied pseudo-randomly across trials using a Gellermann schedule so that mice received equal numbers of left and right presentations. A variety of fixed extra-maze cues surrounded the apparatus. On the 9th to 10th days, a delay (10, 30, or 60 s) was applied after the sample trial.

T-maze left-right discrimination task

The left-right discrimination task was also conducted using an automatic T-maze (Figure 3o) (Shoji et al., 2012) and food deprivation before the trials as described above. On the day after the adaptation session, mice were subjected to a left-right discrimination task for 20 d (one session consisting of 10 trials, two sessions per day, cut-off time of 50 min). The mouse was able to freely choose either the right or left arm of the T-maze (A1 and A2). The correct arm was randomly assigned to each mouse. If it chose the correct arm, the mouse received a reward at the end of the arm. Choosing the incorrect arm resulted in no reward and confinement to the arm for 10 s. After the

mouse consumed the pellet or the mouse stayed for more than 10 s without consuming the pellet, the door that separated the arm (A1 or A2) and connecting passageway (P1 or P2) was opened and the mouse could return to the starting compartment (S1) via the connecting passageway. On the 9th day, the correct arm was changed for reversal learning. A variety of fixed extra-maze clues surrounded the apparatus.

Startle response/prepulse inhibition test

A startle reflex measurement system was used (O'Hara & Co., Tokyo, Japan). A test session began by placing a mouse in a plexiglass cylinder, where it was left undisturbed for 10 min. A 40 ms duration of white noise was used as the startle stimulus for all trial types. The startle response was recorded for 140 ms (measuring the response every 1 ms), starting with the onset of the prepulse stimulus. The background noise level in each chamber was 70 dB. The peak startle amplitude recorded during the 140 ms sampling window was used as the dependent variable. A test session consisted of six trial types (i.e., two types for “startle-stimulus-only” trials and four types for prepulse inhibition (PPI) trials). The intensity of the startle stimulus was 110 or 120 dB. The prepulse

sound was presented 100 ms before the startle stimulus, and its intensity was 74 or 78 dB. Four combinations of prepulse and startle stimuli were used (74–110, 78–110, 74–120, and 78–120 dB). Six blocks of the six trial types were presented in pseudo-random order such that each trial type was presented once within a block. The average inter-trial interval was 15 s (range: 10–20 s).

Social interaction test in a novel environment

The social interaction test in a novel environment was performed with 11- to 14-week-old male mice. Two mice of identical genotypes that were previously housed in different cages were placed into a box together (40 × 40 × 30 cm) and allowed to explore freely for 10 min. Social behavior was monitored by a CCD camera connected to a computer. Analysis was performed automatically using Image SI software (see "Image analysis"). The total duration of contact, number of contacts, number of active contacts, mean duration per contact, and total distance traveled were measured. The number of active contacts was defined as follows: Images were captured at 1 frame per second, and the distance traveled between two successive frames was calculated for

each mouse. If the two mice contacted each other and the distance traveled by either mouse was greater than 5 cm, the behavior was considered an “active contact.”

Sociability and social novelty preference test

The social testing apparatus consisted of a rectangular, three-chambered box and a lid fitted with an infrared video camera (Ohara & Co., Tokyo, JAPAN). Each chamber was 20 × 40 × 22 cm in size, and the dividing walls were made from clear plexiglass, with small square openings (5 × 3 cm) allowing access into each chamber. An unfamiliar C57BL/6J male (stranger 1), which had had no prior contact with the subject mice, was placed in one of the side chambers. The location of stranger 1 in the left vs. the right side chamber was systematically alternated between trials. The stranger mouse was enclosed in a small, round wire cage, which allowed nose contact between the bars but prevented fighting. The cage was 11 cm in height, with a bottom diameter of 9 cm, vertical bars 0.5 cm and horizontal bars spaced 1 cm apart. The subject mouse was first placed in the middle chamber and allowed to explore the entire social test box for a 10 min session to quantify social preference for the first stranger. The amount of time spent

around each cage was measured with the aid of the camera fitted on top of the box. After the first 10 min session, a second unfamiliar mouse, also enclosed in an identical small wire cage, was placed in the chamber that had been empty during the first 10 min session. The mouse subjected to the test thus had a choice between the first, already-investigated unfamiliar mouse (stranger 1), and the novel unfamiliar mouse (stranger 2). The amount of time spent around each cage during the second 10-minutes was measured as described above. Time spent around each cage by each genotype was compared using a one-tailed paired t-test. Data acquisition and analysis were performed automatically using an ImageJ based original program (Image CSI: see "Image analysis").

Nest-building test

To test the individual nest building behavior, mice were housed individually in cages containing paper chip bedding and one square of pressed cotton, "Nestlets" (Ancare, Bellmore, NY, USA). No other nesting material (e.g. wood or wool) was present. The following morning, the manipulation of the Nestlet and the constitution of the built nest

were assessed according to a five-point scale as described previously (Deacon, 2006): (1) Nestlet not noticeably touched (more than 90% intact); (2) Nestlet partially torn (50–90% remaining intact); (3) Nestlet mostly shredded but with no identifiable nest site (less than 50% of the Nestlet remains intact, but less than 90% is within a quarter of the cage floor area (i.e., the cotton is not gathered into a nest but rather spread around the cage), with the material may sometimes in a broadly defined nest area, but, critically, with 50–90% shredded); (4) an identifiable but flat nest (more than 90% of the Nestlet is torn, the material is gathered into a nest within a quarter of the cage floor area, but the nest is flat with walls higher than mouse body height (of a mouse curled up on its side) for less than 50% of its circumference; and (5) a (near) perfect nest (more than 90% of the Nestlet is torn, and the nest is a crater, with walls higher than mouse body height for more than 50% of its circumference).

Hot plate test

A hot plate test was used to evaluate sensitivity to a painful stimulus. Mice were placed on a hot plate (Columbus Instruments, Columbus, OH, USA) at 55.0 (± 0.3)°C, and

latency to the first paw response was recorded. A paw response was a foot shake, or a paw lick, or lifting both forepaws simultaneously.

Locomotor activity monitoring in the home cage

A system that automatically analyzes the locomotor activity of mice in their home cage was used. The system contained a home cage (29 × 18 × 12 cm) and a filtered cage top, separated by a 13 cm-high metal stand containing an infrared video camera, which was attached to the top of the stand. Each mouse was individually housed in each home cage, and their locomotor activity was monitored for 1 week. Outputs from the video cameras were fed into a computer. Images from each cage were captured at a rate of one frame per second, and distance travelled was measured automatically using Image HA software (see “Image analysis”).

Elevated plus maze test

The elevated plus maze apparatus consisted of two open arms (25 × 5 cm) and two enclosed arms of the same size, with transparent walls15 cm high (Komada et al., 2008). The arms and central square were made of white plastic plates and were elevated 55 cm above the floor. To minimize the likelihood of animals falling from the apparatus, 3 mm-high plexiglass ledges were provided for the open arms. Arms of the same type were arranged on opposite sides. Each mouse was placed in the central square of the maze (5 × 5 cm) facing one of the closed arms. Behavior was recorded during a 10 min test period. The number of entries into and the time spent on open and enclosed arms was recorded. For data analysis, the following four measures were employed: the percentage of entries into open arms, the stay time on the open arms (s), the number of total entries, and the total distance traveled (cm). To specify the locations of the mice, the center of balance was used (i.e., "entry" indicates that center of the mass of the mice enters into the other arm). Data acquisition and analysis were performed automatically, using an ImageJ-based original program (Image EP: see “Image analysis”)

Sucrose preference test

The sucrose preference test was performed as previously described (Snyder et al., 2011). Mice were individually housed prior to the experiment. Animals were given a water bottle containing water and a second containing 1% sucrose, with the left/right location balanced across animals, for 3 successive days. Both bottles were removed between 15:30 and 18:30 on each day and weighed. Sucrose preference was calculated according to the formula:

$$\% \text{ preference} = (\Delta \text{weight}_{\text{sucrose}})/(\Delta \text{weight}_{\text{sucrose}} + \Delta \text{weight}_{\text{water}}) \times 100$$

Porsolt forced swim test

The apparatus consisted of four plexiglass cylinders (20 cm height × 10 cm diameter). The cylinders were filled with water (23°C), up to a height of 7.5 cm. Mice were placed in the cylinders, and immobility and distance traveled were recorded over a 10 min test period. Images were captured at one frame per second. For each pair of successive frames, the amount of area (pixels) within which the mouse moved was measured.

When the amount of area was below a certain threshold, the mouse was judged to be "immobile." When the area equaled or exceeded the threshold, the mouse was considered to be "moving." The optimal threshold was determined by adjusting it to the degree of immobility measured by human observation. Immobility lasting for less than 2 s was not included in the analysis. Data acquisition and analysis were performed automatically using an ImageJ based original program (Image TS: see “Image analysis”).

Pharmacological treatment

MK-801: Animals they were placed and recorded in the open filed as described in “*Open field test.*” After 60 min, the animals were removed from the apparatus and injected with MK-801 (0.2 mg/kg, ip) or the vehicle solution.

Haloperidol: Mice were acclimated to the procedure room for at least 30 min before administration of drug or vehicle. Haloperidol (1 or 3 mg/kg, ip) or the vehicle solution was administered ip 30 min prior to the startle response/prepuse inhibition and the open

filed test. The dose of haloperidol was chosen based its efficacy in animal models designed to study the action of antipsychotic drugs (Duncan et al., 2006; Ouagazzal et al., 2001).

Clozapine: Mice were acclimated to the procedure room for at least 30 min before administration of drug or vehicle. Clozapine (1 mg/kg, ip) or the vehicle solution was administered ip 30 min prior to the open filed test. For the open field test, 1 mg/kg, 3 mg/kg or the vehicle solution was administered ip 30 min prior to the test.

Rolipram and ibupurofen treatment: Rolipram (4mg/kg, ip) or the vehicle solution was administrated to the animals for at least 3 weeks. At the same time, mice were fed with ibuprofen chow containing ibuprofen or no drug.

Image analysis

The applications used for the behavioral studies (Image LD, Image EP, Image RM, Image FZ, Image SI, Image TS, Image TM, Mimage CSI and Image HA) were based on the public domain ImageJ program (http://rsb.info.nih.gov/ij/) and were modified for

each test by I and collaborators (those software are available through O'Hara & Co., Tokyo, Japan, and some of them are freely available on the “Mouse Phenotype Database” website URL = http://www.mouse-phenotype.org/software.html).

Statistical analysis

Statistical analysis was conducted using StatView (SAS Institute, Cary, NC, USA). Data were analyzed by unpaired t-test, one-way ANOVA, two-way ANOVA or two-way repeated measures ANOVA, unless noted otherwise. Values in Tables and graphs are expressed as the mean ± s.e.m.

2.3 Dopamine signaling Assay

Dopamine receptor autoradiography

Frozen brains were obtained from 12-week-old wild (n = 6) and Shn-2 KO (n = 6) mice, and were cut into 20-mm-thick coronal sections with a HM560 cryotome (Thermo Fisher Scientific Inc., Waltham, MA, USA). The sections were mounted on slide

glasses (Matsunami Glass, Osaka, Japan) and stored at −80 °C pending analyses. Levels of dopamine D1 and NMDA receptors were determined by autoradiographically analyzing specific binding of [^{3}H]SCH233090 (1.5 nM) and [^{3}H]PHNO (2 nM), respectively, to the brain slices. The conditions of buffers and incubation time were as described in previous reports (Mansour et al., 1990; Nobrega & Seeman, 1994). Non-specific binding of [^{3}H]SCH23390 and [^{3}H]PHNO was determined by adding 10 mM of flupenxiol and 10 mM of raclopride, respectively. Following the incubation, the samples were rinsed with ice-cold buffer, and were desalted with ice-cold distilled water. The slices were subsequently dried under blowing air and were contacted to an imaging plate (Fuji Film, Tokyo, Japan) for 7 days. The imaging plates were subsequently scanned by a BAS5000 system (Fuji Film, Tokyo, Japan). Regions of interest (ROIs) were defined on the images using a Multi Gauge® software (Fuji Film, Tokyo, Japan), and densitometric assay for each ROI was performed using autoradiographic [^{3}H]micro-scales (GE Healthcare Bio-Sciences Corp., Piscataway, NZ, USA).

Preparation and incubation of neostriatal slices

Shn-2 KO mice and wildtype mice were sacrificed by decapitation. The brains were rapidly removed and placed in ice-cold, oxygenated Krebs-HCO_3^- buffer (124 mM NaCl, 4 mM KCl, 26 mM $NaHCO_3$, 1.5 mM $CaCl_2$, 1.25 mM KH2PO_4, 1.5 mM $MgSO_4$ and 10 mM D-glucose, pH 7.4). Coronal slices (350 μm) were prepared using a vibrating blade microtome, VT1000S (Leica Microsystems, Nussloch, Germany). Dentate gyrus was dissected from the slice in ice-cold Krebs-HCO3- buffer. Slices were devided into polypropylene incubation tube (3-4 slices in each tube) with 2 ml fresh Krebs-HCO3- buffer. The slices were preincubated at 30˚C under constant oxygenation with 95 % O_2 / 5% CO_2 for 60 min. The buffer was replaced with fresh Krebs-HCO3- buffer after 30 min of preincubation. Slices were treated with a dopamine D1 agonist, (±)-SKF81297 (Tocris Bioscience, Bristol, United Kingdom). After drug treatment, slices were transferred to Eppendorf tubes, frozen on dry ice, and stored at –80˚C until assayed.

Frozen tissue samples were sonicated in a solution of boiling 1% sodium dodecyl sulfate (SDS), then boiled for an additional 10 min. Small aliquots of the

homogenate were retained for protein determination by the BCA protein assay method (Pierce, Rockford, IL, USA). Equal amounts of protein (40 μg) were separated by 4-12% polyacrylamide Bis-Tris gels (Bio-Rad, Hercules, CA, USA), and transferred to nitrocellulose membranes (0.2 μm) (Schleicher and Schuell, Keene, NH, USA).

2.4 Gene expression and bioinformatics analysis

Gene expression analysis

Microarray experiments were performed using the medial prefrontal cortex and dentate gyrus of 32- to 35-week-old male mice (three control mice and three mutant mice), and the hippocampus of 15- to 35-week-old male mice (four control mice and four mutant mice). The dentate gyrus and medial prefrontal cortex were sampled from the same mice. RNA was isolated from brain tissues using the TRIzol method (Invitrogen, Carlsbad, CA, USA) from brain tissues, followed by purification, using RNeasy columns (Qiagen, Valencia, CA, USA). Double-stranded cDNA was synthesized from the total RNA, and the *in vitro* transcription reaction was performed using biotin-labeled

RNA generated from the cDNA. Labeled RNA was hybridized to the Mouse Genome 430 2.0 Array (Affymetrix, Santa Clara, CA, USA) containing 45101 probe sets and washed according to the manufacturer's recommendations. The hybridized probe array was then stained with streptavidin-conjugated phycoerythrin, and each GeneChip was scanned by an Affymetrix GeneChip Scanner 3000 (GCS3000). Raw data were corrected for background using the robust multichip average (RMA) algorithm and quantile normalization (Irizarry et al., 2003) with the Affymetrix Expression Console 1.1 software. To determine whether genes were differentially expressed between the two groups, a two-tailed, unpaired Welch's t test was performed on the normalized data set. Only genes showing a *P* value from the t test < 0.05 and an absolute value of fold change > 1.2 were considered to be differentially expressed.

Bioinformatics analysis

Gene expression pattern in the brains of Shn-2 KO mice were compared with publicly available microarray data obtained from the web-based search engine software, NextBio (Cupertino, CA, USA). Fold changes are calculated by dividing the mutant/disease

value by the wild-type/normal value. For the graphs, these raw fold change values are used. In the text and tables, fold change values are converted into the negative reciprocal, or -1/(fold change), if the fold change is less than one. Public microarray datasets were queried using NextBio, a database of microarray results (accessed on May 4th, 2011). NextBio is a repository of analyzed microarray datasets that allows the investigator to search results and the expression profiles of publicly available microarray datasets. Gene overlaps were examined using Running Fisher test.

In Figure 4A–D, genes that showed differential expression both in the hippocampus of Shn-2 KO mice and in one of the four inflammation-related biosets that are deposited in NextBio database. The following data sets were used for each of the plots: (a) LPS: Mus musculus, Hippocampal tissue from mice inoculated with NBH + 500 μg/kg LPS 18 wk after _vs_ saline (GSE23182); (b) Injury: Mus musculus, Spinal cord below impact site 72 h after injury _vs_ naïve (GSE5296); (c) Prion infection: Mus musculus, Hippocampal tissue of mice treated with 500 μg/kg saline 18 wk after ME7 infection _vs_ uninfected (GSE23182); (d) Aging: Mus musculus, Hippocampus from spatial

memory unimpaired aged animals _vs_ young (GSE13799). The Gene Expression Omnibus (GEO) accession IDs are shown in parentheses.

NextBio was used to identify diseases or experiments that demonstrated gene expression patterns (signatures) similar to that of Shn-2 KO mice, I utilized NextBio (for Figure 6 and Table 2 NextBio was accessed on September 29 in 2011, for Figure 16A-D accessed on April 20 in 2011, for Table 3, NextBio was accessed on May 4 in 2011, and for Table 4 NextBio was accessed on March 8 (Schizophrenia), and on April 6 (Shn-2 KO mice) in 2012). NextBio compares the signatures in publicly available microarray databases with a signature provided by the user using a "Running Fisher" algorithm, as previously described (Kupershmidt et al., 2010). The overlap *P* value, the direction of correlation between two given gene signature sets (*b1*, *b2*), and the *P* values between subsets of gene signatures are calculated as follows:

First, each gene signature set was rank-ordered according to the absolute value of the fold change. The upregulated and downregulated genes are denoted by positive and negative signs, respectively, to imply directionality. A directional subset is generated for each direction, such as *b1+*, *b1-*, *b2+*, and *b2-*. Second, all the subset pairs are

identified as *b1Di*, *b2Dj*, where *Di* and *Dj* are the available directions (+ or -) in *b1* and *b2*, respectively. The Running Fisher algorithm is applied to each subset pair. The top-ranking genes in the first subset *b1Di* are collected as a group, *G*, and the second subset *b2Dj* was scanned from top to bottom in rank order to identify each rank with a gene matching a member in group *G*. At each matching rank, *K*, the scanned portion of the second subset *b2Dj* consists of *N* genes, and the overlap between group *G* and *N* genes is defined as *M*. A Fisher's exact test is performed at rank *K*, to evaluate the statistical significance of observing *M* overlaps between a set of size *G* and a set of size *N*, where the set of size *G* comes from platform *P1* and the set of size *N* comes from platform *P2*, given the sizes of *P1* and *P2* as well as the overlap between *P1* and *P2*. At the end of the scan, the best *P* value is retained, and a multiple hypothesis testing correction factor is applied. The negative log of the multiple testing corrected best *P* value ($P_{b1Di \rightarrow b2Dj}$) is a score ($S_{b1Di \rightarrow b2Dj}$) for the subset pair. Here, the subscript of $b1Di \rightarrow b2Dj$ indicates that *b*1*Di* is the first subset that is used to define the top genes *G* and *b*2*Dj* is the second subset that is used for the scan.

$$S_{b1Di \rightarrow b2Dj} = -\ln P_{b1Di \rightarrow b2Dj}. \quad (1)$$

Next, the Running Fisher algorithm is performed in the reverse direction. The same procedure in this reverse direction produces another score ($S_{b2Dj \rightarrow b1Di}$) for the same subset pair. The two scores were averaged to represent the magnitude of the similarity between the two subsets.

$$S_{b1Dib2Dj} = \frac{S_{b1Di \rightarrow b2Dj} + S_{b2Dj \rightarrow b1Di}}{2} . \quad (2)$$

The *P* value ($P_{b1Dib2Dj}$) between *b1Di* and *b2Dj* is calculated by the following equation:

$$P_{b1Dib2Dj} = exp\left(-S_{b1Dib2Dj}\right). \quad (3)$$

A positive sign is given to pairwise correlation scores (S_{b1+b2+} and S_{b1-b2-}) for a subset pair of the same direction (*b1+b2+*, *b1-b2-*), and a negative sign is given to ones (S_{b1+b2-} and S_{b1-b2+}) for a subset pair of opposite directions (*b1+b2-*, *b1-b2+*). Then, the overall score (S_{b1b2}) between *b1* and *b2* is calculated from the correlation scores (S_{b1+b2+}, S_{b1-b2-}, S_{b1+b2-}, and S_{b1-b2+}) of subset pairs using the following equation:

$$S_{b1b2} = \frac{S_{b1+b2+} + S_{b1-b2-}}{2} - \frac{S_{b1+b2-} + S_{b1-b2+}}{2} . \quad (4)$$

The sign of S_{b1b2} determines whether the two signatures are positively or negatively correlated. The overall *P* value (P_{b1b2}) between *b1* and *b2* is calculated using the following equation:

$$P_{b1b2} = exp(-|S_{b1b2}|). \quad (5)$$

This overall *P* value is referred as an overlap *P* value between two gene expression patterns in this paper.

2.5 Two-Dimensional Fluorescence Difference Gel Electrophoresis (2D-DIGE)

The DG was dissected out (Hagihara et al., 2009), frozen with liquid nitrogen, and stored at −80 °C until use. Twenty micrograms of each protein were dissolved in 30 mM Tris, pH 8.5 containing 2 M thiourea, 7 M urea, and 4% w/v CHAPS and minimally labeled with CyDye DIGE fluors according to the manufacturer's instructions (GE Healthcare, Little Chalfont, UK). In brief, the dyes were added to the protein extract (8 pmol/μg protein). Internal pools were generated by combining equal

amounts of all samples and labeled with Cy2. After vortexing, centrifugation, and incubation (30 min in the dark at 4 °C), 10 mM L-lysine (Sigma-Aldrich, St. Louis, MI, USA) was added to stop the reaction (10 min in the dark at 4 °C). Equal amounts of Cy2-, Cy3-, and Cy5-labeled protein samples were mixed, and rehydration buffer (GE Healthcare, Milwaukee, WI, USA) was added to a final volume of 125 µl. Isoelectric focusing was performed using Immobiline DryStrip (pH 3–10, 7 cm, GE Healthcare, Milwaukee, WI, USA) and an Ettan IPGphorIII (GE Healthcare, Milwaukee, WI, USA) at 300 V for 200 V·h, 1 kV for 300 V·h, and 5 kV for 6 kV·h. After the reduction and alkylation of disulfide bonds with 10 mg/ml DTT and 25 mg/ml iodoacetamide, respectively, the second-dimension separation was run on NuPAGE gels (Invitrogen, Carlsbad, CA, USA). The gels were scanned on a Typhoon 9400 imager (GE Healthcare, Milwaukee, WI, USA). Excitation and emission wavelengths were chosen specifically for each dye according to the manufacturer's recommendations. Intra-gel spot detection and intra-gel matching were performed using DeCyder software (GE Healthcare, Milwaukee, WI, USA). Differentially expressed protein spots were

determined by pairwise comparison of the mutants with the respective control data using Student's t-test.

2.6 Protein Identification by Mass Spectrometry

In-gel trypsin digestion and mass spectrometry (MS) analysis were carried out essentially according to the method described previously (Kurosawa et al, 2009). SyproRuby (Invitrogen)-stained 2D gels were used. Protein spots on the gel were excised, washed, dehydrated, added to 20 μg/μl trypsin (Promega, Fitchburg, WI, USA) solution, and digested overnight at 37 °C. Peptide segments were extracted sequentially in 0.1% trifluoroacetic acid (TFA)/60% acetonitrile (ACN), 0.1% TFA/80% ACN, and 0.1% TFA/100% ACN. The supernatant was concentrated by centrifugal evaporator and added to 0.1% TFA/2% ACN.

The obtained peptides were separated using a nano-flow multidimensional HPLC system (Paradigm MS4; Michrom Bio Resources, Auburn, CA, USA) and analyzed by electrospray ionization ion trap MS (LCQDECAXP; Thermo Fisher

Scientific, Waltham, MA, USA) under optimum conditions (Kurosawa et al, 2009). MS/MS spectra were acquired in a data-dependent mode. The resulting spectra were analyzed, and the peptide sequences were searched against a protein database (MSDB) using MASCOT software (Matrix Science, London, UK).

2.7 Immunoblotting

The membranes were immunoblotted using phosphorylation state-specific antibodies raised against phospho-peptides: phospho-Ser845 GluR1, a site phosphorylated by PKA (p1160-845; 1:250 dilution) (PhosphoSolutions, Aurora, CO, USA); phospho-Thr202/Tyr204 ERK (1:2,000 dilution) (New England BioLabs, Beverly, MA, USA). Antibodies generated against GluR1 (E-6, 1:250 dilution) (Santa Cruz Biotechnology, Santa Cruz, CA, USA), ERK (1:1,000 dilution) (New England BioLabs), which are not phosphorylation state-specific, were used to determine the total amount of proteins. The membranes were incubated with goat anti-rabbit Alexa 680-linked IgG (1:5,000 dilution) (Molecular Probes, Eugene, OR, USA) and goat anti-mouse IRDyeTM800-linked IgG (1:5,000 dilution) (Rockland Immunochemicals, Gilbertsville, PA, USA).

Fluorescence at infrared wavelengths was detected by the Odyssey infrared imaging system (LI-COR Biosciences, Lincoln, NE, USA), and quantified using Odyssey software.

2.8 Immunohistochemistry

Mice were deeply anesthetized and transcardially perfused with 4% paraformaldehyde in 0.1 M phosphate buffer, pH 7.4. The brains were dissected, immersed overnight in the same fixative, and transferred to 30% sucrose in PBS for at least 3 days for cryoprotection. Brain samples were mounted in Tissue-Tek (Miles, Elkhart, IN), frozen, and cut into 50-μm-thick coronal sections using a microtome (CM1850, Leica Microsystems, Wetzlar, Germany). The sections were washed with Tris-buffered saline containing Tween 20 (pH 7.4). For immunostaining, the cryostat sections were incubated at 4°C for 18 h with the following primary antibodies: calbindin (mouse monoclonal antibody 300 and rabbit polyclonal antibody D-28k; Swant, Bellinzona, Switzerland), calretinin (mouse monoclonal antibody 6B3 and rabbit polyclonal antibody 7699/4; Swant), GAD67 (MAB5406; Millipore, Temecula, CA, USA), mouse

anti-CNPase monoclonal (C5922, Sigma-Aldrich, St. Louis, MO, USA), GFAP (G9269; Sigma-Aldrich, St. Louis, MO, USA), p22-phox (sc-20781; Santa Cruz Biotechnology, San Diego, CA, USA), goat polyclonal antibody for parvalbumin (PVG-214; Swant, Burgdorf. Switzerland). To detect antigen localization, the sections were incubated at 4°C for 2 h with Alexa Fluor (488 or 594)-conjugated goat anti-mouse IgM or IgG antibody (1:400 dilution; Invitrogen) and/or Alexa Fluor (488 or 594)-conjugated goat anti-rabbit IgG antibody (1:400 dilution; Invitrogen). Fluorescent signals were detected using a confocal laser-scanning microscope (LSM 700, Carl Zeiss, Oberkochen, Germany) or a fluorescence microscope (Axioplan-2, Carl Zeiss, Oberkochen, Germany).

2.9 Immunofluorescence Analysis

Adult (2- to 8-month-old) mice were used. They were perfused through the heart with ice-cold PBS and then with 4% paraformaldehyde (PFA) in 0.1 M PBS, pH 7.4. After perfusion, the brains were immediately removed and then immersed in the same fixative at 4°C overnight, followed by successive immersions in 30% sucrose in PBS. The

brains were mounted in Tissue-Tek (Miles Inc., Elkhart, NY, USA), frozen and stored in −80°C until use. Brain sections were prepared 50 μm thick on a cryostat (CM1850, Leica Microsystems, Wetzlar, Germany). Resulting sections were washed in PBS for at least 2 h. The sections were incubated with primary antibodies in PBS-GB (4% normal goat serum (Vector Laboratories, Burlingame, CA, USA) and 1% bovine serum albumin in PBS) at room temperature overnight. The following primary antibodies were used: anti-calbindin (mouse monoclonal antibody 300 and rabbit polyclonal antibody D-28k; Swant, Bellinzona, Switzerland), anti-calretinin (mouse monoclonal antibody 6B3 and rabbit polyclonal antibody 7699/4; Swant), mouse anti-CNPase monoclonal (C5922, Sigma-Aldrich, St. Louis, MO, USA), anti-GAD67 (MAB5406; Millipore, Temecula, CA, USA), rabbit polyclonal anti-active Caspase-3 (BD Pharmingen, San Diego, CA, USA), GFAP (G9269; Sigma-Aldrich, St. Louis, MO, USA), anti-p22-phox (sc-20781; Santa Cruz Biotechnology, San Diego, CA, USA), anti-Iba1 (019-19741; Wako Pure Chemicals, Osaka, Japan), mouse anti-vimentin polyclonal (BD Pharmingen, San Diego, CA, USA), and goat polyclonal anti-parvalbumin (PVG-214; Swant). After washing in PBS for 60 min, the sections were incubated for 2 h at room

temperature with Alexa488- or Alexa594-conjugated secondary antibodies (Molecular Probes, Eugene, OR, USA). Nuclear staining was performed with Hoechst 33258 (Polyscience, Warrington, PA, USA). The sections were mounted on glass slides and air-dried. The sections were then embedded with Permafluor (Thermo Shandon, Pittsburgh, PA, USA). A confocal microscope (LSM700; Zeiss, Oberkochen, Germany) was used to obtain images of the stained sections.

Quantification of the numbers of immunopositive cells

For the quantification of the numbers of immunopositive cells, I used ImageJ with WCIF ImageJ bundle (http://www.uhnres.utoronto.ca/facilities/wcif/). Images from the confocal microscope were converted into 8-bit black and white images. Image thresholds were automatically determined by a plugin “maximum entropy threshold”, and the binary images were obtained. Once the images were segmented, the number of dVenus-positive cells was automatically counted by a command “Analyze/Analyze particles”. To exclude objects that are clearly not objects of interest in the binary image, the minimum size and maximum size were set at range of 5-25 μm, which were

corresponded to the cell body sizes of small GABAergic interneurons and large pyramidal neurons. The immunoreactive cells for GFAP, Iba1, PSA-NCAM and calbindin were visually counted on the binary images obtained by procedures described above. For the quantification of fluorescence intensity of immunostained images, I used ZEN software (Carl Zeiss). The region of interest of the acquired images was traced, and optical densities were obtained from at least four sections. The intensity of background staining was subtracted using nonstained portions of the each section. The values were then averaged within each brain and by group. All data collected for quantitative analysis were statistically evaluated using (Student's t test for comparison of means).

Quantification of the number of dVenus-positive cells in Shn-2 KO mice.

To analyze dVenus expression under the Arc promoter, electric shocks (0.6 mA, 125 V) were delivered to control mice (3-4 months old, n = 5) and Shn-2 KO mice (3-4 months old, n = 5) 10 times through the metal grids in the bottom of a chamber. The duration of each foot shock was 1 s, and the interval between pairs of shocks was 30 s. Five hours

after exposure to the last foot shock, mice were fixed with 4% PFA in 0.1 M PBS. The brains were removed and further incubated in the same fixative at 4°C overnight and cryoprotected in 30% sucrose in PBS. Coronal sections were prepared 50 μm thick on a cryostat (CM1850, Leica Microsystems, Wetzlar, Germany). The resulting sections were counter-stained with Hoechst 33258 and mounted on glass slides. The glass slides were embedded with Permafluor (Thermo Shandon, Pittsburgh, PA, USA). Images of dVenus-positive cells within the specified regions or subdivisions were taken by a confocal microscope (LSM 700, Zeiss, Göttingen, Germany). The brain regions were carefully determined according to the mouse brain atlas (Paxinos & Franklin, 2004). Microscopic analysis was performed using a 20× objective lens (Plan-Apochromat, NA 0.8, Zeiss) and a pinhole setting that corresponded to a focal plane thickness of less than 1-μm.

The number of dVenus expressing cells was counted using ImageJ with the WCIF ImageJ bundle (http://www.uhnres.utoronto.ca/facilities/wcif/). The following procedures are previously described in the paragraph "*Quantification of the numbers of immunopositive cells.*"

Quantification of cortical thickness and cell number

I used three age groups: postnatal days (P) 14-16 (WT: 5 males and 4 females; Shn-2 KO: 2 males and 5 females), P30 and 31 (WT: 4 males and 4 females; Shn-2 KO: 8 males and 10 females), and adult (WT, 3-4 month-old males, $n = 6$; Shn-2 KO, 3-4 month-old males, $n = 8$). Brains were fixed as described above. Fixed brains were sliced sagittally into 50 μm thick sections on a cryostat (CM1850, Leica Microsystems). The resulting sections were mounted on glass slides and air-dried. The sections were stained with Cresyl violet (Merck, Darmstadt, Germany) for 30 min at room temperature. After washing twice in dH_2O for 1 min, the sections were sequentially dehydrated in 70%, 90%, 95%, 2×100% ethanol, 50% ethanol/50% xylene, cleared in xylene, and embedded with new MX mounting reagent (Matsunami Glass, Osaka, Japan). Digital images were captured by using a light microscope (DM3000, Leica, Wetzlar, Germany) with a × 5 objective (N Plan, numerical aperture 0.12, Leica) and a digital camera (DS-Vi1, Nikon, Tokyo, Japan).

For the quantification of region size, cortical thickness, and cell number, I used ImageJ with the WCIF ImageJ bundle (http://www.uhnres.utoronto.ca/facilities/wcif/). Quantification of cell number was performed as described in the paragraph *"Quantification of the number of dVenus-positive cells in Shn-2 KO mice"*. For the quantification of region size, the regions were defined as follows: neocortex, hippocampus, and basal ganglia were defined as cerebrum; and diencephalon, midbrain, pons, and medulla oblongata were defined as brain stem. The sections for measurement were selected at 0.36 mm laterals from the midline. For the quantification of the thickness and cell number of each neocortical region, I used each coordinate: prelimbic area, 0.36 mm lateral from the midline; motor area, 1.20 mm lateral from the midline; somatosensory and visual areas, 2.76 mm lateral from the midline.

2.10 Electrophysiology

Whole-cell patch clamp and field potential recordings

Male Shn-2 KO mice and their wild-type littermates (15-19 weeks old) were used for electrophysiological experiments. Mice were decapitated under halothane anesthesia and both hippocampi were isolated. Transverse hippocampal slices (380 μm) were cut using a tissue slicer. Slices were maintained in a humidified interface holding chamber at room temperature before use, and electrophysiological recordings were made in a submersion-type chamber superfused at 2 ml/min with the standard saline composed of (in mM): NaCl, 125; KCl, 2.5; NaH_2PO_4, 1.0; $NaHCO_3$, 26.2; glucose, 11;$CaCl_2$, 2.5; $MgCl_2$, 1.3 (equilibrated with 95% O_2/5% CO_2) and maintained at 27-27.5 ºC. Whole-cell recordings were made from granule cells in the dentate gyrus by using the blind whole-cell patch-clamp technique. Current-clamp recordings were made with a glass pipette filled with a solution composed of (in mM) potassium gluconate (140), HEPES (20), NaCl (8), MgATP (2), Na_2GTP (0.3), EGTA (0.05) (pH adjusted to 7.2 with KOH) using a Multiclamp 700B amplifier (Molecular Devices, Sunnyvale, CA, USA). Hyperpolarizing and depolarizing currents (400 ms) were injected through the recording pipette to measure the input resistance and to assess properties of action potential firing, respectively. Field excitatory postsynaptic potentials (EPSPs) arising from mossy fibers

(MFs) were recorded from the CA3 region of the hippocampus. Bipolar stimulating electrodes were placed in the dentate granule cell layer and a recording glass electrode filled with 2M NaCl was placed in the stratum lucidum of the CA3 region. EPSPs were evoked at the frequency of 0.05 Hz unless otherwise specified. A criterion used to identify the MF input was more than 85% block of EPSP by the group II metabotropic glutamate receptor agonist (2S,2´R,3´R)-2-(2´,3´-Dicarboxycyclopropyl)glycine (DCG-IV; Tocris Bioscience, Bristol, UK). Statistical significance was evaluated by two-tailed Student's t-test with the significance level $p < 0.05$. All procedures were approved by the Animal Care and Use Committee, Nippon Medical School.

Electroencephalogram (EEG) recording

Mice were anesthetized with pentobarbital (50 mg/kg) and implanted with epidural stainless steel screw electrodes (1.2 mm-diameter) for electroencephalogram (EEG) recording. Electrodes (four pins located ± 2.5 mm lateral of bregma, ± 2.5 mm anterior or posterior to bregma) were connected to a multi-channel cable-free data-logging device NeuroLogger (NewBehavior AG, Zürich, Switzerland) that weights 2.8 g

including batteries and can be plugged into or removed from a connector embedded in a dental cement socket on the skull of the animal (Etholm et al., 2010). EEG recording from implanted mice was conducted in their homecage (12 h light/dark cycle). Food and water were available ad libitum during the recording. The sampling rate was 200 Hz. Spectral analysis of the EEG was performed by fast Fourier transform (FFT) using the SPIKE2 program (version 6, Cambridge Electronic Design, Cambridge, UK). This analysis yielded a power spectral profile over a 0–128 Hz window divided into delta (1–4 Hz), theta (4–9 Hz), alpha (9–12 Hz), and beta (12-25 Hz), and gamma (25–70 Hz) waves.

2.11 Analysis of SNPs in the MHC region

To identify SNPs that potentially influence transactivation of NF-κB and/or Shn-2 in the MHC region, I conducted the following *in silico* analyses. First, I picked up SNPs that are significantly associated with schizophrenia (Bergen et al., 2012; Purcell et al., 2009; J. Shi et al., 2009; Y. Shi et al., 2011; Stefansson et al., 2009), and that are located in or close (~50 bp) to binding sites for NF-κB in the MHC region. The selection was

performed using TRANSFAC, a library of transcription factor binding sites (Wingender et al., 1997) and MATCH, a web-based application for searching putative transcription factor binding sites in DNA sequences (Kel et al., 2003). Due to strong linkage disequilibrium (LD) across the extended MHC region (Purcell et al., 2009; J. Shi et al., 2009; Y. Shi et al., 2011), SNPs in the region could be involved in susceptibility to schizophrenia. I next screened SNPs in NF-κB binding sites from approximately 87,000 SNPs in the extended MHC region (chr6:25,900,000-33,533,000, GRCh37/hg19) (Horton et al., 2004) by using UCSC Table Browser (Karolchik, 2004) for retrieving the data of both SNPs and conserved transcription factor binding sites (TFBSs) (Liu et al., 2008), and Galaxy (Giardine et al., 2005) for mapping those SNPs to TFBSs. Then, I collected genes located in the 20 kbp region up- or down-stream of the 52 schizophrenia-associated SNPs in or close (~50 bp) to binding sites of NF-κB in the MHC region and 58 SNPs in binding sites of NF-κB in the MHC region. The latest gene information was obtained using 1000 Genomes Browser (http://www.ncbi.nlm.nih.gov/variation/tools/1000genomes/). I listed 32 genes that are

differentially expressed in post-mortem brains of schizophrenic patients and brains of Shn-2 KO mice with the NextBio search engine.

2.12 Measurement of skull size

Adult male mice were used (WT, 3-7 month-old, *n* = 9; Shn-2 KO, 3-7 month-old, *n* = 7). Mice were deeply anesthetized with chloral hydrate and perfused with 4% PFA. The scalp was incised along the midline, and the skull was completely exteriorized. In order to precisely measure skull size, connective and muscular tissues were removed. Each cranial size was defined as follows: cranial length, the anterior border of the frontal bone to the posterior border of the occipital bone; cranial width, the maximum width between the temporal bones; cranial depth, the maximum length between the bottom of the temporal bone to the top of parietal bone. Cranial size was measured with a caliper. The fixed brains were stored until use.

2.13 Electron microscopy

Brain tissues were fixed with 4% paraformaldehyde / 0.2% glutaraldehyde / 100 mM sodium cacodylate, pH 7.2 at 4°C by perfusion from left ventricles for 15 min, and small pieces of hippocampus were then fixed by immersion overnight with 4% paraformaldehyde / 6% glutaraldehyde / 100 mM sodium cacodylate, pH 7.2 following the procedure by Shepherd and Harris (Shepherd & Harris, 1998). After fixation with 1% osumium tetroxide / 100 mM sodium cacodylate, pH 7.2 at 4°C for 1 h and then washing with 100 mM sodium phosphate, pH 7.4 / 150 mM sodium chloride, the small pieces of hippocampus were dehydrated in a graded series of ethanol and acetone. They were then embedded in Epok812 (Oken, Tokyo, Japan) and polymerized by heating at 60°C. Thin sections of 2 μm thickness were cut on an ultramicrotome, collected on glass slides, and stained with 0.1% toluidine blue O / 100 mM sodium phosphate, pH 7.4. Areas of the hippocampus, CA1, CA3, and dentate gyrus were trimmed under the microscope and ultra-thin sections of 0.1 μm thickness were cut on an ultramicrotome and collected on nickel grids with a polyvinyl formal membrane. Specimens were observed through a JEM1010 transmission electron microscope (JEOL, Tokyo, Japan) at an accelerating voltage of 80 kV after staining with uranyl acetate and lead citrate.

Image acquisition was done with a Gatan BioScan model 792 CCD camera and Digital Micrograph software (ver. 3.9.3) (Gatan, Pleasanton, CA, USA).

3. RESULTS

3.1 Shn-2 KO Mice Display Behavioral Abnormalities Reminiscent of Schizophrenia

Hyperactivity is one of the most common phenotypes in animal models of schizophrenia or bipolar disorder. Since Shn-2 KO mice were reported to show hyperactivity during open field testing (Takagi et al., 2006), I subjected them to a comprehensive behavioral test battery (Yamasaki et al., 2008) to further analyze the behavioral effects of Shn-2 deficiency. Shn-2 KO mice showed no obvious deficits in general health, physical characteristics, or basic sensorimotor functions compared with their wild-type littermates, apart from decreased sensitivity to pain in the hot plate test (Figure 2b) and a lower body weight (Table 1). Shn-2 KO mice displayed severe working memory deficits in the eight-arm radial maze (Figure 3a and b) and T-maze

forced-alternation task (Figure 3c and d), while their performance in the T-maze left–right discrimination task was normal (Figure 3e). In reversal learning, mutants performed even better than controls (Figure 3e). This working memory impairment is commonly found in schizophrenia patients and is referred to as a cognitive endophenotype of schizophrenia (Kalkstein et al., 2010). Shn-2 KO mice also showed a series of other schizophrenia-related abnormal behaviors: Prepulse inhibition (PPI), the phenomenon by which a weak pre-stimulus suppresses the response to a startling stimulus, is often decreased in schizophrenic patients compared with healthy controls (Swerdlow et al., 2006). In Shn-2 KO mice, while the amplitude of the acoustic startle response was comparable with that of wild-type controls (Figure 3f; Figure 2a), the PPI of the acoustic startle response was markedly reduced (Figure 3g). High-dose administration of haloperidol, a typical antipsychotic, significantly improved this impairment in PPI in Shn-2 KO mice (Figure 3g).

Social withdrawal has been identified as one of the common negative symptoms in schizophrenia patients (Bobes, Arango, Garcia-Garcia, & Rejas, 2011). Mutant mice showed impaired sociability and novelty preference in Crawley's

sociability and social novelty preference test (Figure 3h and i). Mutant mice also displayed decreased social interaction in the conventional social interaction test in a novel environment (Figure 3j; Figure 4g and h). Consistent with a previous report (Takagi et al., 2006), Shn-2 KO mice displayed hyperactivity in the open field test (Figure 4a) and in their home cages (Figure 4b). Prior treatment with the antipsychotic haloperidol (0.3 mg/kg) or clozapine (1.0 mg/kg) decreased hyperactivity in Shn-2 KO mice to that of saline-treated control mice (Figure 3k and l). MK-801, an NMDA antagonist that causes schizophrenia-like psychosis in humans, produced significantly higher levels of drug-stimulated motor activation in Shn-2 KO mice (Figure 4j and k). The social activity of nest building in rodents is disrupted by the administration of psychomimetic agents (Schneider & Chenoweth, 1970). Nestlet shredding and nest building was severely impaired in Shn-2 KO mice (Figure 3m and n); Nestlets were left intact by ~80% of mutant mice, while all wild-type mice built nests within 24 h. Depression-like behavior of Shn-2 KO mice was increased in sucrose preference test (Figure 19n). In the Porsolt forced swim test, a reduction of immobility was observed in Shn-2 KO mice (Figure 4f), possibly due to hyperactivity.

The improvement in PPI observed after haloperidol administration suggests that dopaminergic receptor signaling is altered in Shn-2 KO mice; therefore, I performed dopamine receptor binding assays to examine this. Because Shn-2 KO mice showed significantly reduced expression of D1 dopamine receptors in the DG (Figure 5a), I examined the effects of D1 receptor activation on the phosphorylation status of the AMPA receptor, GluA1, at Ser845 (the PKA site) and extracellular signal-regulated kinase 2 (ERK2) at Thr202/Tyr204. The increases in GluA1 and ERK2 phosphorylation induced by SKF81297, a D1 receptor agonist, were greater in Shn-2 KO mice than in control mice (Figure 5d–g). Normalization of phosphorylated GluA1 against total GluA1, which is decreased in Shn-2 KO mice (Figure 5f, right), made these differences even greater (Figure 5f, center). The increased levels of ERK2 phosphorylation observed in Shn-2 KO mice resulted from increased expression of ERK2 (Figure 5g).

3.2 Shn-2 KO Mice Share Gene Expression Alterations with Postmortem Schizophrenia Brain

The medial prefrontal cortex (mPFC) (Goldman-Rakic, 1995) and DG (Gilbert & Kesner, 2006) have been suggested to play key roles in working memory, and in Shn-2 KO mice this working memory was severely impaired. Therefore, gene chip analysis was conducted to assess gene expression in the mPFC of Shn-2 KO mice. Significant up- or downregulation of 856 genes (980 probes) was observed in the mutants (P-value < 0.05, fold-change < −1.2 or > 1.2). I then compared the gene expression pattern in Shn-2 KO mice with those in patients with mental disorders from publicly available array data using the NextBio search engine. The highest degree of gene expression overlap was detected in postmortem schizophrenic and control tissue from the frontopolar part of the frontal cortex, Brodmann area 10 (BA10) (previously reported by (Maycox et al., 2009); Figure 6a, $P = 9.5 \times 10^{-14}$), with 100 genes altered in both Shn-2 KO mice and schizophrenia patients. Seventy-six genes out of those genes showed the same directional change in expression (Figure 6b–d) and, of these genes, 42 genes were downregulated ($P = 3.6 \times 10^{-16}$) and 34 were upregulated ($P = 6.1 \times 10^{-13}$). It is noteworthy that HIVEP2 (SHN2) was significantly decreased in the schizophrenic BA10 (FC = −1.29, P = 0.0009) (Maycox et al., 2009). Within these groups, I noted a

large number of genes previously implicated in schizophrenia or bipolar disorder (Table 2). Eighty-nine of 100 genes showing significant similarities in terms of expression have been identified as being related to these disorders (Table 2). Interestingly, six of the top 10 ranked genes were involved in inflammatory or immune responses. In addition, seven of the top 10 ranked upregulated biogroups showing significant overlap between postmortem schizophrenia brain tissue and the PFC of Shn-2 KO mice were related to inflammatory or immune responses (Table 3).

3.3 Molecular Alterations in the Hippocampus of Shn-2 KO Mice

The granule cells of the hippocampal DG are compromised in schizophrenia (Altar et al., 2005; Tamminga et al., 2010). Because the DG is involved in spatial working memory (Gilbert & Kesner, 2006; Vann et al., 2000), deficits of which are cardinal features of schizophrenia, I analyzed the DG transcriptome of Shn-2 KO mice. Under the same criteria used for mPFC analysis, the expression of 1497 probes (1220 genes) was significantly up- or downregulated in the mutants. The top 500 genes are listed in Table 4. I also compared the DG transcriptome of Shn-2 KO mice to a study of laser-

captured DG from human schizophrenia patients (Altar et al., 2005). Calb1 (Shn-2 KO, FC = −5.36, P = 0.001; Schizo, FC = −1.82, P = 0.001), a marker of mature granule neurons, and Rab33a (Shn-2 KO, FC = −1.25, P = 0.0023; Schizo, FC = −1.96, P = 0.0001), a Ras-associated small GTPase, were both downregulated in the DG of Shn-2 KO mice and human schizophrenia patients.

I further analyzed the DG proteome in Shn-2 KO mice using two-dimensional difference gel electrophoresis (2D-DIGE) and found 116 proteins differentially expressed between mutant and control mice (Table 5). When sorted by functional category, proteins in the same category were differentially expressed in both schizophrenia and Shn-2 KO mice. Table 6 lists the genes and proteins with altered expression in both schizophrenic DG and Shn-2 KO brains (Altar et al, 2005) (including the DG (Tables 4 and 5) and whole hippocampus (Table 5)). Notably, the expression of aldo-keto reductase genes (particularly AKR1A1 and AKR1B1 and their mouse equivalents) was reduced in human patients and Shn-2 KO mice. Cytochrome-related genes UQCRFS1 and CYC1 were reduced in the DG of schizophrenia and the hippocampus of Shn-2 KO mice, as were genes encoding glucose phosphate isomerase,

NADH dehydrogenase, phosphoglycerate-related molecules, proteasome, ubiquitin-related molecules, and syntaxins (Altar et al., 2005).

Immunohistochemistry of Shn-2 KO brains revealed several features observed in the postmortem brains of schizophrenia patients (Benes et al, 2007; Flynn et al, 2003; Reynolds and Beasley, 2001). Parvalbumin-positive neuronal number was decreased in the mPFC (Figure 7a and b) and hippocampal CA1 region (Figure 7c and d). The expression of glutamic acid decarboxylase 67 (GAD67) was lower in the mutant hippocampus (Figure 7e and f). The expression of 2′,3-cyclic nucleotide 3′-phosphodiesterase (CNPase), a marker for mature oligodendrocytes, was also reduced (Figure 7g and h) and cell-packing density was higher in the DG of Shn-2 KO mice (Figure 7i and j).

3.4 Arc Induction Is Reduced in the Brains of Shn-2 KO Mice

Induction of the immediately early gene protein products has been used to assess neural activation. I crossed Shn-2 KO with transgenic mice expressing destabilized Venus

(dVenus) under the control of the activity-regulated cytoskeletal-associated protein (Arc) promoter (Eguchi and Yamaguchi, 2009), allowing fluorescence-based visualization of Arc expression. I compared Arc-dVenus expression between Shn-2 KO and wild-type mice with the Arc-dVenus-positive background. To maximize Arc induction in the DG physiologically, mice received electrical shocks in a novel environment. Expression of Arc-dVenus in the DG 5 h after stimulation was dramatically reduced throughout the entire brain of Shn-2 KO mice (Figure 8), including amygdala (Figure 8a and d), sensory cortex (Figure 8b and d), motor cortex (Figure 8d), and PFC (Figure 8d). In the hippocampus of Shn-2 KO mice, dVenus expression was almost completely abolished in the DG (Figure 8c and d), with only minimal changes in CA regions. Reduced induction of Arc-dVenus was also observed 5 h after exposure to a novel environment without electrical shocks (Figure 9).

3.5 Schizophrenia-Related Cortical Abnormalities in Shn-2 KO Mice

Shn-2 mutant mice display significantly thinner cortex and reduced cell density in the prelimbic and primary visual cortices (PrL and V1, respectively) when compared with

wild-type mice (Figure 10a–c), which is consistent with observations in human patients (Pierri et al., 1999). Although the mutants demonstrated a reduction in cortical thickness, increased apoptosis was not appreciated in the brains of Shn-2 KO mice (Figure 11). No obvious hallmarks of neurodegeneration, such as cell swelling, protein deposition, or nuclear condensation, were not found by electron microscopic analysis in the mutants (Figure 12). The size of the whole brain (Figure 13a and b), cerebrum (Figure 13c left), and cerebellum (Figure 13c right) was not significantly different between genotypes. The size of skull was also measured, which was not significantly different (Figure 13e). Previous studies report increased low-frequency (Moran & Hong, 2011; Sponheim et al., 1994) and decreased high-frequency (Gallinat et al., 2004; Moran & Hong, 2011) energy in EEG studies of schizophrenia patients. I measured cortical EEG in freely moving mice using Neurologger spectral analysis technology (Figure 10e) and observed a significant increase of power in the theta band and decrease in the gamma band of Shn-2 KO mice compared with that in the controls (Figure 10d).

3.6 Maturation Deficits of Dentate Gyrus in Adult Shn-2 KO Mice

The behavioral abnormalities shown by Shn-2 KO mice resembled those observed in α-CaMKII$^{+/-}$ mice, which also show locomotor hyperactivity and severe working memory deficits (Yamasaki et al., 2008). To identify further similarities, I compared the hippocampal transcriptome patterns of both mouse models. Shn-2 KO mice and α-CaMKII$^{+/-}$ mice showed strikingly similar expression patterns (Figure 14a), with over 100 genes similarly altered. Moreover, the fold changes in differentially expressed genes were quite similar between strains (Figure 14a and b), indicating shared molecular pathophysiology between these mutants. In the hippocampus of α-CaMKII$^{+/-}$ mice, dentate granule cells fail to mature, which is termed "immature dentate gyrus". This immature dentate gyrus, abbreviated "iDG" is characterized by increased expression of the immature-neuronal marker calretinin and decreased expression of the mature granule cell marker calbindin in the DG. Calbindin expression within the Shn-2 KO hippocampus is also dramatically decreased (Figure 14b and c) and was almost completely abolished in the DG (Figure 14c). As observed in α-CaMKII$^{+/-}$ mice, the number of cells positive for calretinin (Figure 14d) and PSA-NCAM (a late-progenitor and immature-neuron marker) (Figure 15) was increased dramatically in the Shn-2 KO

DG. Collectively, these findings suggest that the number of immature neurons increases and that of mature neurons decreases, within the hippocampi of the two mutant mouse strains, that exhibited behavioral abnormalities related to schizophrenia.

Whole-cell recordings were made from granule cells in the DG. The cell membrane capacitance of Shn-2 KO mice decreased compared with that in controls (Figure 14e), indicating a smaller cell surface area. Granule cells in the DG of Shn-2 KO mice had a normal resting membrane potential (data not shown) and high input resistance (Figure 14f). In response to the current injection, Shn-2 KO cells demonstrated a lower current threshold for firing (Figure 14g), a short latency to the first spike (Figure 14h), and a decreased number of spikes during sustained depolarization (Figure 14i). Consistent with their immunohistological profile, granule cells in the mutant DG showed somatic electrophysiological features similar to those of immature granule cells (Schmidt-Hieber et al., 2004; Yamasaki et al., 2008).

I also examined synaptic transmission at the granule cell output, the mossy fiber (MF) synapse. The ratio of peak MF excitatory postsynaptic potential (EPSP) amplitude to fiber volley amplitude was increased in the mutant (Figure 14j), indicating

significant augmentation of basal synaptic transmission. Strong frequency facilitation, an index of mature presynaptic function at the MF synapse (Kobayashi et al., 2010; Yamasaki et al., 2008), was greatly decreased in mutant mice (Figure 14k).

3.7 Evidence of CNS Inflammation within Shn-2 KO Mice

To characterize the molecular events happening in the Shn-2 KO mouse brain, correlation between Shn-2 KO gene expression data and thousands of publicly available array data sets were computed using the NextBio search engine using a rank-based algorithm (Sung et al., 2009). The top 300 biosets with the highest correlation scores with Shn-2 KO mice are categorized in Table 7. Seven of the top 10 correlating biosets were categorized as ‘aging.’ Among the top 300 correlating biosets, 59 were categorized as aging, 18 as infection, 13 as injury, 12 as tumor, and 11 as neurodegeneration. Conspicuously, almost all biosets exhibiting gene expression changes similar to those in the brains of Shn-2 KO mice were related to inflammatory or immune responses. Similar gene perturbation patterns were found in the case of LPS

treatment (Figure 16a, $P = 5.6 \times 10^{-9}$), injury (Figure 16b, $P = 5.7 \times 10^{-24}$), prion infection (Figure 16c, $P = 1.0 \times 10^{-18}$) and aging (Figure 16d, $P=1.4 \times 10^{-26}$).

These results were particularly compelling, considering that Shn-2 is an endogenous inhibitor of NF-κB and that NF-κB is activated in Shn-2-deficient cells (Kimura et al., 2005). The expression of NF-κB-dependent genes such as *Ccnd1* (FC = 2.33, $P = 0.0004$), *Hmox1* (FC = 1.69, $P = 0.0215$), *Pdyn* (FC = 1.66, $P = 0.0364$), *Ptgs2* (also known as *Cox2*, FC = 1.625, $P = 0.0161$), *Traf1* (FC = 1.418, $P = 0.0148$), and *Vim* (FC = 1.87, $P = 0.0057$) was increased in the hippocampus of Shn-2 KO mice. Notably, genes related to the inflammatory/immune response such as *Serpina3n*, *C1qa*, *C1qb*, *C1qc*, *Cyba*, *H2-Ab1*, *Tgfbr1*, *Cebpb*, *Ctsc*, *Lyn*, and *Tgfb1* were upregulated in the mPFC of Shn-2 KO mice and in postmortem brains of schizophrenia patients (Table 2). I compared the gene expression patterns across various human brain disorders with that of Shn-2 KO mice (Table 8). The biosets derived from schizophrenia patient groups showed the highest similarity to the bioset derived from Shn-2 KO mice ($P = 9.50 \times 10^{-14}$), although the biosets derived from neurodegenerative disorders such as Alzheimer's disease and Parkinson's disease also

showed significant similarities in expression to the biosets derived from Shn-2 KO mice. However, in spite of the similarities with neurodegenerative disorders, no obvious apoptosis or neurodegeneration was appreciated in the brains of Shn-2 KO mice (Figures 10 and 11).

Next, immunohistochemistry was performed to detect molecular-level regulation by NF-κB. The expression of p22 phox NADPH oxidase, which causes inflammation via the release of reactive oxygen species (Manea et al., 2007), was increased in the DG and CA1 of Shn-2 KO mice (Figure 16e and f). Vimentin, an NF-κB-regulated (Kumar et al., 2004) intermediate filament protein found in immature astrocytes, was similarly increased (Figure 16g and h), as was glial fibrillary acidic protein (GFAP; Figure 16i and j). Although the area of GFAP-positive cells increased (Figure 16j), the number of GFAP-positive cells that was counted by staining with Hoechst was unchanged (Figure 16k and l). While astrocytes were activated in Shn-2 KO mice, microglias were not, as indicated by unaltered expression of the microglia marker, Iba1 (Figure 17).

Interestingly, pre-weaned animals showed no significant differences in calbindin (Figure 18a and b), calretinin (Figure 18e and f), p22 phox (Figure 18i and j), or GFAP (Figure 18m and n) expression between genotypes. The expression of p22 phox in older (1-month-old) mutant animals was increased (Figure 18k and l) whereas that of GFAP was not significantly different (Figure 18o and p). Calbindin expression was decreased (Figure 18c and d), and calretinin was increased (Figure 18g and h) in the DG of 1-month-old Shn-2 KO mice compared to that of wild-type mice, indicating an immature dentate gyrus (iDG) phenotype.

To assess whether inflammation plays any role in the behavioral abnormalities shown by Shn-2 KO mice, I treated them with anti-inflammatory drugs (chronic administration of 4 mg/kg rolipram and fed chow containing 400 ppm ibuprofen) for 3 weeks. Treatment with anti-inflammatories reduced the number of activated astrocytes, which reflect inflammation within the hippocampi of the Shn-2 KO mice (Figure 19a and b), but did not affect the number of activated astrocytes in the PFC (Figure 19c). The decrease in parvalbumin (in the CA1 and PFC; Figure 19d and e), calbindin (in the DG; Figure 19h), and GAD67 (in the DG; Figure 19i) expression

observed in the mutant mice was not rescued by treatment with anti-inflammatory drugs. Interestingly, the increase in the expression of doublecortin and calretinin in the DG of Shn-2 KO mice was reversed by treatment with anti-inflammatory drugs (Figure 19f and g). Moreover, working memory, as measured by the T-maze test and nest-building behavior were significantly improved in Shn-2 KO mice (Figure 19j and k). On the other hand, the increased locomotor activity observed in the open field test, the impaired PPI observed during the startle response, and the anhedonia in the sucrose preference test did not improve (Figure 19l–n). These results indicate that mild chronic inflammation occurring in the adult brain contributes to at least some of the behavioral deficits and cellular/molecular phenotypes seen in Shn-2 KO mice.

4 DISCUSSION

In the course of large-scale behavioral screening for mouse models of neuropsychiatric disorders, I discovered that Shn-2 KO mice display a series of schizophrenia-related behavioral abnormalities including severe working memory deficits, decreased social interaction, impaired nest-building behavior, and impaired PPI. I also identified

conserved genetic and molecular phenotypes shared by both Shn-2 KO mice and postmortem brains of schizophrenia patients. Transcriptome patterns in the mPFC of Shn-2 KO mice and the PFC of schizophrenia patients are strikingly similar. Table 9 summarizes the phenotypes of the Shn-2 KO mice and the abnormalities associated with schizophrenia. Since the disorder is composed of a heterogeneous population, even an 'ideal' animal model of schizophrenia, if any, will not necessarily exhibit the abnormalities observed in all schizophrenia-relevant phenotypes (Powell & Miyakawa, 2006). However, Shn-2 KO mice exhibit an unusually high number of similarities compared with other existing animal models of schizophrenia.

Shn-2 KO mice possessed an immature DG (iDG) phenotype that has also been identified in α-CaMKII$^{+/-}$ mice, which display behavioral abnormalities similar to those observed in Shn-2 KO mice (Yamasaki et al., 2008). In addition, several other mouse strains have similar phenotypes: SNAP-25 KI mice (Ohira et al., 2013), calcineurin cKO mice (Hagihara et al., 2022), fluoxetine treated mice (Kobayashi et al., 2010), pilocarpine-induced epirepsy model mice (Shin et al., 2013), and mice subjected to electroconvulsive shock (ECS) (Imoto et al., 2017), all of which had immature

dentate gyrus, similar to Shn-2 KO mice. There are also similarities in behavioral phenotypes in these mice, such as hyperactivity and impaired working memory. Considering the present results and these reports together, iDG phenotype can be caused by a variety of genetic mutations and abnormalities in neural activity.

Of the top 20 biogroups whose genes that showed significant overlap with those whose expression was changed in postmortem schizophrenia brains (Maycox et al., 2009), 14 were involved in immune responses. Most of the genes within these biogroups were upregulated (Table 3), suggesting that inflammation or immune activation occurs in the brains of both schizophrenic patients and Shn-2 KO mice. The overall hippocampal transcriptome pattern of Shn-2 KO mice exhibited similarities to patterns identified in a number of inflammatory conditions, including aging, injury, prion infection, and adjuvant treatment (Table 7), in which NF-κB signaling is activated. I found significant increases in the expression level of many complement genes and MHC/HLA genes in Shn-2 KO mice (Table 10). Notably, C1qa, C1qb, C1qc, H2-Aa (HLA-DQA1), and H2-Ab1 (HLA-DQB1) were upregulated in the brains of both Shn-2 KO mice and patients with schizophrenia. Another complement, C4, has

also been reported to increase in the postmortem brains of schizophrenic patients (Sekar et al., 2016). C4 expression was also increased in the DG of Shn-2 KO mice, 2.4 times that of controls. C1q (Fourgeaud & Boulanger, 2007; Presumey et al., 2017) and C4 (Presumey et al., 2017) are proposed to act as a spreading 'punishment signals' that bind to weaker synapses resulting in their physical removal. In this regard, it is of interest to note that the expression of the genes related to 'synaptic transmission,' the dysregulation of which is also thought to be involved in schizophrenia (Mirnics et al., 2001; Stephan et al., 2006), tended to be downregulated in the brains of both Shn-2 KO mice and schizophrenic patients (Table 3). Upregulation of C1q genes could be a potential interface between inflammation and synaptic dysfunctions. Interestingly, the levels of majority of pro-inflammatory cytokines, including those that play a role in acute inflammation (eg, IL-1 and TNF-α), were unchanged in the brains of Shn-2 KO mice and schizophrenic patients (Table 10). These data indicate the atypical nature of inflammation happening in the brains of Shn-2 KO mice and, potentially, in those of schizophrenic patients. The precise manner in which these genes are altered is likely to be complex and remains to be determined. A number of SNPs in the MHC region

associated with schizophrenia (Purcell et al., 2009; J. Shi et al., 2009; Stefansson et al., 2009; Yue et al., 2011). Table 11 lists the SNPs located in, or close to, NF-κB-binding sites that may be associated with susceptibility to schizophrenia. Some of the genes surrounding these SNPs are dysregulated in the postmortem brains of schizophrenic patients and/or the PFC of Shn-2 KO mice. Abnormal transcription of these genes may be induced by dysregulated NF-κB signaling pathways, without any deficiency or mutation in Shn-2 itself.

Astrocytes were activated in the hippocampus of Shn-2 KO mice, while microglias were largely inactive. In humans, type-I and type-II immune responses are defined by the respective cytokines activated. The type-I response mainly promotes cell-mediated immune responses against intracellular pathogens with the activation of Th1 CD4+ cells and microglias (Muller & Schwarz, 2006). The type-II immune response is largely directed against extracellular pathogens in which Th2 CD4+ cells and astrocytes are activated (Muller & Schwarz, 2006). This atypical pattern of inflammation is also observed in schizophrenia patients, who demonstrate attenuated type-I immune responses and activated type-II immune responses (Muller & Schwarz,

2006). This so-called ‘Th2 slant’ can be observed in the CNS, with astrocytes reflecting the type-2 immune response and microglias reflecting the type-1 immune response (Muller & Schwarz, 2006), in schizophrenia patients as well as Shn-2 KO mice (Kimura et al., 2007). Accordingly, the astrocyte activation observed in Shn-2 KO and schizophrenia may result from type-2 immune activation. Microglial activation is also reported in schizophrenia, but only within a small percentage of postmortem brains, possibly as a side effect of medication (Bayer et al., 1999; Muller & Schwarz, 2006). Pharmacological experiments indicate that deficits in working memory and nest-building behavior could be rescued by treatment with anti-inflammatory drugs, which also reduced GFAP expression, a widely used inflammation marker, in the brains of Shn-2 KO mice. These results suggest that mild chronic inflammation caused by deficiency of Shn-2 underlies at least some behavioral abnormalities related to schizophrenia.

The well-established role of inflammation in the etiology of schizophrenia is often referred to as the inflammation hypothesis (Keshavan, Nasrallah, et al., 2011; Muller & Schwarz, 2006; Nawa & Takei, 2006; Patterson, 2009). The link between

prenatal infection and schizophrenia was first identified in an epidemiological study demonstrating increased schizophrenia risk in the offspring of women exposed to influenza during pregnancy (Muller & Schwarz, 2006). Several other infectious factors have also been implicated in the pathogenesis of schizophrenia (Muller & Schwarz, 2006), suggesting that the disease may result from maternal immune response to infection. To this end, prenatal Poly I:C treatment, viral infection, and LPS treatment are used as rodent models of schizophrenia (Nawa & Takei, 2006; Patterson, 2009). To the best of my knowledge, the Shn-2 KO mouse is the first animal model of schizophrenia with multiple inflammatory-like phenomena arising from a single gene knockout.

In schizophrenia patients, the number of parvalbumin-positive neurons decreases in the cortex (Reynolds & Beasley, 2001) and hippocampus (Zhang & Reynolds, 2002), which could cause a deficit in the density of certain GABAergic neuronal subtypes. Inflammatory responses evoked by neonatal LPS treatment were reported to induce a reduction in parvalbumin-expressing neurons in the rat hippocampus (Jenkins et al., 2009). Overexpression of IL-6 (Heyser et al., 1997), which

is secreted during type-II immune responses, also reduces the number of parvalbumin-positive neurons (Muller & Schwarz, 2006). Similarly, a previous study reported that IL-6 mediates age-related loss of critical parvalbumin-expressing GABAergic interneurons through increased neuronal NADPH oxidase-derived superoxide production (Dugan et al., 2009). Consistently, IL-6 was increased in the T cells (Kimura et al., 2005) of Shn-2 KO mice.

Attenuation of molecular markers for schizophrenia may also result from inflammation. Ketamine exposure, which has been used as a model of schizophrenia based on NMDA hypofunction, reduces parvalbumin and GAD67 expression through increased NADPH oxidase and p22 phox, suggesting inflammation (Behrens et al., 2007). Schizophrenia patients express lower levels of GABAergic neuron-expressed GAD67 in the stratum oriens of CA2/3 (Benes et al., 2007), suggesting the possibility that these deficits lead to neuronal GABA hypofunction. I also observed several potential deficits in key oligodendrocyte markers, including decreases in CNPase and myelin basic protein (MBP). Decreased CNPase protein levels have been reported in schizophrenia (Flynn et al., 2003). Similarly, MBP mRNA levels, a major constituent of

the myelin sheath of oligodendrocytes and Schwann cells, were decreased in the mPFC of Shn-2 KO mice (Table 2). Inflammatory cytokines and autoimmune components are suggested to damage oligodendrocytes (Calzà et al., 1998). Thus, CNPase and MBP downregulation suggests a possible inflammation-related abnormality in Shn-2 KO oligodendrocytes, consistent with the so-called ‘oligodendrocyte hypothesis’ of schizophrenia.

Adult but not juvenile Shn-2 KO mice display an abnormally thin cortex, which is also observed in schizophrenia patients (Pierri et al., 1999). Cortical thickness is reduced by aging (Salat et al., 2004), which in turn is associated with inflammation. Gene expression patterns in the cortex of Shn-2 KO mice significantly overlapped ($P = 1.1 \times 10^{-17}$) with a previous data set comparing whole-brain gene expression patterns in young (8-week-old) and aged (2-year-old) mice. These data suggest that similar mechanisms may underlie the reduction of cortical thickness in aging and Shn-2 KO mice.

In addition to anatomical abnormalities, the Shn-2 KO mouse cortex displays physiological alterations. Upon cortical EEG analysis, mutant mice displayed increases

in slow waves and decreases in fast waves, both of which are observed in schizophrenia patients (Gallinat et al., 2004; Moran & Hong, 2011; Sponheim et al., 1994). Computational model study suggested that downregulation of parvalbumin neurons reduced gamma oscillation (Volman et al., 2011), agreeing with my observations of Shn-2 KO mice. Immaturity of DG in Shn-2 KO mice may underlie their abnormal theta rhythm in their cortex, considering the close functional relationship between hippocampus and mPFC as demonstrated by their coordinated activity (Jones & Wilson, 2005).

Induction of Arc transcription after receiving foot shocks in a novel environment was generally reduced in almost all regions of the Shn-2 KO brain. Despite this near-ubiquitous reduction of Arc, I observed comparable Arc expression in the CA1 and CA3 regions of the hippocampus in Shn-2 KO and wild-type mice. The relatively higher Arc expression in these regions suggests that CA areas in Shn-2 KO may be comparatively more active than other brain regions. This idea is consistent with increased glutamate level in the hippocampus of Shn-2 KO mice (Figure 20). In stark contrast to control mice, virtually no Arc induction was observed in the Shn-2 KO

mouse DG, which displays significant immaturity. The gene expression pattern associated with iDG-like phenomena has been observed in fluoxetine-treated (Kobayashi et al., 2010) and α-CaMKII$^{+/-}$ mice, whose DG also shows dramatically reduced expressions of immediately early genes, such as c-Fos and/or Arc (Kobayashi et al., 2010; Matsuo et al., 2009; Yamasaki et al., 2008). Although such an extreme phenotype may not be common in schizophrenic patients, this finding is particularly interesting for several reasons. Reduced expression of Arc mRNA in the PFC (Guillozet-Bongaarts et al., 2014; Maycox et al., 2009) of postmortem schizophrenia brains has been reported. A recent *de novo* copy-number variation (CNV) analysis suggests that Arc protein complexes play a role in the pathogenesis of schizophrenia (Kirov et al., 2012). Specifically, *de novo* CNVs found in schizophrenic patients are significantly enriched in the postsynaptic density (PSD) proteome; these include Arc protein complexes. It was recently shown that, upon synaptic activation, Arc is translocated to neighboring inactive synapses. This may potentially increase the signal-to-noise ratio at plastic synapses (Okuno et al., 2012). Loss or dysfunction of the Arc complex may impair the synaptic input into neurons and subsequently cause cognitive

deficits in both schizophrenic patients and animal models of the disease. Interestingly, DG granule cells of mice treated with chronic fluoxetine produced repeated spikes but generated little immediate-early gene expression (Kobayashi et al., 2010). Thus, altered signal transmission likely reduces Arc induction.

An increasing number of schizophrenia mouse models show impairment in hippocampus-dependent tasks. Mouse mutants of disrupted-in-schizophrenia 1 (DISC1) (Li et al., 2007) and dysbindin-1 (Takao et al., 2008), which are widely accepted models of schizophrenia, show deficits in spatial working memory, which is a DG-dependent function. DISC1 is highly expressed in the DG during adulthood (Meyer & Morris, 2008), and mice lacking a C-terminal portion of DISC1 show morphological abnormalities in the DG and spatial working memory deficits (Li et al., 2007). Dysbindin-1 is expressed at high levels in the DG and MF. In schizophrenia patients, the reduction of dysbindin-1 is relatively restricted to the DG and MF terminal field (Talbot et al., 2004). Sdy mutant mice lacking the dysbindin-1 gene show working memory impairment (Takao et al., 2008) and reduced frequency facilitation in hippocampal MF-CA3 synapse (Kobayashi et al., 2011). α-CaMKII$^{+/-}$ mice display

severe working memory deficits and have well-defined features of iDG (Matsuo et al., 2009; Yamasaki et al., 2008). It is reported that calretinin, an immature-neuronal marker, is significantly upregulated in the DG of postmortem brains in human schizophrenia/bipolar patients (Walton et al., 2012). Thus, the iDG phenotype may represent an additional 'endophenotype' that is shared by human schizophrenic patients and some schizophrenia mouse models. Since iDG neurons can produce spikes with lower current injection compared with mature neurons, the hippocampus harboring iDG may have a lower activation threshold. In the Shn-2 KO mouse brain, hippocampal hyperactivation was suggested by the fact that Arc induction in CA1 and CA3 was comparable to wild-type levels, while other regions exhibited an overall reduction. These observations suggest that the Shn-2 KO mouse hippocampus may be activated to a higher degree than that of controls. There was a marked reduction in strong frequency facilitation at the MF-CA3 synapse, a form of short-term plasticity, in Shn-2 KO mice. In agreement with this, the number of synapses per MF terminal was lower in postmortem schizophrenia brain tissue than in healthy control tissue (Tamminga et al., 2010). Reduced frequency facilitation was also reported in DISC1 mutant mice (Kvajo

et al., 2011). These studies and results of my study collectively suggest that schizophrenia patients and some animal models of the disease may have hippocampal abnormalities, including iDG phenotype.

Pre-weaned animals showed no significant differences in calbindin, calretinin, p22 phox, or GFAP expression between genotypes. Calbindin expression was decreased, and calretinin was increased in the DG of 1-month-old Shn-2 KO mice compared to that of wild-type mice, indicating an iDG phenotype. These observations suggest that neither astrocyte activation, increase of reactive oxygen species production, nor 'iDG' phenotype are present in the brain of Shn-2 KO mice before weaning, and that these phenotypes emerged during postnatal development, which is consistent with the fact that most cases of schizophrenia appear in late adolescence or early adulthood.

After publishing the report of Shn-2 KO mice as schizophrenia model (Takao et al., 2013), several studies were conducted examining Shn-2 gene expression in human postmortem brains. Volk et al., reported that Shn-2 mRNA level are lower in schizophrenia patients compared to healthy controls (Volk et al., 2015). Weickert and her colleagues examined more detail in postmortem brains and found that mRNA of

Shn-2 were reduced in schizophrenia with high inflammation (Murphy, Lawther, et al., 2020). They further investigated in which cell types decreased gene expression occurred in schizophrenia, and revealed that Shn-2 was downregulated by pyramidal neurons in layers 2–6 of the dorsolateral PFC in inflammation-associated schizophrenia (Murphy, Kondo, et al., 2020). These studies support the involvement of Shn-2 in the pathogenesis of schizophrenia with inflammation.

Although Shn-2 gene mutations in schizophrenia have not been reported, mutations have been reported in related disorders. In bipolar disorder, a *de novo* missense mutation in HIVEP2 (Shn-2) was also reported (Kataoka et al., 2016; Nishioka et al., 2023). Bipolar disorder and schizophrenia are considered to constitute a spectrum (Keshavan, Morris, et al., 2011) and are therefore difficult to clearly separate in terms of biological phenomena.

Shn-2 is also essential for normal brain function and neurodevelopment in humans. A number of human genetic studies have focused on Shn-2 were also conducted after the publication of the schizophrenia-like phenotype in Shn-2 KO mice. Whole exome sequencing studies showed that some mentally retarded individuals had

distinct *de novo* mutations in SHN-2 (HIVEP2) (Goldsmith et al., 2019; Jain & Atwal, 2019; Park et al., 2019; Srivastava et al., 2016; Steinfeld et al., 2016). Deficiency of Shn-2 in mice caused a schizophrenia-like phenotype, but the loss-of-function mutation in humans caused neurodevelopmental disorders but not schizophrenia.

Shn-2 deficiency leads to neurological dysfunction both in mice and humans, however, there are differences in the phenomena that occur respectively. In this study, mice were reared in SPF, which eliminates infectious effects as much as possible. In the case of humans, people live in the presence of many microorganisms throughout the embryonic and developmental stages, therefore, infectious effects cannot be eliminated. These differences in the microbiological environment may have caused differences in inflammation in the brain during embryonic and developmental stages, resulting in differences in the symptoms and phenomena that are manifested.

SHN-2 has family genes such as SHN-1 (HIVEP1) and SHN-3 (HIVEP3), those contain a ZAS domain and bind to kappa Kappa-B motif. Notably, *de novo* mutations were detected in the schizophrenic PFC in the gene encoding Shn-1 (also called Hivep1), another member of the Schnurri family, which was suggested to be

involved in pathways important for brain development (Gulsuner et al., 2013). Another SHNs family gene, HIVEP3 were also reported to have Protein-coding missense *de novo* mutations associated to schizophrenia (Howrigan et al., 2020). These reports support that SHN-2 deficiency contributes pathogenesis of schizophrenia,

As discussed above, Shn-2 KO mice exhibited a genetic inflammatory condition that may be responsible for various schizophrenia-like abnormalities. There was an argument that mice are not a good model for humans in inflammatory diseases (Seok et al., 2013). They showed that genomic responses to different acute inflammatory stressors are highly similar in humans but very poorly reproduced in the corresponding mouse models (Seok et al., 2013). I reevaluated the same gene expression datasets used in the previous study (Seok et al., 2013) by focusing on genes whose expression levels were significantly changed in both humans and mice. Contrary to the previous findings, the gene expression levels in the mouse models showed extraordinarily significant correlations with those of the human conditions (Figure 21). I reanalyzed the dataset with nonparametric ranking analysis by NextBio. The hypothesis that mouse models show only coincidental overlap of the directionality of gene changes

with those in human burn conditions was rejected with extraordinarily high confidence (Figure 22; overlap P value = 3.9×10^{-34}, 6.3×10^{-13}, 1.2×10^{-35}, 6.5×10^{-11}, and 3.4×10^{-35} for mouse models of burn, trauma, sepsis (GSE19668), sepsis (GSE26472), and infection, respectively). These results show that the directionality of the changes in mouse models was highly similar to that in human burn conditions. These findings demonstrate that gene expression patterns in mouse models closely recapitulate those in human inflammatory conditions and strongly argue for the utility of mice as animal models of human disorders.

The original paper by Seok et al. that denied the usefulness of the mouse model was cited 2997 times, while our paper (Takao & Miyakawa, 2015) that showed the usefulness of the mouse model was cited 562 times (google scholar, accessed Jan 26, 2024). I would like to discuss what might account for this difference in the number of citations. The argument that mouse models are useless for the study of human disease was fresh and received with surprise by the research community. It was especially welcomed by those involved in animal welfare, the development of biochips, and those involved in these areas. However, many animal experiments using mice have been

conducted before and since then, and continue to produce useful results. The first paper by Seok et al. was published online in 2013, whereas a search on PubMed for papers from 2014 onward using the terms “mouse” + “inflammation” yields 116,963 hits (PubMed, accessed Jan 26, 2024). The number of published papers continues to grow each year, which clearly demonstrates the usefulness of model mice for research in this field.

Shn-2 KO mice are also a model of inflammatory disease, and their inflammatory gene expression signatures shared well with those of the schizophrenia patients. In addition, various behavioral abnormalities and brain characteristics were similar to those of the patient, which suggests that Shn-2 KO mice are an excellent model for schizophrenia.

Together, results of my study demonstrate that Shn-2 deficiency caused atypical inflammation and associated hippocampal and cortical abnormalities, imbalance of GABA-glutamate, and abnormal myelination. These alterations, as a whole, may bring about behavioral abnormalities related to schizophrenia in Shn-2-

deficient mice. Thus, the Shn-2 KO mouse displays good face and concept validity, and may be useful in elucidating the pathogenesis and pathophysiology of schizophrenia.

5. FIGURES

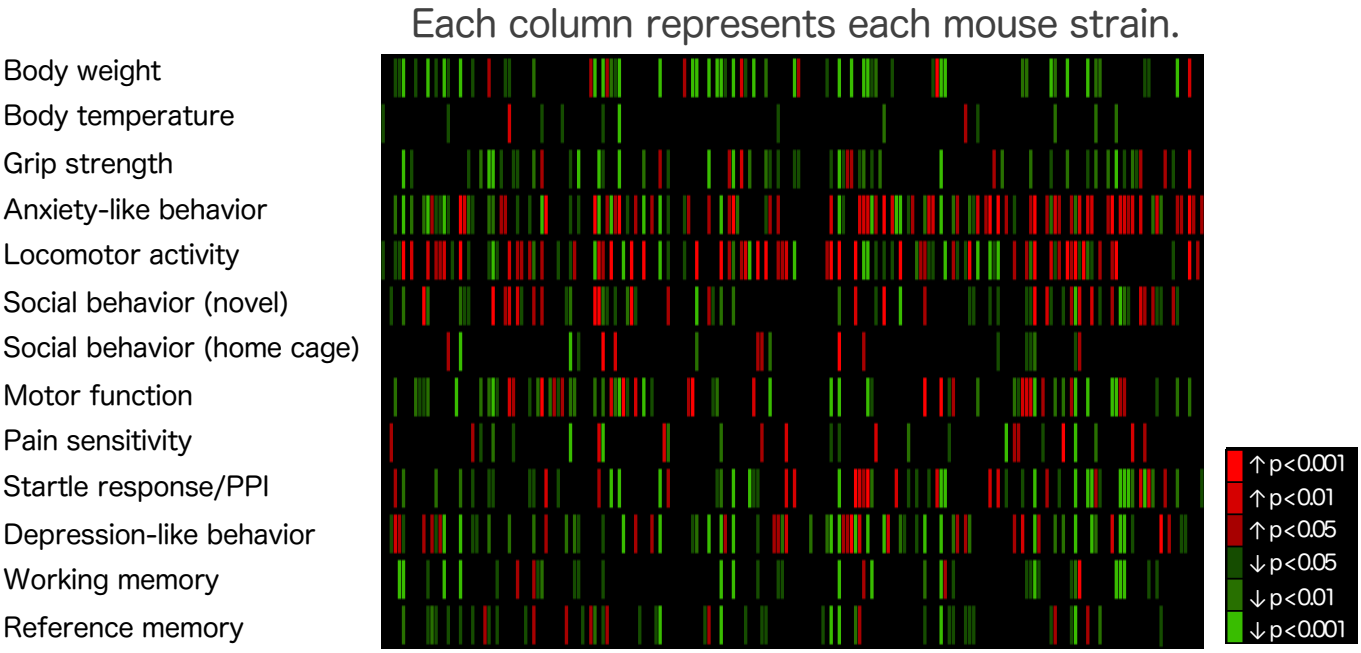

Figure 1.
(a) Comprehensive behavioral test battery for mice. (b) "Animal-model-array" of psychiatric disorders. Each column represents the strain of genetically-engineered mice that has been analyzed in the laboratory of the authors' group (202 strains including unpublished data). Each row represents a category of behavior assessed by comprehensive behavior test battery. Note that most of the genetically-engineered mice bearing a mutation of a gene expressed in the brain showed at least some behavioral phenotype(s), when assessed with the comprehensive behavioral test battery. Colors represent an increase (red) or decrease (green) in a comparison between the wild-type and mutant strains.

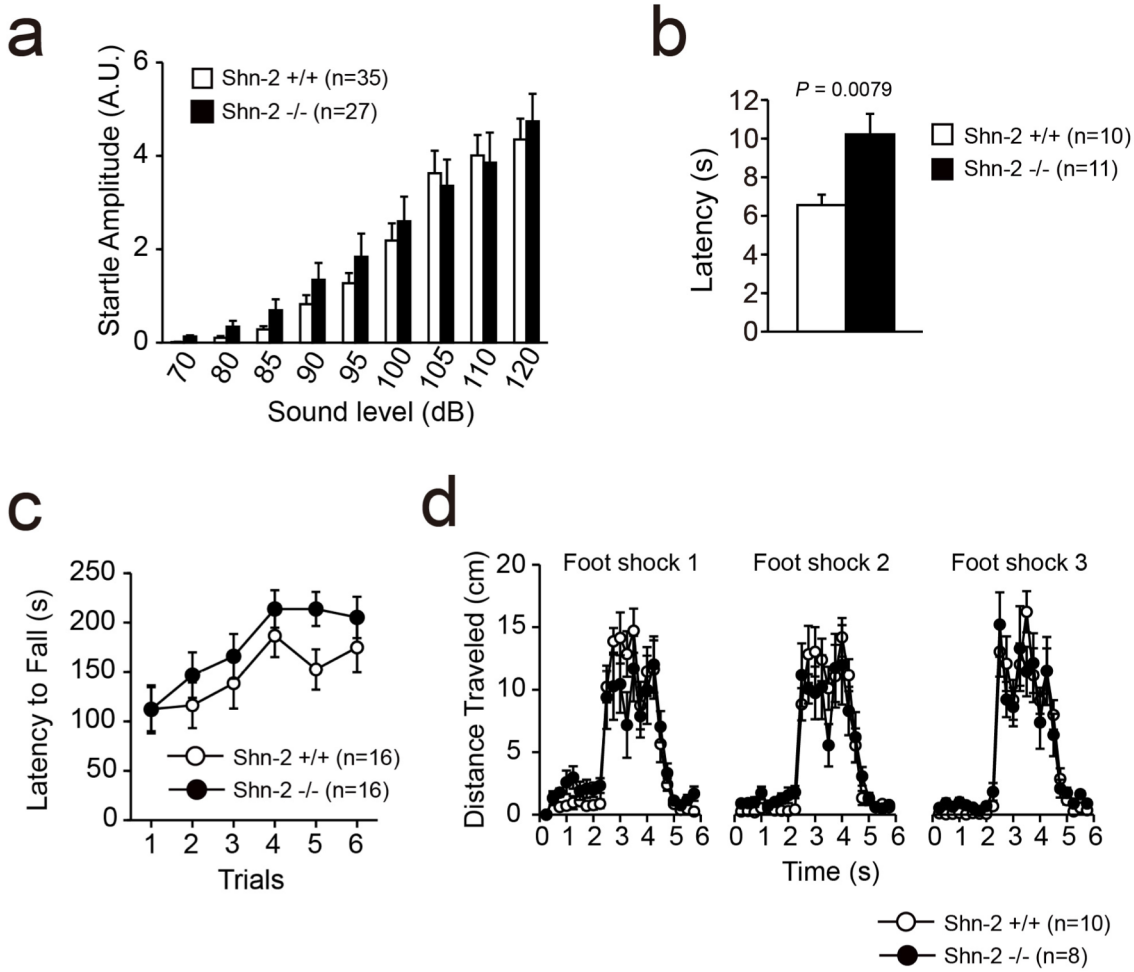

Figure 2.
Sensory/motor functions in Shn-2 KO mice. (a) Shn-2 KO mice showed an acoustic startle response comparable to that observed in wild-type control mice (genotype effect: P = 0.5359). (b) Shn-2 KO mice showed decreased pain sensitivity. (c) The performance of Shn-2 KO mice in the rotarod test was comparable to that of the wild-type controls (genotype effect: P = 0.2612). (d) No significant difference was observed in terms of the distance traveled during the foot shock test.

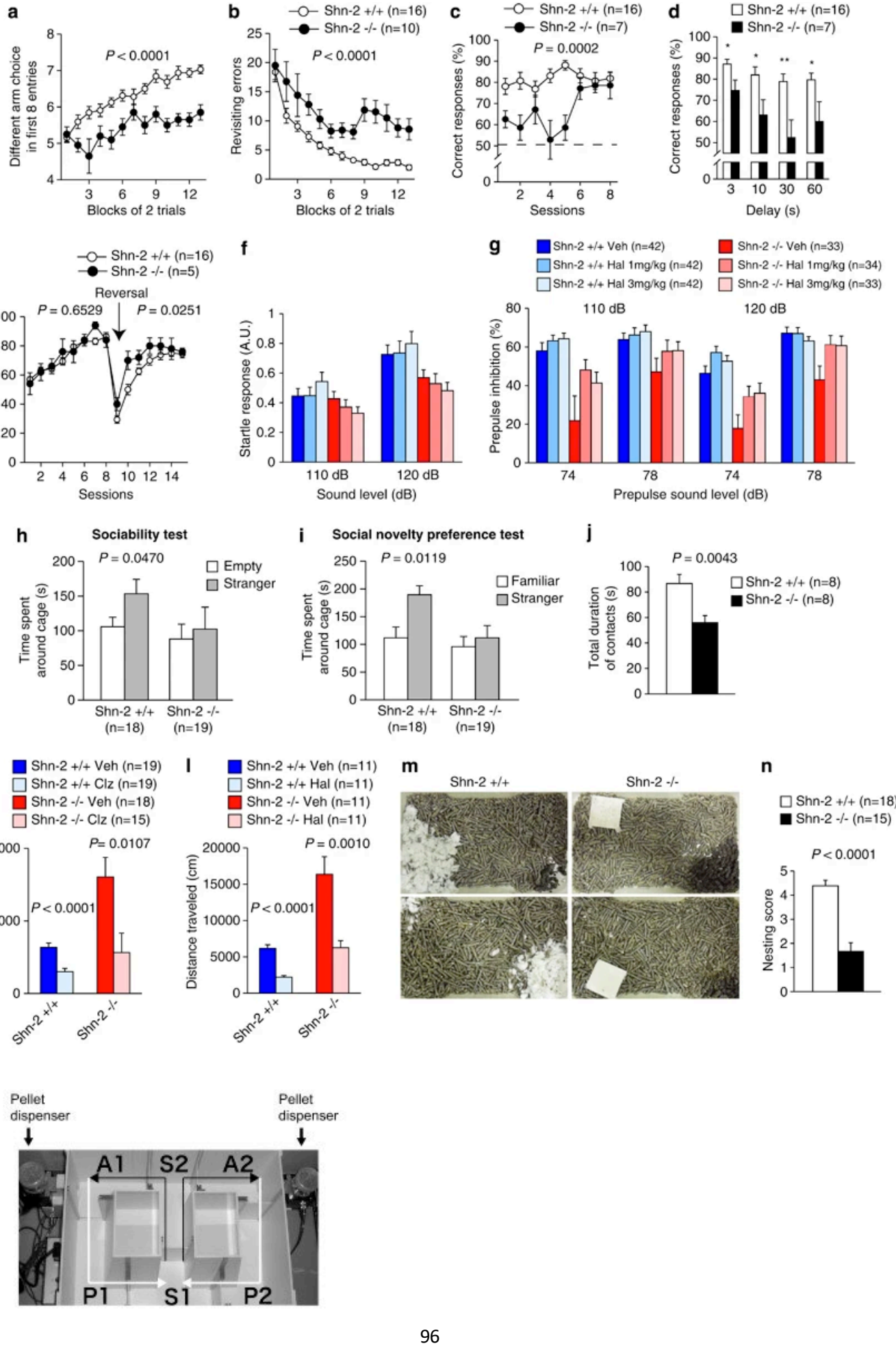
a
Different arm choice in first 8 entries
P < 0.0001
Blocks of 2 trials
b
Shn-2 +/+ (n=16)
Shn-2 -/- (n=10)
Revisiting errors
P < 0.0001
Blocks of 2 trials
c
Shn-2 +/+ (n=16)
Shn-2 -/- (n=7)
Correct responses (%)
P = 0.0002
Sessions
d
Shn-2 +/+ (n=16)
Shn-2 -/- (n=7)
Correct responses (%)
Delay (s)
e
Shn-2 +/+ (n=16)
Shn-2 -/- (n=5)
Reversal
P = 0.6529
P = 0.0251
Correct responses (%)
Sessions
f
Startle response (A.U.)
110 dB
120 dB
Sound level (dB)
g
Shn-2 +/+ Veh (n=42)
Shn-2 +/+ Hal 1mg/kg (n=42)
Shn-2 +/+ Hal 3mg/kg (n=42)
Shn-2 -/- Veh (n=33)
Shn-2 -/- Hal 1mg/kg (n=34)
Shn-2 -/- Hal 3mg/kg (n=33)
110 dB
120 dB
Prepulse inhibition (%)
Prepulse sound level (dB)
h
Sociability test
P = 0.0470
Empty
Stranger
Time spent around cage (s)
Shn-2 +/+ (n=18)
Shn-2 -/- (n=19)
i
Social novelty preference test
P = 0.0119
Familiar
Stranger
Time spent around cage (s)
Shn-2 +/+ (n=18)
Shn-2 -/- (n=19)
j
P = 0.0043
Shn-2 +/+ (n=8)
Shn-2 -/- (n=8)
Total duration of contacts (s)
k
Shn-2 +/+ Veh (n=19)
Shn-2 +/+ Clz (n=19)
Shn-2 -/- Veh (n=18)
Shn-2 -/- Clz (n=15)
P= 0.0107
P < 0.0001
Distance traveled (cm)
Shn-2 +/+
Shn-2 -/-
l
Shn-2 +/+ Veh (n=11)
Shn-2 +/+ Hal (n=11)
Shn-2 -/- Veh (n=11)
Shn-2 -/- Hal (n=11)
P = 0.0010
P < 0.0001
Distance traveled (cm)
Shn-2 +/+
Shn-2 -/-
m
Shn-2 +/+
Shn-2 -/-
n
Shn-2 +/+ (n=18)
Shn-2 -/- (n=15)
P < 0.0001
Nesting score
o
Pellet dispenser
Pellet dispenser
A1
S2
A2
P1
S1
P2

Figure 3.
Schizophrenia-related behavioral abnormalities in Shn-2 KO mice. (a, b) In the spatial working memory version of the eight-arm radial maze, Shn-2 KO mice performed significantly worse with respect to the number of different arm choices in the first eight entries (genotype effect: $F_{1,24}$=62.104, P<0.0001) and made significantly more revisiting errors than controls (genotype effect: $F_{1,24}$=45.597, P<0.0001; genotype × trial block interaction: $F_{12,228}$=1.470, P=0.1345). (c) Mutant mice also showed poor working memory performance in the T-maze forced-alternation task (genotype effect: $F_{1,21}$=20.497, P=0.0002; genotype × session interaction: $F_{7,147}$=3.273, P=0.0029). (d) With increased delay, Shn-2 KO mice exhibited a lower correct percentage than controls (delay=3, 10, 30, and 60 s; P=0.0010, P=0.0047, P=0.0083, and P=0.0026, respectively). (e) Shn-2 KO and wild-type mice were comparable in the left–right discrimination task (genotype effect: $F_{1,19}$=0.209, P=0.6529) and reversal learning (genotype effect: $F_{1,19}$=5.917, P=0.0251). (f) The amplitude of the acoustic startle response was not significantly different between genotypes (Shn-$2^{+/+}$, +Veh *vs* Shn-$2^{-/-}$, Veh, $F_{1,73}$=1.371, P=0.2454). (g) PPI of the acoustic startle response was impaired in Shn-2 KO mice (Shn-$2^{+/+}$, Veh *vs* Shn-$2^{-/-}$, Veh, 110 dB startle, P=0.0027; 120 dB startle, P=0.0003). Administration of haloperidol improved the PPI of Shn-$2^{-/-}$ mice (Shn-$2^{-/-}$, Veh *vs* Shn-$2^{-/-}$,1 mg/kg Hal, 110 dB, P=0.0145; 120 dB, P=0.0059; Shn-$2^{-/-}$, Veh *vs* Shn-$2^{-/-}$, 3 mg/kg Hal, 120 dB, P=0.0044). *Post hoc* Bonferroni's test after two-way repeated-measures ANOVA (level of significance was set at P<0.0167). (h) Shn-2 KO mice display a lower level of social approach in the sociability test. (i) Shn-2 KO mice did not show social novelty preference. (j) Shn-2 KO mice displayed decreased social interaction in a novel environment (total contact duration: $F_{1,14}$=11.569, P=0.0043). (k) Administration of clozapine (1 mg/kg, i.p.) reversed hyperactivity in mutant mice (genotype effect: P=0.0012, drug effect: P=0.0003, genotype × drug interaction: P=0.0574, Shn-$2^{-/-}$, Clz. *vs* Shn-$2^{+/+}$, Veh., P=0.4221). (l) Administration of haloperidol (0.3 mg/kg, i.p.) also reduced hyperactivity in Shn-2 KO mice (genotype effect: P<0.0001, drug effect: P<0.0001, genotype × drug interaction: P=0.0275, Shn-$2^{-/-}$, Hal. *vs* Shn-$2^{+/+}$, Veh., P=0.8957). (m, n) Nest building was impaired in Shn-2 KO mice (P<0.0001). (o) Apparatus of the T-maze task. Veh, Vehicle; Clz, Clozapine; Hal, Haloperidol.

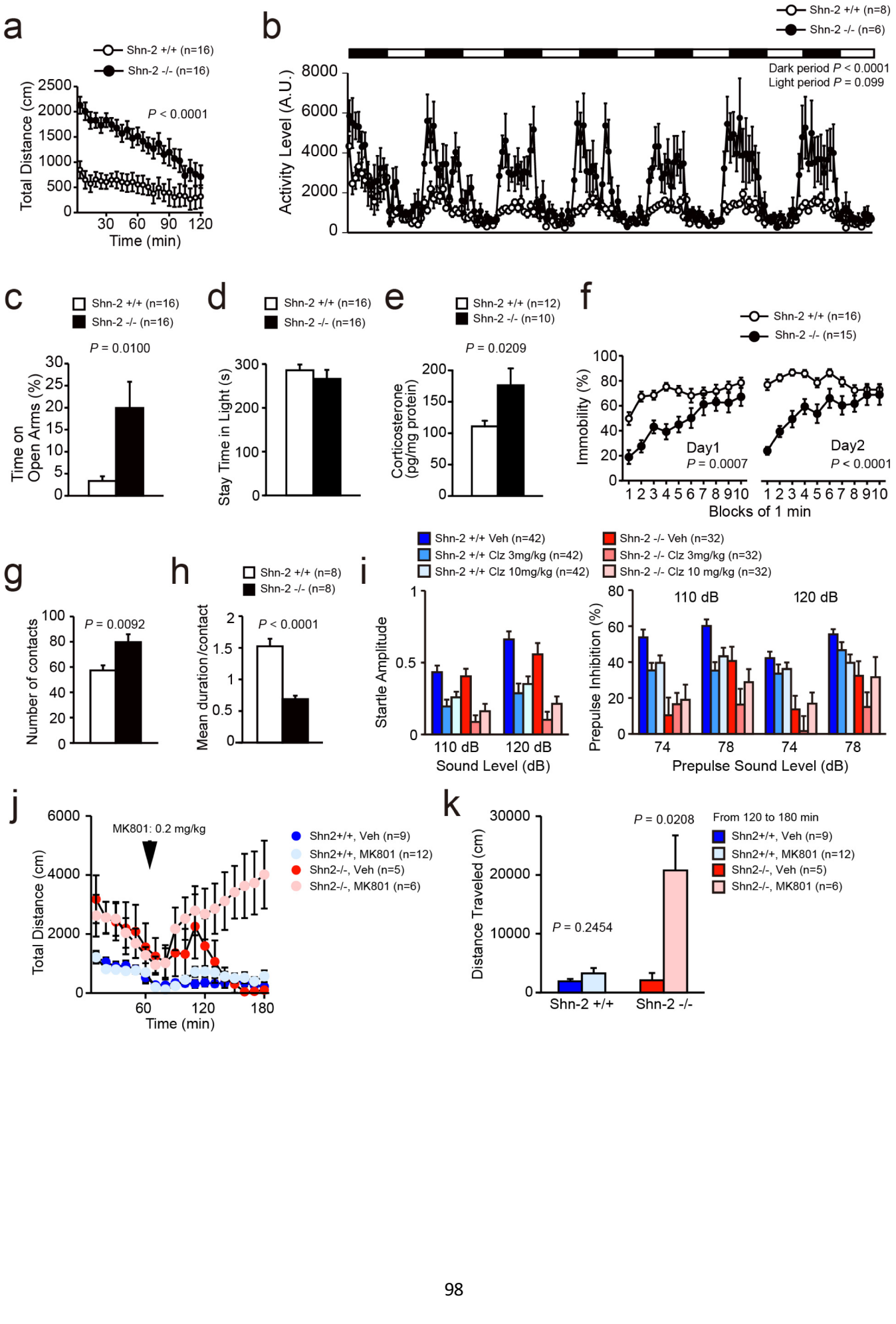
a
Shn-2 +/+ (n=16)
Shn-2 -/- (n=16)
Total Distance (cm)
P < 0.0001
Time (min)
b
Shn-2 +/+ (n=8)
Shn-2 -/- (n=6)
Dark period P < 0.0001
Light period P = 0.099
Activity Level (A.U.)
c
Shn-2 +/+ (n=16)
Shn-2 -/- (n=16)
P = 0.0100
Time on Open Arms (%)
d
Shn-2 +/+ (n=16)
Shn-2 -/- (n=16)
Stay Time in Light (s)
e
Shn-2 +/+ (n=12)
Shn-2 -/- (n=10)
P = 0.0209
Corticosterone (pg/mg protein)
f
Shn-2 +/+ (n=16)
Shn-2 -/- (n=15)
Immobility (%)
Day1
P = 0.0007
Day2
P < 0.0001
Blocks of 1 min
g
P = 0.0092
Number of contacts
h
Shn-2 +/+ (n=8)
Shn-2 -/- (n=8)
P < 0.0001
Mean duration/contact
i
Shn-2 +/+ Veh (n=42)
Shn-2 +/+ Clz 3mg/kg (n=42)
Shn-2 +/+ Clz 10mg/kg (n=42)
Shn-2 -/- Veh (n=32)
Shn-2 -/- Clz 3mg/kg (n=32)
Shn-2 -/- Clz 10 mg/kg (n=32)
Startle Amplitude
110 dB
120 dB
Sound Level (dB)
Prepulse Inhibition (%)
Prepulse Sound Level (dB)
j
MK801: 0.2 mg/kg
Shn2+/+, Veh (n=9)
Shn2+/+, MK801 (n=12)
Shn2-/-, Veh (n=5)
Shn2-/-, MK801 (n=6)
Total Distance (cm)
Time (min)
k
P = 0.0208
From 120 to 180 min
Shn2+/+, Veh (n=9)
Shn2+/+, MK801 (n=12)
Shn2-/-, Veh (n=5)
Shn2-/-, MK801 (n=6)
P = 0.2454
Distance Traveled (cm)
Shn-2 +/+
Shn-2 -/-

Figure 4.
Abnormal behavior in Shn-2 KO mice. (a) Shn-2 KO mice showed hyperactivity in the open field test (genotype effect: $P < 0.0001$). (b) Mutant mice showed hyperlocomotor activity in their home cages in the dark (genotype effect: $P < 0.0001$). (c) In the elevated plus maze test, Shn-2 KO mice displayed increased stay time on open arms, which is usually interpreted as an indication of decreased anxiety-like behavior. (d) No significant differences in anxiety-like behavior were observed between the genotypes in the light/dark transition test. (e) Shn-2 KO mice showed increased plasma corticosterone levels after the elevated plus maze test, which were significantly higher than those in the wild type controls. (f) Shn-2 KO mice were less immobile and more active than the wild type controls in the Porsolt forced swim test (genotype effect: Day1, $P = 0.0007$; Day2, $P < 0.0001$). (g, h) Shn-2 KO mice showed reduced levels of social interaction when placed in a novel environment. (i) Administration of clozapine reduced the startle response (genotype effect: $P = 0.007$; drug effect: $P < 0.0001$; genotype $\times$ drug: $P = 0.7167$). Administration of clozapine improved the PPI in wild type mice (110 dB, Shn-$2^{+/+}$: Veh vs 3 mg/kg Clz, $P = 0.0001$, Veh vs 10 mg/kg Clz, $P = 0.0055$, post hoc Bonferroni's test after two-way repeated measures ANOVA, level of significance was set at $P < 0.0167$), while the treatment did not improve PPI in Shn-2 KO mice. (j, k) Administration of 0.2 mg/kg MK801 activated Shn-2 KO mice (from 120 min to 180 min; genotype effect: $P = 0.0002$; drug effect: $P = 0.0004$; genotype $\times$ drug: $P = 0.0015$, Shn-$2^{-/-}$, Veh vs Shn-$2^{-/-}$, MK801, $P = 0.0208$), but did not activate wild type mice (from 120 min to Shn-$2^{+/+}$, Veh vs Shn-$2^{+/+}$, MK801: $P = 0.2454$). Veh, vehicle; Clz, clozapine; Hal, haloperidol.

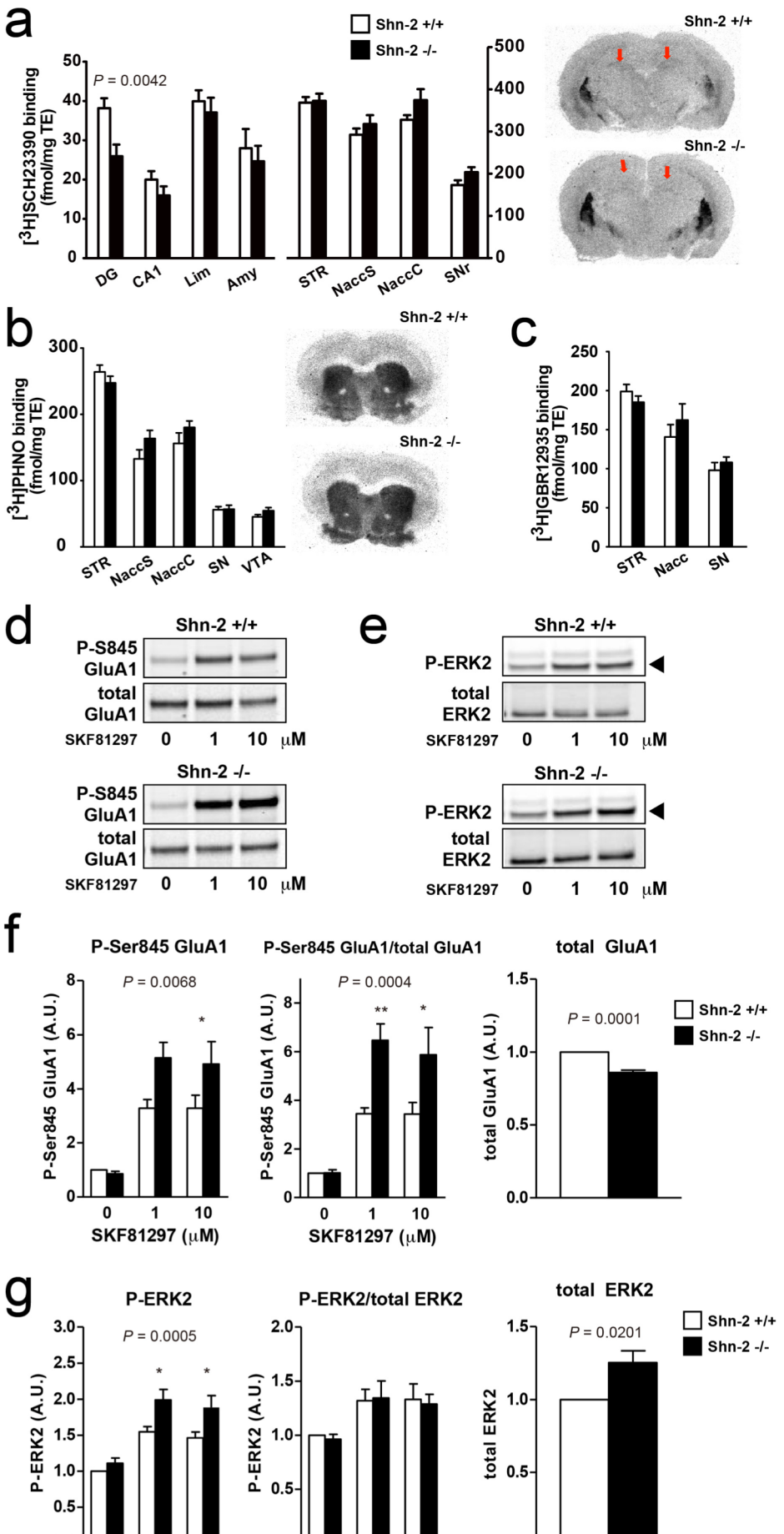
a
Shn-2 +/+
Shn-2 -/-
[3H]SCH23390 binding (fmol/mg TE)
P = 0.0042
DG
CA1
Lim
Amy
STR
NaccS
NaccC
SNr
Shn-2 +/+
Shn-2 -/-
b
[3H]PHNO binding (fmol/mg TE)
STR
NaccS
NaccC
SN
VTA
Shn-2 +/+
Shn-2 -/-
c
[3H]GBR12935 binding (fmol/mg TE)
STR
Nacc
SN
d
Shn-2 +/+
P-S845 GluA1
total GluA1
SKF81297 0 1 10 μM
Shn-2 -/-
P-S845 GluA1
total GluA1
SKF81297 0 1 10 μM
e
Shn-2 +/+
P-ERK2
total ERK2
SKF81297 0 1 10 μM
Shn-2 -/-
P-ERK2
total ERK2
SKF81297 0 1 10 μM
f
P-Ser845 GluA1
P = 0.0068
P-Ser845 GluA1 (A.U.)
SKF81297 (μM)
P-Ser845 GluA1/total GluA1
P = 0.0004
P-Ser845 GluA1 (A.U.)
SKF81297 (μM)
total GluA1
P = 0.0001
total GluA1 (A.U.)
Shn-2 +/+
Shn-2 -/-
g
P-ERK2
P = 0.0005
P-ERK2 (A.U.)
SKF81297 (μM)
P-ERK2/total ERK2
P-ERK2 (A.U.)
SKF81297 (μM)
total ERK2
P = 0.0201
total ERK2
Shn-2 +/+
Shn-2 -/-

Figure 5

Altered dopamine signaling in the dentate gyrus of Shn-2 KO mice. (a) The level of D1 dopamine receptor binding by [^{3}H]SCH23390 was significantly decreased in the dentate gyrus (DG) of Shn-2 KO mice (genotype effect: $P = 0.0042$). (b) There were no significant differences between the genotypes in terms of D2 dopamine receptor binding by [^{3}H]PHNO. (c) The level of dopamine transporter binding by [^{3}H]GBR12935 was not significantly different between the genotypes. (d–g) Acute DG slices were treated with the D1 dopamine receptor agonist, SKF81297 (1 and 10 μM for 10 min), for dopamine D1 receptor-stimulated phosphorylation of GluA1 and ERK2 in DG slices. (d, e) Representative immunoblots showing the amounts of phospho-Ser845 GluA1 (phosphorylated on the PKA-site) and total GluA1 (d), and the amounts of phospho-Thr202/Tyr204 ERK2 (phosphorylated on the MEK-site) and total ERK2 (e). (f) The amount of phosphorylated GluA1 (left, genotype effect: $P = 0.0068$) and the amount of phosphorylated GluA1 normalized to the amount of total GluA1 (center, genotype effect: $P = 0.0004$) were both significantly increased in Shn-2 KO mice. The level of total GluA1 was significantly decreased in mutant mice (right, genotype effect: $P = 0.0001$). (g) The amount of phosphorylated ERK2 was significantly increased in Shn-2 KO mice (left, genotype effect: $P = 0.0005$), whereas the amount of total ERK2 was significantly increased in the mutant mice (right, genotype effect: $P = 0.0201$). There was no significant difference between the genotypes in terms of the amount of phosphorylated ERK2 normalized to the amount of total ERK2. Lim, limbic cortex; Amy, amygdala; STR striatum; NaccS, nucleus accumbens shell; NaccC, nucleus accumbens core; SNr, substantia nigra pars reticulata; SN, substantia nigra; VTR, ventral tegmental area. * $P < 0.05$, ** $P < 0.01$.

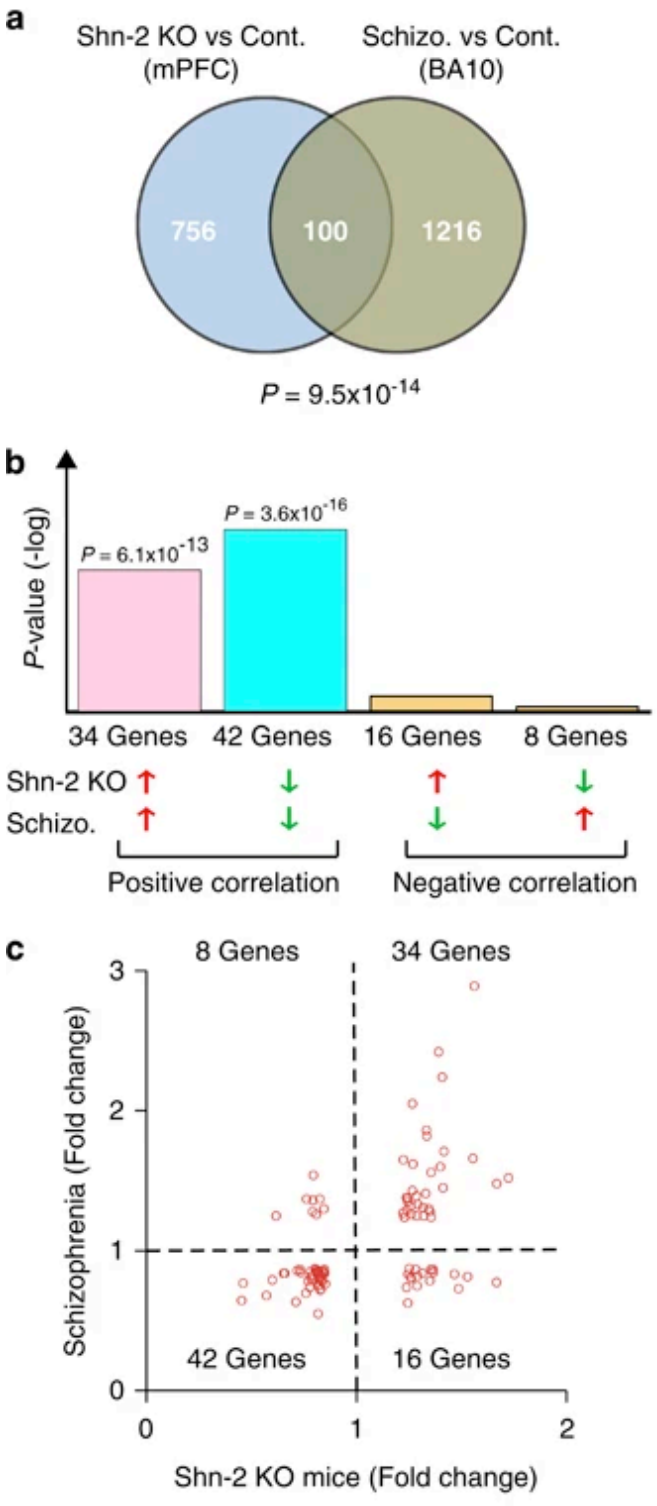

d

Gene symbol	Fold change	
	Shn-2 KO	Schizophrenia
Serpina3n	1.54	2.85
C1qb	1.37	2.38
C1qc	1.39	2.20
C10orf10	1.25	2.01
Rgs4	−1.25	−1.96
Ifitm2	1.31	1.82
C1qa	1.31	1.78
Myt1l	1.22	−1.70
Tac1	−1.44	−1.68
Cebpd	1.40	1.67
Frzb	−2.30	−1.65
Ifitm1	1.53	1.62
Tgfbr1	1.20	1.61
Frzb	−2.30	−1.59
Ddit4	1.25	1.58
Ifitm1	1.53	1.58
Cbln4	−1.81	−1.56
Tgm2	1.38	1.56
Mal2	−1.35	−1.52
Slc14a1	1.34	1.52
Mthfd2	−1.29	1.50
Gfap	1.70	1.48
Rgs4	−1.25	−1.48
D0H4S114	−1.24	−1.47
Fbxo9	−1.23	−1.46
Syn2	1.47	−1.45
Gadd45b	1.65	1.44
Gabra1	−1.32	−1.43
Chml	1.22	−1.43
Cebpb	1.39	1.41
Car10	1.27	−1.41
Rab3b	−1.25	−1.41
Tasp1	−1.24	−1.40
Hk2	1.25	1.39
RP11-35N6.1	−1.20	−1.38
Gng4	−2.26	−1.37
Ms4a6a	1.31	1.37
Klf10	1.65	−1.36
Fcgr3	1.27	1.35
Nrxn3	−1.22	−1.35

Figure 6
Comparison of gene expression profiles between Shn-2 KO mice and individuals with schizophrenia. (a) Venn diagram of genes differentially expressed in the medial prefrontal cortex (mPFC) of Shn-2 KO mice and Brodmann area (BA) 10 of postmortem schizophrenia brain (Schizo.). (b) P-values of overlap between Shn-2 KO mouse and schizophrenia data sets. (c) Scatter plot of gene expression fold change values in Shn-2 KO mice and schizophrenia. (d) Genes differentially expressed in both Shn-2 KO mice and schizophrenia. Red indicates gene upregulation and blue indicates downregulation in both Shn-2 KO mice and schizophrenia. The top 40 genes are included.

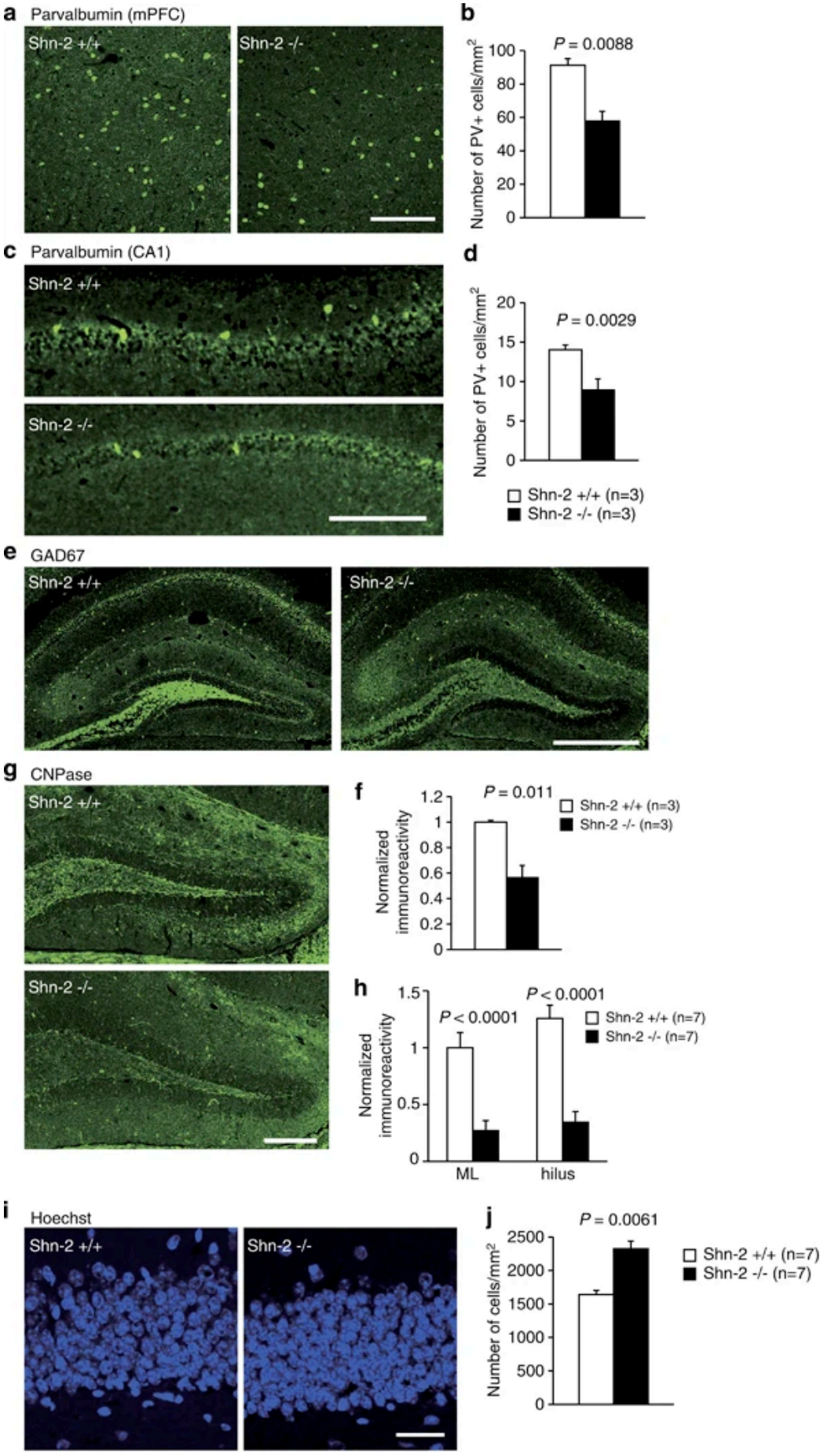
a
Parvalbumin (mPFC)
Shn-2 +/+
Shn-2 -/-
b
P = 0.0088
Number of PV+ cells/mm2
100
80
60
40
20
0
c
Parvalbumin (CA1)
Shn-2 +/+
Shn-2 -/-
d
P = 0.0029
Number of PV+ cells/mm2
20
15
10
5
0
Shn-2 +/+ (n=3)
Shn-2 -/- (n=3)
e
GAD67
Shn-2 +/+
Shn-2 -/-
g
CNPase
Shn-2 +/+
Shn-2 -/-
f
P = 0.011
Normalized immunoreactivity
1.2
1
0.8
0.6
0.4
0.2
0
Shn-2 +/+ (n=3)
Shn-2 -/- (n=3)
h
P < 0.0001
P < 0.0001
Normalized immunoreactivity
1.5
1
0.5
0
ML
hilus
Shn-2 +/+ (n=7)
Shn-2 -/- (n=7)
i
Hoechst
Shn-2 +/+
Shn-2 -/-
j
P = 0.0061
Number of cells/mm2
2500
2000
1500
1000
500
0
Shn-2 +/+ (n=7)
Shn-2 -/- (n=7)

Figure 7
Schizophrenia-related alterations in the Shn-2 KO mouse brain. (a–d) The number of parvalbumin-positive cells is decreased in mPFC (P=0.0088) (a, b) and CA1 (P=0.0029) (c, d) of Shn-2 KO mice. (e, f) The expression of GAD67 in MFs of the hippocampus decreased in mutants (P=0.011). (g, h) Reduced CNPase expression in the DG of Shn-2 KO mice compared with controls (molecular layer, P<0.0001; hilus, P<0.0001). (i, j) DG cell number was evaluated by staining cell nuclei with Hoechst dye. Cell-packing density was higher in Shn-2 KO mice (P=0.0061) (j). GAD67, glutamic acid decarboxylase 67; CNPase, 2′,3-cyclic nucleotide 3′-phosphodiesterase; ML, molecular layer. Scale bars indicate 200 μm (a, c, g), 500 μm (e), 20 μm (i).

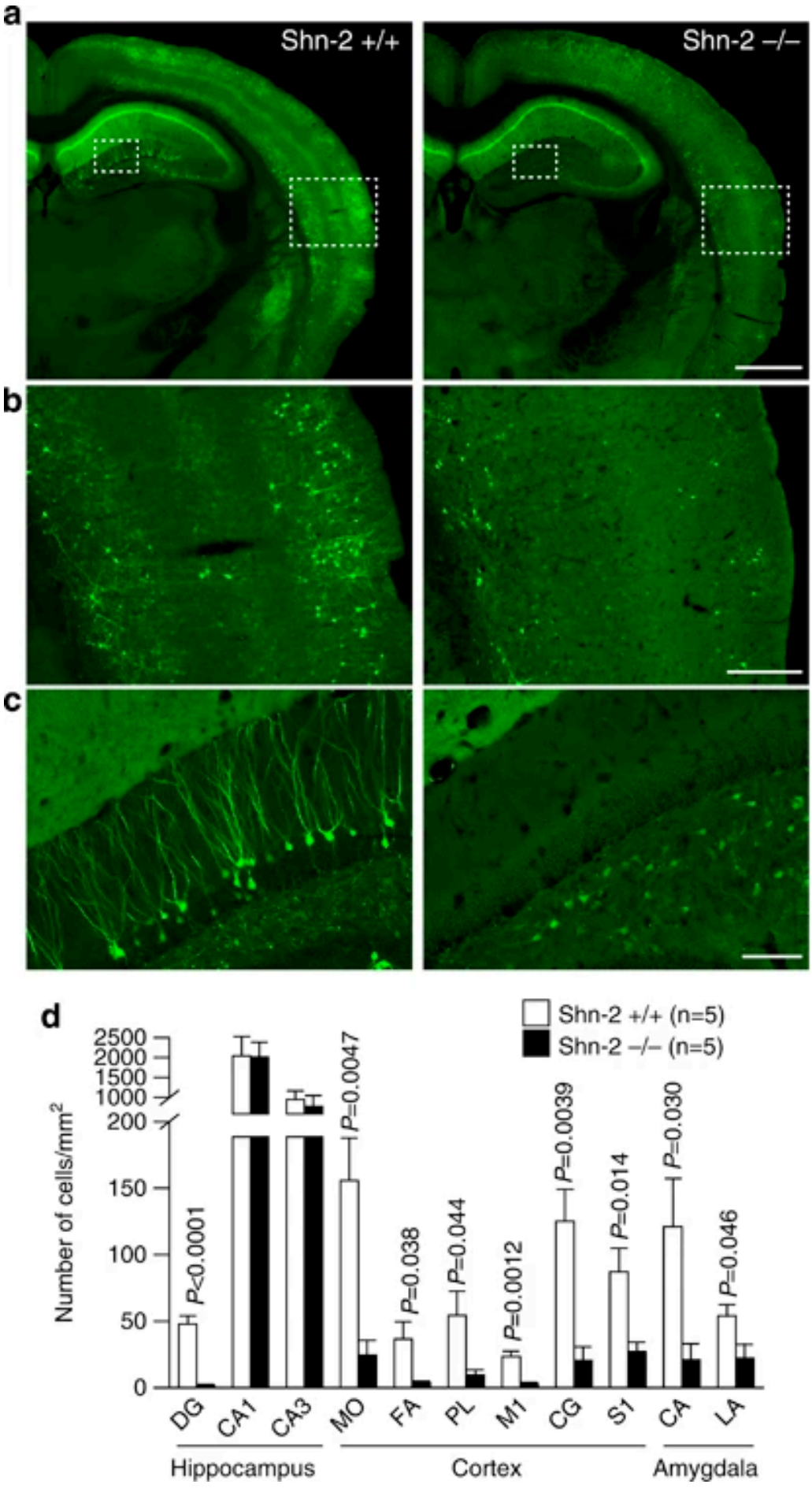
a
Shn-2 +/+
Shn-2 –/–
b
c
d
Shn-2 +/+ (n=5)
Shn-2 –/– (n=5)
Number of cells/mm²
2500
2000
1500
1000
200
150
100
50
0
P<0.0001
P=0.0047
P=0.038
P=0.044
P=0.0012
P=0.0039
P=0.014
P=0.030
P=0.046
DG
CA1
CA3
MO
FA
PL
M1
CG
S1
CA
LA
Hippocampus
Cortex
Amygdala

Figure 8
Reduced Arc induction in Shn-2 KO mice was observed after foot shocks in a novel environment. (a–c) Shn-2 KO mice were mated with transgenic mice expressing dVenus under the Arc promoter. Representative images of both genotypes are shown. (d) In Shn-2 KO mice, Arc-dVenus expression was greatly reduced in the DG and other regions of cortex and amygdala. Arc, activity-regulated cytoskeleton-associated protein. Scale bars indicate 1 mm (a), 250 μm (b), and 100 μm (c). MO, medial orbital cortex; FA, frontal association cortex; PL, prelimbic cortex; M1, primary motor cortex; CG, cingulate cortex; S1, somatosensory cortex; CA, central amygdaloid nucleus; LA, lateral amygdaloid nucleus.

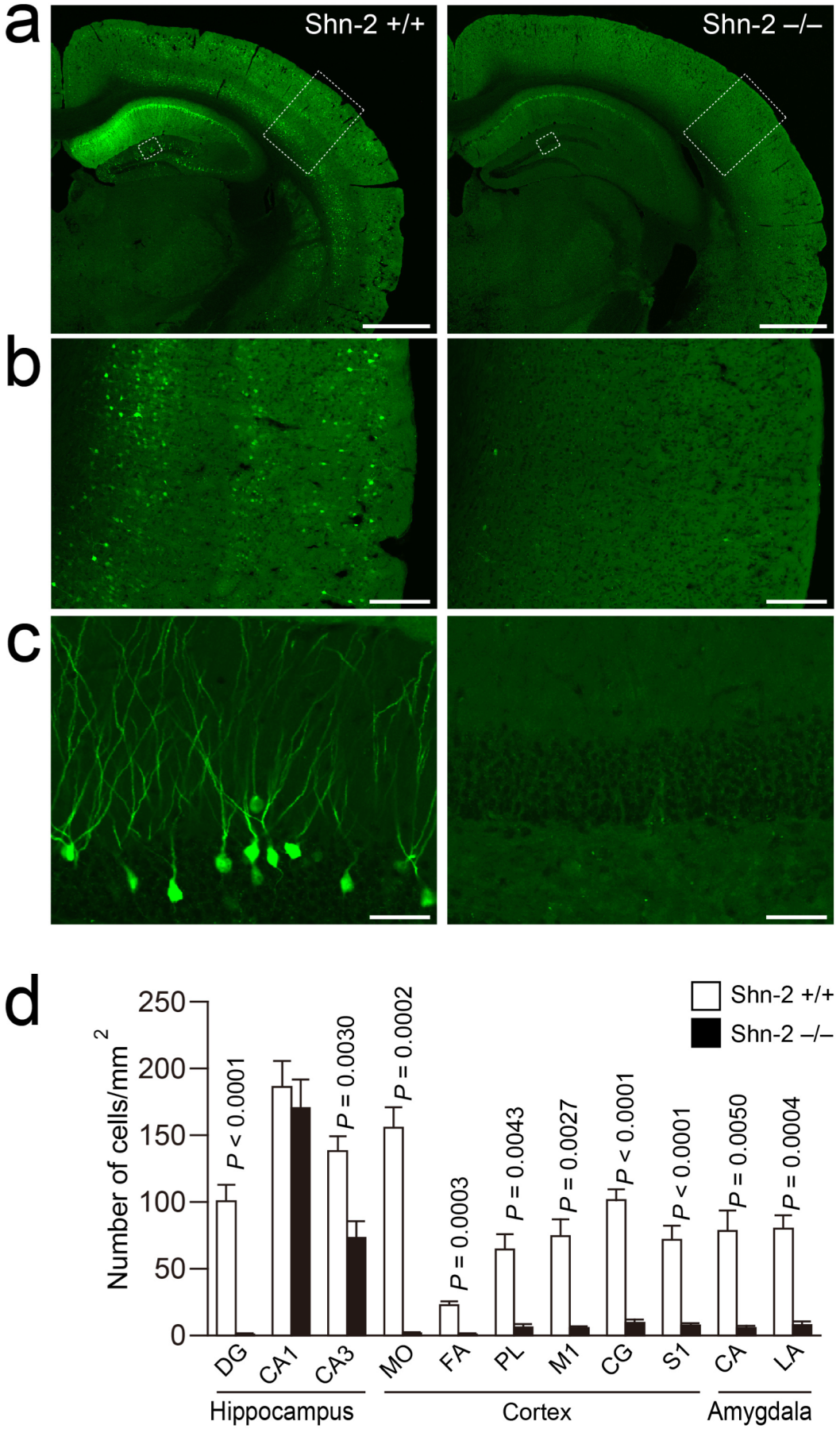
a
Shn-2 +/+
Shn-2 –/–
b
c
d
Shn-2 +/+
Shn-2 –/–
Number of cells/mm 2
250
200
150
100
50
0
P < 0.0001
P = 0.0030
P = 0.0002
P = 0.0003
P = 0.0043
P = 0.0027
P < 0.0001
P < 0.0001
P = 0.0050
P = 0.0004
DG
CA1
CA3
MO
FA
PL
M1
CG
S1
CA
LA
Hippocampus
Cortex
Amygdala

Figure 9
Reduced Arc induction in Shn-2 KO mice exposed to a novel environment. (a–c) Representative images from Shn-2 KO mice and their wild type littermates, both of which were mated with transgenic mice expressing dVenus under the control of the Arc promoter. The mice were fixed with 4% PFA in 0.1 M PBS 5 h after exposure to a novel environment (n= 2, 2). (d) Expression of Arc-dVenus was markedly reduced in the DG, cortical regions, and amygdala of Shn-2 KO mice. P values indicate the genotype effect. Arc, activity-regulated cytoskeleton-associated protein. Scale bars, 1 mm in (a), 200 μm in (c), and 50 μm in (b). DG, dentate gyrus; MO, medial orbital cortex; FA, frontal association cortex; PL, prelimbic cortex; M1, primary motor cortex; CG, cingulate cortex; S1, somatosensory cortex; CA, Central amygdaloid nucleus; LA, lateral amygdaloid nucleus.

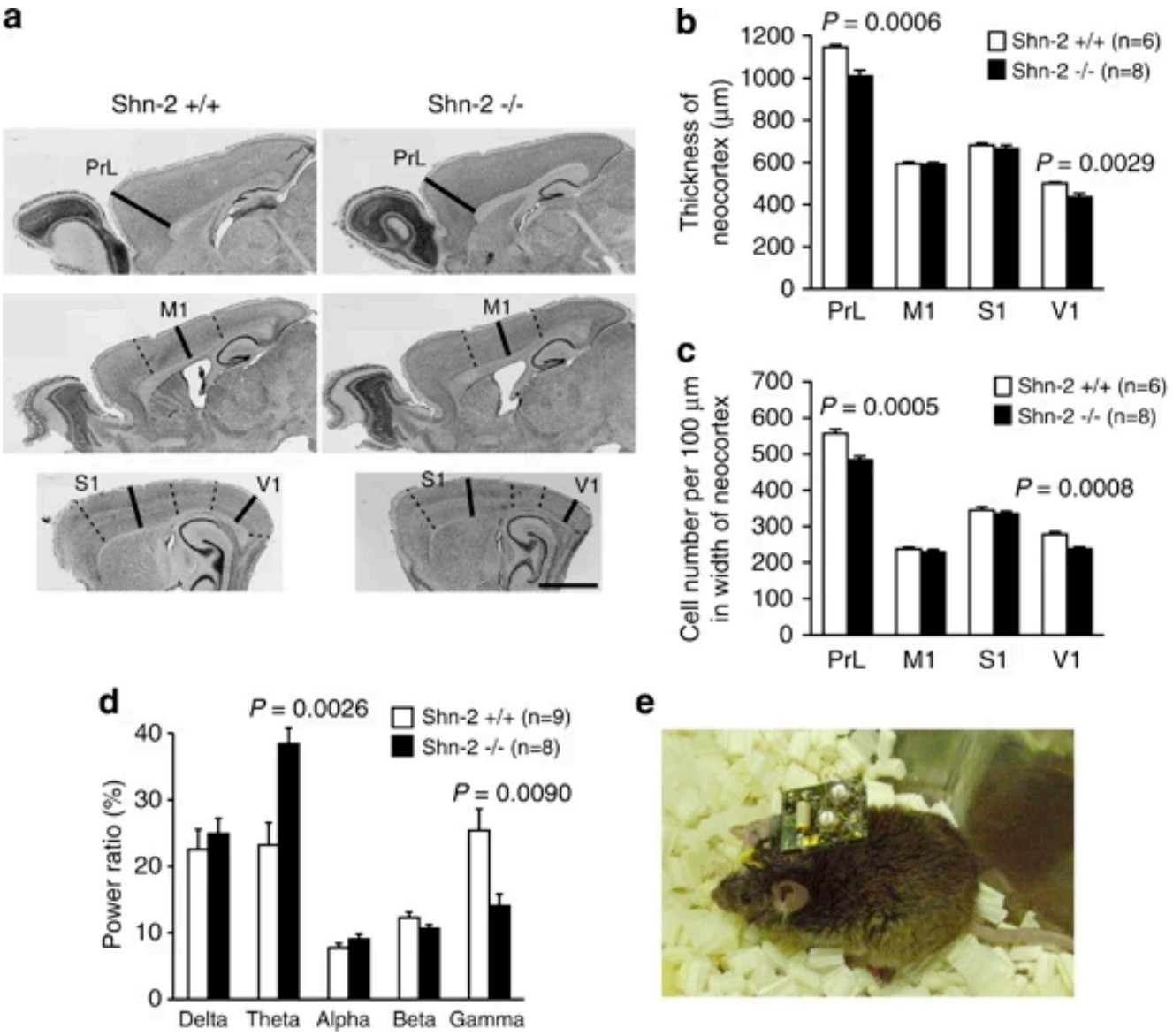

Figure 10

Abnormalities in the cortex of Shn-2 KO mice. (a, b) The cortex of Shn-2 KO mice was thinner than that of wild-type mice. Cortical cell density was also reduced in the prelimbic cortex (PrL) and primary visual cortex (V1) in Shn-2 KO mice (c). (d) Theta band power increased and gamma power decreased in Shn-2 KO mice. (e) A mouse with the Neurologger, a head-mounted EEG data logger device. M1, primary motor cortex; S1, primary somatosensory cortex. Scale bar indicates 1 mm (a).

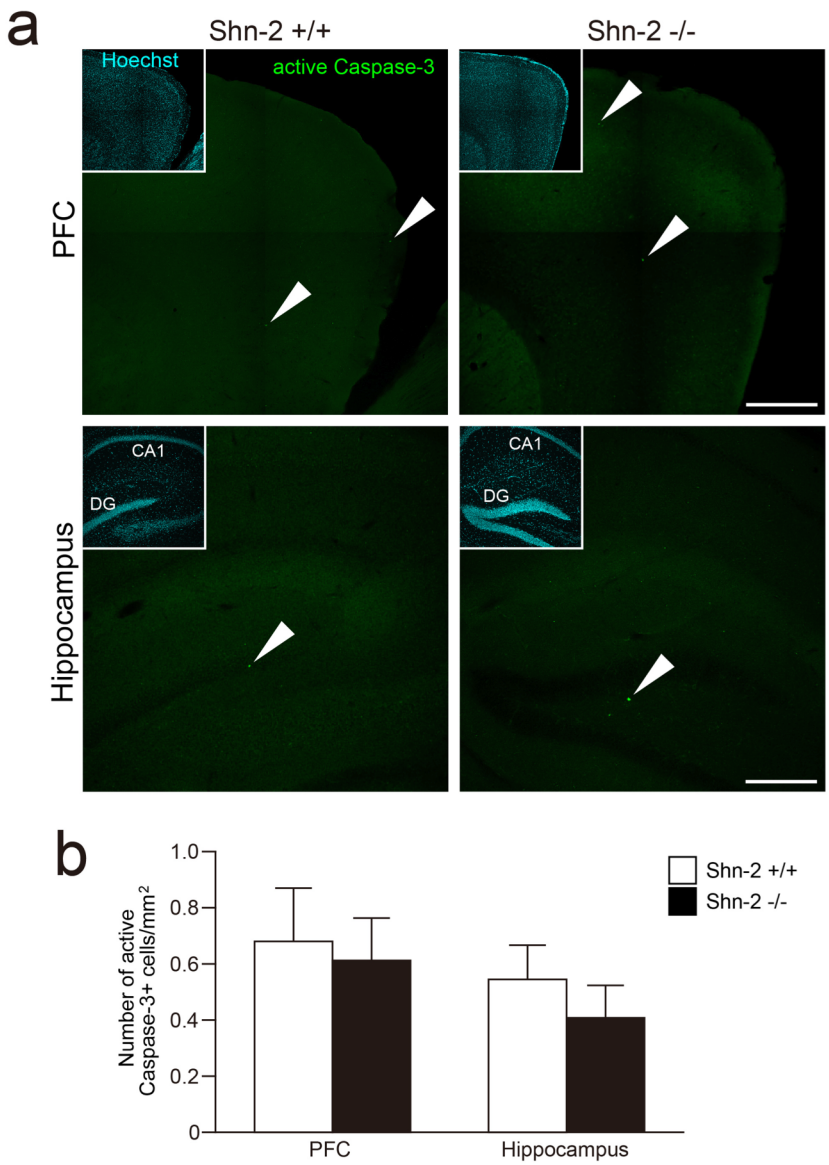

Figure 11
No significant difference was observed between the genotypes in terms of the number of activated Caspase-3-positive cells in the PFC and hippocampus. (a) Representative images of activated caspase-3-positive cells in the PFC and hippocampus. Arrowheads indicate activated caspase-3-positive cells. Scale bars, 500 μm (PFC) and 250 μm (hippocampus). (b) Quantification of the number of activated caspase-3 positive cells. DG, dentate gyrus; PFC, prefrontal cortex.

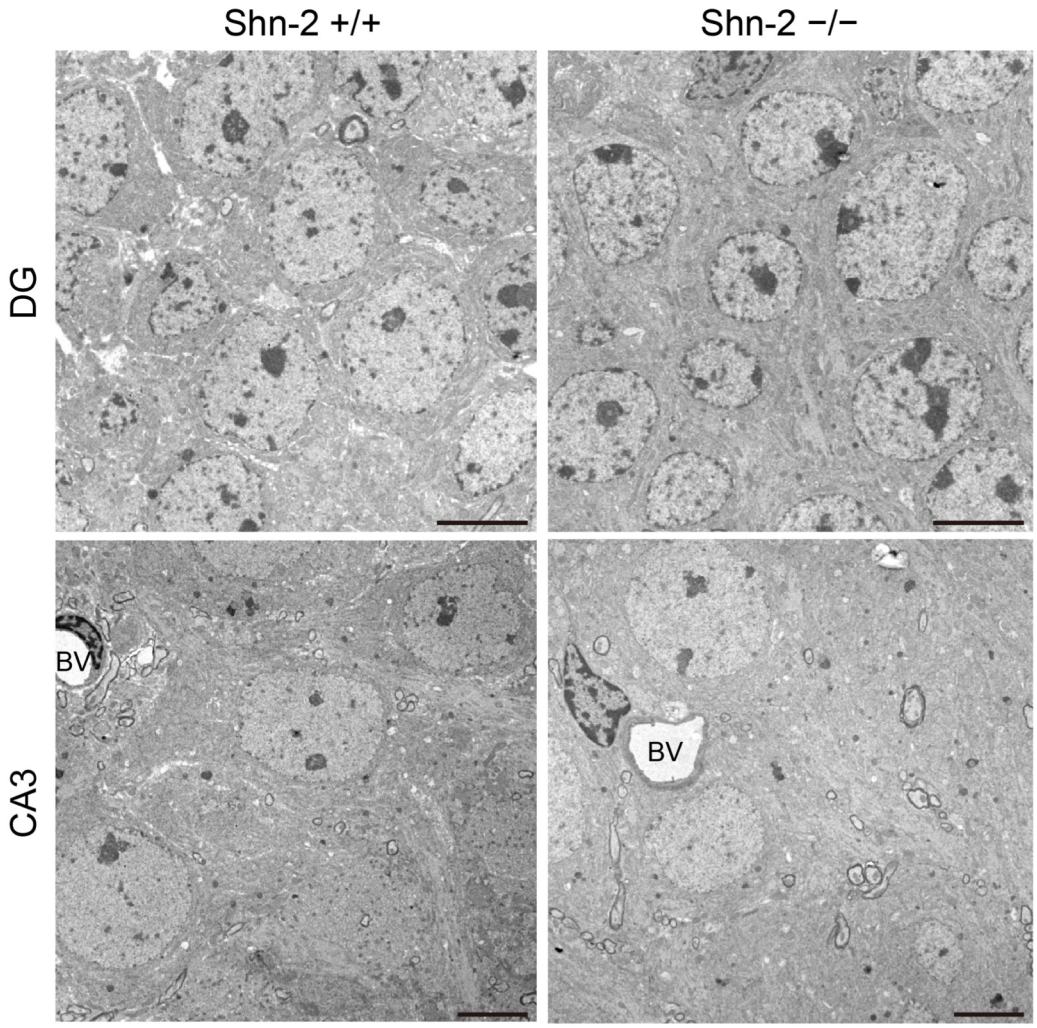

Figure 12
Morphology of the cells within the dentate gyrus (DG) and CA3 regions at the electron microscope level. Representative images of cells in the DG and CA3 regions are shown (upper, DG; lower, CA3). There is no obvious evidence of neurodegeneration, such as cell swelling, protein deposition, or nuclear condensation, in either genotype. BV, blood vessel. Scale bars, 5 μm.

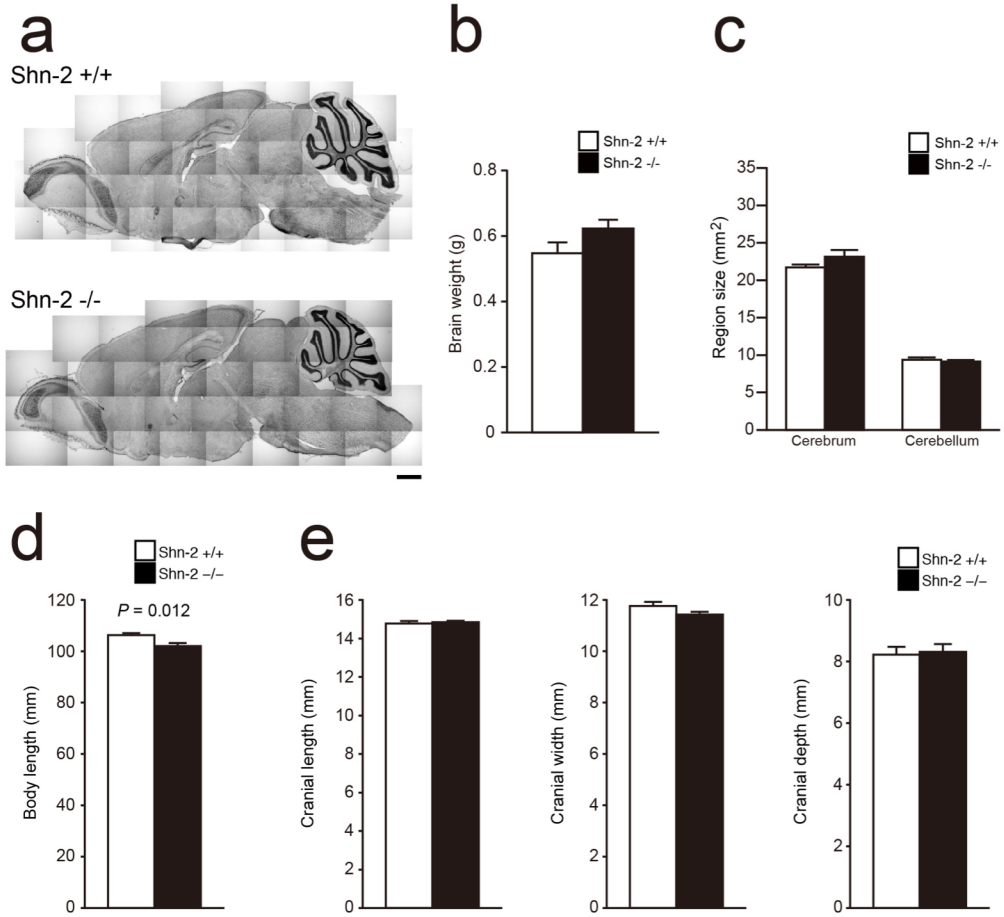

Figure 13
Brain and skull sizes of Shn-2 KO mice. (a) Representative images showing brain sections taken from Shn-2 KO mice (bottom) and wild type controls (top). Scale bar, 1 mm. (b) Brain weight was not significantly different between the genotypes (genotype effect: P = 0.1348, n = 3, 4). (c) The size of the cerebrum (genotype effect: P = 0.1591) and cerebellum (genotype effect: P = 0.5511) was comparable between Shn-2 KO mice and wild type controls (n = 3, 4). (d) Shn-2 KO mice had a shorter body length than wild type control mice (genotype effect: P = 0.012, n = 9, 7). Body length was measured from the nose to the base of the tail. (e) There was no difference in skull size between the genotypes (n = 9, 7). Cranial length (genotype effect: P = 0.665) was measured from the anterior border of the frontal bone to the posterior border of the occipital bone. The cranial width (genotype effect: P = 0.153) is the maximum distance between the temporal bones. The cranial depth (genotype effect: P = 0.807) is the maximum distance between the bottom of the temporal bone and the top of parietal bone.

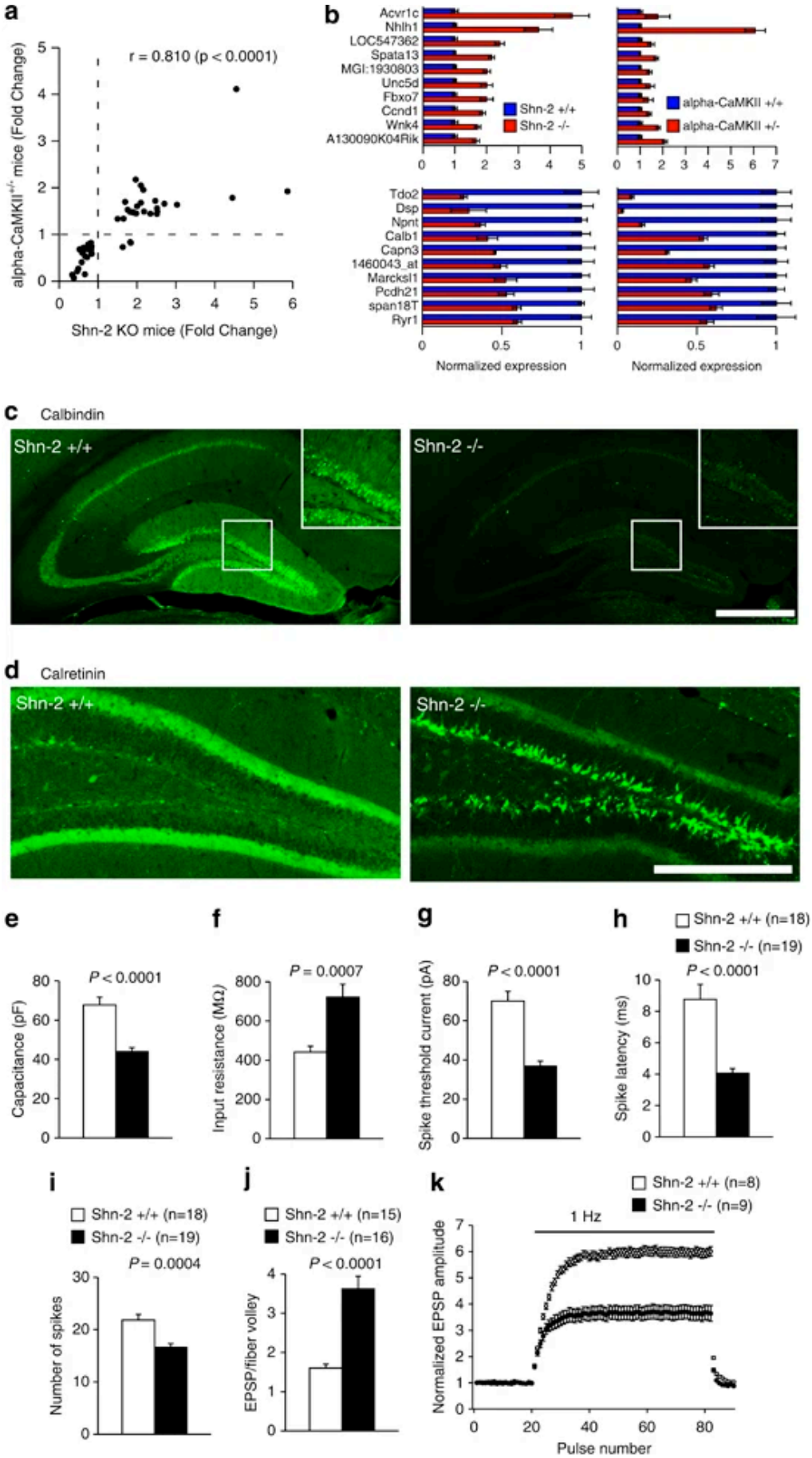
a
r = 0.810 (p < 0.0001)
alpha-CaMKII+/- mice (Fold Change)
Shn-2 KO mice (Fold Change)
b
Acvr1c
Nhlh1
LOC547362
Spata13
MGI:1930803
Unc5d
Fbxo7
Ccnd1
Wnk4
A130090K04Rik
Shn-2 +/+
Shn-2 -/-
alpha-CaMKII +/+
alpha-CaMKII +/-
Tdo2
Dsp
Npnt
Calb1
Capn3
1460043_at
Marcksl1
Pcdh21
span18T
Ryr1
Normalized expression
Normalized expression
c
Calbindin
Shn-2 +/+
Shn-2 -/-
d
Calretinin
Shn-2 +/+
Shn-2 -/-
e
P < 0.0001
Capacitance (pF)
f
P = 0.0007
Input resistance (MΩ)
g
P < 0.0001
Spike threshold current (pA)
h
Shn-2 +/+ (n=18)
Shn-2 -/- (n=19)
P < 0.0001
Spike latency (ms)
i
Shn-2 +/+ (n=18)
Shn-2 -/- (n=19)
P = 0.0004
Number of spikes
j
Shn-2 +/+ (n=15)
Shn-2 -/- (n=16)
P < 0.0001
EPSP/fiber volley
k
Shn-2 +/+ (n=8)
Shn-2 -/- (n=9)
1 Hz
Normalized EPSP amplitude
Pulse number

Figure 14
Dentate granule cells fail to mature in Shn-2 KO mice. (a) The hippocampal transcriptome pattern of Shn-2 KO mice was similar to that of α-CaMKII+/− mice, which also demonstrated maturation failure in the DG. Genes showing differential expression between genotypes at $P<0.005$ in both experiments were plotted. (b) Normalized gene expression of differentially expressed genes in Shn-2 KO and α-CaMKII+/− mice. The top 10 genes are indicated in the graphs. (c) The number of cells expressing the mature neuronal marker calbindin was decreased in Shn-2 KO mice. (d) The expression of the immature-neuronal marker calretinin was markedly increased. (e–k) Physiological properties of granule cells in the DG of Shn-2 KO mice and controls. Physiological features of DG neurons in the mutants were strikingly similar to those of immature DG neurons in normal rodents. Cell capacitance was small in the granule cells of Shn-2 KO mice (e, $P<0.0001$), whereas input resistance was high (f, $P=0.0007$), and the threshold current to induce spikes was low (g, $P<0.0001$). In the current injection (320 pA) experiments, the latency-to-burst spike was shorter (h, $P<0.0001$) and the number of spikes was lower (i, $P=0.0004$) compared with that in wild-type mice. (j) The efficacy of basal transmission at the MF synapse was increased in mutant mice ($P<0.0001$). The ratio of the peak EPSP amplitude to fiber volley amplitude is shown. (k) Shn-2 KO mice display greatly reduced frequency facilitation at 1 Hz (k, genotype effect: $P<0.0001$ at steady level). Scale bars indicate 500 μm (a), 250 μm (d).

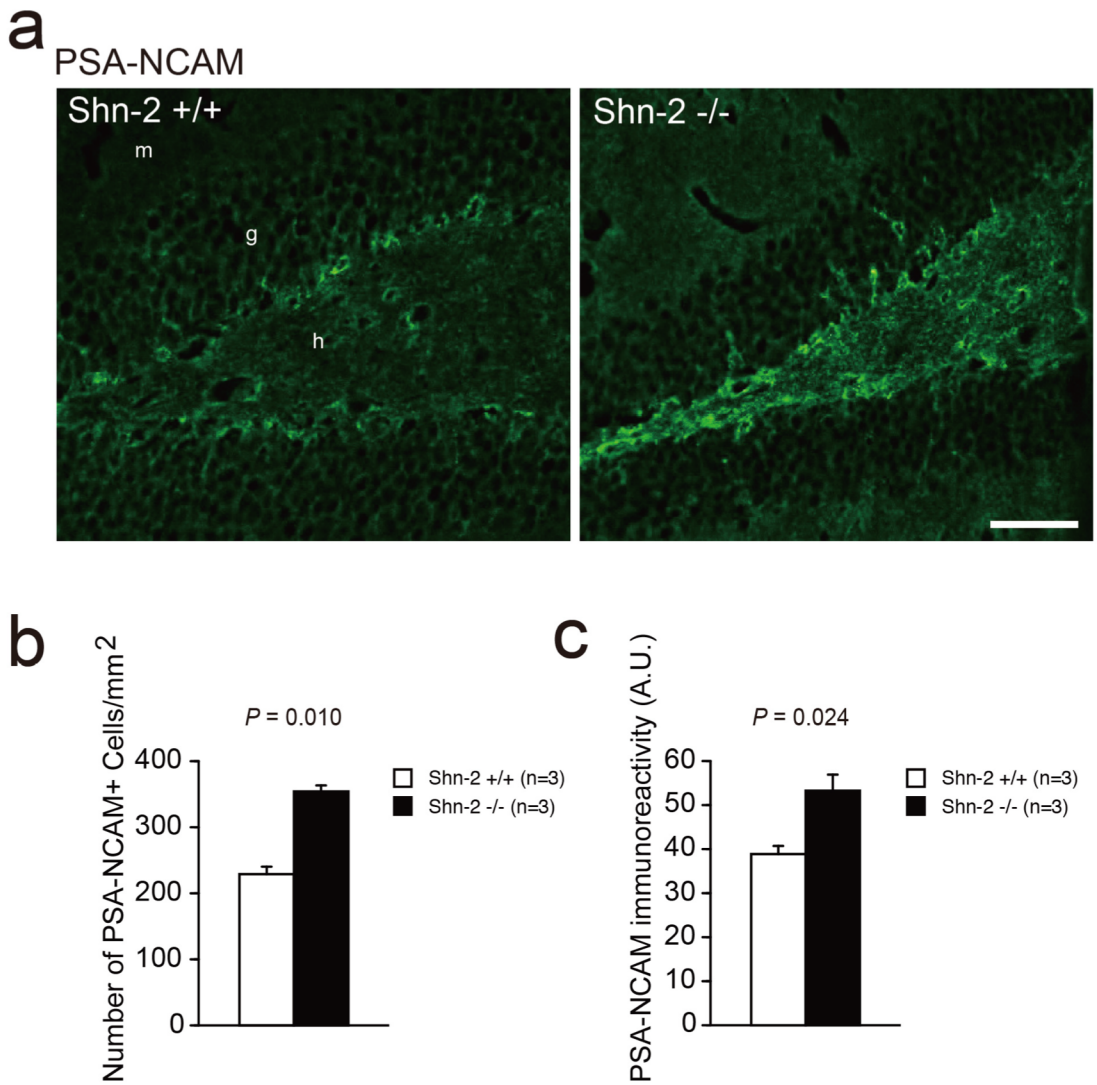

Figure 15
(a) PSA-NCAM expression increased in the DG of Shn-2 KO mice. (b) The number of PSA-NCAM-positive cells also increased in the DG of mutant mice (genotype effect: P = 0.010). (c) PSA-NCAM immunoreactivity was greater in the DG of Shn-2 KO mice than in wild type control mice (genotype effect: P = 0.024). m, molecular layer; g, granule cell layer; h, hilus. Scale bar, 200 μm.

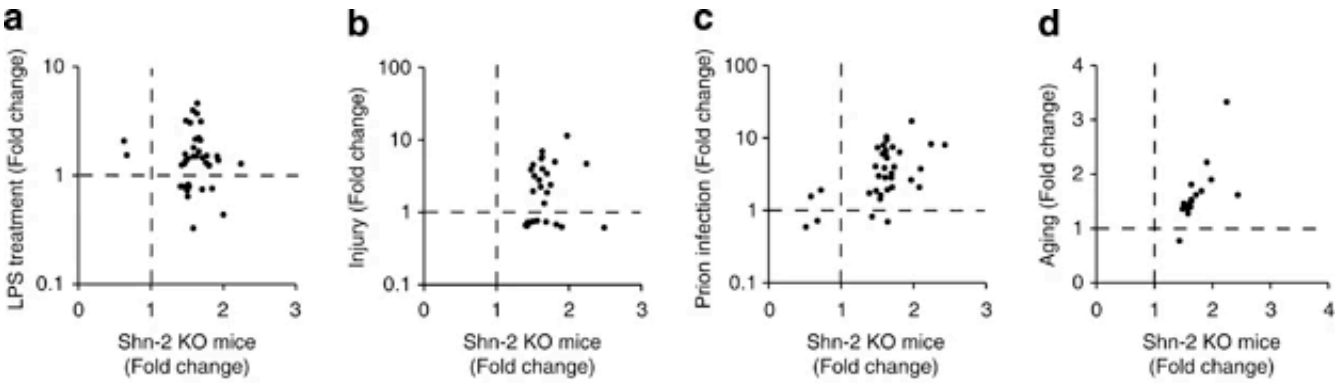
a
LPS treatment (Fold change)
Shn-2 KO mice (Fold change)
b
Injury (Fold change)
Shn-2 KO mice (Fold change)
c
Prion infection (Fold change)
Shn-2 KO mice (Fold change)
d
Aging (Fold change)
Shn-2 KO mice (Fold change)

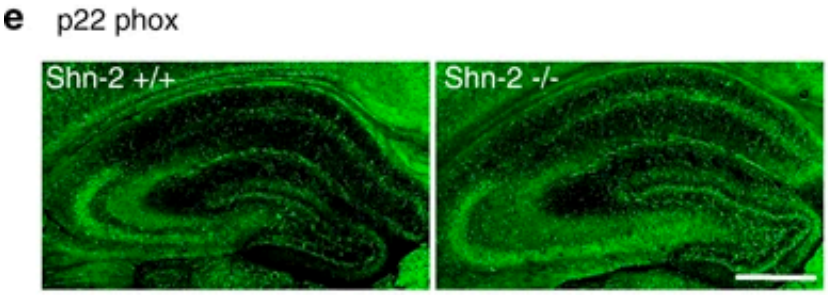
e p22 phox
Shn-2 +/+
Shn-2 -/-

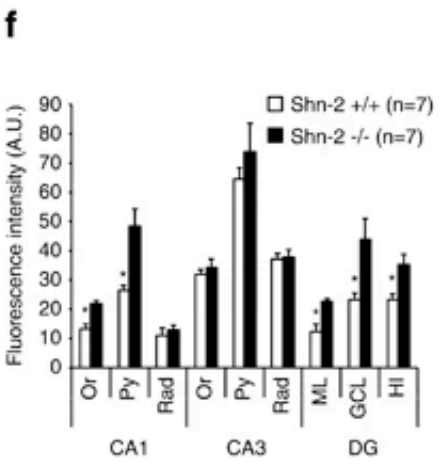
f
Shn-2 +/+ (n=7)
Shn-2 -/- (n=7)
Fluorescence intensity (A.U.)
Or
Py
Rad
Or
Py
Rad
ML
GCL
HI
CA1
CA3
DG

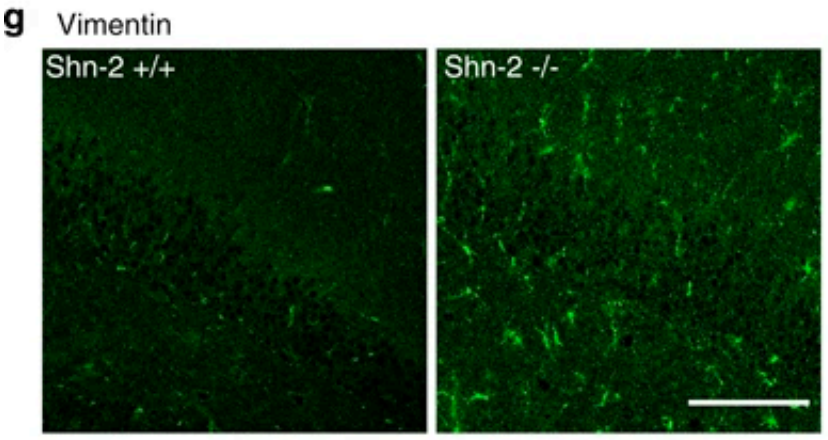
g Vimentin
Shn-2 +/+
Shn-2 -/-

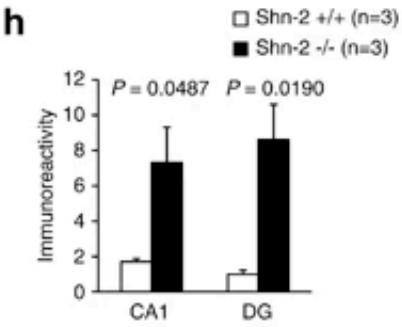
h
Shn-2 +/+ (n=3)
Shn-2 -/- (n=3)
P = 0.0487
P = 0.0190
Immunoreactivity
CA1
DG

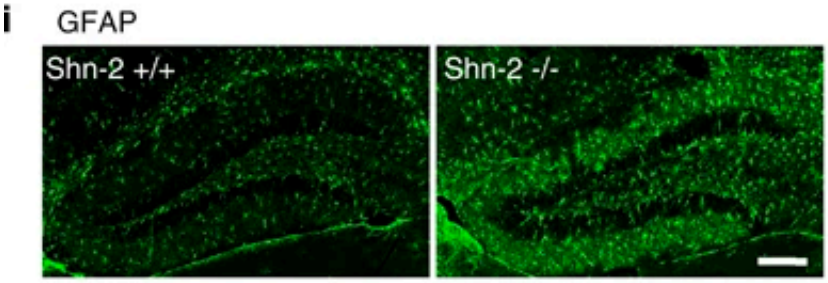
i GFAP
Shn-2 +/+
Shn-2 -/-

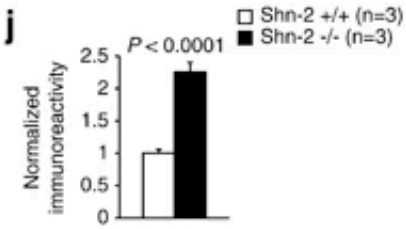
j
Shn-2 +/+ (n=3)
Shn-2 -/- (n=3)
P < 0.0001
Normalized immunoreactivity

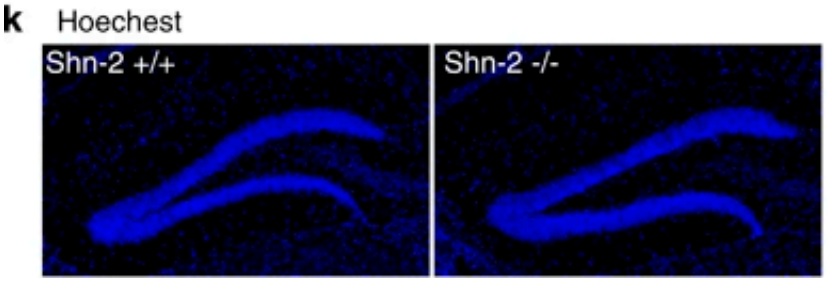
k Hoechest
Shn-2 +/+
Shn-2 -/-

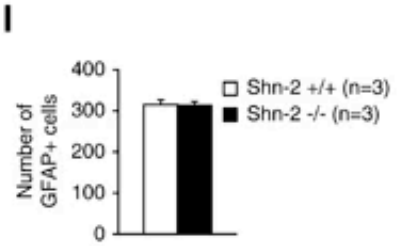
l
Shn-2 +/+ (n=3)
Shn-2 -/- (n=3)
Number of GFAP+ cells

Figure 16
Inflammatory-like phenomena in the hippocampus of Shn-2 KO mice. (a–d) The hippocampal transcriptome pattern of Shn-2 KO mice was similar to the transcriptome data from LPS treatment (a), injury (b), prion infection (c), and aging (d). The Gene Expression Omnibus (GEO) accession numbers for the transcriptome data used for the graphs are GSE23182 (a, c), GSE5296 (b), and GSE13799 (d). Genes that showed differential expression between conditions at $P<0.005$ in Shn-2 KO mice and $P<0.025$ in LPS treatment were plotted in (a). Genes that showed differential expression between conditions at $P<0.005$ in both transcriptome data sets are plotted in (b–d). (e, f) The expression of p22 phox, a component of NADH/NADPH oxidase, was increased in the DG (ML, $P=0.027$; GCL, $P=0.048$; HI, $P=0.039$) and CA1 (Or, $P=0.011$; Py, $P=0.019$) of Shn-2 KO mice. (g, h) The expression of vimentin in the DG of mutants was higher than that of the controls. (i–k) The expression of GFAP was increased in the DG of Shn-2 KO mice. Although the area of GFAP-positive cells increased (j), the number of GFAP-positive cells remained unchanged (k, l), which was confirmed by Hoechest nuclear counterstaining. Or, oriens layer; Py, pyramidal cell layer; Rad, stratum radiatum; ML, molecular layer; GCL, granule cell layer; HI, hilus. Scale bars indicate 500 μm (e), 100 μm (g), and 200 μm (i).

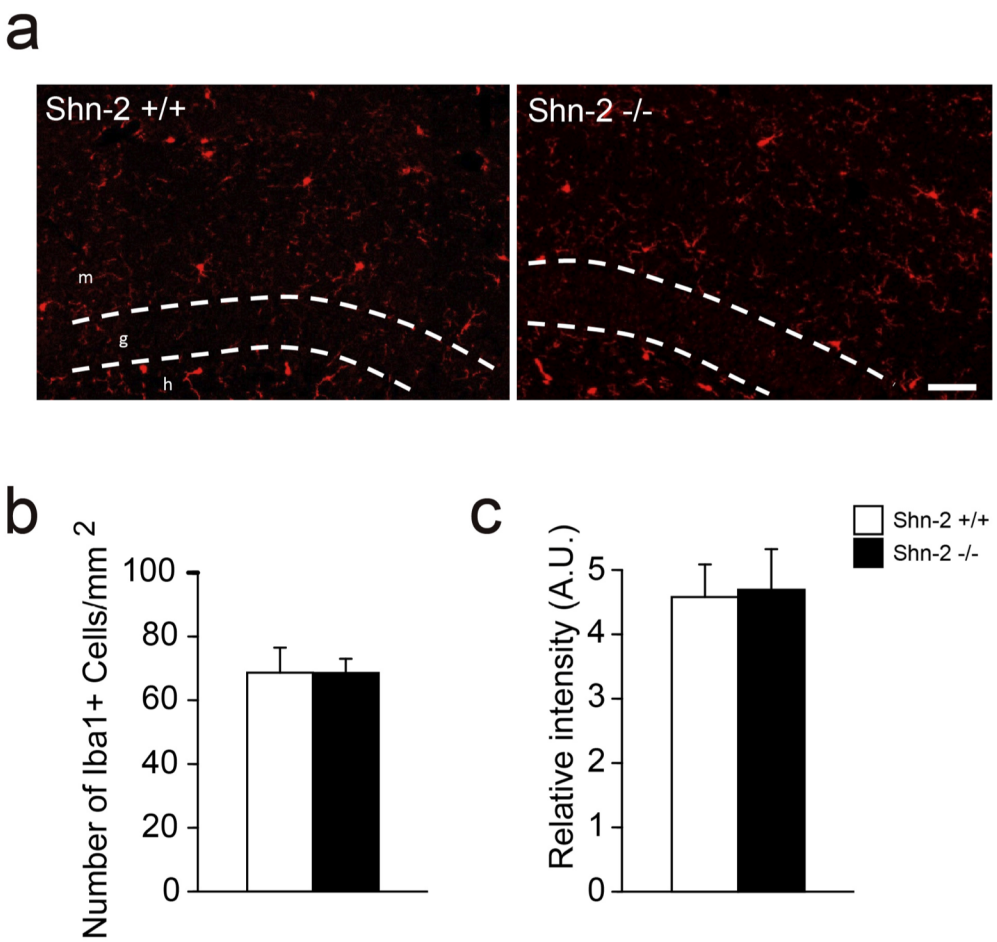

Figure 17
Microglia in the hippocampus of Shn-2 KO mice. (a) The expression of Iba1 was not significantly different between controls (left) and Shn-2 KO mice (right). (b) Number of Iba1-positive cells per unit area did not differ between genotypes (n = 6, 6, genotype effect: P = 0.98). (c) Relative immunofluorescence intensity of Iba1-positive cells (genotype effect: P = 0.74). m, molecular layer; g, granule cell layer; h, hilus. Scale bar indicates 50 mm (a).

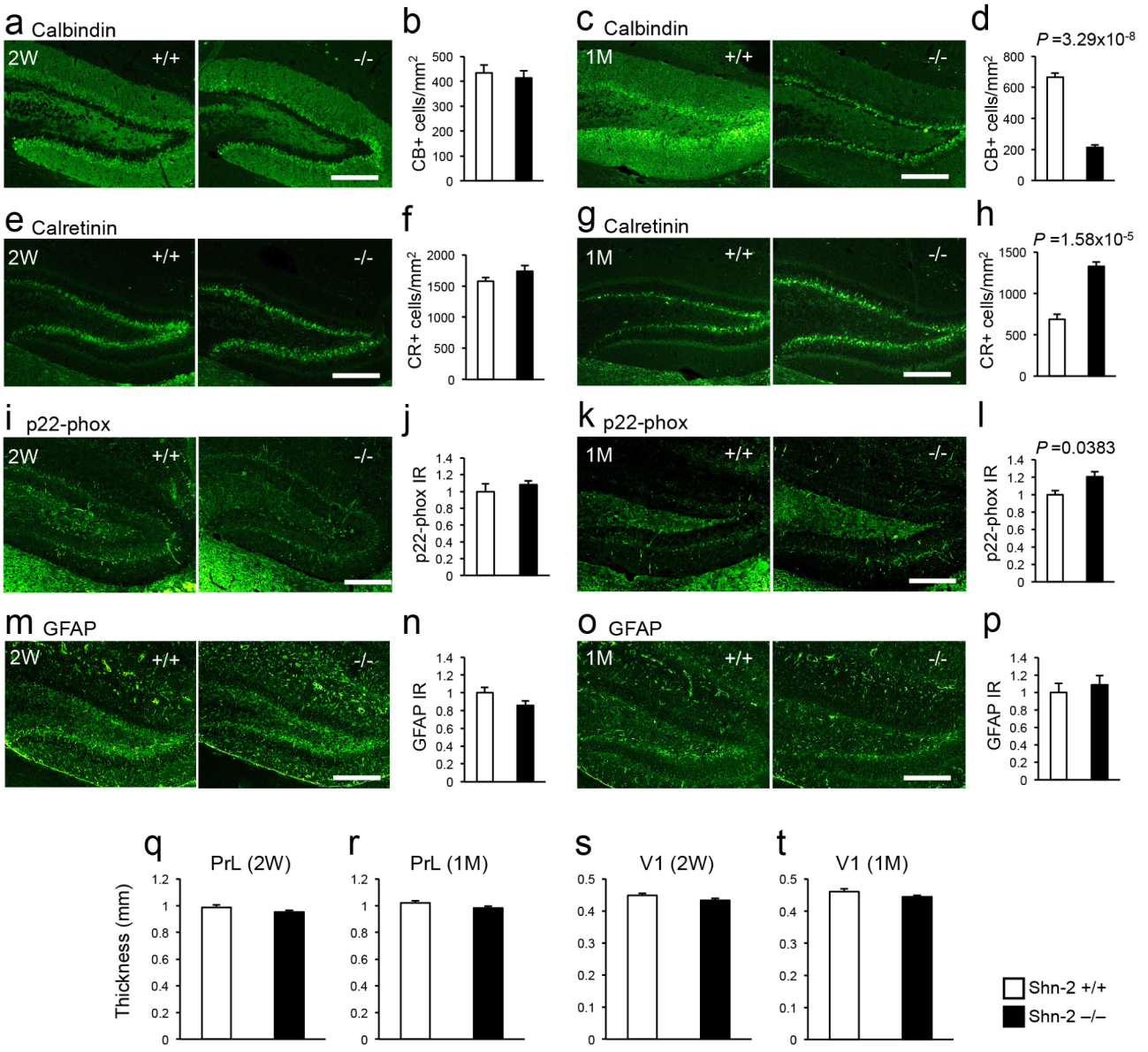

Figure 18

Expression of molecular markers and cortical thickness in Shn-2 KO mice during postnatal development. (a–d) The number of cells expressing calbindin (CB), a maker of mature neurons, was unchanged in Shn-2 KO mice at 2 weeks old (a, b, P =0.653); however, the number decreased significantly by 1 month (c, d, P= 3.29×10^{-8}). (e–h) The number of calretinin (CR)-expressing cells, a marker of immature neurons, was unchanged at 2 weeks old (e, f, P = 0.167); however, the number increased significantly by 1 month (g. h, P= 1.58×10^{-5}). (i–l) Immunoreactivity (IR) of p22-phox in the dentate gyrus (DG) of Shn-2 KO mice was unchanged at 2 weeks old (i, j, P= 0.123); however, a significant increase was observed at 1 month old (k, I). (m–p) There was no significant difference in GFAP expression between control and Shn-2 KO mice at either 2 weeks old (m, n, P= 0.113) or 1 month old (o, p, P= 0.571). (q–t) Cortical thickness was measured in sagittal sections stained with Nissl stain. There was no difference in the thickness of the prelimbic cortex (Prl) (q, 2W, P= 0.0766; r, 1M, P= 0.608) or primary visual cortex (VI) (s, 2W, P= 0.749; t, 1M, P= 0.173) in Shn-2 KO mice at either time point. Scale bars, 200 μm, n= 6–9 mice per group (a–p), n=7–18 mice per group (q–t).

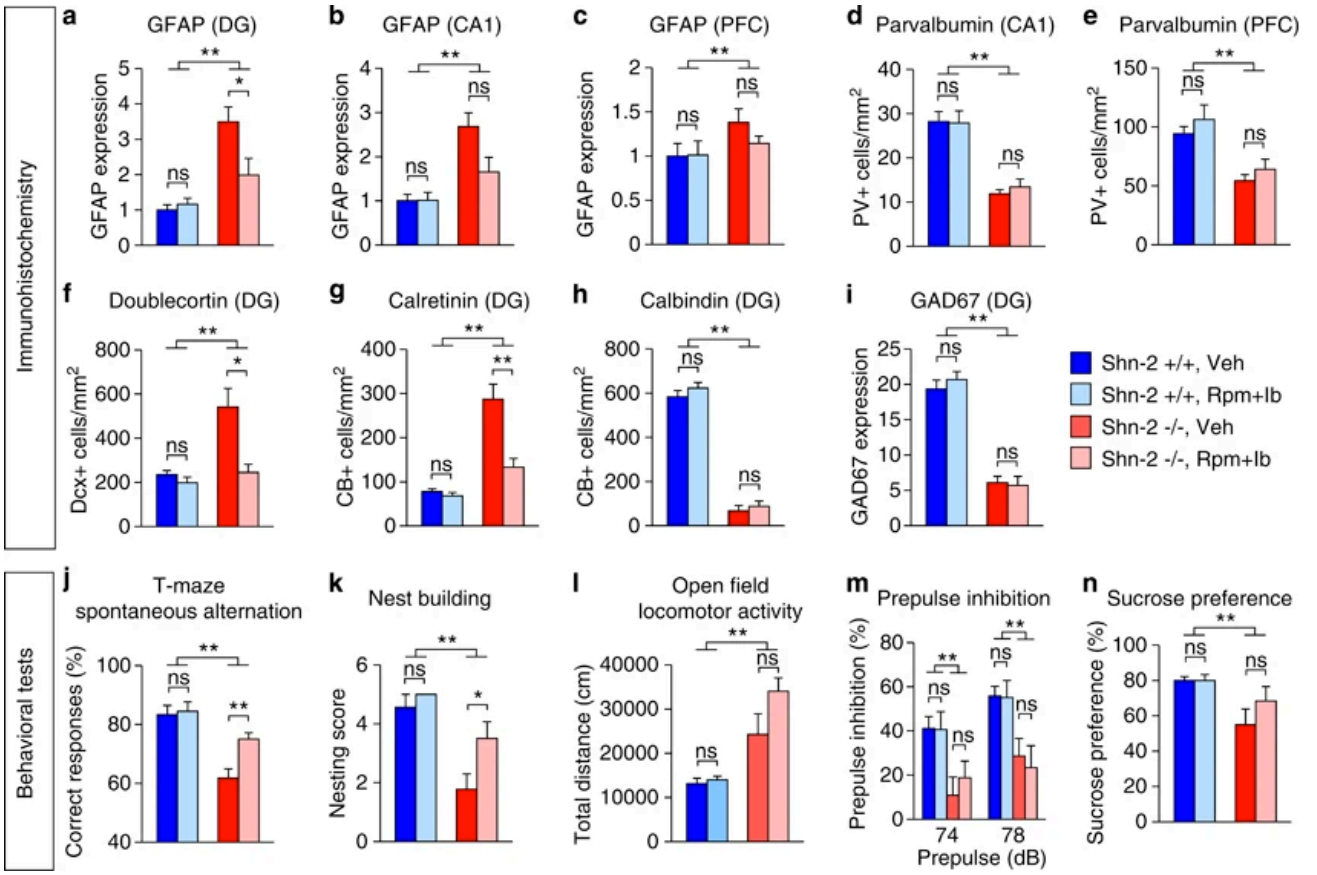

Figure 19
Anti-inflammatory treatment rescued neuronal and behavioral phenotypes of Shn-2 KO mice. Mice were chronically treated with rolipram (Rpm, 4 mg/kg) and ibuprofen (Ib, 400 p.p.m.) for 3 weeks. The treatment significantly decreased GFAP immunoreactivity in the DG of Shn-2 KO mice (a, genotype effect: P<0.0001; genotype × drug interaction: P=0.014; Shn-2−/−, Veh vs Shn-2−/−, Rpm+Ib, P=0.0323). There was a tendency of decrease in GFAP expression in the mutant CA1 (b, genotype effect: P<0.0001; genotype × drug interaction: P=0.053; Shn-2−/−, Veh vs Shn-2−/−, Rpm+Ib, P=0.051). The treatment did not reverse GFAP expression in the PFC of Shn-2 KO mice (c, genotype effect: P=0.0717; genotype × drug interaction: P=0.3662). The reductions of parvalbumin in CA1 (d, genotype effect: P<0.0001) or PFC (e, genotype effect: P=0.0002) were not rescued by the treatment. Increased expression of doublecortin (f, genotype effect: P=0.0014; genotype × drug interaction: P=0.0014; Shn-2−/−, Veh vs Shn-2−/−, Rpm+Ib, P=0.0109) and calretinin (g, genotype effect: P<0.0001; genotype × drug interaction: P=0.0019; Shn-2−/−, Veh vs Shn-2−/−, Rpm+Ib, P=0.0028) in the DG of Shn-2 KO mice were attenuated by the treatment, while decreased expressions of calbindin (h, genotype effect: P<0.0001) or GAD67 (i, genotype effect: P<0.0001) in the mutant DG were not rescued by the treatment. Working memory (j, genotype effect: P<0.0001; genotype × drug interaction: P=0.0504; Shn-2−/−, Veh vs Shn-2−/−, Rpm+Ib, P=0.0042) and nest-building behavior (k, genotype effect: P<0.0001; genotype × drug interaction: P=0.1542; Shn-2−/−, Veh vs Shn-2−/−, Rpm+Ib, P=0.0407) were significantly improved by the anti-inflammatory treatment in Shn-2 KO mice. On the other hand, hyperlocomotor activity (l), impaired PPI (m), or anhedonia in the sucrose preference test (n, genotype effect: P=0.006) were not improved. n=5–10 per group. Rpm, rolipram; Ib, ibuprofen; ns, not significant; *P<0.05, **P<0.01

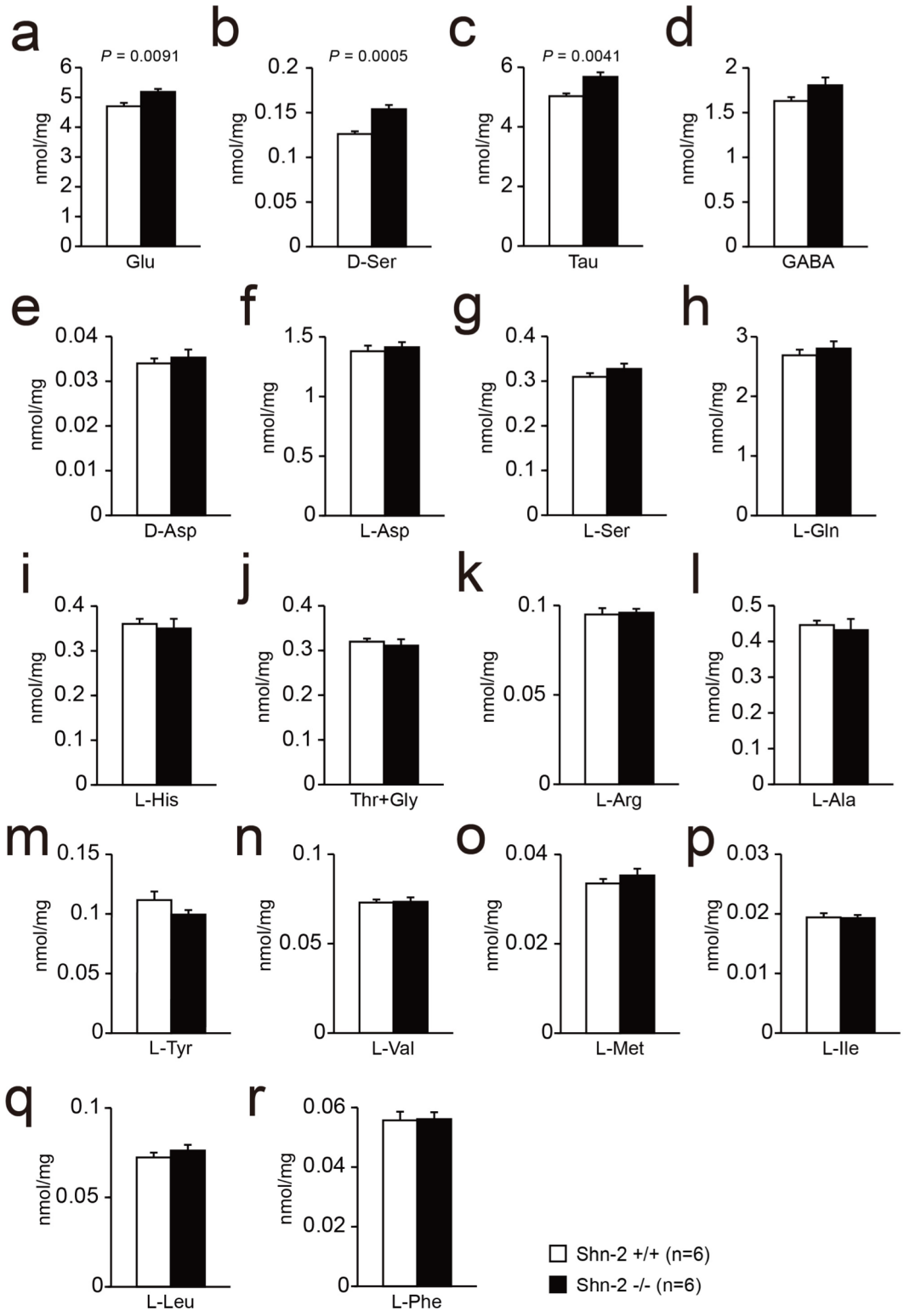

Figure 20
Free amino acids in the hippocampus of Shn-2 KO mice. In Shn-2 KO mice, the levels of glutamate (a), D-serine, and taurine (c) were higher than that of controls. The levels of GABA (d), D-aspartate (e), L-aspartate (f), L-serine (g), L-glutamine (h), L-histidine (i), tyrosine and glycine (j), L-arginine (k), L-alanine (l), L-tyrosine (m), L-valine (n), L-methionine (o), L-isoleucine (p), L-leucine (q), L-phenylalanine (r) were not significantly altered between genotypes.

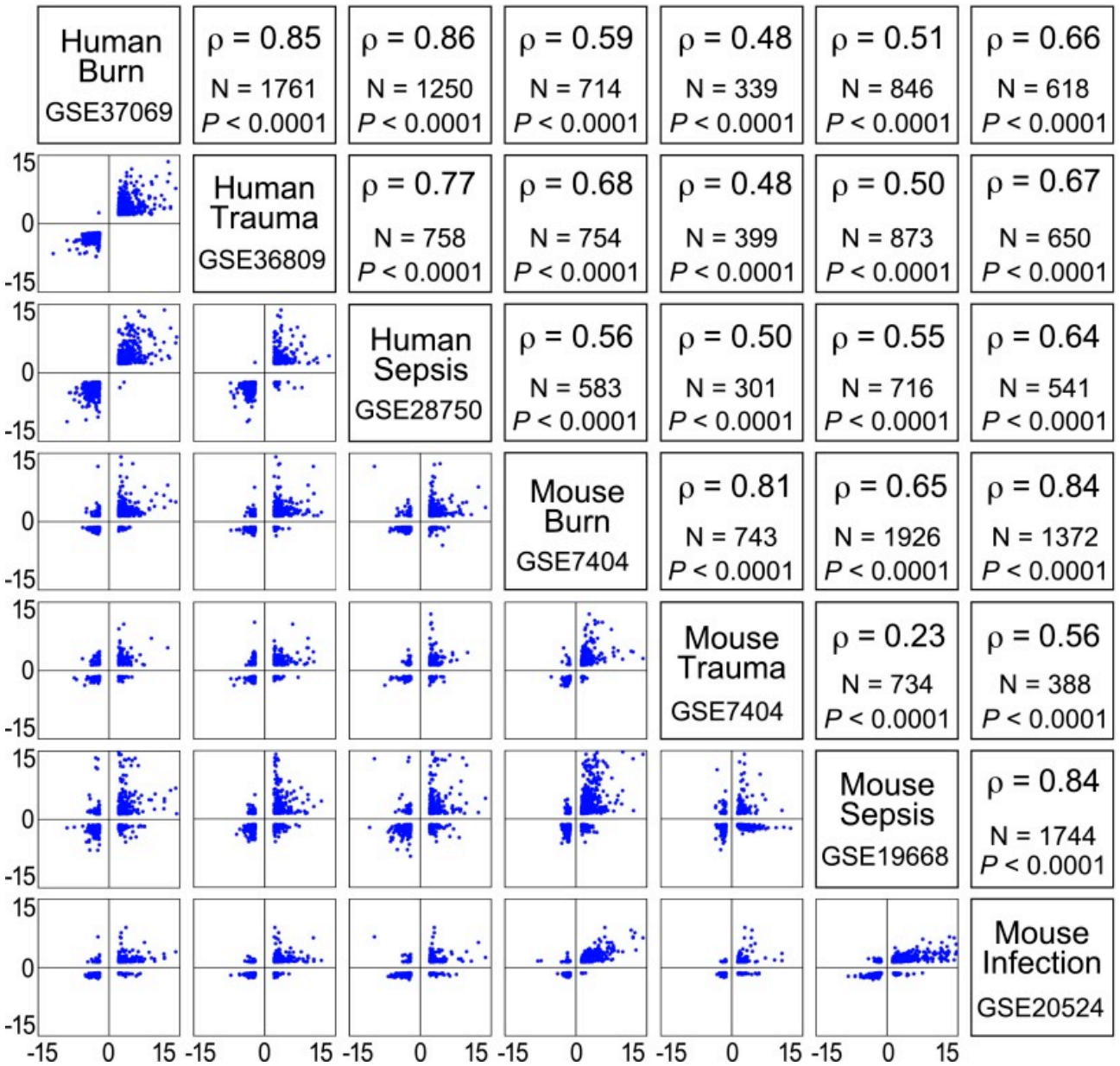

Figure 21
Correlations of gene changes among human burns, trauma, sepsis, and the corresponding mouse models. Scatterplots and Spearman's rank correlations (ρ) of the fold changes. The criteria for gene selection were as follows: absolute fold change > 2.0 in human diseases, absolute fold change > 1.2 in mouse models, P < 0.05 in both conditions. Vertical bar and horizontal bar for each panel represents fold change in right and upper panels, respectively. N represents the number of probes differentially expressed in both conditions of the comparison in each panel. Murine models were highly significantly correlated with human conditions with Spearman's correlation coefficient (ρ = 0.48–0.68; P < 0.0001 for every comparison between human conditions and mouse models). The correlations between different mouse models were also significant (ρ = 0.23–0.84; P < 0.0001 for every comparison).

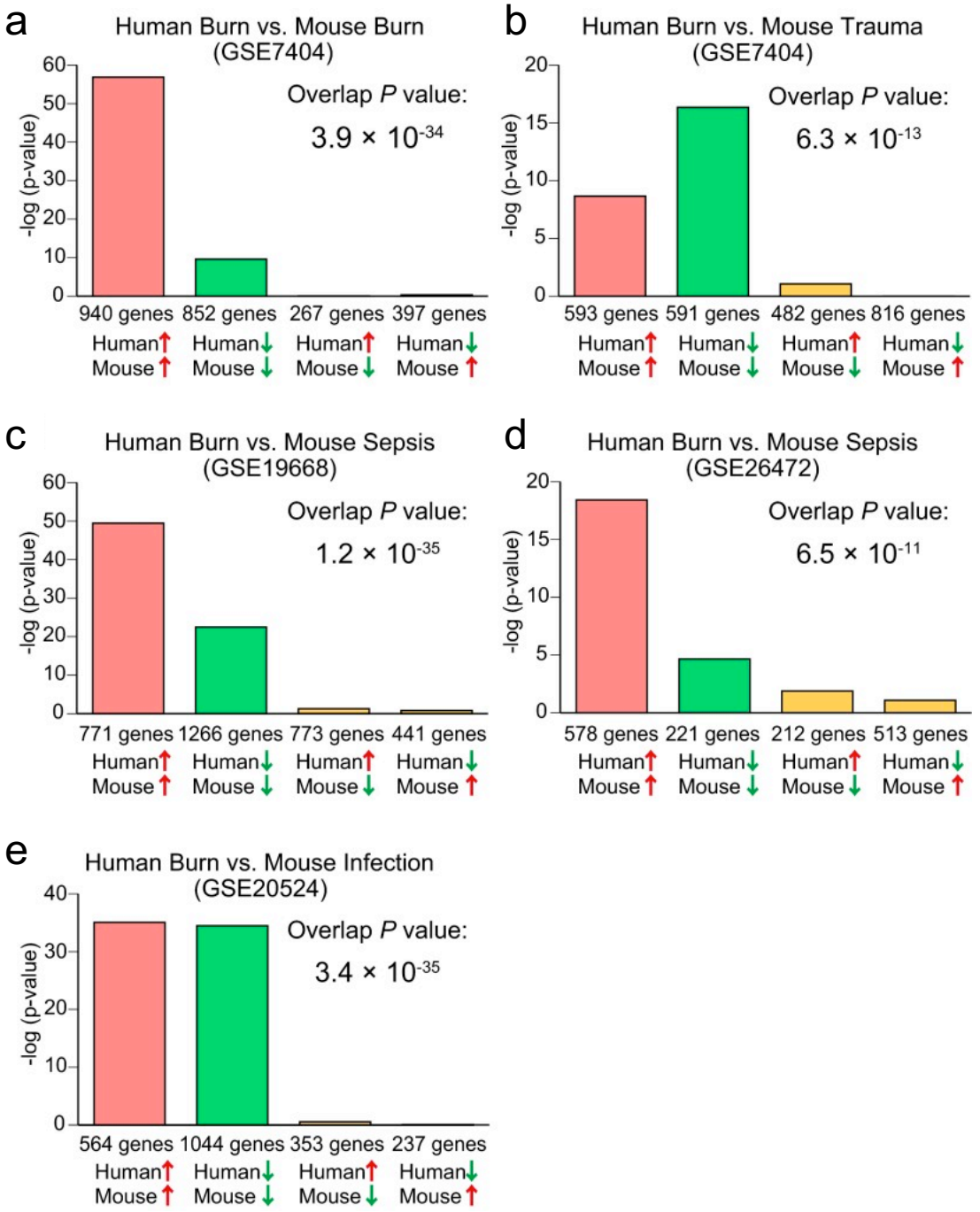

Figure 22
Statistical comparison of the direction of the gene expression changes between human burns and mouse models. Vertical bar represents the significance of the overlap between gene sets. Genes whose expression levels were changed in human burns significantly overlapped with those in the condition of mouse burn (A, overlap P value = 3.9 × 10−34), mouse trauma (B, 6.3 × 10−13), mouse sepsis from GSE19668 (C, 1.2 × 10−35), mouse sepsis from GSE26472 (D, 6.5 × 10−11), and mouse infection (E, 3.4 × 10−35). Value is expressed as the –log 10 of the P value. Statistical significances regarding the directionality of the gene expression changes were derived from the nonparametric ranking method provided by the bioinformatics platform NextBio (currently called illumina Correlation Engine 2.0).

6. TABLES

Table 1. General physical characteristics and neurological screening of Shn-2 KO mice and their wild type littermates.

	Shn-$2^{+/+}$	Shn-$2^{-/-}$
Physical characteristics		
Weight (g)	30.37±0.577	24.15±0.479 *
Whisker (% with)	87.5	87.5
Fur (% with normal)	100	100
Rectal temperature (°C)	36.50±0.148	36.56±0.205
Grip strength (N)	1.187±0.038	1.141±0.025
Sensory motor reflex		
Reaching behavior (% with normal response)	100	100
Eye twitch (% with normal response)	100	93.75
Whisker twitch (% with normal response)	81.25	93.75
Righting reflex (% with normal response)	100	100

Data represent the mean (±SEM) (Shn-$2^{+/+}$, n=16; Shn-$2^{-/-}$, n=16).
*: $P < 0.0001$

Table 2. Genes differentially expressed in both the medial prefrontal cortex (mPFC) of Shn-2 KO mice and Brodmann area (BA) 10 of schizophrenia postmortem brains.

Bioset Rank in schizophrenia	Symbol	Probe ID	PFC in Shn-2 KO		BA10 in schizophrenia[1]		Association/ linkage study[*1]	Other postmortem brain studies[*1, 2]	Neuron from iPS cell[5]	Notes
			Fold chnage	P value	Probe ID	Fold change				
2	Serpina3n	1419100_at	1.54	3.6E-03	202376_at	2.85		↑(2-4)	↓	inflammatory response
4	C1qb	1437726_x_at	1.37	8.0E-03	202953_at	2.38	(6)	↑(7)		inflammatory response
4	C1qb	1417063_at	1.30	7.2E-03						
4	C1qb	1434366_x_at	1.27	1.2E-02						
8	C1qc	1449401_at	1.39	4.0E-04	225353_s_at	2.20				inflammatory response
17	C10orf10	1433837_at	1.25	4.8E-02	209183_s_at	2.01		↑(7)		mitochondrion
22	Rgs4	1416286_at	-1.25	2.0E-02	204338_s_at	-1.96	(8, 9)	↓ (4, 10-13)		calmodulin binding, regulating the duration of postsynaptic signaling for G-coupled neurotransmitter receptors (14)
34	Ifitm2	1417460_at	1.31	2.6E-02	201315_x_at	1.82		↑ (2, 3, 10)	↑	interferon signaling, immune response
37	C1qa	1417381_at	1.31	1.9E-03	218232_at	1.78	(6)	↑(7)		inflammatory response
46	Myt1l	1439702_at	1.22	3.2E-02	1554633_a_at	-1.70	(15)	↓(4)	↑	cell differentiation
49	Tac1	1416783_at	-1.44	1.2E-02	206552_s_at	-1.68	(16, 17)	↓(4, 11)		inflammatory response
54	Cebpd	1423233_at	1.40	3.5E-02	203973_s_at	1.67	(18)	↑(4, 10, 19)		bZIP transcription factor
57	Frzb	1448424_at	-2.30	3.2E-02	203697_at	-1.65			↑	Wnt-protein binding
70	Ifitm1	1424254_at	1.53	1.0E-02	201601_x_at	1.62		↑(3, 10)	↑	interferon signaling
73	Tgfbr1	1420895_at	1.20	1.7E-02	224793_s_at	1.61	(16)	↑(7, 20)		immune system process
84	Frzb				203698_s_at	-1.59			↑	Wnt-protein binding
87	Ddit4	1428306_at	1.25	4.5E-03	202887_s_at	1.58		↑(4, 11)	↑	response to hypoxia
87	Ifitm1				214022_s_at	1.58		↑(3, 10)	↑	interferon signaling
96	Cbln4	1433607_at	-1.81	2.9E-03	234024_at	-1.56	(21)			synapse development and synaptic plasticity (22)
96	Tgm2	1437277_x_at	1.38	3.5E-02	201042_at	1.56	(23, 24)	↑(7)		inflammatory response
96	Tgm2	1433428_x_at	1.36	2.6E-02						
96	Tgm2	1455900_x_at	1.34	2.7E-02						
96	Tgm2	1417500_a_at	1.21	5.0E-02						
123	Mal2	1427042_at	-1.35	1.0E-03	224650_at	-1.52			↑	oligodendrocyte (25)
123	Slc14a1	1428114_at	1.34	2.3E-02	205856_at	1.52		↑(4, 26, 27)		urea transporter
138	Mthfd2	1419254_at	-1.29	2.8E-02	201761_at	1.50			↑	
150	Gfap	1426509_s_at	1.70	4.4E-02	229259_at	1.48	(28)	↓(29, 30, 31)	↓	astrocyte marker, inflammation
150	Rgs4				204339_s_at	-1.48	(8, 9)	↓(4, 10-13)		calmodulin binding, regulating the duration of postsynaptic signaling for G-coupled neurotransmitter receptors (14)
158	D0H4S114	1450839_at	-1.24	2.9E-02	201309_x_at	-1.47		↓(4, 10, 11, 37)	↑	regulation of transforming growth factor beta receptor signaling pathway
173	Fbxo9	1432211_a_at	-1.23	1.8E-02	1566509_s_at	-1.46		↓(4, 11)	↓	protein ubiquitination
181	Syn2	1435511_at	1.47	1.6E-02	210315_at	-1.45	(32)	↓(4, 10)		synaptic transmission
190	Gadd45b	1449773_s_at	1.65	2.1E-02	207574_s_at	1.44		↑(4, 10)		MAPKKK cascade, neural activity dependent (33)
190	Gadd45b	1450971_at	1.56	1.9E-02						
205	Chml	1422322_at	1.22	1.8E-02	226350_at	-1.43				
205	Gabra1	1421280_at	-1.32	8.2E-03	244118_at	-1.43	(34)	↓(4)		GABA receptor
237	Car10	1445497_at	1.27	6.3E-03	220889_s_at	-1.41				
237	Cebpb	1418901_at	1.39	1.3E-02	212501_at	1.41		↑(4)		inflammatory response
237	Cebpb	1427844_a_at	1.34	1.7E-02						
237	Rab3b	1422583_at	-1.25	2.6E-03	227123_at	-1.41		↓(4)		synaptic vesicle protein, inhibitory synapse (35)
256	Tasp1	1424810_at	-1.24	2.0E-02	219443_at	-1.40		↓(4)		
273	Hk2	1422612_at	1.25	2.2E-03	202934_at	1.39				
294	RP11-35N6.1	1436733_at	-1.20	2.1E-02	219732_at	-1.38			↑	
311	Gng4	1417943_at	-2.26	4.0E-04	1555867_at	-1.37				
311	Gng4	1447669_s_at	-2.21	3.0E-04						
311	Ms4a6b	1418826_at	1.31	2.6E-02	219666_at	1.37		↑(4, 7)		
333	Klf10	1416029_at	1.65	3.0E-02	202393_s_at	-1.36				immune system process
366	Cbln4				242524_at	-1.35	(21)			synapse development and synaptic plasticity (22)
366	Fcgr3	1448620_at	1.27	1.0E-02	203561_at	1.35				
366	Nrxn3	1442423_at	-1.22	2.9E-02	215021_s_at	-1.35	(21)	↓(4)	↑	synaptic transmission, cell adhesion
392	Ctsc	1416382_at	1.22	1.6E-02	201487_at	1.34			↑	immune response
392	Etv5	1450082_s_at	-1.33	3.9E-03	203348_s_at	-1.34		↑(10)		
392	Glce	1428374_at	1.33	4.3E-02	213552_at	-1.34				
431	AI593442	1444026_at	-1.23	4.6E-02	236532_at	-1.33		↓(10)		
431	C10orf10				209182_s_at	1.33		↑(7)		
431	Fbxo9				210638_s_at	-1.33		↓(4)	↓	
431	KIAA1199	1429987_at	-1.72	7.3E-05	212942_s_at	-1.33			↑	
431	Pdlim1	1416554_at	-1.35	7.2E-03	208690_s_at	1.33		↑(4), ↓(10)	↑	
431	Pygl	1417741_at	-1.24	4.6E-02	202990_at	1.33			↑	
431	Tyrobp	1450792_at	1.22	9.0E-04	204122_at	1.33				
490	Asph	1425274_at	-1.29	4.8E-03	225008_at	1.32		↑(4), ↓(10)		
490	Mbp	1425264_s_at	-1.30	2.8E-03	210136_at	-1.32	(28, 36)	↓(4)		immune response, myelination
490	Ppp1r14c	1417701_at	-1.25	2.9E-03	226907_at	-1.32		↓(4)	↑	nhibitor of protein phosphatase 1
523	Car10	1458123_at	1.24	2.0E-02	223550_s_at	-1.31				
523	Cyba	1454268_a_at	1.22	1.3E-02	203028_s_at	1.31		↑(4)	↑	inflammatory response
523	Etv5	1428142_at	-1.25	1.0E-02	203349_s_at	-1.31		↑(10)		
523	Fbxo9				212987_at	-1.31		↓(4)	↓	
523	Kcnma1	1425987_a_at	-1.24	7.9E-03	221583_s_at	-1.31	(21)		↓	
523	Kcnma1	1424848_at	-1.20	5.5E-03						
559	Bcl11a	1446293_at	1.24	2.3E-02	222891_s_at	-1.30				immune system process
559	Ms4a6b				223280_x_at	1.30		↑(4)		

612	Cacna1g	1423365_at	1.51	1.2E-02	210380_s_at	−1.29		↓(10)	↑	
612	Gabra1	1421281_at	−1.31	9.9E-03	206678_at	−1.29	(34)	↓(4), ↑(10)		GABA receptor
612	Gabra1	1436889_at	−1.20	9.5E-03						
612	H2-Ab1	1450648_s_at	1.27	2.7E-02	212998_x_at	1.29		↑(4)		immune response
669	Cxadr	1453282_at	−1.23	3.2E-02	226374_at	−1.28				
669	Hlf	1434735_at	−1.30	2.1E-02	204755_x_at	−1.28		↓(37)		
669	Hlf	1434736_at	−1.26	4.5E-02						
669	Lyn	1451318_a_at	1.24	1.0E-04	202625_at	1.28	(21)			immune system process
669	Ms4a6b				224356_x_at	1.28				
669	Tmem200a	1436304_at	1.27	9.7E-03	234994_at	−1.28				
730	Lbh	1429088_at	−1.26	1.1E-03	221011_s_at	−1.27		↓(4)		
730	Rgs4				204337_at	−1.27	(8, 9)	↓(4, 10–13)		calmodulin binding, regulating the duration of postsynaptic signaling for G-coupled neurotransmitter receptors (14)
730	S100a10	1456642_x_at	1.30	4.0E-03	200872_at	1.27				interact with 5-HT1bR, calcium ion binding, implicated in depression (38)
730	S100a10	1416762_at	1.26	5.7E-03						
797	Bcl11a				219497_s_at	−1.26				
797	Mbp				1554544_a_at	−1.26				immune response, myelination
797	Nnat	1423506_a_at	1.45	3.9E-02	204239_s_at	−1.26		↓(4)		
797	Pde10a	1419390_at	1.23	2.9E-02	205501_at	−1.26	(39)		↑	cAMP/PKA signaling, PDE10A inhibitors are currently being evaluated in clinical trials for the treatment of schizophrenia(40)
797	Tgfb1	1420653_at	1.32	2.1E-02	203085_s_at	1.26		↑(4)	↓	inflammatory response
797	Zbtb16	1439163_at	−1.21	2.7E-02	244697_at	1.26	(41)	↑(4)	↓	immune system development
894	9430020K01Rik	1428535_at	−1.21	4.9E-03	231841_s_at	−1.25	(42)	↓(4)		
894	Cntnap4	1419044_at	−1.21	3.2E-02	1553442_a_at	−1.25		↓(4)	↑	cell adhesion
894	Cntnap4				1554377_a_at	−1.25				
894	Csf1r	1419873_s_at	1.22	1.5E-02	203104_at	1.25		↓(19)		transmembrane receptor protein tyrosine kinase signaling pathway
894	Csf1r	1419872_at	1.21	1.5E-03						
894	Fam149a	1437950_at	−1.26	3.0E-03	214890_s_at	−1.25		↓(10)		
894	Gfap				203540_at	1.25		↓(10)	↓	
894	Kcnf1	1454768_at	−1.58	6.0E-04	210263_at	−1.25			↓	cellular process
894	Kcnf1	1441300_at	−1.28	5.1E-03						
894	Krt222	1457354_at	−1.22	2.4E-02	244111_at	−1.25		↓(4)		
894	Pvrl3	1423331_a_at	−1.56	6.4E-03	213325_at	−1.25		↑(4)		cell adhesion
894	Pvrl3	1448673_at	−1.48	3.7E-02						
894	Slc30a3	1460654_at	1.29	2.7E-03	207035_at	−1.25				cellular process
986	Ass1	1416239_at	−1.24	1.1E-02	207076_s_at	−1.24		↓(10)	↑	
986	D0H4S114				201310_s_at	−1.24	(41)	↓(4, 37)	↑	
986	H2-T23	1449556_at	−1.30	6.0E-03	200905_x_at	1.24	(43)	↓(10), ↑(11)	↓	immune response
986	Hdac9	1434572_at	−1.40	1.1E-02	1552760_at	−1.24		↓(4)		inflammatory response
986	Lyn				202626_s_at	1.24	(21)	↑(7)		inflammatory response
986	Nrsn1	1418588_at	−1.25	7.7E-06	239293_at	−1.24		↓(4)		
986	Nrxn3				205795_at	−1.24	(21)	↓(4)	↑	neurotransmitter secretion
986	Nrxn3				229649_at	−1.24		↓(4)		
986	Pxn	1456135_s_at	1.33	1.8E-02	201087_at	1.24		↑(10)		cellular response to oxidative stress
986	Pxn	1424027_at	1.27	8.3E-03						
986	Serpinf1	1453724_a_at	1.35	2.0E-02	202283_at	−1.24				regulation of cell development
1101	C3ar1	1419482_at	1.20	4.5E-02	209906_at	1.23				inflammatory response
1101	Cxadr				203917_at	−1.23				regulation of cell proliferation
1101	Epha4	1421928_at	−1.25	1.2E-02	228948_at	−1.23	(44)	↓(4)	↑	transmembrane receptor protein tyrosine kinase signaling pathway
1101	Galnt13	1457045_at	−1.26	1.6E-02	234472_at	−1.23		↓(4)	↓	
1101	Hecw2	1455150_at	−1.31	2.6E-02	232080_at	−1.23	(45)	↓(10)		
1101	Ms4a6b				223922_x_at	1.23				
1101	Spa17	1417635_at	−1.22	4.8E-02	205406_s_at	−1.23		↓(10)		
1218	Cntnap4				232388_at	−1.22				
1218	Epha4				229374_at	−1.22				
1218	Fam19a1	1457092_at	−1.43	1.8E-02	230923_at	−1.22	(21)			
1218	Psrc1	1417323_at	−1.27	2.0E-04	201896_s_at	1.22			↓	
1218	Ptprn2	1457874_at	−1.22	3.2E-02	203030_s_at	−1.22	(21, 46)	↓(4), ↑(10)	↑	
1218	Rhoc	1448605_at	1.24	3.8E-02	200885_at	1.22			↓	
1218	Slc8a1	1440201_at	−1.25	8.3E-03	241752_at	−1.22	(47)	↓(4), ↑(4)		cytosolic calcium ion homeostasis
1356	1810041L15Rik	1429440_at	1.33	6.7E-03	52837_at	−1.21			↑	
1356	1810041L15Rik	1455515_at	1.22	9.0E-03						
1356	6330527O06Rik	1423853_at	−1.40	2.6E-02	219463_at	−1.21			↑	
1356	Aif1	1418204_s_at	1.27	5.1E-03	215051_x_at	1.21		↓(37)		inflammatory response
1356	Etv5				216375_s_at	−1.21		↑(10, 11), ↓(19)		cellular response to oxidative stress
1356	Fam149a				214889_at	−1.21		↓(10)		
1356	Fstl5	1436800_at	1.35	1.9E-02	232010_at	−1.21	(45)		↑	
1356	Hpca	1450930_at	1.26	4.2E-03	205454_at	−1.21				
1356	Hpca	1425833_a_at	1.22	3.9E-02						
1356	Idi1	1423804_a_at	−1.27	4.9E-02	208881_x_at	−1.21		↓(4)		
1356	N28178	1455023_at	−1.21	2.9E-02	213636_at	−1.21		↓(4)		
1356	S1pr3	1438658_a_at	−1.67	4.8E-06	228176_at	1.21			↑	inflammatory response
1356	S1pr3	1437173_at	−1.28	3.8E-03						inflammatory response
1356	Sla	1420819_at	1.30	1.2E-02	203760_s_at	1.21				

1517	Bcl11a				219498_s_at	−1.20		↓(11)	immune system development
1517	Cd53	1448617_at	1.21	3.1E−03	203416_at	1.20		↓(19)	
1517	Rnf149	1440344_at	1.21	3.9E−02	243178_at	1.20		↓(4), ↑(4, 10)	
1517	Sept6	1460286_at	−1.28	5.7E−03	1555526_a_at	−1.20		↓(4, 10) ↑	
1517	Slc8a1				238546_at	−1.20	(47)		cytosolic calcium ion homeostasis
1517	Syn2	1460230_at	1.23	3.8E−02	229039_at	−1.20		↓(4, 10), ↑(7)	neurotransmitter secretion
1517	Tns1	1449405_at	1.34	1.6E−02	221748_s_at	1.20		↑(4, 10, 11)	
1517	Tns1	1419283_s_at	1.32	9.5E−03					

PFC, prefrontal cortex; iPS cell, induced pluripotent Stem Cell

up−regulated genes in both Shn−2 KO mice and schizophrenia

down−regulated genes in both Shn−2 KO mice and schizophrenia

*1: Studies of schizophrenia or bipolar disorder

*2: Genes up− (↑) or down−regulated (↓) in the post−mortem brains of SCZ and/or BD patients (identified by curated studies in NextBio (http://www.nextbio.com))

References

(1) Maycox PR, Kelly F, Taylor A, Bates S, Reid J, Logendra R, et al. Analysis of gene expression in two large schizophrenia cohorts identifies multiple changes associated with nerve terminal function. Mol. Psychiatry. 2009; 14: 1083−1094.

(2) Saetre P, Emilsson L, Axelsson E, Kreuger J, Lindholm E, Jazin E. Inflammation−related genes up−regulated in schizophrenia brains. BMC Psychiatry. 2007; 7: 46.

(3) Arion D, Unger T, Lewis DA, Levitt P, Mirnics K. Molecular evidence for increased expression of genes related to immune and chaperone function in the prefrontal cortex in schizophrenia. Biol. Psychiatry. 2007; 62:711−721.

(4) Narayan S, Tang B, Head SR, Gilmartin TJ, Sutcliffe JG, Dean B, et al. Molecular profiles of schizophrenia in the CNS at different stages of illness. Brain Res. 2008;1239: 235−248.

(5) Brennand KJ, Simone A, Jou J, Gelboin−Burkhart C, Tran N, Sangar S, et al. Modelling schizophrenia using human induced pluripotent stem cells. Nature. 2011; 473: 221−225.

(6) Zakharyan R, Khoyetsyan A, Arakelyan A, Boyajyan A, Gevorgyan A, Stahelova A, et al. Association of C1QB gene polymorphism with schizophrenia in Armenian population. BMC Med. Genet. 2011; 12: 126.

(7) Barnes MR, Huxley−Jones J, Maycox PR, Lennon M, Thornber A, Kelly F, et al. Transcription and pathway analysis of the superior temporal cortex and anterior prefrontal cortex in schizophrenia. Journal of Neuroscience Research. 2011; 89: 1218−1227.

(8) Chowdari KV, Mirnics K, Semwal P, Wood J, Lawrence E, Bhatia T, et al. Association and linkage analyses of RGS4 polymorphisms in schizophrenia. Hum. Mol. Genet. 2002; 11: 1373−1380.

(9) Morris DW, Rodgers A, McGhee KA, Schwaiger S, Scully P, Quinn J, et al. Confirming RGS4 as a susceptibility gene for schizophrenia. Am. J. Med. Genet. B Neuropsychiatr. Genet. 2004; 125B: 50−53.

(10) Harris LW, Wayland M, Lan M, Ryan M, Giger T, Lockstone H, et al. The cerebral microvasculature in schizophrenia: a laser capture microdissection study. PLoS ONE. 2008; 3(12): e3964.

(11) Ryan MM, Lockstone HE, Huffaker SJ, Wayland MT, Webster MJ, Bahn S. Gene expression analysis of bipolar disorder reveals downregulation of the ubiquitin cycle and alterations in synaptic genes. Molecular Psychiatry. 2006; 11: 965−978.

(12) Mirnics K, Middleton FA, Stanwood GD, Lewis DA, Levitt P. Disease−specific changes in regulator of G−protein signaling 4 (RGS4) expression in schizophrenia. Mol. Psychiatry. 2001; 6: 293−301.

(13) Le−Niculescu H, Balaraman Y, Patel S, Tan J, Sidhu K, Jerome R e., et al. Towards understanding the schizophrenia code: An expanded convergent functional genomics approach. American Journal of Medical Genetics Part B: Neuropsychiatric Genetics. 2007; 144B: 129−158.

(14) De Vries L, Zheng B, Fischer T, Elenko E, Farquhar MG. The Regulator of G Protein Signaling Family. Annual Review of Pharmacology and Toxicology. 2000; 40: 235−271.

(15) Vrijenhoek T, Buizer−Voskamp JE, van der Stelt I, Strengman E, Sabatti C, Geurts van Kessel A, et al. Recurrent CNVs disrupt three candidate genes in schizophrenia patients. Am. J. Hum. Genet. 2008; 83: 504−510.

(16) Yan WL, Guan XY, Green ED, Nicolson R, Yap TK, Zhang J, et al. Childhood−onset schizophrenia/autistic disorder and t(1; 7) reciprocal translocation: identification of a BAC contig spanning the translocation breakpoint at 7q21. Am. J. Med. Genet. 2000; 96: 749−753.

(17) Ekelund J, Lichtermann D, Hovatta I, Ellonen P, Suvisaari J, Terwilliger JD, et al. Genome−wide scan for schizophrenia in the Finnish population: evidence for a locus on chromosome 7q22. Hum. Mol. Genet. 2000; 9: 1049−1057.

(18) Lee C−H, Liu C−M, Wen C−C, Chang S−M, Hwu H−G. Genetic copy number variants in sib pairs both affected with schizophrenia. J. Biomed. Sci. 2010; 17: 2.

(19) Iwamoto K, Kakiuchi C, Bundo M, Ikeda K, Kato T. Molecular characterization of bipolar disorder by comparing gene expression profiles of postmortem brains of major mental disorders. Mol. Psychiatry. 2004; 4: 406−416.

(20) Benes FM, Lim B, Matzilevich D, Walsh JP, Subburaju S, Minns M. Regulation of the GABA cell phenotype in hippocampus of schizophrenics and bipolars. Proc. Natl. Acad. Sci. U.S.A. 2007; 104: 10164−10169.

(21) Shi J, Levinson DF, Duan J, Sanders AR, Zheng Y, Pe'er I, et al. Common variants on chromosome 6p22.1 are associated with schizophrenia. Nature. 2009; 460: 753−757.

(22) Yuzaki M. Cbln and C1q family proteins: new transneuronal cytokines. Cell. Mol. Life Sci. 2008; 65: 1698−1705.

(23) Bradford M, Law MH, Stewart AD, Shaw DJ, Megson IL, Wei J. The TGM2 gene is associated with schizophrenia in a British population. Am. J. Med. Genet. B Neuropsychiatr. Genet. 2009; 150B: 335−340.

(24) Bradford M, Law MH, Megson IL, Wei J. The functional significance of the TGM2 gene in schizophrenia: A correlation of SNPs and circulating IL−2 levels. Journal of Neuroimmunology. 2011; 232: 5−7.

(25) Bello−Morales R, de Marco MC, Aranda JF, Matesanz F, Alcina A, López−Guerrero JA. Characterization of the MAL2−positive compartment in oligodendrocytes. Exp. Cell Res. 2009; 315: 3453−3465.

(26) Shao L, Vawter MP. Shared Gene Expression Alterations in Schizophrenia and Bipolar Disorder. Biol Psychiatry. 2008; 64: 89−97.

(27) Iwamoto K, Bundo M, Kato T. Altered expression of mitochondria−related genes in postmortem brains of patients with bipolar disorder or schizophrenia, as revealed by large−scale DNA microarray analysis. Hum. Mol. Genet. 2005; 14: 241−253.

(28) Lewis CM, Levinson DF, Wise LH, DeLisi LE, Straub RE, Hovatta I, et al. Genome scan meta−analysis of schizophrenia and bipolar disorder, part II: Schizophrenia. Am. J. Hum. Genet. 2003; 73: 34−48.

(29) Rajkowska G, Miguel−Hidalgo JJ, Makkos Z, Meltzer H, Overholser J, Stockmeier C. Layer−specific reductions in GFAP−reactive astroglia in the dorsolateral prefrontal cortex in schizophrenia. Schizophr. Res. 2002; 57: 127−138.

(30) Johnston−Wilson NL, Sims CD, Hofmann JP, Anderson L, Shore AD, Torrey EF, et al. Disease−specific alterations in frontal cortex brain proteins in schizophrenia, bipolar disorder, and major depressive disorder. The Stanley Neuropathology Consortium. Mol. Psychiatry. 2000; 5: 142−149.

(31) Webster MJ, O'Grady J, Kleinman JE, Weickert CS. Glial fibrillary acidic protein mRNA levels in the cingulate cortex of individuals with depression, bipolar disorder and schizophrenia. Neuroscience. 2005; 133: 453−461.

(32) Lee HJ, Song JY, Kim JW, Jin S−Y, Hong MS, Park JK, et al. Association study of polymorphisms in synaptic vesicle−associated genes, SYN2 and CPLX2, with schizophrenia. Behav Brain Funct. 2005; 1: 15.

(33) Ma DK, Jang M−H, Guo JU, Kitabatake Y, Chang M, Pow−anpongkul N, et al. Neuronal Activity−Induced Gadd45b Promotes Epigenetic DNA Demethylation and Adult Neurogenesis. Science. 2009; 323: 1074 −1077.

(34) Petryshen TL, Middleton FA, Tahl AR, Rockwell GN, Purcell S, Aldinger KA, et al. Genetic investigation of chromosome 5q GABAA receptor subunit genes in schizophrenia. Mol. Psychiatry. 2005; 10: 1074−1088

(35) Tsetsenis T, Younts TJ, Chiu CQ, Kaeser PS, Castillo PE, Südhof TC. Rab3B protein is required for long−term depression of hippocampal inhibitory synapses and for normal reversal learning. Proceedings of the National Academy of Sciences. 2011; 108: 14300 −14305.

(36) Straub RE, MacLean CJ, Ma Y, Webb BT, Myakishev MV, Harris−Kerr C, et al. Genome−wide scans of three independent sets of 90 Irish multiplex schizophrenia families and follow−up of selected regions in all families provides evidence for multiple susceptibility genes. Mol. Psychiatry. 2002; 7: 542−559.

(37) Perrone−Bizzozero N. perro−affy−human−186940 [Internet]. 2006. Available from: http: //www.ncbi.nlm.nih.gov/projects/geo/query/acc.cgi?acc=GSE4036

(38) Svenningsson P, Greengard P. p11 (S100A10)—an inducible adaptor protein that modulates neuronal functions. Curr Opin Pharmacol. 2007; 7: 27−32.

(39) Lindholm E, Ekholm B, Shaw S, Jalonen P, Johansson G, Pettersson U, et al. A schizophrenia−susceptibility locus at 6q25, in one of the world's largest reported pedigrees. Am. J. Hum. Genet. 2001; 69: 96−105.

(40) Sano H, Nagai Y, Miyakawa T, Shigemoto R, Yokoi M. Increased social interaction in mice deficient of the striatal medium spiny neuron−specific phosphodiesterase 10A2. Journal of Neurochemistry. 2008; 105: 546−556.

(41) Need AC, Ge D, Weale ME, Maia J, Feng S, Heinzen EL, et al. A Genome−Wide Investigation of SNPs and CNVs in Schizophrenia. PLoS Genet. 2009; 5: e1000373.

(42) Purcell SM, Wray NR, Stone JL, Visscher PM, O'Donovan MC, Sullivan PF, et al. Common polygenic variation contributes to risk of schizophrenia and bipolar disorder. Nature. 2009; 460: 748−752.

(43) Consortium TSPG−WAS (GWAS). Genome−wide association study identifies five new schizophrenia loci. Nature Genetics. 2011; 43: 969−976.

(44) Alkelai A, Lupoli S, Greenbaum L, Giegling I, Kohn Y, Sarner−Kanyas K, et al. Identification of new schizophrenia susceptibility loci in an ethnically homogeneous, family−based, Arab−Israeli sample. FASEB J. 2011; 25: 4011−4023.

(45) Sklar P, Smoller JW, Fan J, Ferreira M a. R, Perlis RH, Chambert K, et al. Whole−genome association study of bipolar disorder. Molecular Psychiatry. 2008; 13: 558−569.

(46) Curtis D, Vine AE, McQuillin A, Bass NJ, Pereira A, Kandaswamy R, et al. Case−case genome−wide association analysis shows markers differentially associated with schizophrenia and bipolar disorder and implicates calcium channel genes. Psychiatr. Genet. 2011; 21: 1−4.

(47) Ikeda M, Aleksic B, Kinoshita Y, Okochi T, Kawashima K, Kushima I, et al. Genome−Wide Association Study of Schizophrenia in a Japanese Population. Biological Psychiatry. 2011; 69: 472−478.

Table 3. Biogroups showing significant overlap with both postmortem schizophrenia brain tissue and the PFC in Shn-2 KO mice.

			BA10 in schizophrenia					PFC in Shn-2 KO				
Rank	Biogroup name	Source	Common genes	Direction	P value	common genes (opposite direction)	P value	Common genes	Direction	P value	Common genes (opposite direction)	P value
1	response to stress	GO	125	up	5.4E-44	78	1.0E-04	36	up	1.9E-03	18	8.3E-01
2	immune response	GO	76	up	3.9E-37	17	3.8E-01	24	up	4.3E-07	5	8.9E-01
3	response to wounding	GO	65	up	3.5E-34	22	1.1E-01	22	up	4.8E-08	7	4.4E-01
4	inflammatory response	GO	49	up	6.8E-33	12	1.2E-01	19	up	7.4E-10	4	1.3E-01
5	synaptic transmission	GO	57	down	5E-32	10	1.5E-01	11	down	2.5E-02	7	5.5E-01
6	transmission of nerve impulse	GO	59	down	3.2E-29	12	1.4E-01	12	down	4.1E-02	9	4.7E-01
7	cell–cell signaling	GO	74	down	5.5E-28	26	5.0E-03	18	down	5.9E-03	16	6.5E-02
8	immune effector process	GO	33	up	4.7E-24	5	6.5E-01	14	up	4.6E-06	2	7.2E-01
9	regulation of response to stimulus	GO	46	up	7.7E-24	21	1.7E-01	23	up	2.5E-07	6	5.1E-01
10	regulation of immune system process	GO	41	up	1.3E-21	12	6.6E-01	18	up	2.9E-06	6	4.2E-01
11	leukocyte mediated immunity	GO	25	up	2.5E-20	4	3.2E-01	14	up	1.1E-07	1	6.1E-01
12	Neutrophil Pathway	Broad MSigDB – Canonical Pathways	6	up	2.8E-20	0		0			0	
13	neuron projection	GO	51	down	8.3E-20	8	9.1E-01	22	up	3.3E-06	15	1.6E-02
14	positive regulation of immune system process	GO	33	up	1.1E-19	5	1.7E-01	15	up	8.9E-07	4	6.2E-01
15	regulation of immune response	GO	31	up	5.2E-19	7	6.9E-01	14	up	7.7E-06	1	7.3E-01
16	transport	GO	170	down	9.9E-19	91	3.1E-06	61	up	2.1E-02	45	1.6E-01
17	adaptive immune response based on somatic recombination of immune receptors built from immunoglobulin superfamily domains	GO	20	up	1.9E-18	3	8.4E-01	11	up	9.6E-08	1	5.2E-01
18	response to other organism	GO	33	up	3.3E-18	10	2.2E-01	5	up	2.2E-01	2	5.8E-01
19	positive regulation of signal transduction	GO	31	up	3.3E-18	8	4.1E-01	8	up	3.8E-06	6	1.3E-01
20	adaptive immune response	GO	20	up	3.8E-18	3	8.6E-01	11	up	9.6E-08	1	5.2E-01
21	response to organic substance	GO	57	up	5.6E-18	52	3.3E-05	27	up	1.5E-05	10	5.5E-01
22	Metallothionein superfamily, eukaryotic	InterPro	6	up	6E-18	0		0			0	
23	Metallothionein, vertebrate	InterPro	6	up	6E-18	0		0			0	
24	Monocyte Pathway	Broad MSigDB – Canonical Pathways	6	up	2.1E-17	0		1	down	1.7E-01		
25	E12 binding site geneset 2	Broad MSigDB – Regulatory Motifs	150	down	7.6E-17	80	6.4E-06	62	up	3.0E-04	57	1.3E-03
26	cell death	GO	68	up	8.3E-17	61	1.0E-04	30	up	8.1E-05	16	7.9E-01
27	death	GO	68	up	1E-16	61	1.0E-04	30	up	9.1E-05	16	8.0E-01
28	lymphocyte mediated immunity	GO	19	up	1.2E-16	3	8.3E-01	11	up	1.7E-07	1	5.3E-01
29	acute inflammatory response	GO	17	up	1.3E-16	3	1.4E-01	11	up	4.9E-09	2	2.3E-01
30	cell proliferation	GO	68	up	1.6E-16	47	2.5E-02	35	up	4.8E-08	17	1.8E-01
31	synapse	GO	44	down	2.3E-16	5	8.6E-01	14	down	1.5E-03	17	3.1E-03
32	Lymphocyte Pathway	Broad MSigDB – Canonical Pathways	5	up	2.9E-16	0		1	down	1.4E-01	0	
33	Hematopoietic Cell Lineage	Broad MSigDB – Canonical Pathways	16	up	3.7E-16	1	9.0E-01	5	up	2.7E-05	1	6.4E-01
34	response to external stimulus	GO	40	up	1.8E-15	29	9.7E-02	17	up	4.0E-05	5	8.1E-02
35	cytokine binding	GO	18	up	2E-15	0		0			0	
36	Predicted Gene Targets for miR-30	TargetScan miRNA targets DB	70	down	3.3E-15	22	4.7E-02	23	down	4.6E-03	24	8.0E-03
37	response to hypoxia	GO	19	up	8.5E-15	7	2.9E-01	4	down	1.4E-02	3	1.6E-02
38	Predicted Gene Targets for miR-381	TargetScan miRNA targets DB	55	down	8.5E-15	15	1.8E-01	15	down	1.9E-01	7	9.5E-01
39	Complement and Coagulation Cascades	Broad MSigDB – Canonical Pathways	11	up	1.3E-14	0		6	up	6.9E-06	1	3.7E-01
40	cell differentiation	GO	84	up	1.5E-14	87	1.7E-06	55	up	3.9E-06	51	2.0E-04
41	vasculature development	GO	30	up	3.6E-14	13	6.9E-01	20	up	2.9E-07	11	3.8E-02
42	Cell Adhesion Molecules (CAMs)	Broad MSigDB – Canonical Pathways	21	up	4.2E-14	5	3.0E-01	5	down	5.2E-02	4	1.9E-01
43	Calcium Regulation In Cardiac Cells	Broad MSigDB – Canonical Pathways	25	down	4.2E-14	4	7.3E-01	6	down	1.7E-03	4	3.3E-01
44	Cytokine Cytokine Receptor Interaction	Broad MSigDB – Canonical Pathways	25	up	4.6E-14	4	9.3E-01	9	up	9.2E-03	4	8.2E-02
45	cellular component movement	GO	40	up	4.7E-14	41	8.6E-05	21	up	2.0E-04	16	8.6E-02
46	MMP Cytokine Connection	Broad MSigDB – Canonical Pathways	7	up	9.1E-14	0		0			0	
47	MAZ binding site geneset 2	Broad MSigDB – Regulatory Motifs	130	down	9.8E-14	73	9.5E-05	62	up	1.9E-06	48	6.9E-02
48	ATF3 binding site geneset 3	Broad MSigDB – Regulatory Motifs	47	down	1.2E-13	14	2.1E-01	14	up	2.4E-02	10	1.2E-01
49	CREBP1 binding site geneset 2	Broad MSigDB – Regulatory Motifs	30	down	2.7E-13	8	3.2E-01	8	down	3.8E-03	4	4.1E-01
50	positive regulation of response to stimulus	GO	29	up	2.7E-13	11	5.3E-02	15	up	1.4E-07	5	2.8E-01
51	AP1 binding site geneset 9	Broad MSigDB – Regulatory Motifs	69	down	3.1E-13	41	3.4E-05	35	up	2.0E-04	26	5.1E-03
52	innate immune response	GO	25	up	4.1E-13	3	5.0E-01	7	up	1.0E-04	1	6.5E-01
53	ATF1 binding site geneset 1	Broad MSigDB – Regulatory Motifs	25	down	4.5E-13	6	6.8E-01	7	down	9.0E-02	2	8.6E-01
54	ion transport	GO	60	down	5.2E-13	20	1.1E-01	8	up	1.0E-04	21	3.0E-04
55	LEF1 binding site geneset 4	Broad MSigDB – Regulatory Motifs	128	down	5.6E-13	62	2.0E-04	44	down	2.3E-02	43	5.1E-01
56	Immunoglobulin-like fold	InterPro	41	up	5.7E-13	12	8.2E-01	20	up	2.0E-06	7	5.4E-01
57	negative regulation of response to stimulus	GO	12	up	6E-13	7	1.8E-01	8	up	1.7E-03	1	2.1E-02
58	response to endogenous stimulus	GO	34	up	7.5E-13	37	8.8E-05	12	up	5.6E-03	6	2.4E-01
59	immune system development	GO	30	up	8.9E-13	9	4.3E-01	18	up	3.2E-05	6	2.3E-01
60	regulation of anatomical structure morphogenesis	GO	28	up	1E-12	15	8.5E-02	19	up	1.7E-05	12	2.6E-03
61	SP1 binding site geneset 6	Broad MSigDB – Regulatory Motifs	156	down	1.2E-12	65	6.0E-01	56	down	5.7E-02	58	2.8E-01
62	AP4 binding site geneset 5	Broad MSigDB – Regulatory Motifs	92	down	1.4E-12	49	1.7E-03	49	up	1.8E-05	36	1.3E-03
63	Calcium Signaling Pathway	Broad MSigDB – Canonical Pathways	24	down	2.3E-12	4	8.2E-01	5	up	1.6E-01	5	2.5E-01
64	leukocyte migration	GO	15	up	2.7E-12	3	4.5E-01	0			0	
65	production of molecular mediator of immune response	GO	11	up	2.8E-12	3	4.8E-01	0			0	
66	growth	GO	27	up	3.5E-12	20	4.6E-01	18	up	1.7E-02	8	7.5E-01
67	CREB binding site geneset 1	Broad MSigDB – Regulatory Motifs	28	down	3.6E-12	7	5.0E-01	7	down	2.8E-02	0	
68	response to hormone stimulus	GO	32	up	4.1E-12	31	1.4E-03	12	up	2.0E-03	6	1.6E-01

69	wound healing	GO	18	up	4.5E−12	5	8.2E−01	0			0	
70	Predicted Gene Targets for miR−330	TargetScan miRNA targets DB	37	down	5.6E−12	9	6.3E−01	9	down	1.5E−01	5	9.4E−01
71	cell projection part	GO	37	down	5.8E−12	6	9.1E−01	10	down	2.5E−02	7	1.8E−01
72	Immunoglobulin−like	InterPro	36	up	6E−12	14	5.5E−01	20	up	5.9E−06	7	3.9E−01
73	regulation of cell size	GO	18	up	7.9E−12	12	2.6E−01	8	up	6.4E−02	3	7.2E−01
74	cell growth	GO	17	up	8.7E−12	12	1.9E−01	8	up	4.2E−02	3	6.6E−01
75	positive regulation of programmed cell death	GO	33	up	1E−11	23	3.1E−02	17	up	4.8E−08	6	6.3E−01
76	cell junction	GO	48	down	1.1E−11	21	5.0E−04	22	up	1.2E−05	10	9.5E−02
77	CREBP1CJUN binding site geneset 1	Broad MSigDB − Regulatory Motifs	27	down	1.4E−11	6	5.0E−01	6	down	7.2E−02	0	
78	hemopoiesis	GO	26	up	1.9E−11	9	3.8E−01	14	up	4.0E−04	5	3.0E−01
79	learning or memory	GO	18	down	1.9E−11	1	6.6E−01	6	down	2.8E−03	5	4.7E−02
80	Predicted Gene Targets for miR−181	TargetScan miRNA targets DB	49	down	2E−11	20	5.3E−02	14	down	1.1E−01	12	6.4E−01
81	Predicted Gene Targets for miR−539	TargetScan miRNA targets DB	33	down	2E−11	10	2.7E−01	12	down	2.8E−03	5	4.6E−01
82	cell activation	GO	31	up	2.1E−11	17	3.0E−03	17	up	5.0E−04	9	2.7E−01
83	activation of immune response	GO	18	up	2.2E−11	3	3.2E−01	0			0	
84	cell migration	GO	31	up	2.2E−11	29	1.1E−03	16	up	1.2E−03	11	1.9E−01
85	hemopoietic or lymphoid organ development	GO	27	up	2.2E−11	9	4.0E−01	16	up	2.0E−04	6	1.9E−01
86	Complement Pathway	Broad MSigDB − Canonical Pathways	6	up	2.4E−11	0		0			0	
87	NRSF binding site geneset 1	Broad MSigDB − Regulatory Motifs	16	down	2.4E−11	0		3	up	2.2E−01	1	5.8E−01
88	regulation of neurological system process	GO	20	down	3E−11	4	5.7E−01	4	down	1.2E−01	5	3.9E−01
89	regulation of angiogenesis	GO	13	up	3E−11	3	4.6E−01	0			0	
90	ATF binding site geneset 2	Broad MSigDB − Regulatory Motifs	23	down	3.3E−11	4	7.0E−01	4	down	1.4E−01	0	
91	Smooth Muscle Contraction	Broad MSigDB − Canonical Pathways	22	down	3.4E−11	6	1.5E−01	5	down	2.7E−03	7	3.4E−02
92	membrane raft	GO	18	up	3.5E−11	9	1.1E−01	5	up	5.3E−02	4	2.9E−01
93	vesicle	GO	62	down	3.8E−11	29	4.0E−04	19	up	3.0E−04	13	2.6E−01
94	positive regulation of immune response	GO	21	up	4E−11	3	5.5E−01	11	up	1.3E−05	1	6.0E−01
95	behavior	GO	41	down	4.1E−11	22	4.0E−04	16	down	9.5E−03	14	1.6E−02
96	cellular response to stimulus	GO	50	up	4.3E−11	47	8.6E−03	21	up	2.8E−02	9	9.7E−01
97	MYOD binding site geneset 4	Broad MSigDB − Regulatory Motifs	64	down	4.6E−11	32	2.2E−02	23	down	1.1E−03	28	2.4E−03
98	Predicted Gene Targets for miR−25	TargetScan miRNA targets DB	42	down	5.4E−11	13	6.7E−01	19	up	8.3E−05	11	4.2E−02
99	Gamma−aminobutyric acid A receptor	InterPro	6	down	5.6E−11	0		1	down	3.5E−03	0	
100	immunoglobulin production	GO	8	up	5.9E−11	3	3.1E−01	0			0	
101	transporter activity	GO	71	down	7.1E−11	29	1.3E−01	19	down	2.0E−02	20	2.9E−01
102	regulation of neurotransmitter levels	GO	14	down	8.1E−11	0		4	down	5.3E−02	3	2.0E−01
103	regulation of transmission of nerve impulse	GO	19	down	8.4E−11	4	5.3E−01	4	down	9.1E−02	4	4.1E−01
104	cytoplasmic vesicle	GO	60	down	1.1E−10	28	4.0E−04	17	up	1.3E−03	13	1.8E−01
105	regulation of peptidyl−tyrosine phosphorylation	GO	8	up	1.1E−10	2	1.8E−01	4	up	5.4E−02	1	4.5E−01
106	calmodulin binding	GO	18	down	1.2E−10	5	5.5E−01	6	up	8.0E−04	4	3.8E−03
107	localization of cell	GO	31	up	1.3E−10	30	1.6E−03	16	up	2.5E−03	12	1.6E−01
108	Interferon−induced transmembrane protein	InterPro	3	up	1.5E−10	0		0			0	
109	membrane−bounded vesicle	GO	57	down	1.5E−10	29	9.1E−05	10	up	3.0E−02	10	1.5E−01
110	locomotion	GO	37	up	1.7E−10	35	4.0E−04	17	up	6.2E−03	12	3.1E−01
111	cytokine production	GO	21	up	1.9E−10	5	7.4E−01	11	up	2.0E−04	4	9.1E−03
112	receptor binding	GO	63	down	2.4E−10	46	5.3E−09	18	up	1.2E−03	20	3.9E−03
113	complement activation	GO	10	up	2.5E−10	0		0			0	
114	Predicted Gene Targets for miR−26	TargetScan miRNA targets DB	47	down	2.6E−10	17	1.7E−01	0			0	
115	response to bacterium	GO	20	up	2.7E−10	6	3.1E−01	4	up	1.5E−01	1	4.9E−01
116	cytoplasmic membrane−bounded vesicle	GO	56	down	3E−10	28	1.0E−04	10	down	1.1E−01	8	1.2E−01
117	regulation of immune effector process	GO	13	up	3E−10	2	9.4E−01	5	up	5.9E−02	1	4.7E−01
118	NFAT binding site geneset 3	Broad MSigDB − Regulatory Motifs	110	down	4.3E−10	64	1.7E−05	48	down	2.0E−04	44	3.0E−02
119	FOXO4 binding site geneset 3	Broad MSigDB − Regulatory Motifs	121	down	4.4E−10	75	1.6E−06	50	down	1.2E−03	34	5.7E−01
120	regulation of cellular component movement	GO	22	up	4.9E−10	17	1.4E−02	0			0	
121	response to steroid hormone stimulus	GO	21	up	5.2E−10	13	1.0E−01	4	down	2.7E−02	4	1.3E−01
122	ATF binding site geneset 1	Broad MSigDB − Regulatory Motifs	26	down	5.2E−10	4	7.7E−01	5	down	5.4E−03	3	5.7E−01
123	site of polarized growth	GO	12	down	5.3E−10	1	7.9E−01	4	up	8.0E−04	2	5.1E−01
124	axon	GO	25	down	5.4E−10	4	8.1E−01	8	down	7.6E−02	4	8.4E−01
125	positive regulation of developmental process	GO	28	up	5.8E−10	12	6.8E−01	22	up	5.7E−09	16	1.0E−04
126	axon part	GO	17	down	5.9E−10	8	6.1E−10	5	down	3.6E−02	0	
127	positive regulation of cellular component movement	GO	16	up	7.3E−10	10	3.1E−02	5	up	7.9E−02	3	1.0E−01
128	morphogenesis of a branching structure	GO	13	up	7.3E−10	2	9.9E−01	8	up	3.0E−04	5	4.7E−02
129	leukocyte activation	GO	27	up	7.7E−10	14	2.8E−03	16	up	5.0E−04	8	3.2E−01
130	MAPK Signaling Pathway	Broad MSigDB − Canonical Pathways	26	down	8.2E−10	16	2.4E−03	16	up	3.1E−06	5	6.5E−01
131	negative regulation of developmental process	GO	22	up	9.1E−10	14	1.9E−01	14	down	7.0E−04	12	3.2E−02
132	ATF3 binding site geneset 2	Broad MSigDB − Regulatory Motifs	24	down	9.6E−10	4	7.8E−01	6	down	3.0E−02	0	
133	myeloid cell differentiation	GO	16	up	9.7E−10	4	7.9E−01	11	up	4.3E−06	2	1.2E−01
134	neuronal cell body	GO	24	down	9.9E−10	4	7.9E−01	19	up	9.0E−10	9	2.6E−02
135	response to organic cyclic substance	GO	13	up	9.9E−10	9	2.6E−02	0			0	
136	Predicted Gene Targets for miR−1	TargetScan miRNA targets DB	40	down	9.9E−10	10	7.0E−01	11	down	6.5E−02	6	2.8E−01
137	cell surface	GO	23	up	1.0E−09	13	5.3E−01	15	up	1.1E−07	9	7.3E−02
138	CD44 antigen	InterPro	1	up	1.1E−09	0		0			0	
139	CREB binding site geneset 4	Broad MSigDB − Regulatory Motifs	28	down	1.1E−09	7	5.2E−01	5	up	3.1E−02	8	8.2E−02
140	generation of a signal involved in cell−cell signaling	GO	18	down	1.2E−09	4	7.0E−01	11	down	2.1E−03	10	6.0E−03

BA10, Brodmann Area 10; PFC, prefrontal cortex; GO, the Gene Ontology.

"Biogroup name": A collection of genes that are associated with a specific biological function, pathway, or similar criteria.
"Source": Data source from which the biogroups are derived as follows:
Gene Ontology (biological processes, cellular components, molecular functions)

MSigDB (canonical pathways, positional gene sets, regulatory motif gene sets)
InterPro (protein families)
TargetScan (predicted miRNA targets)
"Common genes": Number of overlapping genes in the bioset and the biogroup
"Direction": direction of expression for each gene in the biosets (up-regulated or down-regulated)
"p-value": Probability that such an overlap would occur by chance assuming that there is no biological link between the bioset and the biogroup
"Common genes (opposite direction)": Number of overlapping genes between the bioset and the biogroup, but the direction of the expression change was differenct from each other

	Biogroups related to inflammation
up	up-regulated genes expressed in each bioset
down	down-regulated genes expressed in each bioset

Bioset vs Biogroups record downloaded from NextBio(2012/03/08 21:37:19)
Bioset: Brain BA10 from all schizophrenic samples _vs_ controls above control group mean pH6.5
Study: Post-mortem tissue from brain BA10 region of schizophrenic and control patients
Bioset vs Biogroups record downloaded from NextBio(2012/04/06 17:12:16)
Bioset: Prefrontal cortex from Shn2 KO mice _vs_ wildtype mice
Study: Shn2_PFC
https://www.nextbio.com/b/search/bg/?type=bioset&id=101611

Table 4. Genes differentially expressed in the dentate gyrus of Shn-2 KO mice.

Symbol	Description	Probe ID	Fold Change	P value	Rank
Tdo2	tryptophan 2,3-dioxygenase	1419093_at	-13.69	3.60E-06	1
Capn3	calpain 3	1426043_a_at	-8.22	3.90E-08	2
1441102_at		1441102_at	7.84	5.20E-06	3
Capn3	calpain 3	1433681_x_at	-6.74	1.20E-07	4
Rgs13	regulator of G-protein signaling 13	1442263_at	6.62	0.0010	5
Ifi205	interferon activated gene 205	1452348_s_at	6.28	6.50E-07	6
Wnk4	WNK lysine deficient protein kinase 4	1427196_at	5.82	6.60E-05	7
1426906_at		1426906_at	5.63	3.60E-07	8
Gpr115	G protein-coupled receptor 115	1429460_at	5.50	0.0005	9
Calb1	calbindin 1	1448738_at	-5.36	0.0010	10
Acvr1c	activin A receptor, type IC	1443225_at	5.30	8.00E-10	11
Mm.132167		1460043_at	-5.25	0.0004	12
Fxyd7	FXYD domain-containing ion transport regulator 7	1419200_at	5.23	0.0001	13
Prlr	prolactin receptor	1437397_at	5.22	3.70E-05	14
Batf3	basic leucine zipper transcription factor, ATF-like 3	1453076_at	5.16	0.0037	15
1456934_at		1456934_at	-5.13	0.0003	16
Ifi205	interferon activated gene 205	1452231_x_at	5.09	1.30E-06	17
Ntf3	neurotrophin 3	1434802_s_at	-4.91	0.0149	18
1438309_at		1438309_at	4.73	1.30E-09	19
Pcdh21	protocadherin 21	1418304_at	-4.72	0.0001	20
Gfra2	glial cell line derived neurotrophic factor family receptor alpha 2	1433716_x_at	-4.64	4.30E-05	21
1458836_at		1458836_at	-4.61	0.0003	22
Zcchc5	zinc finger, CCHC domain containing 5	1437355_at	-4.56	7.00E-05	23
6130401L20Rik	RIKEN cDNA 6130401L20 gene	1459246_at	-4.53	8.30E-06	24
Ryr1	ryanodine receptor 1, skeletal muscle	1427306_at	-4.48	8.20E-06	25
1449337_at		1449337_at	-4.44	1.60E-08	26
Aldh1a3	aldehyde dehydrogenase family 1, subfamily A3	1448789_at	4.35	0.0003	27
1457558_at		1457558_at	-4.35	1.30E-05	28
Gpr12	G-protein coupled receptor 12	1457702_at	-4.19	0.0005	29
Ifi203	interferon activated gene 203	1448775_at	4.16	3.40E-05	30
1442613_at		1442613_at	-4.11	2.40E-05	31
Wnt9a	wingless-type MMTV integration site 9A	1436978_at	-4.11	0.0057	32
Fam160a1	family with sequence similarity 160, member A1	1437371_at	-4.10	1.80E-05	33
Tdo2	tryptophan 2,3-dioxygenase	1455770_at	-4.05	1.50E-07	34
Nhlh1	nescient helix loop helix 1	1419533_at	4.04	0.0183	35
Necab3	N-terminal EF-hand calcium binding protein 3	1431946_a_at	4.00	0.0008	36
Igsf1	immunoglobulin superfamily, member 1	1433652_at	-3.93	9.60E-06	37
Fbln2	fibulin 2	1423407_a_at	3.91	0.0122	38
Kcnf1	potassium voltage-gated channel, subfamily F, member 1	1454768_at	-3.85	0.0003	39
Gm4658	predicted gene 4658	1443888_at	-3.84	4.10E-08	40
Spon1	spondin 1, (f-spondin) extracellular matrix protein	1451342_at	-3.80	2.50E-06	41
Ogn	osteoglycin	1419663_at	-3.79	0.0013	42
1452107_s_at		1452107_s_at	-3.73	0.0032	43
Calb1	calbindin 1	1417504_at	-3.70	0.0004	44
Ntf3	neurotrophin 3	1450803_at	-3.69	0.0097	45
Mm.293522		1457729_at	-3.69	0.0004	46
Sulf1	sulfatase 1	1438200_at	3.66	0.0021	47
1424415_s_at		1424415_s_at	-3.60	8.10E-06	48
Nrxn3	neurexin III	1445217_at	3.60	2.10E-05	49
AW547468		1440657_at	-3.59	0.0004	50
1429313_at		1429313_at	-3.59	1.10E-08	51
1452106_at		1452106_at	-3.58	0.0023	52

Chst9	carbohydrate (N-acetylgalactosamine 4-0) sulfotransferase 9	1431897_at	-3.56	0.0003	53
Grp	gastrin releasing peptide	1424525_at	3.56	0.0009	54
Nrxn3	neurexin III	1460101_at	3.51	8.00E-07	55
Tox3	TOX high mobility group box family member 3	1436600_at	-3.48	0.0004	56
Spink10	serine peptidase inhibitor, Kazal type 10	1438444_at	-3.44	1.20E-07	57
Pmepa1	prostate transmembrane protein, androgen induced 1	1422706_at	3.42	0.0053	58
Mm.91794		1443322_at	-3.41	0.0001	59
A930035E12Rik	RIKEN cDNA A930035E12 gene	1429906_at	3.40	1.60E-06	60
AK220484	cDNA sequence AK220484	1439341_at	-3.40	6.50E-05	61
Cntn3	contactin 3	1438628_x_at	-3.38	8.00E-07	62
Dsp	desmoplakin	1435493_at	-3.37	0.0060	63
Tgfa	transforming growth factor alpha	1421943_at	-3.37	1.40E-08	64
Dsp	desmoplakin	1435494_s_at	-3.36	0.0043	65
Pmepa1	prostate transmembrane protein, androgen induced 1	1422705_at	3.33	0.0037	66
A930041H05Rik	RIKEN cDNA A930041H05 gene	1442157_at	3.33	4.00E-06	67
Slc27a2	solute carrier family 27 (fatty acid transporter), member 2	1416316_at	-3.30	0.0001	68
Cpne9	copine family member IX	1454653_at	3.30	0.0016	69
Prlr	prolactin receptor	1448556_at	3.27	0.0001	70
Nrxn3	neurexin III	1432931_at	3.21	8.10E-07	71
Npy2r	neuropeptide Y receptor Y2	1417489_at	-3.21	0.0014	72
AU042950	expressed sequence AU042950	1458648_at	-3.17	7.40E-05	73
5930433N17Rik	RIKEN cDNA 5930433N17 gene	1440721_at	3.17	2.40E-06	74
Cst12	cystatin 12	1424627_at	3.13	0.0073	75
1436319_at		1436319_at	3.13	0.0029	76
Ryr1	ryanodine receptor 1, skeletal muscle	1457347_at	-3.13	2.80E-06	77
6330417G04Rik	RIKEN cDNA 6330417G04 gene	1440849_at	-3.12	8.70E-06	78
Klf10	Kruppel-like factor 10	1416029_at	3.09	0.0093	79
Clec1a	C-type lectin domain family 1, member a	1460039_at	-3.07	2.40E-06	80
A330050F15Rik	RIKEN cDNA A330050F15 gene	1441166_at	-3.07	3.10E-06	81
Pmepa1	prostate transmembrane protein, androgen induced 1	1452295_at	3.07	0.0017	82
Tagln	transgelin	1423505_at	3.06	0.0200	83
Gpr12	G-protein coupled receptor 12	1449472_at	-3.01	0.0007	84
Tesc	tescalcin	1418743_a_at	2.96	9.10E-08	85
Iyd	iodotyrosine deiodinase	1451547_at	-2.94	2.20E-07	86
Itga4	integrin alpha 4	1436037_at	-2.94	0.0003	87
Bcl6	B-cell leukemia/lymphoma 6	1421818_at	-2.94	5.60E-06	88
9030425E11Rik	RIKEN cDNA 9030425E11 gene	1448250_at	2.93	1.70E-05	89
Rspo3	R-spondin 3 homolog (Xenopus laevis)	1455607_at	-2.92	0.0004	90
Col3a1	collagen, type III, alpha 1	1427883_a_at	2.91	0.0205	91
Rgs2	regulator of G-protein signaling 2	1447830_s_at	2.90	0.0200	92
1448251_at		1448251_at	2.90	2.90E-06	93
Fat4	FAT tumor suppressor homolog 4 (Drosophila)	1460574_at	-2.89	0.0014	94
Necab3	N-terminal EF-hand calcium binding protein 3	1447907_x_at	2.87	0.0004	95
6130401L20Rik	RIKEN cDNA 6130401L20 gene	1430430_at	-2.86	1.10E-05	96
Fat4	FAT tumor suppressor homolog 4 (Drosophila)	1459749_s_at	-2.86	0.0025	97
Cnih3	cornichon homolog 3 (Drosophila)	1419517_at	-2.85	0.0115	98
Ifi203	interferon activated gene 203	1419858_at	2.84	0.0048	99
Tspan18	tetraspanin 18	1442174_at	-2.84	5.60E-05	100
Gfra2	glial cell line derived neurotrophic factor family receptor alpha 2	1459847_x_at	-2.84	0.0002	101
1429905_at		1429905_at	-2.84	0.0054	102
Ogn	osteoglycin	1419662_at	-2.83	0.0005	103
P2rx7	purinergic receptor P2X, ligand-gated ion channel, 7	1439787_at	2.83	0.0002	104
Trhr	thyrotropin releasing hormone receptor	1449571_at	-2.83	0.0015	105
Hrk	harakiri, BCL2 interacting protein (contains only BH3 domain)	1439854_at	-2.82	0.0010	106

Rasgrp1	RAS guanyl releasing protein 1	1431749_a_at	2.81	0.0009	107
1438375_at		1438375_at	2.80	0.0179	108
Arl4d	ADP-ribosylation factor-like 4D	1418250_at	2.80	0.0474	109
Col22a1	collagen, type XXII, alpha 1	1453084_s_at	-2.78	5.50E-06	110
Ctgf	connective tissue growth factor	1416953_at	2.77	0.0262	111
Gfap	glial fibrillary acidic protein	1426509_s_at	2.75	0.0126	112
BI076661		1443253_at	-2.74	3.10E-05	113
Gfap	glial fibrillary acidic protein	1426508_at	2.72	0.0150	114
H2-Aa	histocompatibility 2, class II antigen A, alpha	1435290_x_at	2.71	0.0026	115
Rreb1	ras responsive element binding protein 1	1428657_at	-2.70	1.20E-05	116
Parp8	poly (ADP-ribose) polymerase family, member 8	1451474_a_at	2.70	2.00E-05	117
Gsg1l	GSG1-like	1436013_at	2.68	0.0020	118
Grb14	growth factor receptor bound protein 14	1417673_at	-2.68	0.0009	119
Fmod	fibromodulin	1456084_x_at	2.68	0.0160	120
Rgs2	regulator of G-protein signaling 2	1419247_at	2.67	0.0137	121
Tesc	tescalcin	1418744_s_at	2.67	4.80E-08	122
Tmsb10	thymosin, beta 10	1417219_s_at	2.66	1.10E-06	123
Tmsb10	thymosin, beta 10	1436902_x_at	2.64	1.50E-07	124
Vwf	Von Willebrand factor homolog	1435386_at	2.63	0.0077	125
Frmd4b	FERM domain containing 4B	1452123_s_at	-2.63	0.0014	126
Orc4l	origin recognition complex, subunit 4-like (S. cerevisiae)	1439643_at	-2.62	7.70E-05	127
Pla2g4e	phospholipase A2, group IVE	1429862_at	-2.62	0.0001	128
Stc1	stanniocalcin 1	1450448_at	-2.62	0.0001	129
Htr1a	5-hydroxytryptamine (serotonin) receptor 1A	1438710_at	-2.62	2.20E-07	130
Clec1a	C-type lectin domain family 1, member a	1456318_at	-2.61	3.20E-07	131
Pip5k1b	phosphatidylinositol-4-phosphate 5-kinase, type 1 beta	1450389_s_at	-2.61	0.0005	132
Gprc5c	G protein-coupled receptor, family C, group 5, member C	1452947_at	2.61	0.0055	133
Unc5d	unc-5 homolog D (C. elegans)	1440484_at	2.61	9.20E-05	134
1441823_at		1441823_at	2.58	0.0018	135
Gal	galanin	1460668_at	2.58	0.0369	136
Ccdc88c	coiled-coil domain containing 88C	1427138_at	2.57	0.0036	137
Rgs2	regulator of G-protein signaling 2	1419248_at	2.56	0.0142	138
Frmd4b	FERM domain containing 4B	1438169_a_at	-2.56	0.0046	139
Cdkn1a	cyclin-dependent kinase inhibitor 1A (P21)	1421679_a_at	2.54	0.0254	140
Fam129b	family with sequence similarity 129, member B	1426812_a_at	2.53	0.0010	141
Il20rb	interleukin 20 receptor beta	1437876_at	-2.53	0.0045	142
Rasgrp1	RAS guanyl releasing protein 1	1450143_at	2.49	0.0027	143
Gstm7	glutathione S-transferase, mu 7	1419072_at	-2.49	0.0002	144
1435311_s_at		1435311_s_at	2.48	1.20E-05	145
4930578M01Rik	RIKEN cDNA 4930578M01 gene	1456421_at	-2.48	9.30E-05	146
Pdzrn4	PDZ domain containing RING finger 4	1456512_at	-2.48	3.70E-07	147
Cdkn1a	cyclin-dependent kinase inhibitor 1A (P21)	1424638_at	2.48	0.0147	148
Cd83	CD83 antigen	1416111_at	-2.47	2.90E-05	149
Rwdd3	RWD domain containing 3	1430167_a_at	-2.47	1.00E-06	150
Pip5k1b	phosphatidylinositol-4-phosphate 5-kinase, type 1 beta	1421834_at	-2.47	0.0006	151
Itga4	integrin alpha 4	1456498_at	-2.46	8.10E-05	152
1435771_at		1435771_at	2.46	0.0014	153
Lhx9	LIM homeobox protein 9	1441313_x_at	-2.46	0.0010	154
Ifi203	interferon activated gene 203	1451567_a_at	2.46	4.10E-06	155
C4b	complement component 4B (Childo blood group)	1418021_at	2.46	0.0028	156
Ahcyl2	S-adenosylhomocysteine hydrolase-like 2	1443468_at	-2.45	0.0011	157
6030442H21Rik	RIKEN cDNA 6030442H21 gene	1432746_at	-2.45	1.90E-06	158
Spata13	spermatogenesis associated 13	1437865_at	2.44	0.0018	159
Matn2	matrilin 2	1419442_at	-2.44	0.0072	160

Ap1s3	adaptor-related protein complex AP-1, sigma 3	1455735_at	-2.44	1.40E-06	161
Nrxn3	neurexin III	1457212_at	2.44	2.70E-06	162
Grik3	glutamate receptor, ionotropic, kainate 3	1440177_at	-2.43	0.0157	163
Slc39a6	solute carrier family 39 (metal ion transporter), member 6	1424674_at	-2.43	1.40E-09	164
Ccbe1	collagen and calcium binding EGF domains 1	1440053_at	-2.42	6.90E-07	165
Fst	follistatin	1434458_at	-2.42	0.0016	166
Ccbe1	collagen and calcium binding EGF domains 1	1437385_at	-2.42	5.20E-07	167
1455179_at		1455179_at	2.42	0.0215	168
Slc39a6	solute carrier family 39 (metal ion transporter), member 6	1441949_x_at	-2.41	1.20E-05	169
Scn9a	sodium channel, voltage-gated, type IX, alpha	1442810_x_at	-2.40	0.0013	170
Tgfb3	transforming growth factor, beta 3	1417455_at	2.40	0.0048	171
Pik3r1	phosphatidylinositol 3-kinase, regulatory subunit, polypeptide 1 (p8	1425514_at	2.40	0.0085	172
Gm715	predicted gene 715	1445503_at	2.39	0.0029	173
Sv2c	synaptic vesicle glycoprotein 2c	1453715_at	2.39	0.0001	174
BG061080		1453841_at	2.39	3.40E-05	175
AW551984	expressed sequence AW551984	1433434_at	2.39	0.0116	176
Slc39a6	solute carrier family 39 (metal ion transporter), member 6	1424675_at	-2.39	3.90E-05	177
Il16	interleukin 16	1448686_at	-2.38	0.0008	178
Ror1	receptor tyrosine kinase-like orphan receptor 1	1442067_at	-2.38	5.00E-05	179
Pcolce	procollagen C-endopeptidase enhancer protein	1437165_a_at	2.38	0.0129	180
1439665_at		1439665_at	-2.37	3.20E-05	181
Mgp	matrix Gla protein	1448416_at	2.37	0.0055	182
Matn2	matrilin 2	1455978_a_at	-2.37	0.0030	183
Col27a1	collagen, type XXVII, alpha 1	1429549_at	2.36	0.0096	184
Col27a1	collagen, type XXVII, alpha 1	1453191_at	2.36	0.0091	185
Tmsb10	thymosin, beta 10	1437185_s_at	2.35	6.50E-08	186
Cp	ceruloplasmin	1448734_at	2.35	0.0044	187
Plcb4	phospholipase C, beta 4	1425338_at	2.35	0.0014	188
Acvr1c	activin A receptor, type IC	1428032_at	2.35	1.80E-05	189
Ddit4l	DNA-damage-inducible transcript 4-like	1439332_at	-2.34	1.60E-06	190
Rreb1	ras responsive element binding protein 1	1438216_at	-2.34	4.30E-05	191
1436329_at		1436329_at	2.33	0.0006	192
Gng4	guanine nucleotide binding protein (G protein), gamma 4	1447669_s_at	-2.32	0.0027	193
Pip5k1b	phosphatidylinositol-4-phosphate 5-kinase, type 1 beta	1421833_at	-2.32	0.0004	194
Nid1	nidogen 1	1416808_at	2.30	0.0081	195
Wisp1	WNT1 inducible signaling pathway protein 1	1448594_at	2.29	0.0218	196
1421595_at		1421595_at	-2.29	0.0018	197
Bcl6	B-cell leukemia/lymphoma 6	1450381_a_at	-2.28	3.30E-06	198
Stard13	StAR-related lipid transfer (START) domain containing 13	1452604_at	-2.28	1.10E-06	199
Spata13	spermatogenesis associated 13	1454656_at	2.28	0.0019	200
Ccnd1	cyclin D1	1417419_at	2.28	6.50E-05	201
Rwdd3	RWD domain containing 3	1451809_s_at	-2.27	1.10E-05	202
Crym	crystallin, mu	1416776_at	-2.27	0.0067	203
Acvr1	activin A receptor, type 1	1448460_at	2.26	0.0027	204
Ddit4l	DNA-damage-inducible transcript 4-like	1444139_at	-2.26	5.30E-07	205
Il16	interleukin 16	1417391_a_at	-2.24	0.0001	206
Fndc1	fibronectin type III domain containing 1	1453321_at	-2.24	0.0029	207
Acvr1	activin A receptor, type 1	1416786_at	2.24	0.0122	208
1437382_at		1437382_at	-2.24	6.50E-05	209
Lhx9	LIM homeobox protein 9	1419324_at	-2.24	0.0065	210
Fxyd5	FXYD domain-containing ion transport regulator 5	1418296_at	2.24	0.0030	211
Itga8	integrin alpha 8	1454966_at	-2.24	0.0072	212
Aff3	AF4/FMR2 family, member 3	1441172_at	2.24	0.0003	213
Col1a2	collagen, type I, alpha 2	1450857_a_at	2.24	0.0114	214

Rasgrp1	RAS guanyl releasing protein 1	1421176_at	2.23	0.0099	215
Pnck	pregnancy upregulated non-ubiquitously expressed CaM kinase	1422711_a_at	-2.23	0.0081	216
Lrrc6	leucine rich repeat containing 6 (testis)	1420660_at	2.23	2.90E-05	217
Aplnr	apelin receptor	1438651_a_at	2.22	0.0229	218
ENSMUSG0000006	predicted gene, ENSMUSG00000068790	1452731_x_at	-2.22	3.80E-07	219
Dusp14	dual specificity phosphatase 14	1431422_a_at	2.22	0.0251	220
1443187_at		1443187_at	-2.21	0.0002	221
Spp1	secreted phosphoprotein 1	1449254_at	2.21	0.0465	222
Kcnk2	potassium channel, subfamily K, member 2	1449158_at	-2.21	0.0010	223
AI663975	expressed sequence AI663975	1440084_at	-2.21	0.0013	224
P2rx7	purinergic receptor P2X, ligand-gated ion channel, 7	1419853_a_at	2.21	0.0170	225
Mkx	mohawk homeobox	1437492_at	-2.21	0.0002	226
Slc4a4	solute carrier family 4 (anion exchanger), member 4	1421225_a_at	-2.20	2.00E-06	227
Pacsin2	protein kinase C and casein kinase substrate in neurons 2	1417810_a_at	-2.20	1.50E-05	228
Trdn	triadin	1451801_at	-2.20	9.90E-05	229
1435261_at		1435261_at	-2.20	0.0041	230
Epha10	Eph receptor A10	1436093_at	-2.20	0.0011	231
1435310_at		1435310_at	2.19	7.10E-06	232
Rbm24	RNA binding motif protein 24	1454752_at	-2.19	9.70E-05	233
B3galt5	UDP-Gal:betaGlcNAc beta 1,3-galactosyltransferase, polypeptide 5	1428397_at	-2.19	0.0048	234
1456214_at		1456214_at	2.18	1.80E-05	235
Pmepa1	prostate transmembrane protein, androgen induced 1	1438783_at	2.18	0.0002	236
1460009_at		1460009_at	2.18	0.0098	237
EG240055	predicted gene, EG240055	1435564_at	-2.18	0.0017	238
Frzb	frizzled-related protein	1448424_at	-2.17	0.0009	239
1458240_at		1458240_at	-2.17	0.0008	240
Cp	ceruloplasmin	1455393_at	2.17	0.0146	241
Osmr	oncostatin M receptor	1418674_at	2.17	0.0334	242
Mn1	meningioma 1	1454867_at	-2.17	0.0345	243
Nrxn3	neurexin III	1438193_at	2.17	5.60E-05	244
Gda	guanine deaminase	1422868_s_at	-2.17	0.0063	245
Ccnd1	cyclin D1	1417420_at	2.16	1.40E-05	246
BB557941	expressed sequence BB557941	1443368_at	-2.16	4.40E-05	247
Cda	cytidine deaminase	1427357_at	2.16	0.0003	248
1440918_at		1440918_at	-2.16	0.0002	249
Gpr68	G protein-coupled receptor 68	1455000_at	2.15	0.0053	250
Rhoj	ras homolog gene family, member J	1418892_at	2.14	0.0201	251
Frmd4b	FERM domain containing 4B	1426594_at	-2.14	0.0008	252
Mm.385139		1440291_at	2.14	5.00E-06	253
Ccnd1	cyclin D1	1448698_at	2.14	5.70E-05	254
Igfbp5	insulin-like growth factor binding protein 5	1452114_s_at	-2.14	0.0023	255
Ecm2	extracellular matrix protein 2, female organ and adipocyte specific	1440096_at	-2.14	0.0498	256
ENSMUSG0000006	predicted gene, ENSMUSG00000068790	1428301_at	-2.14	1.40E-08	257
Pik3r1	phosphatidylinositol 3-kinase, regulatory subunit, polypeptide 1 (p8	1451737_at	2.13	0.0071	258
Trpm3	transient receptor potential cation channel, subfamily M, member 3	1445555_at	-2.13	0.0012	259
Lor	loricrin	1448745_s_at	-2.13	3.10E-05	260
Gdf10	growth differentiation factor 10	1424007_at	-2.13	0.0019	261
Fnip2	folliculin interacting protein 2	1439189_at	-2.12	0.0002	262
1110002E22Rik	RIKEN cDNA 1110002E22 gene	1447870_x_at	-2.12	0.0023	263
Cp	ceruloplasmin	1417494_a_at	2.12	0.0133	264
Vwa3b	von Willebrand factor A domain containing 3B	1453250_at	-2.12	3.80E-05	265
Grem2	gremlin 2 homolog, cysteine knot superfamily (Xenopus laevis)	1418492_at	-2.11	8.10E-05	266
Parp3	poly (ADP-ribose) polymerase family, member 3	1451969_s_at	2.11	0.0208	267
Kcna5	potassium voltage-gated channel, shaker-related subfamily, membe	1417680_at	-2.10	0.0012	268

Anxa2	annexin A2	1419091_a_at	2.10	0.0273	269
Smpdl3b	sphingomyelin phosphodiesterase, acid-like 3B	1417300_at	-2.10	0.0002	270
Mm.326876		1442556_at	-2.10	0.0106	271
1455137_at		1455137_at	-2.10	8.30E-05	272
Glra2	glycine receptor, alpha 2 subunit	1434098_at	-2.09	2.90E-05	273
1437442_at		1437442_at	2.09	1.80E-05	274
Aldh1a2	aldehyde dehydrogenase family 1, subfamily A2	1422789_at	2.09	0.0118	275
Rasgrp1	RAS guanyl releasing protein 1	1434295_at	2.09	0.0022	276
Cebpb	CCAAT/enhancer binding protein (C/EBP), beta	1418901_at	2.09	0.0005	277
Rfx3	regulatory factor X, 3 (influences HLA class II expression)	1441702_at	-2.09	0.0024	278
Trpm3	transient receptor potential cation channel, subfamily M, member 3	1430268_at	-2.08	0.0011	279
Ddit4l	DNA-damage-inducible transcript 4-like	1451751_at	-2.08	5.50E-05	280
Cebpb	CCAAT/enhancer binding protein (C/EBP), beta	1427844_a_at	2.08	0.0016	281
2900017F05Rik	RIKEN cDNA 2900017F05 gene	1430096_at	-2.07	1.30E-05	282
Mm.313328		1443157_at	-2.07	4.20E-05	283
Gda	guanine deaminase	1435748_at	-2.07	0.0067	284
1453424_at		1453424_at	-2.07	0.0092	285
Fbxo7	F-box protein 7	1443006_at	2.07	0.0011	286
1447040_at		1447040_at	-2.07	9.70E-05	287
1456923_at		1456923_at	-2.07	7.00E-05	288
Glis3	GLIS family zinc finger 3	1430353_at	-2.07	0.0047	289
Zbtb16	zinc finger and BTB domain containing 16	1459557_at	-2.06	0.0188	290
Socs2	suppressor of cytokine signaling 2	1449109_at	2.06	0.0015	291
D16Ertd472e	DNA segment, Chr 16, ERATO Doi 472, expressed	1429897_a_at	-2.06	0.0364	292
Rapgef5	Rap guanine nucleotide exchange factor (GEF) 5	1455840_at	-2.05	0.0002	293
Mycn	v-myc myelocytomatosis viral related oncogene, neuroblastoma de	1417155_at	-2.05	0.0070	294
Onecut2	one cut domain, family member 2	1444980_at	-2.05	0.0006	295
Lmna	lamin A	1457670_s_at	2.05	0.0056	296
1436125_at		1436125_at	-2.05	0.0413	297
4933427G17Rik	RIKEN cDNA 4933427G17 gene	1431905_s_at	-2.05	0.0079	298
1456137_at		1456137_at	2.05	7.10E-05	299
Rgnef	Rho-guanine nucleotide exchange factor	1419457_at	-2.05	0.0007	300
Arsj	arylsulfatase J	1457827_at	2.05	0.0148	301
Ifitm3	interferon induced transmembrane protein 3	1423754_at	2.04	0.0134	302
2610027H17Rik	RIKEN cDNA 2610027H17 gene	1442445_at	-2.04	0.0074	303
Ier5	immediate early response 5	1417612_at	2.04	0.0201	304
Homer2	homer homolog 2 (Drosophila)	1424367_a_at	-2.04	1.60E-06	305
Miat	myocardial infarction associated transcript (non-protein coding)	1455325_at	-2.03	0.0139	306
Marcksl1	MARCKS-like 1	1437226_x_at	-2.03	0.0057	307
Frzb	frizzled-related protein	1416658_at	-2.03	0.0010	308
Itga8	integrin alpha 8	1427489_at	-2.03	0.0086	309
1433788_at		1433788_at	2.03	3.40E-06	310
Ahcyl2	S-adenosylhomocysteine hydrolase-like 2	1459537_at	-2.03	0.0020	311
1418507_s_at		1418507_s_at	2.03	0.0063	312
Cacng5	calcium channel, voltage-dependent, gamma subunit 5	1434785_at	-2.03	0.0003	313
Ppp1r14c	protein phosphatase 1, regulatory (inhibitor) subunit 14c	1443799_at	-2.02	0.0011	314
11-Mar	membrane-associated ring finger (C3HC4) 11	1455947_at	2.02	0.0468	315
Sidt1	SID1 transmembrane family, member 1	1426550_at	-2.02	0.0002	316
Fbln5	fibulin 5	1416164_at	2.01	0.0002	317
Kcnq3	potassium voltage-gated channel, subfamily Q, member 3	1458421_at	2.01	0.0056	318
Acvr1	activin A receptor, type 1	1457551_at	2.01	0.0015	319
Rbm24	RNA binding motif protein 24	1456180_at	-2.01	5.60E-05	320
1419730_at		1419730_at	-2.01	0.0015	321
Cyp11a1	cytochrome P450, family 11, subfamily a, polypeptide 1	1448804_at	2.01	0.0212	322

Lamb1-1	laminin B1 subunit 1	1424114_s_at	-2.01	1.80E-06	323
Aff3	AF4/FMR2 family, member 3	1433939_at	2.01	0.0002	324
Inha	inhibin alpha	1422728_at	-2.01	0.0230	325
Rgnef	Rho-guanine nucleotide exchange factor	1419458_at	-2.00	0.0011	326
Gda	guanine deaminase	1435749_at	-2.00	0.0084	327
1110002E22Rik	RIKEN cDNA 1110002E22 gene	1430786_at	-2.00	0.0016	328
Myh14	myosin, heavy polypeptide 14	1428835_at	2.00	0.0315	329
1438824_at		1438824_at	2.00	0.0071	330
Ifi205	interferon activated gene 205	1452349_x_at	2.00	0.0002	331
Slc6a15	solute carrier family 6 (neurotransmitter transporter), member 15	1426712_at	-1.99	4.60E-06	332
Prdm8	PR domain containing 8	1455925_at	-1.99	0.0012	333
Lphn3	latrophilin 3	1459295_at	1.99	0.0154	334
1439899_at		1439899_at	-1.99	0.0263	335
Scn4b	sodium channel, type IV, beta	1434008_at	1.99	0.0254	336
Rhou	ras homolog gene family, member U	1449027_at	-1.98	8.20E-07	337
1700011I03Rik	RIKEN cDNA 1700011I03 gene	1438059_at	1.98	0.0025	338
LOC626082	hypothetical protein LOC626082	1446282_at	-1.98	0.0023	339
Rfx3	regulatory factor X, 3 (influences HLA class II expression)	1441253_at	-1.98	0.0014	340
BM115624		1441746_at	1.98	0.0049	341
Kl	klotho	1423400_at	-1.98	0.0001	342
1446224_at		1446224_at	-1.97	0.0332	343
Wisp1	WNT1 inducible signaling pathway protein 1	1448593_at	1.97	0.0226	344
Rasgrf1	RAS protein-specific guanine nucleotide-releasing factor 1	1424734_at	-1.97	0.0037	345
Fmod	fibromodulin	1437718_x_at	1.97	0.0316	346
BC048546	cDNA sequence BC048546	1436503_at	-1.97	3.40E-06	347
1458140_at		1458140_at	-1.96	0.0011	348
Map2k6	mitogen-activated protein kinase kinase 6	1441482_at	-1.96	0.0454	349
6430597G12Rik	RIKEN cDNA 6430597G12 gene	1431153_at	1.96	0.0008	350
Lpar4	lysophosphatidic acid receptor 4	1452424_at	-1.96	0.0003	351
Bgn	biglycan	1416405_at	1.95	0.0257	352
Bgn	biglycan	1448323_a_at	1.95	0.0182	353
Fmod	fibromodulin	1437685_x_at	1.95	0.0192	354
AU023617	expressed sequence AU023617	1444974_at	-1.95	0.0169	355
Baiap3	BAI1-associated protein 3	1427509_at	-1.95	0.0016	356
Plcb4	phospholipase C, beta 4	1425339_at	1.94	0.0002	357
Itpr1	inositol 1,4,5-triphosphate receptor 1	1460203_at	-1.94	0.0004	358
Adcy1	adenylate cyclase 1	1445359_at	-1.94	6.50E-06	359
5830456J23Rik	RIKEN cDNA 5830456J23 gene	1433169_at	-1.93	0.0003	360
1435424_x_at		1435424_x_at	-1.93	0.0057	361
1460038_at		1460038_at	-1.93	0.0059	362
9330120H11Rik	RIKEN cDNA 9330120H11 gene	1457671_at	-1.93	1.50E-06	363
Cdh13	cadherin 13	1423551_at	-1.92	0.0002	364
1457440_at		1457440_at	-1.92	0.0004	365
Slc16a10	solute carrier family 16 (monocarboxylic acid transporters), membe	1457851_at	-1.92	0.0004	366
Mm.381253		1441430_at	1.92	0.0030	367
BM247146		1438295_at	1.92	0.0013	368
Npnt	nephronectin	1426560_a_at	-1.92	0.0008	369
Cp	ceruloplasmin	1417495_x_at	1.92	0.0296	370
Lphn3	latrophilin 3	1427809_at	1.91	0.0115	371
1428891_at		1428891_at	-1.91	0.0004	372
9830166K06Rik	RIKEN cDNA 9830166K06 gene	1457389_at	-1.91	0.0064	373
Iigp1	interferon inducible GTPase 1	1419043_a_at	-1.91	0.0030	374
Pdzrn3	PDZ domain containing RING finger 3	1416846_a_at	-1.91	0.0007	375
Gadd45a	growth arrest and DNA-damage-inducible 45 alpha	1449519_at	1.91	0.0311	376

1436996_x_at		1436996_x_at	1.91	0.0260	377
Serpinf1	serine (or cysteine) peptidase inhibitor, clade F, member 1	1416168_at	1.91	0.0315	378
Isoc1	isochorismatase domain containing 1	1425050_at	−1.90	0.0016	379
Rabgap1l	RAB GTPase activating protein 1-like	1429196_at	1.90	0.0001	380
Zfp521	zinc finger protein 521	1451332_at	1.90	0.0001	381
1300014I06Rik	RIKEN cDNA 1300014I06 gene	1428851_at	−1.90	7.40E-06	382
Usp29	ubiquitin specific peptidase 29	1419237_at	1.90	6.60E-06	383
Epha3	Eph receptor A3	1443273_at	1.90	0.0003	384
Ifitm1	interferon induced transmembrane protein 1	1424254_at	1.90	0.0215	385
Cobl	cordon-bleu	1434917_at	1.90	0.0083	386
Gpc3	glypican 3	1450990_at	−1.90	0.0455	387
Srl	sarcalumenin	1436867_at	−1.90	0.0021	388
Adcy2	adenylate cyclase 2	1444633_at	1.90	0.0002	389
AK220484	cDNA sequence AK220484	1442703_at	−1.89	1.60E-05	390
9330154F10Rik	RIKEN cDNA 9330154F10 gene	1433325_at	1.89	0.0056	391
1437574_at		1437574_at	1.89	0.0124	392
Igfbp7	insulin-like growth factor binding protein 7	1423584_at	1.89	0.0162	393
Itpr1	inositol 1,4,5-triphosphate receptor 1	1417279_at	−1.89	5.40E-05	394
C230098O21Rik	RIKEN cDNA C230098O21 gene	1433988_s_at	−1.89	0.0009	395
Cntn3	contactin 3	1420739_at	−1.89	1.40E-05	396
Chn2	chimerin (chimaerin) 2	1428573_at	−1.89	0.0069	397
Otop2	otopetrin 2	1443043_at	1.88	0.0389	398
Synm	synemin, intermediate filament protein	1457275_at	−1.88	0.0003	399
Zfhx4	zinc finger homeodomain 4	1437556_at	−1.88	0.0002	400
Ccbe1	collagen and calcium binding EGF domains 1	1439327_at	−1.88	8.90E-05	401
Klhl32	kelch-like 32 (Drosophila)	1458375_at	−1.88	0.0010	402
Smo	smoothened homolog (Drosophila)	1427048_at	−1.88	0.0012	403
C230034O21Rik	RIKEN cDNA C230034O21 gene	1439707_at	−1.88	0.0011	404
Isoc1	isochorismatase domain containing 1	1425052_at	−1.88	0.0040	405
1435458_at		1435458_at	1.88	0.0233	406
1431402_at		1431402_at	−1.88	0.0034	407
Postn	periostin, osteoblast specific factor	1423606_at	1.87	0.0031	408
Gfra1	glial cell line derived neurotrophic factor family receptor alpha 1	1450440_at	−1.87	0.0144	409
Rbm24	RNA binding motif protein 24	1458624_at	−1.87	0.0008	410
Rasgrf2	RAS protein-specific guanine nucleotide-releasing factor 2	1421621_at	−1.87	0.0020	411
1440555_at		1440555_at	1.87	0.0029	412
Foxd1	forkhead box D1	1418876_at	1.87	0.0206	413
Mm.381347		1445207_at	−1.87	0.0003	414
Thbd	thrombomodulin	1448529_at	1.87	0.0064	415
Lamb1-1	laminin B1 subunit 1	1424113_at	−1.87	0.0005	416
Stat3	signal transducer and activator of transcription 3	1426587_a_at	1.87	1.80E-05	417
1700086L19Rik	RIKEN cDNA 1700086L19 gene	1455085_at	−1.87	0.0069	418
Mrc1	mannose receptor, C type 1	1450430_at	1.87	0.0064	419
Syt10	synaptotagmin X	1450347_at	−1.87	1.10E-05	420
AW146388		1454388_at	−1.86	0.0026	421
Fst	follistatin	1421365_at	−1.86	0.0011	422
Fbln1	fibulin 1	1422540_at	−1.86	4.80E-05	423
Tgfbi	transforming growth factor, beta induced	1448123_s_at	1.86	0.0226	424
1438470_at		1438470_at	1.86	0.0058	425
1443086_at		1443086_at	−1.86	6.50E-05	426
Fmod	fibromodulin	1415939_at	1.86	0.0209	427
D16Ertd472e	DNA segment, Chr 16, ERATO Doi 472, expressed	1451466_at	−1.86	0.0466	428
Slc20a1	solute carrier family 20, member 1	1448568_a_at	1.86	1.10E-05	429
Chst15	carbohydrate (N-acetylgalactosamine 4-sulfate 6-O) sulfotransfer	1452092_at	−1.86	0.0038	430

Agxt2l1	alanine-glyoxylate aminotransferase 2-like 1	1452975_at	1.86	0.0266	431
BC046404	cDNA sequence BC046404	1436195_at	1.85	6.70E-06	432
Kcns2	K+ voltage-gated channel, subfamily S, 2	1421342_at	1.85	0.0002	433
Slc30a3	solute carrier family 30 (zinc transporter), member 3	1460654_at	1.85	4.90E-05	434
Lrrtm1	leucine rich repeat transmembrane neuronal 1	1455883_a_at	-1.85	4.40E-05	435
Apod	apolipoprotein D	1416371_at	1.85	0.0229	436
Marcksl1	MARCKS-like 1	1435627_x_at	-1.85	0.0058	437
1444275_at		1444275_at	-1.85	1.50E-05	438
Rab26	RAB26, member RAS oncogene family	1435500_at	-1.85	0.0115	439
Ncapg	non-SMC condensin I complex, subunit G	1455686_at	-1.85	0.0250	440
Trdn	triadin	1426143_at	-1.84	0.0025	441
Kcnt2	potassium channel, subfamily T, member 2	1440030_at	1.84	0.0013	442
1441127_at		1441127_at	-1.84	3.00E-05	443
Lyz2	lysozyme 2	1423547_at	1.84	0.0135	444
AI663975	expressed sequence AI663975	1442725_at	-1.84	0.0033	445
Fibcd1	fibrinogen C domain containing 1	1435482_at	-1.84	0.0427	446
6330406I15Rik	RIKEN cDNA 6330406I15 gene	1426937_at	1.84	0.0005	447
1438724_at		1438724_at	-1.84	0.0034	448
5330423I11Rik	RIKEN cDNA 5330423I11 gene	1431473_at	-1.84	0.0109	449
Plscr2	phospholipid scramblase 2	1448961_at	1.84	0.0168	450
Fmod	fibromodulin	1437324_x_at	1.84	0.0190	451
Ccdc3	coiled-coil domain containing 3	1428549_at	1.84	0.0197	452
F13a1	coagulation factor XIII, A1 subunit	1448929_at	1.84	0.0169	453
Marcksl1	MARCKS-like 1	1435415_x_at	-1.83	0.0039	454
Col22a1	collagen, type XXII, alpha 1	1429280_at	-1.83	0.0004	455
Slit2	slit homolog 2 (Drosophila)	1440650_at	-1.83	0.0005	456
Dpyd	dihydropyrimidine dehydrogenase	1427946_s_at	-1.83	1.10E-05	457
Col1a2	collagen, type I, alpha 2	1423110_at	1.83	0.0054	458
Onecut2	one cut domain, family member 2	1460044_at	-1.83	0.0003	459
Fbn1	fibrillin 1	1460208_at	-1.83	0.0003	460
3-Mar	membrane-associated ring finger (C3HC4) 3	1436614_at	1.83	0.0208	461
Zfp703	zinc finger protein 703	1436026_at	1.82	0.0208	462
Hrasls	HRAS-like suppressor	1428991_at	1.82	0.0108	463
Mkx	mohawk homeobox	1446811_at	-1.82	0.0102	464
9130213B05Rik	RIKEN cDNA 9130213B05 gene	1424214_at	-1.82	0.0003	465
Kcnt2	potassium channel, subfamily T, member 2	1459971_at	1.82	0.0002	466
Lcorl	ligand dependent nuclear receptor corepressor-like	1446571_at	-1.82	0.0419	467
BB637274		1431248_at	-1.82	0.0046	468
1427086_at		1427086_at	-1.82	1.00E-04	469
Slit2	slit homolog 2 (Drosophila)	1424659_at	-1.82	0.0005	470
1439709_at		1439709_at	-1.82	0.0343	471
Sphkap	SPHK1 interactor, AKAP domain containing	1446364_at	-1.81	0.0011	472
Olfml2b	olfactomedin-like 2B	1423915_at	-1.81	0.0339	473
Kndc1	kinase non-catalytic C-lobe domain (KIND) containing 1	1428599_at	1.81	2.30E-07	474
Il11ra1	interleukin 11 receptor, alpha chain 1	1417505_s_at	-1.81	7.20E-07	475
Plcb4	phospholipase C, beta 4	1441531_at	1.81	0.0036	476
2900064F13Rik	RIKEN cDNA 2900064F13 gene	1432813_at	1.81	0.0038	477
1439947_at		1439947_at	1.81	0.0249	478
Crtac1	cartilage acidic protein 1	1426606_at	1.81	8.00E-05	479
Mpzl2	myelin protein zero-like 2	1416236_a_at	1.80	0.0262	480
A230067G21Rik	RIKEN cDNA A230067G21 gene	1455750_at	-1.80	0.0039	481
Adamts3	a disintegrin-like and metallopeptidase (reprolysin type) with throm	1441693_at	-1.80	0.0018	482
Actn2	actinin alpha 2	1456968_at	-1.80	0.0007	483
Rassf3	Ras association (RalGDS/AF-6) domain family member 3	1448546_at	1.80	0.0024	484

Aff3	AF4/FMR2 family, member 3	1453395_at	1.80	0.0025	485
Nrxn3	neurexin III	1444700_at	1.80	4.60E-05	486
Slc27a3	solute carrier family 27 (fatty acid transporter), member 3	1427180_at	1.80	0.0310	487
1458479_at		1458479_at	-1.80	0.0103	488
AW554440		1446596_at	-1.80	0.0076	489
Popdc3	popeye domain containing 3	1423856_at	-1.79	0.0091	490
1451430_at		1451430_at	-1.79	0.0113	491
1441499_at		1441499_at	-1.79	2.80E-05	492
Txnrd3	thioredoxin reductase 3	1449623_at	1.79	0.0391	493
B3galt5	UDP-Gal:betaGlcNAc beta 1,3-galactosyltransferase, polypeptide 5	1428398_at	-1.79	0.0056	494
Bcl6	B-cell leukemia/lymphoma 6	1453595_at	-1.79	0.0005	495
D5Ertd505e	DNA segment, Chr 5, ERATO Doi 505, expressed	1458934_at	-1.79	0.0007	496
Rhou	ras homolog gene family, member U	1449028_at	-1.79	9.00E-07	497
Gm266	predicted gene 266	1436115_at	-1.78	0.0100	498
Fgfbp1	fibroblast growth factor binding protein 1	1419086_at	1.78	0.0298	499
S100a11	S100 calcium binding protein A11 (calgizzarin)	1460351_at	1.78	0.0289	500

Table 5. Proteins differentially expressed in the whole hippocampus or the dentate gyrus of Shn-2 KO mice.

		Hippocampus		Dentate gyrus	
Symbol	Description	Fold Change	P value	Fold Change	P value
GFAP	grial fibrillary acidic protein	3.60	0.0007	2.05	0.0007
ATP5K	ATP synthase e chain, mitochondrial	−1.66	0.0017	−1.99	0.0042
ATP5F1	ATP synthase, H+ transporting, mitochondrial F0 complex, subunit b, isoform 1			−1.10	0.0073
ATP6V1A	ATPase, H+ transporting, lysosomal 70kDa, V1 subunit A			1.46	0.0004
ATP6V1B2	vacuolar H+ ATPase B2 isoform 2			1.42	0.0014
UB	1d8 ubiquitin mutant	−1.60	0.0054		
UBB	ubiquitin B	−1.60	0.0054		
CALB2	calbindin 2			1.45	0.0010
HPCA	hippocalcin			1.44	0.0190
INPP1	inositol polyphosphate-1-phosphatase	1.43	0.0480	−1.25	0.0450
EG628438	CPN10-like protein	−1.42	0.0120		
HSPE1	heat shock protein 1 (chaperonin 10)	−1.42	0.0120	−1.99	0.0042
UQCRFS1	ubiquinol-cytochrome C reductase, Rieskeiron-sulfer polypeptide 1	−1.41	0.0180	−1.12	0.0200
ARPC5	actin related protein 2/3 complex, subunit 5			−1.41	0.0006
GPD1	glycerol-3-phosphate dehydrogenase 1			1.40	0.0057
COX5B	cytochrome C oxidase, subunit V6			1.40	0.0004
CKMT1	Creatin kinase, mitochondrial 1	−1.37	0.0170	−1.26	0.0013
PPP3CA	calcineurin A alpha	1.37	0.0230	1.27	0.0031
STMN1	stathmin 1	−1.35	0.0310	−1.23	0.0270
ADAM5	a disintegrin and metallopeptidase domain 5	−1.33	0.0082		
KLHL10	kelch-like 10	−1.33	0.0490		
VDAC2	voltage-dependent anion chanel 2	−1.32	0.0300		
ATP5D	ATP-synthase, H+ transporting mitcondrial F1 complex, delta subunit precursor	−1.31	0.0200	−1.15	0.0320
MYL6	myosin, light chain 6, allcali, smooth muscle and non-muscle isoform 1	−1.31	0.0200		
SNCB	synuclein, beta	−1.31	0.0200	−1.15	0.0320
SEPT2	septin 2	−1.29	0.0015		
NAPB	N-ethylmaleimide sensitive fusion protein attachment protein beta			1.29	0.0002
FIS1	fission 1 (mitochondrial outer membrane) homolog			−1.28	0.0150
PHGDH	D-3-phosphoglycerate dehydrogenase	1.27	0.0320		
SEPT5	septin 5	−1.27	0.0003	−1.08	0.0480
DBF4	activator of S phase kinase	−1.26	0.0270		
GSTM5	glutathione S-transferase, mu5	−1.25	0.0120	−1.21	0.0002
HPRT1	hypoxanthine phosphoribosyl transferase 1	−1.25	0.0120	−1.21	0.0002
MED6	Mediator of RNA polymerase II transcription, subunit 6 homolog	−1.25	0.0150		
UCHL3	ubiquitin carboxyl-terminal hydrolase isozyme L3	−1.25	0.0120		
YWHAH	tyrosine 3-monooxygenase/ tryptophan 5-monooxygenase activation protein	−1.25	0.0120	1.26	0.0006
ACTR3	ARP3 actin-related protein 3 homolog			−1.25	0.0033
BDNF	brain-derived neurotrophic factor	−1.24	0.0360		
GLOD4	glyoxalase domain-containing protein 4	1.24	0.0380	1.25	0.0012
LOC574157	similar to sperm surface protein Sp17	−1.24	0.0360		
NAPA	N-etylmaleimide sensitive fusion protein attachment protein alpha	1.24	0.0380	1.25	0.0012
SPA17	sperm surface protein Sp17 (sperm autoantigenic protein 17)	−1.24	0.0360		
GON4L	gon-4 like isoform a	−1.23	0.0240		
STX18	syntaxin-18			1.23	0.0031
ARBP	acidic ribosomal phosphoprotein	−1.22	0.0480		
RPLP0	ribosomal protein P0	−1.22	0.0480		
PCBP1	poly (rc) binding protein 1			1.22	0.0063
AKR1	aldose reductase (aldo-keto reductase family 1)	−1.21	0.0370		
AKR1B3	aldo-keto reductase family 1, member B3 (aldose reductase)			1.40	0.0057
CORO1A	Coronin-1A	−1.21	0.0061	−1.18	0.0001
ACO2	mitochondrial aconitase 2			−1.21	0.0002
GRIA2	glutamate receptor, ionotropic, AMPA2 isoform 3			−1.21	0.0002
YWHAG	tyrosine 3-monooxygenase/tryptophan 5-monooxygenase activation protein, gamma polypeptide			1.21	0.0012
CAPZB	capping protein (actin filament) muscle Z-like, beta			−1.20	0.0001
DLD	dihydrolipoamide dehydrogenase			−1.19	0.0140
MAPK1	mitogen activated protein kinase 1			1.19	0.0180
GBAS	protein NipSnap homolog 2 (Glioblastoma-amplified sequence)			−1.19	0.0057
GSTM1	glutathione S-transferase, mu1			−1.19	0.0110
UQCRC1	ubiquinol-cytocrome C reductase core protein 1	−1.18	0.0200		

DLAT	dihydrolipoamide S-acetyltransferase (E2 component of pyruvate dehydrogenase complex)			1.18	0.0044
PRDX1	peroxiredoxin-1			1.18	0.0260
ALDOA	aldolase 1, A isoform	1.17	0.0100	-1.22	0.0010
CAR2	carbonic anhydrase 2	-1.17	0.0030		
ETFA	Electron transfer flavoprotein subunit alpha, mitcondrial precursor	-1.17	0.0340	-1.10	0.0004
FABP5	fatty acid-binding protein 5	-1.17	0.0021		
NDUFS1	NADH dehydrogenase (ubiquinone) Fe-S protein 1	-1.17	0.0350		
NDUFA10	NADH dehydrogenase (ubiquinone) 1, alpha subunit 10			-1.15	0.0003
PGAM1	phosphoglycerate mutase	-1.17	0.0030		
UBCRC2	ubiquinol cytochrome c reductase core protein 2			-1.17	0.0080
UQCRB	ubiquinol-cytochrome C reductase binding protein			1.17	0.0100
ALDH2	aldehyde dehydrogenase 2, mitcondrial	-1.16	0.0130		
CS	Citrate synthase	-1.16	0.0450	-1.09	0.0085
HSP60	heat shock protein 60	1.16	0.0280		
HSP90AB1	heat shock 90kDa protein 1 beta			1.19	0.0190
HSPA8	heat shock 70kDa protein 8 isoform 1			1.17	0.0220
SNTG2	syntrophin, gammma 2	1.16	0.0280		
VDAC1	voltage-dependent anion chanel 2	-1.16	0.0026	-1.17	0.0006
CFL1	cofilin-1	-1.15	0.0380	-1.11	0.0310
DOK7	downstream of tyrosine kinase 7 (docking protein 7)	-1.15	0.0058	-1.15	0.0003
HNRPK	heterogeneous nuclear ribonucleoprotein K	-1.15	0.0480		
HNRNPH1	heterogeneous nuclear ribonucleoprotein H1			-1.07	0.0480
MDH1	cytosolic malate dehydrogenase	1.15	0.0088		
PITPNA	phosphatidylinositol transfer protein, alpha	1.15	0.0088		
FREQ	Neuronal calcium sensor 1 (Frequenin homolog)	1.14	0.0280		
GSN	gelsolin	1.14	0.0340		
PLG	Plasminogen	1.14	0.0340		
ATP5A1	ATP synthase, H+-transporting, mitochondrial F1 complex, alpha subunit	1.13	0.0260	-1.17	0.0026
CD40	tumor necrosis factor receptor surperfamily, member 5 isoform 1 (CD40 antigen)	-1.13	0.0300	1.24	0.0370
CT75	cancer/ testis antigen 75	-1.13	0.0026		
DNAH7	dynein, axonemal, heavy chain 7	1.13	0.0037		
LDHA	L-lactate dehydrogenase A	-1.13	0.0120		
UCHL1	ubiquitin carboxyl-terminal hydrolase isozyme L1	1.12	0.0480	1.40	0.0007
AK1	adenylate kinase 1	-1.11	0.0110		
AK3	adenylate kinase 3			-1.19	0.0057
PVALB	parvalbumin	-1.11	0.0170		
SH3BGRL	SH3-binding domain glutamic acid-rich protein like	-1.11	0.0170		
TXN1	thioredoxin	-1.11	0.0170		
GPI1	glucose phosphate isonerase 1			-1.10	0.0130
CDCREL-1	CDCrel-1AI	-1.09	0.0420		
NDUFS8	NADH dehydrogenase (ubiquinone) Fe-5 protein 8	-1.09	0.0420		
PEBP1	phosphatidylethanolamine binding protein 1	-1.09	0.0420		
PGK1	phosphoglycerate kinase 1	-1.06	0.0330		
PSMA6	proteasome subunit, alpha type 6			-1.05	0.0400
PSMB5	proteasome subunit, beta type 5			-1.16	0.0000
PSMB1	proteasome subunit, beta type 1			-1.10	0.0073

Table 6. Groups of molecules and genes altered in both postmortem brains and the dentate gyrus (DG) and hippocampus (HC) of Shn-2 KO mice.

	DG Microarray (schizophrenia)		DG Genechip		DG Proteome		HC Genechip		HC Proteome	
	Altar et al.	Shn2 KO mice	P value	Fold Change	P value	Fold Change	P value	Fold Change	P value	Fold Change
Aldo-Keto Reductase	AKR1A1	Akr1b3			0.0057	1.4	0.0276	−1.05		
	AKR1B1	Akr1a4					0.0254	−1.05		
		Akr1c18	0.0038	1.27			0.0216	1.36		
		Akr1							0.0370	−1.21
		Aldoa							0.0100	1.17
ATP related	ATP6V1E1	Atp6v1a			3.60E−04	1.46				
	ATP5A1	Atp5a1			0.0026	−1.17			0.0260	1.13
	ATP1B1	Atp6v1b2			0.0014	1.42				
		Atp2b2	0.0014	1.36						
		Atp5k			0.0042	−1.99			1.70E−03	−1.66
		Atp5f1/Psmb1			0.0073	−1.10				
		Atp5d			0.032	−1.15			0.0200	−1.31
		Atp6v1g2					0.0118	1.06		
		Atp6v0e2					0.0120	1.06		
		Atp6v1e1					0.0242	1.05		
		Atp6v0d2					0.0483	−1.21		
		Atp5g3					0.0123	−1.06		
		Atp5h					0.0350	−1.07		
		Atp11c	4.00E−04	1.33						
		Atp2b3	0.0016	1.30						
		Atp2c1	5.30E−06	−1.25						
		Atp2a3	4.00E−04	1.22						
		Atp6v1g1	4.50E−07	1.21						
Cytochrome related	UQCRFS1	Uqcrfs1			0.02	−1.12			0.0180	−1.41
		Ubcrc2			0.008	−1.17				
	CYC1	Cyc1					0.0325	−1.08		
	SCO1	Cox5b			4.20E−04	1.40				
	COX7A2	Uqcrb			0.01	1.17				
	CYB5R3	Uchl1			0.00073	1.4			0.0480	1.12
		Cyp3a13					0.0025	1.11		
		Cybrd1					0.0030	1.65		
		Cyba					0.0195	1.31		
		Cyb561	0.0049	−1.28						
		Uqcrh					0.0470	−1.08		
Glucose phosphate isomerase	GPI	Gpi1			0.013	−1.10	0.0491	−1.03		
NADH dehydrogenase	NDUFB2	Ndufa10			2.60E−04	−1.15	0.0417	1.12		
	NDUFB5									
	NDUFS4									
		Ndufs1							0.0350	−1.17
		Ndufs8							0.0420	−1.09
Phosphoglycerate related	PGAM1								0.0030	−1.17
		Pgk1			0.033	−1.06				
		Phgdh	0.0022	−1.44			0.0393	−1.10	0.0320	1.27
Proteasome	PSMC6	Psma6			0.04	−1.05				
	PSMD8	Psmb5			2.90E−05	−1.16				
	PSMD9	Psmb1 / Atp5f1			0.0073	−1.10				
	PSME1	Psmb8					0.0386	1.23		
	PSMA1	Psmg2	2.30E−04	−1.27						
	PSMB6									
Ubiquitin related	UCHL1	Uchl1			7.30E−04	1.40			0.0480	1.12
	UBB	Ubb							0.0054	−1.60
	UBE2D1	Uchl3					0.0120	−1.25		
	UBL4A	Usp22					0.0017	1.15		
		Usp29	6.60E−06	1.90			0.0034	1.18		
		Ubl5					0.0042	1.38		
		Ube2l3					0.0105	1.10		
		Ube2b					0.0116	−1.06		
		Usp22					0.0130	1.14		
		Ube2d2					0.0140	1.09		
		Ube2e2					0.0168	1.17		
		Usp38					0.0192	1.15		
		Usp16					0.0220	1.14		
		Usp40					0.0391	−1.24		
		Wwp2					0.0444	−1.18		
		Usp39					0.0476	1.05		
		Usp25					0.0487	1.17		
		Ups48	0.0035	1.21						
		Usp27x	0.0049	1.27						
		Ube2v2	0.0006	1.24						
		Uhrf2	0.0020	−1.27						
		Hace1	0.0013	−1.43						
		Nub1	0.0050	1.22						
Calbindin	CALB1	Calb1	0.0010	−5.36			1.42E−05	−2.02		
Syntaxin related	STX8	Stx18			0.0031	1.23				
		Stxbp6					0.0123	1.32		
		Stx6	0.0029	1.28			0.0337	1.13		
		Stx4a					0.0342	−1.19		
		Stx2	0.0029	−1.45						
		Stxbp3a	0.0010	1.42						
		Stxbp1	0.0002	1.24						

Downregulated genes or proteins

Upregulated genes or proteins

Genes or proteins whose direction of the regulation is not consistent in Shn-2 KO mice

Table 7. Biosets highly correlated with the hippocampal transcriptome of Shn-2 KO mice.

Rank in p-value	Group	Public id	Bioset Name	Correlation	Common Genes	P value
1	Tumor	GSE21687	Ependymona cell lines _vs_ primary tumors	-	993	1.10E-48
2	Aging	GSE11528	Whole brain from Mus musculus - P56 young adult mice _vs_ P0 newborn mice	+	756	1.00E-44
3	Relative gene expression	GSE4734	C57BL_6J hippocampus - relative gene expression compared to the median of its expression across 5 brain regions in 6 strains	+	1411	1.40E-42
4	Aging	GSE11528	Whole brain from Mus musculus - P14 mice pups _vs_ P0 newborn mice	+	682	3.40E-41
5	Aging	GSE8150	Neocortex from aged mice treated with alpha- and gamma-tocopherol _vs_ young untreated mice	+	447	1.90E-40
6	Aging	GSE8150	Neocortex from aged mice treated with alpha-tocopherol _vs_ young untreated mice	+	448	2.90E-40
7	Relative gene expression	GSE4734	C3H_HeJ hippocampus - relative gene expression compared to the median of its expression across 5 brain regions in 6 strains	+	1411	6.60E-40
8	Aging	GSE11528	Whole brain from Mus spretus - P14 mice pups _vs_ P0 newborn mice	+	652	1.10E-38
9	Aging	GSE11528	Whole brain from Mus spretus - P56 young adult mice _vs_ P0 newborn mice	+	716	2.80E-38
10	Genetic modification	E-MEXP-962	Alpha-CaMKII HKO mice _vs_ wild type	+	211	1.40E-37
11	Aging	GSE8150	Neocortex from aged mice _vs_ young untreated mice	+	405	3.10E-36
12	Tumor	GSE6463	Granule neuron precursors from Ink4c-p53- mice overexpressing Cyclin D1 _vs_ not overexpressing	+	349	4.70E-36
13	Aging	GSE13120	Mouse neocortex 30mo _vs_ 5mo	+	396	2.20E-35
14	Aging	GSE12454	Forebrain from wildtype C57BLx129 mice - P0.5 _vs_ E13.5	+	689	1.20E-34
15	Comparison of tissues	GSE8044	Mus musculus brown adipose tissue _vs_ white adipose tissue	-	681	1.20E-33
16	Aging	GSE20547	Cerebellum of wildtype female mice 20-22 mo _vs_ 6 mo old	+	464	6.90E-33
17	TRAP	GSE13379	TRAP astrocyte RNA from mouse cortex _vs_ unbound RNA	-	836	6.90E-33
18	Aging	GSE19677	Whole striatum of YAC128 transgenic Huntingtin's model mice - 24mo old _vs_ 12mo old_GPL1261	+	777	1.50E-32
19	Relative gene expression	GSE4734	FVB_NJ hippocampus - relative gene expression compared to the median of its expression across 5 brain regions in 6 strains	+	1411	2.20E-32
20	Relative gene expression	GSE4734	DBA_2J hippocampus - relative gene expression compared to the median of its expression across 5 brain regions in 6 strains	+	1411	2.50E-32
21	Aging	GSE12454	Forebrain from Atrx-null C57BLx129 mice - P0.5 _vs_ E13.5	+	864	1.10E-31
22	TRAP	GSE13379	TRAP cholinergic neuronal RNA from mouse corpus striatum _vs_ unbound RNA	-	707	3.70E-31
23	Comparison of tissues	GSE13394	Drd1a subclass of medium spiny neurons from mouse striatum _vs_ Purkinje neurons from cerebellum	+	818	6.40E-31
24	Comparison of tissues	GSE13394	Drd2 subclass of medium spiny neurons from mouse striatum _vs_ Purkinje neurons from cerebellum	+	829	9.20E-31
25	Comparison of tissues	GSE19534	Neural tissues from wildtype 21mo post-natal mice - striata _vs_ cerebella	+	890	2.00E-30
26	Relative gene expression	GSE4734	A_J hippocampus - relative gene expression compared to the median of its expression across 5 brain regions in 6 strains	+	1411	6.80E-30
27	Neurodegeneration	GSE10263	Striatum from R6-2 transgenic mice _vs_ WT_GPL1261	-	411	6.90E-30
28	Relative gene expression	GSE4734	129S6_SvEvTac hippocampus - relative gene expression compared to the median of its expression across 5 brain regions in 6 strains	+	1411	1.80E-29
29	Comparison of tissues	GSE19534	Neural tissues from wildtype 6mo post-natal mice - striata _vs_ cerebella	+	778	4.80E-29
30	Aging	GSE20954	Lung of ICR strain postnatal day 2 _vs_ embryonic day 12	+	646	1.70E-28
31	Drug treatment	GSE22307	Colon tissue from mice treated with 3 percent dextran sodium sulfate (DSS) for 4d _vs_ untreated	+	483	2.30E-28
32	Comparison of tissues	GSE19534	Neural tissues from SNCA KO 6mo post-natal mice - striata _vs_ cerebella	+	789	3.40E-28
33	Aging	GSE20954	Lung of ICR strain postnatal day 10 _vs_ embryonic day 12	+	563	9.10E-28
34	TRAP	GSE13379	TRAP cholinergic neuronal RNA from mouse basal forebrain _vs_ unbound RNA	-	758	1.10E-27
35	Comparison of tissues	GSE18281	Peri-medullary thymic cortex microdissected from C57BL6 mice _vs_ whole thymic medulla	-	917	1.40E-27
36	Relative gene expression	GSE1479	E14.5 atrial chamber of heart - relative gene expression compared to the median of its expression across 5 brain regions in 6 strains	+	1411	1.50E-27
37	Aging	GSE20547	Cerebellum of SNCA-A53T-overexpressing female mice (TgB) 20-22 mo _vs_ 6 mo old	+	419	2.00E-27
38	Comparison of tissues	GSE19534	Neural tissues from SNCA KO 21mo post-natal mice - striata _vs_ cerebella	+	909	2.10E-27
39	TRAP	GSE13379	TRAP Pnoc+ neuronal RNA from mouse cerebellum _vs_ unbound RNA	-	438	3.00E-27
40	Genetic modification	GSE19402	Hippocampus of Camk2a-Cre driven G9a KO mice _vs_ GLP KO mice	+	555	4.00E-27
41	TRAP	GSE13379	TRAP mixed oligodendroglia RNA from mouse cortex _vs_ unbound RNA	-	562	6.80E-27
42	Comparison of tissues	GSE7897	Tissue from mice younger than 76d- Lymphomas of Eu-Myc mice _vs_ wild type lymph node	-	793	9.10E-27
43	TRAP	GSE13379	TRAP Purkinje neuronal RNA from mouse cerebellum _vs_ unbound RNA	-	947	1.00E-26
44	Aging	GSE13799	Hippocampus from spatial memory unimpaired aged animals _vs_ young	+	149	1.40E-26
45	TRAP	GSE13379	TRAP Bergmann glia RNA from mouse cerebellum _vs_ unbound RNA	-	846	2.50E-26
46	Neurodegeneration	GSE3621	Brain from 18wk old mice - R6/1 Huntington's model _vs_ wildtype	-	178	3.90E-26
47	Neurodegeneration	GSE3621	Brain from 22wk old mice - R6/1 Huntington's model _vs_ wildtype	-	204	2.50E-25
48	Drug treatment	GSE22307	Colon tissue from mice treated with 3 percent dextran sodium sulfate (DSS) for 6d _vs_ untreated	+	559	2.80E-25
49	Aging	GSE8091	Heads from embryonic mice- E13.5 _vs_ E9.5	+	986	3.90E-25
50	Aging	GSE20547	Cerebellum of SNCA-A53T-overexpressing female mice (TgA) 20-22 mo _vs_ 6 mo old	+	427	4.20E-25
51	Neurodegeneration	GSE23182	Hippocampal tissue of mice treated with 500ug/kg LPS 18wk after ME7 infection _vs_ uninfected	+	335	5.40E-25
52	Relative gene expression	GSE1479	E12.5 heart ventricles - relative gene expression compared to the median of its expression across 5 brain regions in 6 strains	-	1411	6.60E-25
53	Comparison of tissues	GSE13563	Protective calvarial bone of skull _vs_ weight bearing mandibular bone	+	358	8.20E-25
54	Genetic modification	GSE10263	Striatum from CHL2 knock-in mice _vs_ WT_GPL1261	-	415	1.20E-24
55	Aging	GSE18597	Spinal cord SOD1 G93A mutant - 98 day old _vs_ 28 day old	+	445	1.60E-24
56	Aging	GSE10000	Aorta of ApoE null mice - 78wk old _vs_ 6wk old_GPL1261	+	556	5.30E-24
57	Genetic modification	GSE7897	Early onset Lymphoma from Eμ-Myc transgenic mice _vs_ normal wild type lymph node	-	770	5.70E-24
58	Injury	GSE5296	Spinal cord below impact site 72h after injury _vs_ naive	+	349	5.70E-24
59	Aging	GSE19677	Whole striatum of wildtype mice - 24mo old _vs_ 12mo old_GPL1261	+	681	7.30E-24
60	Relative gene expression	GSE1479	E16.5 atrial chamber of heart - relative gene expression compared to the median of its expression across 5 brain regions in 6 strains	+	1411	7.60E-24
61	Aging	GSE20954	Lung of ICR strain postnatal day 30 _vs_ embryonic day 12	+	689	7.70E-24
62	Genetic modification	GSE8396	Liver from mice Wy14643 treated 6hr - PPARa-null _vs_ wildtype	+	450	1.00E-23
63	Comparison of tissues	GSE7897	Late onset Lymphoma from Eu-Myc transgenic mice _vs_ normal wild type lymph node	-	739	1.10E-23
64	Treatment	GSE18341	Lungs of 16wk adult C57BL6 mice + mechanical ventilation for 2hr _vs_ untreated 2hr	-	465	1.30E-23
65	Genetic modification	GSE17511	Skin basal cells from mouse overexpressing tissue-specific IKK-beta _vs_ wildtype	+	307	1.60E-23
66	Treatment	GSE13432	White adipose tissue of mouse housed at 4 degrees 5wk _vs_ room temperature	-	473	1.90E-23
67	Injury	GSE5296	Spinal cord below impact site 28d after injury _vs_ sham-injury	+	154	2.00E-23

68	Relative gene expression	GSE1479	E18.5 atrial chamber of heart – relative gene expression compared to the median of its expression across 5 brain regions in 6 strains	+	1411	2.20E-23
69	Relative gene expression	GSE2882	Cingulate cortex_G42_GABA neurons homogenate – relative gene expression compared to the median of its expression across 5 brain regions in 6 strains	+	929	2.40E-23
70	Injury	GSE5296	Spinal cord above impact site 72h after injury _vs_ naive	+	320	2.60E-23
71	Genetic modification	GSE18597	Spinal cord from 112 day old mice – SOD1 G93A mutant _vs_ wildtype	+	378	3.20E-23
72	Relative gene expression	GSE4734	FVB_NJ pituitary gland – relative gene expression compared to the median of its expression across 5 brain regions in 6 strains	–	1411	4.00E-23
73	Comparison of tissues	GSE5038	Wildtype mouse tissue – motor neurons _vs_ total spinal cord	–	931	4.50E-23
74	Drug treatment	GSE6476	Hippocampus from mice treated 21d with 18mg/kg/d fluoxetine _vs_ untreated	+	95	5.50E-23
75	Relative gene expression	GSE4734	C3H_HeJ periaqueductal gray – relative gene expression compared to the median of its expression across 5 brain regions in 6 strains	–	1411	5.60E-23
76	TRAP	GSE13394	Purkinje neurons from mouse cerebellums – TRAP purified _vs_ unbound RNA	–	850	7.40E-23
77	Comparison of tissues	GSE18281	Medullary thymocytes (CD3hi CD45+) FACs from C57BL6 mice _vs_ whole medulla of thymus	–	745	9.80E-23
78	Genetic modification	GSE8396	Liver from mice C22-6 treated 6hr – PPARa-null _vs_ wildtype	+	316	1.80E-22
79	Tumor	GSE22406	Mammary tumors of mice expressing inducible c-myc – primary _vs_ recurrent after deinduction	+	531	2.10E-22
80	Aging	GSE10000	Aorta of ApoE null mice – 32wk old _vs_ 6wk old_GPL1261	+	367	2.60E-22
81	Treatment	GSE15155	Satellite muscle cells from adult mice – cultured 3d activated _vs_ fresh isolated quiescent cells	–	753	3.20E-22
82	Genetic modification	GSE16585	Retina of 28d old mice – Nrl overexpression and Rorb KO _vs_ wildtype	+	631	4.40E-22
83	Aging	GSE13799	Hippocampus from spatial memory impaired aged animals _vs_ unimpaired young	+	223	5.10E-22
84	Comparison of tissues	GSE6383	E18.5 small intestine- epithelium _vs_ mesenchyme	–	797	5.30E-22
85	Aging	GSE4818	Testes post natal day2 _vs_ day11	+	676	6.50E-22
86	Drug treatment	GSE12413	Heart of C57BL mice treated 14d with 120ug/g/day isoproterenol _vs_ untreated	+	699	7.10E-22
87	Aging	GSE5333	Epididymus gd18 _vs_ gd12	+	436	8.90E-22
88	Genetic modification	GSE18597	Spinal cord from 98 day old mice – SOD1 G93A mutant _vs_ wildtype	+	141	9.20E-22
89	Treatment	GSE7699	Liver from mice on ketogenic diet _vs_ chow	+	326	1.20E-21
90	Relative gene expression	GSE4734	129S6_SvEvTac periaqueductal gray – relative gene expression compared to the median of its expression across 5 brain regions in 6 strains	–	1411	1.50E-21
91	Comparison of tissues	GSE18281	Whole medulla of thymus from C57Bl6 mice _vs_ whole thymic cortex	+	788	2.00E-21
92	Aging	GSE15209	Neural stem cells derived from the foetal cortex _vs_ normal brain cortex	–	770	2.00E-21
93	TRAP	GSE13394	Drd1a subclass of medium spiny neurons from mouse striatum – TRAP purified _vs_ unbound RNA	+	439	2.60E-21
94	Aging	GSE20954	Lung of ICR strain embryonic day 18 _vs_ embryonic day 12	+	569	2.70E-21
95	Injury	GSE5296	Spinal cord above impact site 24h after injury _vs_ naive	+	246	2.80E-21
96	Drug treatment	GSE13044	Fetal livers from timed pregnant mice exposed gestation days 1-17 – 10mg/kg/day PFOA _vs_ vehicle	–	368	3.50E-21
97	Comparison of tissues	GSE6933	Mouse multipotent adult progenitor cells – clone 3 _vs_ clone 2	+	742	4.20E-21
98	Comparison of tissues	GSE23782	Skin from 4-OHT treated K14NICDER transgenic mice expressing Notch – epidermis _vs_ whole skin	–	587	5.00E-21
99	Comparison of tissues	GSE7685	Mouse tibiae Zone III of growth plate _vs_ Zone I	+	606	5.70E-21
100	Aging	E-MEXP-1504	Liver from wild type mouse aged 130 weeks old _vs_ young 13 weeks old	+	166	5.90E-21
101	Comparison of tissues	GSE8024	Mouse embryonic fibroblasts _vs_ murine neural precursor cells differentiated from ES cells	+	675	6.70E-21
102	Comparison of tissues	GSE8034	E14 cortex glial cells- GFAP-GFP High _vs_ low	–	405	7.90E-21
103	Comparison of tissues	GSE23782	Skin from 4-OHT treated K14NICDER transgenic mice expressing Notch – epidermis _vs_ dermis	–	450	8.70E-21
104	Aging	GSE3231	V6.5 embryonic cells differentiating to embryoid bodies 14d _vs_ 0hr	+	515	9.30E-21
105	Aging	GSE10965	Retinal Pigmental epithelium and Choroid – 4mo old_CHGN vs 26mo old	–	400	1.10E-20
106	Comparison of tissues	GSE19979	P7 bladder epithelium from Theiler stage 6 mice – uroplakin positive _vs_ negative	–	528	1.30E-20
107	TRAP	GSE13379	TRAP cholinergic neuronal RNA from mouse spinal cord _vs_ unbound RNA	–	762	1.90E-20
108	Treatment	GSE11679	CA1 region of hippocampus from postnatally handled mice _vs_ non handled mice	+	688	2.40E-20
109	Drug treatment	GSE13044	Fetal livers from timed pregnant mice exposed gestation days 1-17 – 5mg/kg/day PFOA _vs_ vehicle	–	368	2.60E-20
110	Genetic modification	GSE8396	Liver from mice fenofibrate treated 6hr – PPARa-null _vs_ wildtype	+	344	2.80E-20
111	Relative gene expression	GSE4734	C57BL_6J pituitary gland – relative gene expression compared to the median of its expression across 5 brain regions in 6 strains	–	1411	3.00E-20
112	Treatment	GSE13071	Knee joint synovium – collagen induced arthritis moderate inflammation _vs_ healthy control	+	767	3.10E-20
113	Genetic modification	GSE7897	Tissue from 253-649d old mice – Lymphomas of Eu-Myc mice _vs_ wild type normal lymph node	–	643	3.80E-20
114	Comparison of tissues	GSE6933	Mouse multipotent adult progenitor cells – clone 3 _vs_ clone 1	+	797	4.30E-20
115	Aging	GSE15452	Lung of wildtype mice – 28d old _vs_ 1d old	+	489	4.60E-20
116	Infection	GSE8966	Liver from SCID mice + Arkansas strain E. chaffeensis 15d _vs_ mock infected	+	389	4.70E-20
117	Genetic modification	GSE7020	Spleen from Nix KO mice _vs_ WT	–	504	5.40E-20
118	Comparison of tissues	GSE6933	Mouse multipotent adult progenitor cells _vs_ marrow stromal cells	–	601	6.60E-20
119	Treatment	GSE8790	Lungs of AJ mice + 8d cigarette smoke at 5hr per day _vs_ air	+	635	7.50E-20
120	Comparison of tissues	GSE13071	Knee joint synovium – collagen induced arthritis mild inflammation _vs_ no inflammation	+	472	8.20E-20
121	Comparison of tissues	GSE8024	Mouse embryonic fibroblasts _vs_ murine embryonic stem cells	+	815	1.20E-19
122	Infection	GSE8966	Liver from SCID mice + Wakulla strain E. chaffeensis 15d _vs_ mock infected	+	615	1.20E-19
123	Comparison of tissues	GSE13394	Drd1a subclass of medium spiny neurons from mouse striatum _vs_ motor neurons from brainstem	+	772	1.30E-19
124	Genetic modification	GSE19402	Hypothalamus of Camk2a-Cre driven G9a KO mice _vs_ GLP KO mice	+	581	1.30E-19
125	Aging	GSE5333	Epididymus gd16 _vs_ gd12	+	424	1.50E-19
126	Genetic modification	GSE17478	Left ventricle of mice exposed to particulate matter – dominant negative CREB _vs_ wildtype	+	323	1.50E-19
127	Genetic modification	GSE15541	Bone marrow transformed with NUP98-HOXD13 + wildtype MEIS1 overexpression _vs_ control	–	458	1.60E-19
128	Relative gene expression	GSE1806	Diaphragm_8wk – relative gene expression compared to the median of its expression across 5 brain regions in 6 strains	+	1411	2.00E-19
129	Comparison of tissues	GSE3822	E11.5 embryonic metanephric mesenchyme _vs_ ureteric bud	+	548	2.10E-19
130	Comparison of tissues	GSE13071	Knee joint synovium – collagen induced arthritis severe inflammation _vs_ no inflammation	+	693	2.20E-19
131	Genetic modification	GSE9355	Sorted mammary tumor from RAG2 KO mice _vs_ WT hyperplastic mammary cells	–	293	3.10E-19
132	Treatment	GSE4786	Cochlea from calorie restricted mice _vs_ middle aged control	+	619	3.30E-19
133	Aging	GSE11186	Dorsal skin of mouse during second postnatal hair growth cycle – 29d postnatal _vs_ 23d postnatal	–	504	3.50E-19
134	Genetic modification	GSE14242	Long bones from 12d old Hyp mutant mice – Phex mutation _vs_ wildtype	+	284	3.70E-19
135	Injury	GSE5296	Spinal cord below impact site 28d after injury _vs_ naive	+	271	4.30E-19
136	Comparison of tissues	GSE13071	Knee joint synovium – collagen induced arthritis severe inflammation _vs_ healthy control	+	718	4.40E-19
137	Comparison of tissues	GSE9763	Transformed glial progenitors cells- postnatals _vs_ embryonic progenitors	+	875	6.40E-19
138	Aging	GSE8091	Heads from embryonic mice- E11.5 _vs_ E9.5	+	893	7.30E-19
139	Comparison of tissues	GSE13071	Knee joint synovium – collagen induced arthritis moderate inflammation _vs_ no inflammation	+	695	7.40E-19

140	Relative gene expression	GSE4734	129S6_SvEvTac hypothalamus – relative gene expression compared to the median of its expression across 5 brain regions in 6 strains	–	1411	1.00E-18
141	Neurodegeneration	GSE23182	Hippocampal tissue of mice treated with 500ug/kg saline 18wk after ME7 infection _vs_ uninfected	+	427	1.00E-18
142	Genetic modification	GSE15541	Bone marrow transformed with NUP98-HOXD13 + MEIS1-homeodomain deletion overexpression _vs_ control	–	527	1.10E-18
143	TRAP	GSE13379	TRAP Drd2+ medium spiny neuronal RNA from mouse striatum _vs_ unbound RNA	+	454	1.20E-18
144	Aging	E-MEXP-454	Genital ridges from Sf1-eGFP transgenic male mice E13.5 _vs_ E10.5	+	468	1.20E-18
145	Treatment	GSE23006	Mucosa of tongue from Balb-c mice – 5d post-wound _vs_ unwounded	+	494	1.30E-18
146	Aging	GSE20547	Cerebellum of SNCA-A53T-overexpressing female mice 20-22 mo _vs_ 6 mo old	+	407	1.50E-18
147	Injury	GSE5296	Spinal cord impact site 7d after injury _vs_ sham-injury	+	599	1.80E-18
148	Infection	GSE5555	Lungs- Nippostrongylus brasiliensis infected _vs_ uninfected mice	+	475	1.90E-18
149	Comparison of tissues	GSE6933	Mouse marrow stromal cells _vs_ embryonic stem cells	+	803	2.00E-18
150	Genetic modification	GSE7676	E12.5 placenta- pcdh12 KO _vs_ wildtype	+	326	3.00E-18
151	Neurodegeneration	GSE3621	Brain from 27wk old mice – R6/1 Huntington's model _vs_ wildtype	–	282	3.10E-18
152	Drug treatment		Splenic macrophages from aged mice – treated 6hr with 1ug per mL LPS _vs_ untreated	–	496	3.30E-18
153	Comparison of tissues	GSE3483	Mouse satellite cells in activated state _vs_ non myogenic cells	–	548	3.40E-18
154	Comparison of tissues	GSE15209	Oligoastrocytoma _vs_ normal brain cortex	–	658	3.50E-18
155	Genetic modification	GSE2372	Aorta of 32 week old mice – ApoE KO _vs_ wildtype	+	181	4.00E-18
156	Relative gene expression	GSE1479	E10.5 whole heart – relative gene expression compared to the median of its expression across 5 brain regions in 6 strains	–	1411	4.50E-18
157	Injury	GSE7404	WBC from spleen after burn injury sham at 1d _vs_ 2hr	+	307	4.50E-18
158	Aging	GSE3501	Mammary glands from mice overexpressing LH and erbb2 – 10wk _vs_ 5wk	–	503	4.70E-18
159	Aging	E-MEXP-878	Mice hippocampal neurons differentiating for 16d _vs_ 0.25d	+	675	5.00E-18
160	Genetic modification	GSE11897	P0.5 ovarian tissue from LHX8 null mice _vs_ WT_GPL1261	+	514	7.10E-18
161	Treatment	GSE13432	White adipose tissue of mouse housed at 4 degrees 1wk _vs_ room temperature	–	537	7.80E-18
162	Neurodegeneration	E-MEXP-1005	Brain from ME7-inoculated mice after 150d _vs_ not inoculated	+	190	7.90E-18
163	Genetic modification	GSE15303	Oligodendrocytes Myelin-gene Regulatory Factor heterozygote _vs_ oligodendrocyte progenitors	+	592	8.30E-18
164	Relative gene expression	GSE4734	129S6_SvEvTac pituitary gland – relative gene expression	–	1411	8.40E-18
165	Drug treatment	GSE7793	Kidney of mice treated IP 7d with vancomycin 400mg-kg-d _vs_ saline	+	861	9.40E-18
166	Not categorized yet	GSE15267	Pluripotent cells induced from serum-free fibroblast + Oct4 +Sox2 +Klf4 _vs_ serum-free MEFs	–	409	9.80E-18
167	Aging	GSE2154	Chondrocyte micromass cultures from E11.5 limb buds differentiated for 12d _vs_ 3d	+	387	1.10E-17
168	Genetic modification	GSE8156	Untreated granulosa cell tumor of Smad8+/- Smad1 Smad5 flox KO _vs_ WT granulosa cells+PMSG	+	409	1.30E-17
169	TRAP	GSE13379	TRAP Drd1+ medium spiny neuronal RNA from mouse striatum _vs_ unbound RNA	+	354	1.40E-17
170	Infection	GSE8966	Liver from SCID mice + Liberty strain E. chaffeensis 15d _vs_ mock infected	+	398	1.40E-17
171	Tumor	GSE6482	Kaposi-like tumor _vs_ mECK36 cells post KSHVBac36 transfection	+	252	1.40E-17
172	Aging	GSE2297	Female brain 8-wk _CHGN vs 1 wk	+	272	1.60E-17
173	Infection	GSE17509	Splenocytes CD45 heterozygotes expressing 62% normal levels of CD45 + EBOV 9d _vs_ uninfected	+	667	1.80E-17
174	Genetic modification	GSE12073	Pancreatic islets of NOD Rats- insulin promoter driven AIRE expression _vs_ nontransgenic islets	+	301	1.90E-17
175	Not categorized yet	GSE5350	Ambion human brain reference RNA _vs_ Stratagene universal reference RNA_Affy platform_GPL570	+	885	1.90E-17
176	Injury	E-MEXP-703	Skeletal muscle 12d post cardiotoxin injury in CnAa transgenic mice _vs_ untreated	+	313	1.90E-17
177	Infection	E-MEXP-1190	Spleen from C57BL-6 mice T. congolense-infected for 9d _vs_ uninfected	–	463	2.10E-17
178	Genetic modification	GSE10000	Aorta of 32wk old mice – ApoE null _vs_ wildtype_GPL1261	+	197	2.20E-17
179	Drug treatment	GSE12466	CD3+ T-cells from C57BL mouse + 1 mg/ml anti-CD3 + 3 mg/ml anti/CD28 _vs_ untreated	–	402	2.20E-17
180	Drug treatment	GSE12333	Embryoid bodies derived from D3 ES cell line + retinoic acid 10d _vs_ control	–	362	2.70E-17
181	Infection	GSE7814	Brain of cerebral-malaria-susceptible mice infected for 6 days _vs_ uninfected	+	208	3.20E-17
182	Aging	GSE11186	Dorsal skin of mouse during second postnatal hair growth cycle – 44d postnatal _vs_ 23d postnatal	+	437	3.30E-17
183	Drug treatment	GSE18341	Lungs of 16wk adult C57BL6 mice + LPS 30min + mechanical ventilation 2hr _vs_ untreated 2hr	–	510	4.40E-17
184	Comparison of tissues	GSE9763	Postnatal glial progenitor cells- transformed _vs_ normal	+	673	5.30E-17
185	Genetic modification	GSE10784	Hippocampus from Df(16)A+ mouse model of human 22q11 microdeletion syndrome _vs_ wildtype	+	144	5.40E-17
186	Genetic modification	GSE15303	Oligodendrocytes Myelin-gene Regulatory Factor conditional KO _vs_ oligodendrocyte progenitors	+	601	5.50E-17
187	Drug treatment	GSE12466	CD3+ T-cells from C57BL mouse + 1 mg/ml anti-CD3 _vs_ untreated	–	394	6.50E-17
188	Drug treatment	GSE17886	Two-cell embryo from maternal pronuclei strain C57BL-6 treated with alpha-amanitin _vs_ untreated	+	1010	7.90E-17
189	Aging	GSE2154	Chondrocyte micromass cultures from E11.5 limb buds differentiated for 9d _vs_ 3d	+	325	8.20E-17
190	Drug treatment	GSE11898	Mesangial cells of kidney stimulated 6hr with double stranded DNA _vs_ lipofectamine control	–	394	8.80E-17
191	TRAP	GSE13394	Drd2 subclass of medium spiny neurons from mouse striatum – TRAP purified _vs_ unbound RNA	+	441	1.00E-16
192	Tumor	GSE6482	Kaposi-like tumor _vs_ mEC cells + empty vector	+	545	1.00E-16
193	Aging	GSE2154	Chondrocyte micromass cultures from E11.5 limb buds differentiated for 15d _vs_ 3d	+	342	1.10E-16
194	Aging	GSE4818	Testes gestational day18 _vs_ day11	+	602	1.40E-16
195	Drug treatment	GSE15457	RAW264.7 mouse macrophages + 2.1 mM HOCl 6hr _vs_ untreated	–	382	1.40E-16
196	Treatment	GSE15129	Liver of 14mo old SAMP1 mouse fed diet supplemented with reduced coenzyme Q10 _vs_ control diet	+	212	1.50E-16
197	Aging	GSE5333	Epididymus pnd2 _vs_ gd12	+	296	1.80E-16
198	Comparison of tissues	GSE15209	Glioblastoma _vs_ normal brain cortex	–	725	1.80E-16
199	Drug treatment	GSE17880	Spleen of mice treated with 900mg/kg/d 2-butoxyethanol 7d _vs_ vehicle	–	847	1.80E-16
200	Comparison of tissues	GSE15580	Adult mouse Sca1-low transit-amplifying cells _vs_ embryonic prostate stem cells	+	575	1.80E-16
201	Neurodegeneration	E-MEXP-1005	Brain from mice after 120d ME7-inoculated _vs_ mock	+	119	2.10E-16
202	Comparison of tissues	GSE10871	MEF derived partly reprogrammed SSEA+ MCV8 cells with Oct4 Klf4 C-Myc Sox2 _vs_ Oct4 MVC8 iPS	+	685	2.20E-16
203	Treatment	GSE17825	Femur fracture tissue in 6wk old mice 5d post fracture _vs_ 1d post fracture	+	720	2.20E-16
204	Neurodegeneration	E-MEXP-1005	Brain from mice after 150d ME7-inoculated _vs_ mock	+	200	2.50E-16
205	Aging	GSE17783	Callosal projection neurons – P14 _vs_ E18	+	259	2.60E-16
206	Not categorized yet	GSE5876	Lacrimal gland from female MPR-lpr mice _vs_ Non-obese diabetic female mice_GPL339	+	189	2.60E-16
207	Genetic modification	GSE12956	Telencephalon of E14.5 embryo – Arx mutant _vs_ WT	+	344	2.70E-16
208	Genetic modification	GSE5037	Spinal cord from SOD1-null mice _vs_ wild-type	+	120	3.00E-16
209	Aging	GSE18567	Cochlea of nicotinic cholinergic receptor (alpha9 subunit) null mice – P60 _vs_ P3	+	425	3.00E-16
210	Comparison of tissues	GSE15767	Non-immunized subcapsular sinus macrophages of female C57BL/6 mice _vs_ medullary macrophages	–	409	3.10E-16
211	Treatment	GSE6858	Lung from wildtype mice + allergen ovalbumin _vs_ vehicle control	+	346	3.20E-16
212	Drug treatment	E-TABM-310	Macrophages from wild type rat + PAM2 60min _vs_ untreated	–	357	3.20E-16
213	Aging	GSE15452	Lung of FGFR3 FGFR4 double knockout mice – 28d old _vs_ 1d old	+	577	3.50E-16
214	Genetic modification	GSE10849	Heart from caveolin-1 knockout mice _vs_ wildtype	+	150	3.50E-16

215	Infection	E-MEXP-1190	Liver from C57BL-6 mice T. congolense-infected for 7d _vs_ uninfected	+	296	3.80E-16
216	Infection	GSE8025	FVBN mouse colon infected 9d _vs_ non-infected	-	594	4.50E-16
217	Comparison of tissues	GSE12618	Embryonic bladder mesenchymal cells _vs_ epithelial cells	+	367	4.50E-16
218	Neurodegeneration	E-MEXP-1005	Brain from ME7-inoculated mice after 120d _vs_ not inoculated	+	195	4.70E-16
219	Comparison of tissues	GSE11274	Germline pluripotent stem cells derived from adult Oct4-GFP GSCs _vs_ MEFS from E12.5 mice	-	829	5.40E-16
220	Tumor	GSE15904	Mammary tumor from MMTV-MYC mice of Epithelial-Mesenchymal Transition subtype _vs_ MMTV-Neu tumors	+	577	5.70E-16
221	Drug treatment	GSE3293	Gallbladders of leptin deficient obese mice + Leptin _vs_ Saline injections	+	344	5.90E-16
222	Infection	GSE7814	Cerebral-malaria-susceptible infected by Plasmodium for 6 days _vs_ cerebral-malaria resistant	+	179	6.10E-16
223	Comparison of tissues	GSE7809	Mouse ICC from Myenteric Plexus _vs_ Tunica Muscularis	-	289	7.30E-16
224	Drug treatment	GSE6674	AM14 B cells+anti-IgM+CpG _vs_ AM14 B cells untreated	-	382	7.40E-16
225	Treatment	GSE23006	Mucosa of tongue from Balb-c mice - 10d post-wound _vs_ unwounded	+	298	7.50E-16
226	Drug treatment	GSE6689	Stem cells+growth factor stimulation-Time point 2 _vs_ naive	+	450	8.40E-16
227	Infection	E-MEXP-1190	Spleen from C57BL-6 mice T. congolense-infected for 3d _vs_ uninfected	-	270	8.50E-16
228	Relative gene expression	GSE4734	DBA_2J periaqueductal gray - relative gene expression compared to the median of its expression across 5 brain regions in 6 strains	-	1411	8.80E-16
229	Drug treatment	GSE13044	Fetal livers from timed pregnant mice exposed gestation days 1-17 - 3mg/kg/day PFOA _vs_ vehicle	-	274	9.80E-16
230	Aging	GSE18567	Cochlea of wildtype mice - P60 _vs_ P3	+	343	9.90E-16
231	Tumor	GSE11859	Olig2-tva-cre:SmoM2 mice - Cerebellar tumor _vs_ non-tumor cerebellar tissue	-	635	1.10E-15
232	Treatment	GSE19403	Demyelinated spinal cord white matter from wildtype mice - induced by lysolecithin 15d _vs_ 4d	+	633	1.10E-15
233	Injury	GSE5296	Spinal cord impact site 28d after injury _vs_ sham-injury	+	388	1.20E-15
234	Aging	GSE15452	Lung of FGFR3 FGFR4 double heterozygous mice - 28d old _vs_ 1d old	+	654	1.30E-15
235	Drug treatment	GSE18660	CGR8 ESC differentiated 5d treated 10d with 1mM 1-ethyl-2-benzimidazolinone _vs_ untreated 10d	-	512	1.30E-15
236	Infection	GSE18293	Liver of Braun lipoprotein KO mutant Y. pestis infected mouse at 48hr post infection _vs_ uninfecte	+	571	1.40E-15
237	Aging	GSE16585	Retina overexpressing Nrl - 28d old mice _vs_ 14d	-	318	1.50E-15
238	Comparison of tissues	GSE15330	Ikaros-shRNA transfected - megakaryo-erythrocyte progenitors _vs_ hematopoetic stem cells	-	378	1.50E-15
239	Genetic modification	GSE10634	Kidney of P7 aquaporin 11 knockout mouse _vs_ wildtype	+	292	1.60E-15
240	Genetic modification	GSE13104	Osteosarcoma arisen from p53 heterozygous mouse _vs_ mc3T3 mouse osteoblast	+	480	1.60E-15
241	Comparison of tissues	GSE13074	Retinal pigment epithelium from light damaged BALBc mice _vs_ dark adapted	+	122	1.70E-15
242	TRAP	GSE13379	TRAP motor neuronal RNA from mouse brainstem _vs_ unbound RNA	-	605	1.80E-15
243	TRAP	GSE13394	Motor neurons from mouse brainstems - TRAP purified _vs_ unbound RNA	-	601	2.10E-15
244	Infection	E-MEXP-1190	Liver from BALBc mice T. congolense-infected for 7d _vs_ uninfected	+	392	2.10E-15
245	Infection	E-MEXP-1190	Liver from A J mice T. congolense-infected for 7d _vs_ uninfected	+	493	2.20E-15
246	Aging	GSE5334	Gonad development at pnd 2 _vs_ gd12	+	487	2.40E-15
247	Relative gene expression	GSE4734	C57BL_6J periaqueductal gray - relative gene expression compared to the median of its expression across 5 brain regions in 6 strains	-	1411	2.50E-15
248	Drug treatment	GSE18800	Mouse lung wildtype 14d after intratracheal bleomycin 1 mg/kg _vs_ no bleomycin	+	564	2.70E-15
249	Genetic modification	GSE16389	Villi enterocytes from transgenic mice with mutant Fabpi-SV40 TAg-N132 _vs_ non-transgenic mice	-	328	2.70E-15
250	Genetic modification	GSE23908	Ovaries from E16 embryos lacking germ cells (homozygous Kit W-v mutation) _vs_ wildtype	+	309	3.30E-15
251	Aging	GSE18597	Spinal cord SOD1 G93A mutant - 126 day old _vs_ 28 day old	+	504	3.50E-15
252	Injury	GSE5296	Spinal cord below impact site 24h after injury _vs_ naive	+	112	4.00E-15
253	Drug treatment	GSE6689	Stem cells+growth factor stimulation-Time point 3 _vs_ naive	+	258	4.00E-15
254	Infection	GSE6765	Small intestine from A. caviae-infected mice _vs_ uninfected	+	202	4.00E-15
255	Not categorized yet	GSE17617	C57BL6J X DBA2J mouse orexin-expressing neurons _vs_ whole brain	-	916	4.40E-15
256	Drug treatment	GSE17297	Mesentery from DBA mice 3d post-intraperitoneal injection 0.5 ml pristane _vs_ untreated control	+	512	4.60E-15
257	Drug treatment	GSE12466	CD3+ T-cells + 1 mg/ml anti-CD3 from Itk KO C57BL mouse _vs_ wildtype C57BL	+	251	4.70E-15
258	Treatment	GSE4066	Dorsal skin CD-1 mice + DMSO & UV irradiation 24h _vs_ sham irradiation	+	233	5.00E-15
259	Not categorized yet	GSE3234	Hematopoietic cells- downstream progenitors (Sca-1-cKit+) _vs_ bone marrow	-	317	5.70E-15
260	Genetic modification	GSE15541	Bone marrow transformed with NUP98-HOXD13 + M33-MEIS1 fusion overexpression _vs_ control	-	413	7.50E-15
261	Tumor	GSE9355	Sorted mammary tumor from WT mice _vs_ hyperplastic mammary cells	-	234	7.50E-15
262	Genetic modification	GSE16585	Retina of 14d old mice - Nrl overexpression and Rorb KO _vs_ wildtype	+	542	8.20E-15
263	Relative gene expression	GSE2882	Cingulate cortex_GIN_GABA neurons homogenate - relative gene expression	+	929	9.00E-15
264	Injury	GSE7404	WBC from spleen at 1d after burn injury _vs_ burn injury sham	-	605	9.80E-15
265	Drug treatment	GSE18341	Lungs of 16wk adult C57BL6 mice + LPS 30min + spontaneous breathing 2hr _vs_ untreated 2hr	-	488	1.00E-14
266	Treatment	GSE5555	Lungs with resolved N. brasiliensis infection- 72hr post HDM in PBS challenge _vs_ no challenge	-	538	1.00E-14
267	Injury	GSE5296	Spinal cord below impact site 7d after injury _vs_ naive	+	339	1.10E-14
268	Tumor	GSE14038	Primary tumor plexiform neurofibroma _vs_ universal tissue reference	+	722	1.10E-14
269	Genetic modification	GSE6789	IRAK4-KD MEFs IL1b-stimulated 1h _vs_ wildtype	+	220	1.10E-14
270	Comparison of tissues	GSE6259	DCs from WT mice sorted for - 33D1+ _vs_ DEC205+	+	381	1.10E-14
271	Aging	GSE5333	Epididymus gd14 _vs_ gd12	+	382	1.20E-14
272	Not categorized yet	GSE3792	ES-D3 cells differentiated 16d toward osteoblasts _vs_ undirected	+	427	1.20E-14
273	Aging	GSE21716	Livers from C57Bl6J mice at 18mo (old age) _vs_ 6mo (young adult)	+	98	1.30E-14
274	Comparison of tissues	GSE17955	Amygdala from 3-4mo old C57BL/6J mice _vs_ hippocampus	-	79	1.40E-14
275	Relative gene expression	GSE4734	A_J pituitary gland - relative gene expression compared to the median of its expression across 5 brain regions in 6 strains	-	1411	1.50E-14
276	Tumor	GSE21603	Colon from BCL9 BCL9L double KO mice - dimethylhydrazine induced colon tumor _vs_ normal epithelium	+	650	1.70E-14
277	Not categorized yet	GSE11141	NgR bitransgenic overexpression in mature brain dentate gyrus _vs_ developing brain	+	202	1.80E-14
278	Aging	GSE19626	Eyes of wildtype mice - E16.5 embyros _vs_ E10.5	+	409	1.90E-14
279	Genetic modification	GSE9892	Liver from TGFbeta1 null mice _vs_ wildtype	+	413	1.90E-14
280	Comparison of tissues	GSE15330	Wildtype megakaryo-erythrocyte progenitors _vs_ hematopoetic stem cells	-	474	2.00E-14
281	Aging	GSE5334	Gonad development at pnd 2 _vs_ gd14	+	420	2.10E-14
282	Comparison of tissues	GSE13394	Purkinje neurons from cerebellum _vs_ motor neurons from brainstem	-	784	2.20E-14
283	Treatment	GSE19322	Non-infarct region of left ventricle of MRL mice - 5d after myocardial infarction _vs_ healthy	+	368	2.20E-14
284	Treatment	GSE5555	Lungs with resolved N. brasiliensis infection- 6hr post PBS challenge _vs_ no challenge	-	424	2.40E-14
285	Not categorized yet	GSE5350	Ambion human brain reference RNA _vs_ Stratagene universal reference RNA_Illumina plat_GPL2507	+	735	2.40E-14
286	Comparison of tissues	GSE15724	Tracheal epithelium- basal cells (KRT5-GFP- lectin+) _vs_ columnar cells (KRT5-GFP- lectin-).1	+	301	2.40E-14
287	Not categorized yet	GSE10913	Murine decidual response in uterine stroma Bmp2 ff uterus horn _vs_Bmp2 dd uterus horn	-	245	2.50E-14
288	Aging	GSE5334	Gonad development at pnd 0.5 _vs_ gd12	+	519	2.60E-14

289	Tumor	GSE15460	Pool of gastric cancer cell lines _vs_ primary gastric tumors_GPL570	−	743	2.60E−14
290	Comparison of tissues	GSE13394	Drd2 subclass of medium spiny neurons from mouse striatum _vs_ motor neurons from brainstem	+	781	2.70E−14
291	Drug treatment	E−TABM−141	Min6 B1 pancreatic beta cells pretreated with CHX− chlorophenylthio−cAMP + glucose _vs_ no treatment	−	432	2.70E−14
292	Comparison of tissues	GSE13408	Wildtype Embryoid body _vs_ Embryonic Stem Cells	+	481	2.70E−14
293	Neurodegeneration	GSE23182	Hippocampal tissue from mice innoculated with ME7 prion + 500ug/kg LPS 18wk after _vs_ saline	+	198	2.80E−14
294	Tumor	GSE14038	Primary tumor dermal neurofibroma _vs_ universal tissue reference	+	744	2.80E−14
295	Infection	GSE11494	NALT from mice infected with attenuated S. pyogenes lacking M1 and SCPA proteins _vs_ sham infected	+	140	2.80E−14
296	Infection	GSE13522	Skin from Balb/c mice infected by Trypanosoma cruzi Y strain 24hr _vs_ saline control	+	349	2.80E−14
297	Not categorized yet	GSE10011	NIH−3T3 labelled 30min 200uM 4−thiouridine − newly transcribed RNA _vs_ total cellular RNA	−	832	2.90E−14
298	Infection	E−MEXP−1190	Liver from C57BL−6 mice T. congolense−infected for 17d _vs_ uninfected	+	608	3.00E−14
299	Injury	GSE5296	Spinal cord above impact site 7d after injury _vs_ naive	+	248	3.10E−14
300	Relative gene expression	GSE4734	DBA_2J bed nucleus of the stria terminalis − relative gene expression compared to the median of its expression across 5 brain regions in 6 strains	+	1411	3.40E−14

Table 8. Comprehensive comparison of gene expression patterns in human brain disorders and Shn-2 KO mice.

Shn-2 KO PFC　Homo Sapiens, mental or neuronal disorder, Postmortem brain, disease vs normal

							Positive Correlation				Negative Correlation			
Disease	Study Name	Series ID	Bioset Name	Score	P value	Correlation	Common Genes	↑ ↑	P value	↓ ↓	P value	↑ ↓	P value	↓ ↑	P value
Schizophrenia	Post-mortem tissue from brain BA10 region of schizophrenic and control patients	GSE17612	Brain BA10 from all schizophrenic samples _vs_ controls above control group mean pH6.5	6	9.50E-14	+	100	34	6.1E-13	42	3.6E-16	16	0.0790	8	0.3047
Tuberous sclerosis	Gene expression in cortical tubers isolated from tuberous sclerosis complex patients	GSE16969	Postmortem cortical tuber tissue from tuberous sclerosis complex patients _vs_ unaffected	5	1.50E-11	+	275	84	3.5E-15	81	7.2E-09	68	0.5150	47	0.2073
HIV-associated neurocognitive disorders	Brain tissue from postmortem patients with HIV-associated neurocognitive disorders	GSE28160	Brains of HIV-associated neurocognitive disorder patients _vs_ healthy HIV-negative controls	5	2.80E-11	+	215	62	4.6E-15	65	2.5E-15	69	2.9E-07	25	0.5021
Alzheimer	Pyramidal cell gene expression from brain regions in Alzheimer's disease and normal aged brains	GSE5281	Pyramidal cells from primary visual cortex of Alzheimer patient brains _ vs_ from aged normal brains	4	3.90E-10	+	272	69	4.8E-06	116	7.6E-15	63	0.9515	39	0.2483
Alzheimer	Alzheimers disease with and without neurofibrillary tangles	GSE4757	Alzheimer's disease neurons – with neurofibrillary tangles _vs_ normal	3	2.50E-08	+	113	31	1.7E-07	43	5.9E-13	28	0.0007	12	0.2092
Autism spectrum disorder	Cerebellum, frontal cortex, and temporal cortex gene expression from ASD patients	GSE28521	Prefrontal cortex of autism spectrum disorder (ASD) patients _vs_ healthy donor	3	4.10E-08	+	58	24	3.1E-09	19	1.9E-07	10	0.6076	5	0.5696
Parkinson's disease	Substantia nigra and frontal gyrus brain regions in Parkinson's disease patients	GSE8397	Medial substantia nigra from Parkinson's disease patients _vs_ normal donors	3	4.90E-07	+	135	33	6.2E-05	56	1.3E-07	31	0.4574	15	0.7685
Huntingtons disease	Huntington's disease – Cerebellum, Caudate nucleus, Motor cortex BA4, and Prefrontal cortex BA9	GSE3790	Prefrontal Cortex BA9- Huntingtons disease grade 0 _vs_ control_GPL96	3	7.60E-07	–	65	9	0.1259	9	0.081	18	2.6E-05	29	2.3E-10
Schizophrenia	Neuroinflammatory pathways of different neurodegenerative diseases	GSE26927	Grey matter in Brodmann area of Schizophrenia patients _vs_ normal controls	2	3.70E-05	+	58	10	0.0550	11	0.2555	8	0.2638	29	7.5E-11
Schizophrenia	Prefrontal cortex gene expression in schizophrenic patients at different stages of illness	GSE21138	Prefrontal cortex Brodmann area 46 – schizophrenics with intermediate DOI _vs_ healthy controls	2	7.10E-05	+	77	14	0.0492	35	9.1E-10	18	0.3584	13	0.0247
Schizophrenia	Prefrontal cortex gene expression in schizophrenic patients at different stages of illness	GSE21138	Prefrontal cortex Brodmann area 46 – schizophrenics with long DOI _vs_ healthy controls	2	8.40E-05	+	19	3	0.0082	11	2.2E-08	3	0.1520	2	0.1674
Downs Syndrome	Downs Syndrome brains	GSE5390	Postmortem brain Downs syndrome _vs_ healthy controls	2	8.40E-05	+	165	62	0.0007	44	3.5E-07	40	0.0374	22	0.9379
Parkinson's disease	Substantia nigra gene expression in Parkinson's disease patients	GSE20292	Postmortem brain whole substantia nigra from Parkinsons disease patients _vs_ unaffected	1	9.00E-04	+	60	21	0.0029	22	3.9E-05	9	0.8082	8	0.1563
Alzheimer	Genetic control of human brain transcript expression in Alzheimer' s disease	GSE15222	Cortical tissue from male Alzheimer's disease patients _vs_ male normal parietal cortex	2	0.0001	+	193	43	0.0174	66	8.3E-10	65	0.0014	24	0.5513
Alzheimer	Hippocampal gene expression from Alzheimer's diease patients of varying severity	GSE1297	Hippocampal CA1 from severe Alzheimer's disease patients (MMSE<14) _vs_ control (MMSE>25)	2	0.0002	+	98	22	0.0003	37	1.3E-07	30	0.0053	10	0.2200
Bipolar	Endothelial and neuronal cells from normal, bipolar, and schizophrenia patients	GSE12679	Neurons of dorsolateral prefrontal cortex of postmortem bipolar patients _vs_ control	2	0.0002	+	53	13	0.0012	23	9.0E-07	13	0.0578	5	0.3644
Parkinson's disease	Substantia nigra from Parkinson's disease patients	GSE7621	Substantia nigra from Parkinson disease patients _vs_ normal	1	0.001	+	102	32	0.1015	30	1.1E-06	16	0.8031	24	0.1307
Parkinson's disease	Substantia nigra of Parkinson's disease patients	GSE20164	Substantia nigra collected at autopsy from brains of Parkinsons disease patients _vs_ control	1	0.0012	+	25	11	5.7E-06	7	0.0466	6	0.2701	1	0.6529
Alzheimer	Hippocampus of Alzheimer' s disease patients	GSE28146	CA1 hippocampal gray matter from patients with severe Alzheimers Disease _vs_ healthy control	1	0.0016	+	105	29	0.0006	35	2.4E-05	27	0.0522	17	0.1113
Parkinson's disease	Globus pallidus interna from postmortem brains of Parkinson's disease patients	GSE20146	Globus pallidus interna from Parkinsons disease patients _vs_ unaffected	1	0.0019	+	44	14	9.7E-05	13	0.0016	12	0.0776	5	0.5559
Alzheimer	Study of synaptic function and neuroplasticity in incipient AD	GSE12685	Synaptoneurosomes from frontal cortex of Alzheimer's Disease patient with normal MMSE _vs_ control	1	0.0058	–	48	13	0.8230	2	0.5446	5	0.1514	28	0.0001
Bipolar	Human adult postmortem brain tissue from subjects with bipolar disorder	GSE5392	Orbitofrontal cortex from bipolar disorder subjects _CHGN vs healthy control	1	0.0092	+	67	16	0.0012	26	0.0049	14	0.9310	11	0.0786
Parkinson's disease	Brain regions affected and non-affected by Parkinson's disease (PD) in PD and normal patients	GSE28894	Frontal cortex of Parkinson's disease patients _vs_ normal subjects	1	0.0156	+	62	30	3.5E-05	8	0.3887	7	0.9333	18	0.0594
Parkinson's disease	Putamen gene expression in brains of Parkinson's disease patients	GSE20291	Postmortem brain putamen from male Parkinsons disease patients _vs_ unaffected	1	0.0193	+	16	4	0.1444	8	0.0007	2	0.4982	2	0.5243
Parkinson's disease	Substantia nigra pars compacta gene expression in neurons from Parkinson's disease patients	GSE20141	Substantia nigra pars compacta neurons from Parkinsons disease patients _vs_ control	1	0.0204	+	136	54	0.0003	30	0.1155	27	0.8151	32	0.1017
Parkinson's disease	Substantia nigra gene expression in Parkinsons disease patients	GSE20163	Substantia nigra of Parkinsons disease patients _vs_ unaffected individuals	1	0.0271	+	43	2	0.0424	20	8.5E-05	17	0.0534	4	0.0901
Schizophrenia	Cerebellum expression profile from schizophrenic patients	GSE4036	Cerebellum from schizophrenic patients _vs_ normal	1	0.0376	–	15	3	0.1070	2	0.2391	5	0.0071	5	0.0051
Alzheimer	Astrocyte gene expression in the aging brain related to Alzheimer's pathology and ApoE genotype	GSE29652	Astrocytes of Braak stage III-IV Alzheimers patients – APOE e4 positive _vs_ APO e4 negative	1	0.0415	–	7	1	1.0000	1	1.0000	6	0.0034	1	0.5127
Alzheimer	Non-amplified RNA microarray analysis and intra and inter-method reproducibility	GSE30945	Brain RNA non-amplified – Alzheimer patient _vs_ pooled normal donors	1	0.049	+	101	33	0.0012	24	0.1580	30	0.1177	15	0.6580
Schizophrenia	Prefrontal cortex expression profile of bipolar disorder, depression, and schizophrenia patients	GSE12654	Postmortem prefrontal cortex from patients with schizophrenia _vs_ control	1	0.0722	–	8	1	0.0981	0	1	6	0.0030	1	0.1675
Leison	White matter gene expression in lesion areas of patients with fulminant acute multiple sclerosis	GSE32915	White matter – initial lesions of patients with active MS _vs_ healthy controls	0	0.0817	–	90	5	0.6971	30	0.2787	48	0.0058	7	0.2252
Parkinson's disease	Imaging-guided microarray: Identifies molecular markers in the pathogenesis of Parkinson disease	GSE19587	Inferior olivary nucleus of postmortem brain – Parkinsons _vs_ healthy control	1	0.078	–	75	8	0.3639	18	0.0428	40	0.0021	10	0.0441
Parkinson's disease	Substantia nigra from Parkinsons disease patients with incidental Lewy body disease	GSE20159	Substantia nigra from Parkinson disease patients with incidental Lewy body disease _vs_ unaffected	0	0.0812	+	18	6	0.0065	5	0.2422	5	0.8081	2	0.2941
Alzheimer	mRNA expression in parietal lobe cortex in Alzheimer's disease	GSE16759	Parietal lobe of Alzheimers patients _vs_ healthy controls	0	0.148	+	39	15	0.0371	11	0.2241	9	0.5082	6	0.7473
Rett syndrome	Superior frontal gyrus of girls with Rett syndrome	GSE6955	Superior frontal gyrus from girls (2-8years old) with Rett syndrome _vs_ age matched controls	0	0.1526	–	4	1	0.3812	0	1	1	0.0596	2	0.1490
Bipolar	Adult postmortem brain tissue (dorsolateral prefrontal cortex) from bipolar disorder	GSE5388	Postmortem brain from patient with bipolar disease _vs_ healthy control	0	0.1618	+	18	2	0.2635	12	0.0154	3	0.8846	1	0.1754
Parkinson's disease	Dopamine neurons of substantia nigra pars compacta from Parkinsons disease patients	GSE24378	Dopamine neurons of substantia nigra pars compacta from Parkinsons disease patients _vs_ controls	0	0.1733	–	58	13	0.0019	12	0.3866	23	0.0069	11	0.0032
Trisomy 21 and 13	Trisomy 21 and 13 expression from fetal cerebrum, cerebellum, and heart	GSE1397	Fetal cerebrum with trisomy 21 _vs_ euploid	0	0.1737	+	16	4	0.3372	6	0.0579	2	0.8630	4	0.7497
	Prefrontal cortex expression profile of bipolar disorder, depression, and schizophrenia patients	GSE12654	Postmortem prefrontal cortex from patients with bipolar disorder _vs_ control	0	0.1854	–	2	0	1	0	1	2	0.0344	0	1.0000
ALS	Motor neurons from patients with SOD1-related amyotrophic lateral sclerosis (ALS)	GSE20589	Motor neurons from cervical spinal cords of ALS patients with SOD1 mutations _vs_ normal controls	0	0.2012	–	59	12	0.2937	18	0.1153	12	0.8851	18	0.0015
Parkinson's disease	Cerebellum gene expression in Parkinsons disease patients	GSE20314	Cerebellum of Parkinsons disease patients _vs_ unaffected individuals	0	0.5651	–	24	3	0.2976	7	0.0142	8	0.0436	6	0.0308
Major depression	Frontal cortex of HIV patients with and without major depressive disorder (MDD)	GSE17440	Frontal cortex of HIV patients with major depressive disorder _vs_ w-o major depressive disorder	0	0.5767	–	59	21	0.1309	9	0.1550	14	0.0087	16	0.7757
	Prefrontal cortex expression profile of bipolar disorder, depression, and schizophrenia patients	GSE12654	Postmortem prefrontal cortex from patients with depression _vs_ control		Not significant										
Multiple sclerosis	Brain tissue from multiple sclerosis patients	GSE5839			Not signifincant										
Multiple sclerosis	Expression data from patients presenting a first demyelinating event (early multiple sclerosis)	GSE19470			Not signifincant										
ALS	Human motor neuron gene expression in individuals with CHMP2B mutations	GSE19332			Not signifincant										

↑ ↑ genes up-regulated in both Shn-2 KO mice and brain disorder
↓ ↓ genes down-regulated in both Shn-2 KO mice and brain disorder
↑ ↓ genes in up-regulated Shn-2 KO mice and down-regulated in brain disorder
↓ ↑ genes in down-regulated Shn-2 KO mice and down-regulated in brain disorder

Table 9. Phenotypes of Shn-2 KO mice and abnormalities associated with schizophrenia.

	Schizophrenia (1, 2, 3)	Shn-2 KO mice
Positive Signs/Symptoms:	Psychomotor agitation	Increased locomotor activity
Negative Signs/Symptoms:	Social withdrawal	Decreased interaction with a juvenile conspecific, decreased preference for social novelty
	Self neglect	Decreased nest building behavior
Cognitive Signs/Symptoms:	Decreased working memory	Impaired performance in 8-arm radial maze working memory task, impaired working memory in T-maze task
	Deficits in attention/sensorimotor gating	Decreased sensorimotor gating (PPI deficits)
	Inflexibility	Normal performance in reversal learning in T-maze left-right discrimination
Other behavioral signs	Decreased pain sensitivity	Decreased pain sensitivity (5)
	Lack of activity, depressive mood	Increased depression-like behavior in sucrose preference test, Decreased depression-like behavior in forced swim test and tail suspension test (7)
	High prevalence of anxiety disorder/symptomatology (16)	Increased anxiety-related behaviors (4), Increased stay time on open arms in the elevated plus maze (14)
	Increased sensitivity to NMDAR antagonist	Increased sensitivity to MK-801
	Reduction of psychotic agitation by haloperidol (17)	Reduction of increased locomotor activity by haloperidol
	No improvement of PPI by haloperidol (18)	Improvement of PPI by haloperidol
	Reduction of aggression by clozapine (19)	Reduction of increased locomotor activity by clozapine
	Improvement of PPI by clozapine (20)	No improvement of PPI by clozapine
	Poor bilateral transfer (21)	Improved motor coordination in the Rotarod test
Physical signs	Hypercortisolemia (22)	Hypercortisolemia
	Lower body mass index (BMI) (23), no significant BMI difference in male (24), higher BMI in women (24)	Decreased body weight
Physiology (EEG)	Increased delta (25, 26), theta (25) power, Decreased alpha (25, 26), increased gamma power (27), decreased gamma power (28)	Increased Theta wave, decreased Gamma wave
Cortical Thickness	Reduction in frontal lobe and temporal cortex (29), normal (20)	Decreased cortical thickness in PrL and V1
Cortical Cell density	Increase (50, 51), decrease (52, 53), normal (27, 31)	Decrease
Hippocampus Volume	Decrease in bilateral volume (32), Decrease in total volume (33)	Tendency to be large (data not shown)
Parvalbumin	Decrease in hippocampus (34) , PFC (35)	Decreased in hippocampus , PFC
GAD67	Decrease in hippocampus (36), increase in DLPFC (37)	Decreased in hippocampus
Myelination/oligodendrocyte	Decreased CNPase (40), decrease myeline water fraction (5)	Decreased CNPase, MBP was decreased
Astrocytes	Increased GFAP (39, 47), increased S100beta (41, 42, 43, 44) decreased GFAP (38)	Increased GFAP, increased S100beta
Microglia	Increased activated microglia (45), microglia activation (46),	No significant change in Iba-1 expression
Dopamine receptor	Decreased D1R in prefrontal (48)	Decreased D1R binding in dentate gyrus
	Increased D2R in striatum (49)	No significant change in D2R binding

References and notes

(1) Tandon R, Keshavan MS, Nasrallah HA. Schizophrenia, "Just the Facts" : what we know in 2008 part 1: overview. Schizophr. Res. 2008; 100: 4-19.

(2) Keshavan MS, Nasrallah HA, Tandon R. Schizophrenia,「Just the Facts」6. Moving ahead with the schizophrenia concept: from the elephant to the mouse. Schizophr. Res. 2011; 127: 3-13.

(3) Powell CM, Miyakawa T. Schizophrenia-relevant behavioral testing in rodent models: a uniquely human disorder? Biol. Psychiatry. 2006; 59: 1198-1207.

(4) Takagi T, Jin W, Taya K, Watanabe G, Mori K, Ishii S. Schnurri-2 mutant mice are hypersensitive to stress and hyperactive. Brain Res. 2006; 1108: 88-97.

(5) The decreased pain sensitivity in these mice is consistent with reports showing that individuals with schizophrenia are less sensitive to physical pain than unaffected individuals (6).

(6) Dworkin RH. Pain insensitivity in schizophrenia: a neglected phenomenon and some implications. Schizophr Bull. 1994; 20: 235-248.

(7) Shn-2 KO mice were more mobile than wild type controls in the Porsolt forced swim test (Supplementary Figure 2f). We also performed the sucrose preference test, in which a reduced preference for sucrose is considered to represent anhedonia or depression-like behavior (8). Shn-2 KO mice showed a significantly lower preference for sucrose, which suggests increased depression-like behavior (Figure 8n). Anhedonia is a hallmark of schizophrenia (9). Many strains of schizophrenia model mice, including calcineurin KO mice (10), NR2A KO mice (11), and nNOS KO mice (12), appear to show a reduction in depression-like behavior during the forced swim test. However, these mice are not necessarily less sensitive to stress. Rather, this difference may reflect their hyperactive phenotype and/or their increased sensitivity to stress. It should be noted that depression is not included in the DSM IV diagnostic criteria for schizophrenia, although depressive symptoms are common throughout the course of the illness (13). Schizophrenic patients are likely to comprise several biologically distinct heterogeneous populations, which include patients with or without high levels of depression. Clearly, the characteristics of Shn-2 KO mice do not mimic those of the entire schizophrenic population, but rather those of a specific subset of patients. In this regard, the depression-related behavioral abnormalities shown by Shn-2 KO mice may not be inconsistent with the idea that they represent an animal model of schizophrenia.

(8) Nestler EJ, Hyman SE. Animal models of neuropsychiatric disorders. Nature Neuroscience. 2010; 13: 1161-1169.

(9) Der-Avakian A, Markou A. The neurobiology of anhedonia and other reward-related deficits. Trends in Neurosciences. 2012; 35: 68-77.

(10) Miyakawa T, Leiter LM, Gerber DJ, Gainetdinov RR, Sotnikova TD, Zeng H et al.. Conditional calcineurin knockout mice exhibit multiple abnormal behaviors related to schizophrenia. Proc Natl Acad Sci U S A. 2003; 100: 8987-8992.

(11) Boyce-Rustay JM, Holmes A. Genetic Inactivation of the NMDA Receptor NR2A Subunit has Anxiolytic- and Antidepressant-Like Effects in Mice. Neuropsychopharmacology. 2006; 31: 2405-2414.

(12) Tanda K, Nishi A, Matsuo N, Nakanishi K, Yamasaki N, Sugimoto T et al.. Abnormal social behavior, hyperactivity, impaired remote spatial memory, and increased D1-mediated dopaminergic signaling in neuronal nitric oxide synthase knockout mice. Mol Brain. 2009;2:19.

(13) Buckley PF, Miller BJ, Lehrer DS, Castle DJ. Psychiatric Comorbidities and Schizophrenia. Schizophr Bull. 2009; 35: 383-402.

(14) Shn-2 KO mice spent a significantly longer period of time in the open arm during the elevated plus maze test (Supplementary Figure 2c), suggesting decreased anxiety-like behavior. However, there was no significant difference in the anxiety-like behavior in the light/dark transition test between genotypes (Supplementary Figure 2d). During the elevated plus maze test, Shn-2 KO mice spent more time in the open arms and entered the open arms more frequently, which is usually considered a sign of decreased anxiety-like behavior. However, this behavior may simply be attributable to locomotor hyperactivity, and their anxiety-like behavior per se may not differ from that shown by their wild type littermates (it may even be increased). This interpretation stems from our previous findings that: 1) plasma corticosterone levels were significantly greater in KO mice subjected to restraint stress; 2) KO mice subjected to an unfamiliar environment showed behaviors indicative of heightened anxiety, such as backtracking, freezing, stretching, and escaping; and 3) the center stay time in the open field test, a frequently used index of anxiety-like behavior, decreased in Shn-2 KO mice (4). Indeed, plasma corticosterone levels were significantly higher in these mice than in the controls after the elevated plus maze test (Supplementary Figure 2e). Increased time spent in the open arms is sometimes interpreted as "panic-like escaping behavior" in mice showing increased anxiety-like behavior (10, 15), including forebrain-specific calcineurin KO mice, which we previously proposed as an animal model for schizophrenia. It should be noted that anxiety is common throughout the course of the illness (13), although anxiety is not included in the DSM IV diagnostic criteria for schizophrenia. Schizophrenic patients are likely to comprise several biologically distinct heterogeneous populations, which include patients with or without high levels of anxiety. Obviously, the characteristics of Shn-2 KO mice may not mimic those of the entire schizophrenic population, but rather those of a specific subset of patients. In this regard, the anxiety-like behavioral abnormalities shown by Shn-2 KO mice may not be inconsistent with the idea that they represent an animal model of schizophrenia and could be potentially interesting.

(15) Holmes A, Parmigiani S, Ferrari PF, Palanza P, Rodgers RJ. Behavioral profile of wild mice in the elevated plus-maze test for anxiety. Physiol. Behav. 2000; 71: 509-516.

(16) Seedat S, Fritelli V, Oosthuizen P, Emsley RA, Stein DJ. Measuring Anxiety in Patients with Schizophrenia. The Journal of Nervous and Mental Disease. 2007; 195: 320-324.

(17) Villari V, Rocca P, Fonzo V, Montemagni C, Pandullo P, Bogetto F. Oral risperidone, olanzapine and quetiapine versus haloperidol in psychotic agitation. Prog. Neuropsychopharmacol. Biol. Psychiatry. 2008; 32: 405-413.

(18) Wynn JK, Green MF, Sprock J, Light GA, Widmark C, Reist C et al.. Effects of Olanzapine, Risperidone and Haloperidol on Prepulse Inhibition in Schizophrenia Patients: A Double-Blind, Randomized Controlled Trial. Schizophr Res. 2007; 95: 134-142.

(19) Frogley C, Taylor D, Dickens G, Picchioni M. A systematic review of the evidence of clozapine's anti-aggressive effects. Int. J. Neuropsychopharmacol. 2012; 15: 1351-1371.

(20) Kumari V, Soni W, Sharma T. Normalization of information processing deficits in schizophrenia with clozapine. Am J Psychiatry. 1999; 156: 1046-1051.

(21) Mandal MK, Singh SK, Asthana HS, Srivastava P. Bilateral transfer deficit in schizophrenia. Comprehensive Psychiatry. 1992; 33: 319-324.

(22) Altamura AC, Boin F, Maes M. HPA axis and cytokines dysregulation in schizophrenia: potential implications for the antipsychotic treatment. Eur Neuropsychopharmacol. 1999; 10: 1-4.

(23) Sørensen HJ, Mortensen EL, Reinisch JM, Mednick SA. Height, weight and body mass index in early adulthood and risk of schizophrenia. Acta Psychiatrica Scandinavica. 2006; 114: 49-54.

(24) Allison DB, Fontaine KR, Heo M, Mentore JL, Cappelleri JC, Chandler LP et al.. The distribution of body mass index among individuals with and without schizophrenia. J Clin Psychiatry. 1999; 60: 215-220.

(25) Sponheim SR, Clementz BA, Iacono WG, Beiser M. Resting EEG in first-episode and chronic schizophrenia. Psychophysiology. 1994; 31: 37-43.

(26) Wada Y, Takizawa Y, Kitazawa S, Jiang ZY, Yamaguchi N. Quantitative EEG analysis at rest and during photic stimulation in drug-naive patients with first-episode paranoid schizophrenia. Eur Arch Psychiatry Clin Neurosci. 1994; 244: 247-251.

(27) Moran ZD, Williams TJ, Bachman P, Nuechterlein KH, Subotnik KL, Yee CM. Spectral decomposition of P50 suppression in schizophrenia during concurrent visual processing. Schizophrenia Research. 2012; 140: 237-242.

(28) Haig AR, Gordon E, De Pascalis V, Meares RA, Bahramali H, Harris A. Gamma activity in schizophrenia: evidence of impaired network binding? Clin Neurophysiol. 2000; 111: 1461-1468.

(29) Goldman AL, Pezawas L, Doz P, Mattay VS, Fischl B, Verchinski BA et al.. Widespread Reductions of Cortical Thickness in Schizophrenia and Spectrum Disorders and Evidence of Heritability. Arch Gen Psychiatry. 2009; 66: 467-477.

(30) Smiley JF, Konnova K, Bleiwas C. Cortical thickness, neuron density and size in the inferior parietal lobe in schizophrenia. Schizophr. Res. 2012; 136: 43-50.

(31) Analyses of cortical cell density in patients with schizophrenia have yielded conflicting results . This may be due to differences in the experimental methods used and the cortical regions examined in these studies. Two methods are used for cell-counting: a two-dimensional (2D) method and a three-dimensional (3D) method. Previous studies using the 2D method show decreased neuron density in the cortex of patients with schizophrenia, whereas studies using the 3D method seem to suggest the opposite. Also, the studies that failed to show a reduction in cell density focused on dorsolateral areas, such as Brodmann's area (BA) 9 or 47. By contrast, cortical cell density appeares to decrease in the BA 10 area of schizophrenic brains. Our own study used the 2D method to examine cell density in the medial prefrontal cortex, which corresponds to BA 32 and a part of BA10.

(32) Nelson MD, Saykin AJ, Flashman LA, Riordan HJ. Hippocampal volume reduction in schizophrenia as assessed by magnetic resonance imaging: a meta-analytic study. Arch. Gen. Psychiatry. 1998; 55: 433-440.

(33) Koolschijn PCMP, van Haren NEM, Cahn W, Schnack HG, Janssen J, Klumpers F et al.. Hippocampal volume change in schizophrenia. J Clin Psychiatry. 2010; 71: 737-744.

(34) Zhang ZJ, Reynolds GP. A selective decrease in the relative density of parvalbumin-immunoreactive neurons in the hippocampus in schizophrenia. Schizophr. Res. 2002; 55: 1-10.

(35) Reynolds GP, Beasley CL. GABAergic neuronal subtypes in the human frontal cortex—development and deficits in schizophrenia. J. Chem. Neuroanat. 2001; 22: 95-100.

(36) Benes FM, Lim B, Matzilevich D, Walsh JP, Subburaju S, Minns M. Regulation of the GABA cell phenotype in hippocampus of schizophrenics and bipolars. Proc. Natl. Acad. Sci. U.S.A. 2007; 104: 10164-10169.

(37) Dracheva S, Elhakem SL, McGurk SR, Davis KL, Haroutunian V. GAD67 and GAD65 mRNA and protein expression in cerebrocortical regions of elderly patients with schizophrenia. Journal of Neuroscience Research. 2004; 76: 581-592.

(38) Steffek AE, McCullumsmith RE, Haroutunian V, Meador-Woodruff JH. Cortical expression of glial fibrillary acidic protein and glutamine synthetase is decreased in schizophrenia. Schizophrenia Research. 2008; 103: 71-82.

(39) Pennington K, Dicker P, Dunn MJ, Cotter DR. Proteomic analysis reveals protein changes within layer 2 of the insular cortex in schizophrenia. Proteomics. 2008; 8: 5097-5107.

Table10. Expressions of classical inflammatory marker genes in the brains of Shn-2 KO mice and postmortem brains of schizophrenia.

					Shn-2 KO mice				SCZ (1)			Related supplemental table
		Symbol	Description	Probe ID/ ref seq	Assay	Area	Fold change	P value	Probe ID	Fold change	P value	
Complement		C1qa	complement component 1, q subcomponent, alpha polypeptide	1417381_at	expression microarray	mPFC	1.31	0.0019	218232_at	1.78	1.6E-05	2
					expression microarray	DG	1.28	0.0303				4
		C1qb	complement component 1, q subcomponent, beta polypeptide	1437726_x_at	expression microarray	mPFC	1.37	0.0080	202953_at	2.38	2.6E-05	2
		C1qc	complement component 1, q subcomponent, C chain	1449401_at	expression microarray	mPFC	1.39	0.0004	225353_s_at	2.20	0.0001	2
					expression microarray	DG	1.33	0.0239				4
		C1ql2	complement component 1, q subcomponent-like 2	1444687_at	expression microarray	DG	1.63	0.0088				4
		C1ql3	complement component 1, q subcomponent-like 3	1425176_at	expression microarray	DG	-1.48	0.0151				4
		C2	complement component 2 (within H-2S)	1457664_x_at	expression microarray	DG	1.29	0.0223	1554533_at	-1.02	0.2710	4
		C4b	complement component 4B (Childo blood group)	1418021_at	expression microarray	DG	2.46	0.0028				4
		Cfh	complement component factor h	1423153_x_at	expression microarray	DG	1.57	0.0081	213800_at	1.02	0.4178	4
HLA-induction		H2-Aa (HLA-DQA1)	histocompatibility 2, class II antigen A, alpha	1435290_x_at	expression microarray	mPFC	1.41	0.0060	212671_s_at	1.25	0.0788	10 (2)
					expression microarray	DG	2.71	0.0026				4
		H2-Ab1 (HLA-DQB1)	histocompatibility 2, class II antigen A, beta 1	1450648_s_at	expression microarray	mPFC	1.27	0.0270	212998_x_at	1.29	0.0390	2, 10 (2)
		H2-T23 (HLA-E)	histocompatibility 2, class II antigen Q, alpha 1	1449556_at	expression microarray	mPFC	-1.30	0.0060	200905_x_at	1.24	0.0095	10 (2)
		H2-Ea (HLA-DRA)	histocompatibility 2, class II antigen E alpha	1422892_s_at	expression microarray	DG	1.69	0.0191	210982_s_at	1.36	0.0578	4
		H2-D1	histocompatibility 2, D region locus 1	1427651_x_at	expression microarray	DG	1.47	0.0434				4
Cytokines	pro-inflammatory	Il1a	interleukin 1 alpha	NM_010554	quantitative PCR	HIPP	1.34	0.0817	210118_s_at	1.01	0.4413	
				1421473_at	expression microarray	mPFC	1.20	0.0444				
					expression microarray	DG	1.01	0.9189				
		Il1b	interleukin 1 beta	NM_008361	quantitative PCR	HIPP	-1.11	0.6230	39402_at	1.04	0.1604	
				1449399_a_at	expression microarray	mPFC	1.21	0.0327				
					expression microarray	DG	1.09	0.0596				
		Il2	interleukin 2	1449990_at	expression microarray	mPFC	-1.04	0.2027	217181_at	-1.01	0.3951	
					expression microarray	DG	1.03	0.5787				
		Il3	interleukin 3	1450566_at	expression microarray	mPFC	1.03	0.7002	207906_at	-1.04	0.2353	
					expression microarray	DG	1.08	0.1157				
		Il6	interleukin 6	NM_031168	quantitative PCR	HIPP	2.06	0.0746	243977_at	-1.02	0.2821	
				1450297_at	expression microarray	mPFC	1.15	0.0470				
					expression microarray	DG	1.00	0.9975				
		Il12a	interleukin 12a	1425454_a_at	expression microarray	mPFC	-1.36	0.1521	207160_at	-1.01	0.3319	
					expression microarray	DG	1.13	0.0847				
		Il15	interleukin 15	1418219_at	expression microarray	mPFC	1.04	0.3897	217372_at	1.02	0.2544	
					expression microarray	DG	-1.06	0.4606				
		Il17a	interleukin 17 alpha	1421672_at	expression microarray	mPFC	1.06	0.3669	205707_at	1.18	0.0004	
					expression microarray	DG	-1.09	0.1381				
		Il18	interleukin 18	1417932_at	expression microarray	mPFC	1.02	0.5895	206295_at	1.09	0.0631	
					expression microarray	DG	-1.09	0.0654				
		Il31	interleukin 31	1430001_at	expression microarray	mPFC	-1.05	0.1754	1553032_at	-1.00	0.4948	
					expression microarray	DG	1.06	0.1675				
		Tnf	tumor necrosis factor (tumor necrosis factor alpha)	NM_013693	quantitative PCR	HIPP	-1.12	0.6312	207113_s_at	1.04	0.1065	
				1419607_at	expression microarray	mPFC	-1.00	0.9904				
					expression microarray	DG	1.09	0.2969				
		Ccl2	chemokine (C-C motif) ligand 2	NM_011333	quantitative PCR	HIPP	1.70	0.0878	216598_s_at	1.16	0.2467	
				1420380_at	expression microarray	mPFC	1.04	0.3637				
					expression microarray	DG	1.20	0.0657				
		Ccl8	chemokine (C-C motif) ligand 8	1419684_at	expression microarray	mPFC	1.35	2.9E-05	214038_at	-1.09	0.0635	
					expression microarray	DG	1.36	0.0012				4
		Ccl17	chemokine (C-C motif) ligand 17	1419413_at	expression microarray	mPFC	-1.02	0.8010	226960_at	1.03	0.1761	
					expression microarray	DG	1.22	0.0252				4
		Ccl27a	chemokine (C-C motif) ligand 27A	1430375_a_at	expression microarray	mPFC	-1.32	0.0024	207955_at	-1.00	0.4766	
					expression microarray	DG	-1.44	2.1E-08				4
		Cxcl9	chemokine (C-X-C motif) ligand 9	1456907_at	expression microarray	mPFC	-1.04	0.5194	1560791_at	-1.01	0.4244	
					expression microarray	DG	1.13	0.0142				
		Cxcl10	chemokine (C-X-C motif) ligand 10	1418930_at	expression microarray	mPFC	1.01	0.8429	204533_at	1.17	0.1879	
					expression microarray	DG	1.50	0.1164				
		Cxcl16	chemokine (C-X-C motif) ligand 16	1449195_s_at	expression microarray	mPFC	1.06	0.3457	223454_at	1.13	0.0697	
					expression microarray	DG	1.26	0.0435				4
		Ifnb1	interferon beta 1, fibroblast	NM_010510	quantitative PCR	HIPP	-1.08	0.6360	208173_at	1.00	0.4712	
				1422305_at	expression microarray	mPFC	1.05	0.6214				
					expression microarray	DG	1.19	0.1535				
		Ifng	interferon gamma	1425947_at	expression microarray	mPFC	-1.13	0.0122	210354_at	-1.01	0.3638	
					expression microarray	DG	-1.00	0.9683				
	anti-inflammatory	Il4	interleukin 4	1449864_at	expression microarray	mPFC	-1.10	0.2368	207539_s_at	1.05	0.0633	
					expression microarray	DG	1.00	0.9691				
		Il5	interleukin 5	1450550_at	expression microarray	mPFC	1.01	0.7264	207952_at	1.02	0.3105	
					expression microarray	DG	-1.12	0.0173				
		Il10	interleukin 10	1420802_at	quantitative PCR	HIPP	-1.23	0.7710	207433_at	1.02	0.2500	
					expression microarray	mPFC	-1.02	0.6765				
					expression microarray	DG	-1.03	0.7388				
		Il13	interleukin 13	1420802_at	expression microarray	mPFC	-1.01	0.9250	207844_at	1.02	0.3450	
					expression microarray	DG	-1.06	0.1339				
		Il16	interleukin 16	1448686_at	expression microarray	mPFC	-1.16	0.0667	1555016_at	1.04	0.1071	
					expression microarray	DG	-2.38	0.0008				4
		Tgfb1	transforming growth factor, beta 1	1420653_at	expression microarray	mPFC	1.32	0.0212	203084_at	1.04	0.2116	
					expression microarray	DG	1.03	0.6899				

Abbreviations: HIPP, hippocampus; DG, dentate gyrus; PFC, medial prefrontal cortex; BA10, Brodmann area 10; SCZ, schizophrenia

Upregulated genes (fold change > 1.20, and P < 0.05)

Downregulated gene (fold change < −1.20, and P < 0.05)

No probe/no human homologue

(1) Genes differentially expressed in the BA10 of SCZ postmortem brain.
Maycox PR, Kelly F, Taylor A, Bates S, Reid J, Logendra R, et al. Analysis of gene expression in two large schizophrenia cohorts identifies multiple changes associated with nerve terminal function. Mol. Psychiatry. 2009; 14: 1083-1094.

(2) up-regulated in superior temporal cortex and anterior prefrontal cortex of SCZ postmortem brain.
Barnes MR, Huxley-Jones J, Maycox PR, Lennon M, Thornber A, Kelly F, et al. Transcription and pathway analysis of the superior temporal cortex and anterior prefrontal cortex in schizophrenia. Journal of Neuroscience Research. 2011; 89: 1218-1227.

Table 11. SNPs in, or in close proximity to, NF-kB binding sites within the MHC region that play a role in susceptibility to Schizophrenia, and expression of their neighboring genes.

SNP	Position	LD block[*1]	Disease association (reference)	P value	Distance (bp)[*2]	Matching Score[*3]	Putative NF-kB biding sequence[*4]	Neighbouring genes[*5]	Expressions in post-mortem brains of SCZ and/or BD patients[*6]	Expressions in PFC of Shn-2 KO mice[*7]
rs3734534	26240649	Block 1	SCZ(4)	3.33E-02	41	0.819	AAGGGAGGGCGCCAA	HIST1H3E, HIST1H2APS3, HIST1H1D, HIST1H4F, HIST1H4G, HIST1H3F	HIST1H1D: ↑(7) HIST1H3F: ↓(7)	
rs2072803	26392515		SCZ(3)	8.19E-07	5	0.944	GGGGGTTCCC	BTN2A2, BTN3A2, BTN3A1		
rs13219354	27185664		SCZ(3) SCZ(2)	1.12E-07 1.30E-10	−7	0.907	GGTAATGCCC	RPL10P2, TRNAV28, TRNAS7, TRNAR17, TRNAL10, TRNAV12, TRNAI17		
rs6917419	27243480	Block 3	SCZ(4)	1.42E-02	18 17	0.908 0.911	GGATATTCCC AGGATATTCCCG	PRSS16, LOC442172, TRNAI28P, TRNAS32P, TRNAI1, TRNAI11, TRNAV27, TRNAV31, TRANAQ27, TRNAS5		
rs3800316	27256102		SCZ(1) SCZ(3)	3.80E-08 3.81E-08	37	0.826	GGAGGTTTCC	LOC442172, TRNAI28P, TRNAS32P, TRNAI1, TRNAI11, TRNAV27, TRNAV31, TRANAQ27, TRNAS5		
rs7746199	27261324		SCZ(1) SCZ(3)	5.00E-08 5.03E-08	−32	0.911	TGGGAATATCCT	TRNAS5P, TRNAI1, TRNAI11, TRNAV27, TRNAI28P, TRNAV31, TRNAS32P, TRNAQ27, TRNAS5, POM121L2		
rs3800318	27263641	Block 4	SCZ(1) SCZ(3)	6.40E-08 6.38E-08	15	0.885	AGGACTTACC	TRNAI1, TRNAI11, TRNAV27, TRNAI28P, TRNAV31, TRNAS32P, TRNAQ27, TRNAS5, POM121L2		
rs12182446	27745738		SCZ(3)	4.77E-07	41	0.894	AGGAATTACC	TRNAV7, LOC100131289, TRNAM2, RSL24D1P1, TRNAQ27, TRNAQ10, HISTH4PS1, HIST1HNB, HIST1H2AI		
rs17693963	27710165	Block 5	SCZ(3)	2.81E-07	39	0.842	GGGGTTTTTC	TRNAT18, TRNAV15, GPR89P, TRNAV7, LOC100131289		
rs200991	27815494		SCZ(4)	1.37E-02	−9 11	0.820 0.831	GGAAACTGCT TGGTTCTTCC	LOC100996513, HIST1H2AK, HIST1H4K, HIST1H2BN, HIST1H1B, HIST1H2BPS2, HIST1H2AL	HIST1H2BN: ↑(7) HIST1H4K: ↑(8) HIST1H1B:↑(8)	
rs184215243	27925555				0	0.877	GNGAAGTCCC	OR2W6P, OR2B6, RPLP2P1, OR2W4P		
rs1150683	28155314		SCZ(4)	1.72E-02	11	0.831	GGGTTTCTCC	ZNF192P2, ZNF603P		
rs2299030	28198755	Block 6	SCZ(4)	2.85E-02	3	0.805	GTGCATTCCC	ZNF193, TRNAS13, TOB2P1, ZKSCAN4		
rs114108814	28251663				0	0.867	AGGAAGATCCCN	ZNF187, PGBD1		
rs13211507	28257377		SCZ(2)	8.30E-11	−10	0.853	GTGAAGCCCC	PGDB1, ZNF187		
rs6918631	28312456		SCZ(4)	1.06E-04	18	0.920	GGGAATTCCA	ZNF323, ZKSCAN3		
rs13213152	28349698		SCZ(5)	8.43E-06	0	0.805	[A/G]GGAGGTCCC	ZSCAN12, ZKSCAN3		
rs6927023	28454221		SCZ(4)	2.93E-05	−19	0.876	GGAAGAACCC	TRNAL12, TRNAL47P, TRMEP1, TRNAT5, GPX6		
rs2269554	28994989		SCZ(4)	2.96E-02	42	0.847	TGGTCTTGCC	ZNF211, DR2AD1P, LOC100129636		
rs2394514	29023214		SCZ(4)	1.16E-05	−14	0.838	CAGAATTTCC	LOC100129636		
rs11961013	29471934		SCZ(4)	3.11E-02	−29	0.825	CCTGAATATCCCCC	MAS1L, RPS17P1		
rs112248026	29542215				0	0.734	GTGAGGTNCC	UBD, OR2H5P, TMEM183AP1, RPL13AP, OR2H2		
rs3129090	29664131		SCZ(4)	3.24E-02	34	0.894	GGGAACCCCA	ZFP57, ZDHHC20P1		
rs3871467	29677249		SCZ(4)	7.27E-03	−8	0.857	GGCCACTCCC	ZDHHC20P1, HLA-F, HCG4P11, RPL23AP1, HLA-F-AS1		
rs1611388	29680789		SCZ(4)	4.24E-02	28	0.841	AGGGGACTTGCTTC	ZDHHC20P1, HLA-F, HCG4P11, RPL23AP1, HLA-F-AS1		
rs2072898	29692729		SCZ(4)	5.14E-04	−26	0.960	GGAAACCCCA	HCG4P11, HLA-F, RPL23AP1, HLA-F-AS1, MICE		
rs1736913	29704400		SCZ(4)	4.60E-05	1	0.930	TGGTGTTTCC	HCG4P11, HLA-F, RPL23AP1, HLA-F-AS1, MICE, HCG9P5, IFITM4P		
rs9258215	29707307		SCZ(4)	1.50E-02	22	0.828	GAGAGATCCC	HCG4P11, HLA-F, RPL23AP1, HLA-F-AS1, MICE, HCG9P5, IFITM4P		
rs1737055	29733742		SCZ(4)	3.50E-02	10 26	0.991 0.847	GGAAACTCCC AGGGGAACTTCAGA	3.8-1.5, HLA-F-AS1, IFITM4P, MICE, HCG9P5		
rs1737030	29737563		SCZ(4)	3.70E-02	−11	0.858	GGGAATTGTC	3.8-1.5, HLA-F-AS1, IFITM4P, MICE, HCG9P5		
rs2734990	29812505		SCZ(4)	2.14E-02	4	0.820	ATGAGTTTCC	HCG4P8, HLA-G, HCGVIII-2, MICF	HLA-G: ↑(9)	
rs1611637	29836741		SCZ(4)	2.22E-02	−10 19	0.863 0.814	TGGCTTTCCC CAAGTATTTCCCCT	3.8-1.4		
rs9259843	29896001				0	0.810	ATGGAANCTTCCAG	MCCD1P1, 3.8-1.3, HCG4B, HLA-K, HLA-U, HCG4P5, HLA-A		
rs2524005	29899677		SCZ(5) SCZ, BD(5)	3.81E-07 4.95E-07	10	0.824	GTCAAGCCCC	HCG4B, HLA-K, HLA-U, HCG4P5, HLA-A	HLA-A:↑(10)	
rs6925061	29992286		SCZ(4)	1.17E-02	12	0.838	GGAAATTCAA	HLA-J, HCG8, ZNRD1-AS1, ETF1P1, HCG4P3	HLA-J: ↑(8)	
rs11965452	30011802		SCZ(4)	3.98E-02	28	0.835	GGAATCACCT	ZNRD1-AS1, ETF1P1, ZNRD1		
rs145478650	30128479				0	0.801	GGGGACTNCTCC	TRIM40, TRIM10, TRIM15	TRIM15: ↑(7, 9)	
rs12663184	30301600		SCZ(4)	2.80E-02	−42	0.972	CAGGAACTTCCCCA	HCG18, HCG17, TRIM39, TRIM39-RPP21, HLA-N	HCG18: ↑(7)	
rs4713325	30383442		SCZ(4)	2.14E-02	−40 −13	0.921 0.829	AGGCGTTTCC CTGACTTTCC	MICC		
rs4713328	30383876		SCZ(4)	7.51E-03	−15	0.814	GGGGCTTGGC	MICC		
rs2157605	30454076		SCZ(4)	4.12E-03	14	0.808	GGGTGTTTTC	TMPOP1, SUCLA2P1, RANP1, HLA-E		HLA-E: ↓
rs188502980	30530949				0	0.721	TGTGACTTCCNA	GNL1, PRR3, ABCF1	GNL1: ↓(7, 12)	
rs148600920	30670918				0	0.916	TGGGGATTCCCN	PPP1R18, NRM, RPL7P4, MDC1, TUBB		
rs150040417	30680130				0	0.729	GCNGGACTTCCTTC	RPL7P4, MDC1, TUBB	TUBB: ↓(7), ↑(9)	
rs142435078	30864590				0	0.748	AGTGGATTTCCNTC	DDR1, GTF2H4, VARS2	DDR1: ↑(7, 9) GTF2H4: ↑(7)	
rs2530709	30940569		SCZ(4)	3.80E-02	−25	0.830	AGTGGATGTACCCA	DPCR1, LOC100422429, LOC100420530, MUC21,		
rs12528087	30980603		SCZ(4)	4.98E-02	−5	0.847	GGGGCTTTGC	MUC22		
rs9263715	31095801		SCZ(4)	5.48E-04	−40	0.852	GGCAGGGCCC	C6orf15, CDSN, PSORS1C1, PSORS1C2, POLR2LP, CCHCR1		
rs3134762	31210866		SCZ(4)	1.24E-02	30	0.881	AGGATATTCC			
rs1050437	31239585									
rs72558135	31239586									
rs1050438	31239592									
rs41542719					0	0.870	GGAGAGCCCCN	HLA-C, USP8P1, RPL3P2, WASF5P		
rs3177890	31239593									
rs41542719										
rs45574634	31239594									
rs16899205	31266361		SCZ(4)	4.47E-02	−42	0.815	ATGGGAGGTTCTCA	USP8P1, RPL3P2, WASF5P		
rs2524089	31266522		SCZ(4)	1.46E-02	28	0.840	GGGACAGACC	USP8P1, RPL3P2, WASF5P		
rs2844569	31336604	Block 7	SCZ(4)	3.85E-02	36	0.825	AAGGACAATCCACA	HLA-B, DHFRP2, FGFR3P1, ZDHHC20P2, HLA-S	HLA-B: ↓(9)	
rs2524094	31240041				0	0.819	NGGATTCTCC	HLA-C, USP8P1, RPL3P2, WASF5P		
rs2442749	31352040		SCZ(4)	6.65E-04	43	0.923	GGGGACTTCC	DHFRP2, FGFR3P1, ZDHHC20P2, HLA-S, MICA		
rs78961316 rs75369119	31325125				0	0.900	TGGNGAATCCCC	HLA-B, DHFRP2	HLA-B: ↓(9)	
rs191718782	31528188				0	0.884	NGGGGTTCCC	ATP6V1G2-DDX39B, DDX39B, ATP6V1G2, NFKBIL1, LOC100287329, LTA, TNF	ATP6V1G2: ↓(7)	
rs147118182	31550289				0	0.706	GGACTTTCCN	LOC100287329, LTA, TNF, LTB, LST1, LST1	LST1: ↓(11)	
rs2857597	31585000		SCZ(4)	2.57E-02	42	0.914	GGAATCCCCC	UQCRHP1, AIF1, SNORA38, PRRC2A	AIF1: ↓(11), ↑(12)	AIF1: ↑
rs151200532	31601179				0	0.885	CNGGGGCTTCCCCT	AIF1, SNORA38, PRRC2A, BAG6, APOM	AIF1: ↓(11), ↑(12)	AIF1: ↑
rs113819636	31601185									
rs2272593	31601344				0	0.900	GGGGANGCCC	AIF1, SNORA38, PRRC2A, BAG6, APOM	AIF1: ↓(11), ↑(12)	AIF1: ↑
rs1046089	31602967		SCZ(4)	1.19E-02	−38	0.810	GGGAGCAGCC	AIF1, SNORA38, PRRC2A, BAG6, APOM	AIF1: ↓(11), ↑(12)	AIF1: ↑
rs805301	31618121		SCZ(4)	4.55E-03	45	0.821	GGAAATCACA	PRRC2A, BAG6, APOM, C6orf47, GPANK1, CSNK2B, LY6G5B		
rs147925659	31615449				0	0.772	GGGGCANGCTCCTC	PRRC2A, BAG6, APOM, C6orf47, GPANK1, CSNK2B		
rs142009508	31627341				0	0.803	GGACACCCCN	BAG6, APOM, C6orf47, GPANK1, CSNK2B, LY6G5B, LY6G5C		

rs11549123	31702008				0	0.778	TTGGGAACTGNCCA	LY6G6D, LY6G6C, C6orf25, CLIC1, MSH5-SAPCD1, MSH5	CLIC1: ↑(12)	
rs707928	31742590		SCZ(4)	2.34E-03	-10	0.811	TGTGTTTTCC	MSH5, MSH5-SAPCD1, SAPCD1, VMA7, VARS	VMA7: ↓(9)	
rs140366323	31749648				0	0.819	AGNGGACACTCCGA	MSC5, MSH5-SAPCD1, SAPCD1, VWA7, VARS, LSM2	VMA7: ↓(9)	
rs145442830	31749658									
rs41258944	32017242				0	0.891	GGGGGACNGTCCAG	C4A*8, C4B, CYP21A2, TNXB	C4A; ↑(12)	C4A; ↑ C4B; ↑
rs61745920										
rs61746537	32017243									
rs61740712	32021355				0	0.855	CNGGGACCATCCAG	C4A*8, C4B, CYP21A2, TNXB	C4A; ↑(12)	C4A; ↑ C4B; ↑
rs141752970	32021358									
rs142409885	32032790				0	0.758	CGGNGACTGTCCAG	TNXB		
rs3749962	32036357				0	0.806	NGGAACTGTCCA	TNXB		
rs61744966	32036363									
rs112581362	32057142				0	0.806	GGGNCTCGCC	TNXB		
rs117182156	32057148									
rs186990718	32121861				0	0.797	AGAAAGNCCC	PRRT1, LOC100507547, PPT2, PPT2-EGFL8, EGFL8, AGPAT1	PRRT1: ↑(7)	
rs1661134	32155121				0	0.868	TTGGAACTTTCCNA	PPT2-EGFL8, EGFL8, AGPAT1, RNF5, AGER, PBX2, GPSM3, NOTCH4	AGER: ↑(9) PBX2: ↑(8) GPSM3: ↑(8)	
rs146965329	32155125									
rs3131296	32172993		SCZ(2)	2.30E-10	37	0.894	GTGAATTCCC	AGER, PBX2, GPSM3, NOTCH4	AGER: ↑(9) PBX2: ↑(8) GPSM3: ↑(8)	
rs143622513	32181942				0	0.709	AGGTNCCCCC	GPSM3, NOTCH4		
rs146606566	32181945									
rs138205668	32188865				0	0.834	NGTGGACCCTCCTG	NOTCH4		
rs141236527	32188869									
rs146677249	32364137				0	0.864	TNGGAAGGTCCATT	HCG23, BTNL2		
rs115417906	32489822				0	0.894	GGNACTCCCC	HLA-DRB5	HLA-DRB5: ↑(7, 12)	
rs148834340	32489825									
rs3117099	32358270		SCZ(5) SCZ, BD(5)	4.12E-06 2.70E-06	6	0.847	CTGGAAGTCCCT	C6orf10, HCG23, BTNL2		C6orf10: ↑
rs9272219	32602269		SCZ(1) SCZ(3)	6.90E-08 6.88E-08	-2	0.977	AGGAATTTCC	HLA-DQA1	HLA-DQA1: ↑(13)	HLA-DQA1: ↑
rs115222936	32605039				0	0.901	GGGATTNCCC	HLA-DQA1	HLA-DQA1: ↑(13)	HLA-DQA1: ↑
rs9274652	32636235	Block 8			0	0.894	GGGGATTCCN	HLA-DQB1	HLA-DQB1: ↑(7, 12, 13)	
rs9276227	32700684		SCZ(4)	1.06E-02	-15	0.885	GGCAACTCCT	HLA-DQA2		
rs17220178	32794947				0	0.843	TGGAAANTACCT	HLA-DOB, TAP2, PSMB8, LOC100507463, TAP1	TAP2: ↑(9) TAP1: ↑(12)	
rs147219068	32940687									
rs140566548	32940694				0	0.798	NGTGACTCCCCA	HLA-DMA, BRD2	HLA-DMA: ↑(12)	
rs142520217	32940695									
rs34652619	32942636				0	0.901	NGGAGTTCCC	BRD2		
rs1048780	33170841				0	0.754	GGNGACTTTGCC	COL11A2, RXRB, RNY4P10, SLC39A7, MIR219-1, HSD17B8, RING1, ZNF70P1	RXRB: ↓(7), ↑(9)	
rs150581613	33173227				0	0.732	GGCNCCTTCC	COL11A2, RXRB, RNY4P10, SLC39A7, MIR219-1, HSD17B8, RING1, ZNF70P1	RXRB: ↓(7), ↑(9)	

Abbreviations: SNP, single-nucleotide polymorphism; LD, linkage disequilibrium; SCZ, schizophrenia; BD, bipolar disorder

*1: LD blocks reported in a previous study (3) (Blocks 6-8; estimated based on Figure S10 in (3))

*2: distance (bp) between the predicted NF-kappaB binding region and the most proximal (0-40bp) SNP site (plus, 5'->3'; minus, 3'->5'; 0, SNP on NF-kappaB binding region)

*3: matching score between a matrix of NF-kappaB binding sites and an arbitrary section of the input sequence (calculated using Match (http://www.gene-regulation.com/cgi-bin/pub/programs/match/bin/match.cgi) using a library of mononucleotide weight matrices fromTRANSFAC)

*4. NF-kappaB binding site sequence predicted by TRANSFAC (N: position of the SNPs)

*5: genes in the flanking regions (approximately 20-kb) of the SNPs (identified using the 1000 Genomes Browser (http://www.ncbi.nlm.nih.gov/variation/tools/1000genomes/))

*6: genes up- (↑) or down-regulated (↓) in the post-mortem brains of SCZ and/or BD patients (identified by curated studies in NextBio (http://www.nextbio.com))

*7: genes up- or down-regulated in the PFC of Shn-2 KO mice (identified using NextBio)

*8: 26.8kbp apart from rs61745920

References

(1) Purcell SM, Wray NR, Stone JL, Visscher PM, O'Donovan MC, Sullivan PF, et al. Common polygenic variation contributes to risk of schizophrenia and bipolar disorder. Nature. 2009; 460: 748-752.

(2) Stefansson H, Ophoff RA, Steinberg S, Andreassen OA, Cichon S, Rujescu D, et al. Common variants conferring risk of schizophrenia. Nature. 2009; 460: 744-747.

(3) Shi J, Levinson DF, Duan J, Sanders AR, Zheng Y, Pe'er I, et al. Common variants on chromosome 6p22.1 are associated with schizophrenia. Nature. 2009; 460: 753-757.

(4) Shi Y, Li Z, Xu Q, Wang T, Li T, Shen J, et al. Common variants on 8p12 and 1q24.2 confer risk of schizophrenia. Nature Genetics. 2011; 43: 1224-1227.

(5) Bergen SE, O'Dushlaine CT, Ripke S, Lee PH, Ruderfer DM, Akterin S, et al. Genome-wide association study in a Swedish population yields support for greater CNV and MHC involvement in schizophrenia compared with bipolar disorder. Molecular Psychiatry. 2012; 17: 880-886.

(6) Matys V, Fricke E, Geffers R, Gößling E, Haubrock M, Hehl R, et al. TRANSFAC®: transcriptional regulation, from patterns to profiles. Nucl. Acids Res. 2003; 31: 374-378.

(7) Narayan S, Tang B, Head SR, Gilmartin TJ, Sutcliffe JG, Dean B, et al. Molecular profiles of schizophrenia in the CNS at different stages of illness. Brain Res. 2008; 1239: 235-248.

(8) Ryan MM, Lockstone HE, Huffaker SJ, Wayland MT, Webster MJ, Bahn S. Gene expression analysis of bipolar disorder reveals downregulation of the ubiquitin cycle and alterations in synaptic genes. Molecular Psychiatry. 2006; 11: 965-978.

(9) Harris LW, Wayland M, Lan M, Ryan M, Giger T, Lockstone H, et al. The cerebral microvasculature in schizophrenia: a laser capture microdissection study. PLoS ONE. 2008; 3: e3964.

(10) Saetre P, Emilsson L, Axelsson E, Kreuger J, Lindholm E, Jazin E. Inflammation-related genes up-regulated in schizophrenia brains. BMC Psychiatry. 2007; 7: 46.

(11) Perrone-Bizzozero N. perro-affy-human-186940 [Internet]. 2006. Available from: http://www.ncbi.nlm.nih.gov/projects/geo/query/acc.cgi?acc=GSE4036

(12) Maycox PR, Kelly F, Taylor A, Bates S, Reid J, Logendra R, et al. Analysis of gene expression in two large schizophrenia cohorts identifies multiple changes associated with nerve terminal function. Mol. Psychiatry. 2009; 14: 1083-1094.

(13) Barnes MR, Huxley-Jones J, Maycox PR, Lennon M, Thornber A, Kelly F, et al. Transcription and pathway analysis of the superior temporal cortex and anterior prefrontal cortex in schizophrenia. Journal of Neuroscience Research. 2011; 89: 1218-1227.

7. REFARENCES

Altar, C. A., Jurata, L. W., Charles, V., Lemire, A., Liu, P., Bukhman, Y., Young, T. A., Bullard, J., Yokoe, H., Webster, M. J., Knable, M. B., & Brockman, J. A. (2005). Deficient hippocampal neuron expression of proteasome, ubiquitin, and mitochondrial genes in multiple schizophrenia cohorts. *Biological Psychiatry*, *58*(2), 85–96. https://doi.org/10.1016/j.biopsych.2005.03.031

Bayer, T. A., Buslei, R., Havas, L., & Falkai, P. (1999). Evidence for activation of microglia in patients with psychiatric illnesses. *Neuroscience Letters*, *271*(2), 126–128. https://doi.org/10.1016/s0304-3940(99)00545-5

Behrens, M. M., Ali, S. S., Dao, D. N., Lucero, J., Shekhtman, G., Quick, K. L., & Dugan, L. L. (2007). Ketamine-induced loss of phenotype of fast-spiking interneurons is mediated by NADPH-oxidase. *Science (New York, N.Y.)*, *318*(5856), 1645–1647. https://doi.org/10.1126/science.1148045

Benes, F. M., Lim, B., Matzilevich, D., Walsh, J. P., Subburaju, S., & Minns, M. (2007). Regulation of the GABA cell phenotype in hippocampus of schizophrenics and bipolars. *Proceedings of the National Academy of Sciences*

of the United States of America, *104*(24), 10164–10169. https://doi.org/10.1073/pnas.0703806104

Bergen, S. E., O'Dushlaine, C. T., Ripke, S., Lee, P. H., Ruderfer, D. M., Akterin, S., Moran, J. L., Chambert, K. D., Handsaker, R. E., Backlund, L., Ösby, U., McCarroll, S., Landen, M., Scolnick, E. M., Magnusson, P. K. E., Lichtenstein, P., Hultman, C. M., Purcell, S. M., Sklar, P., & Sullivan, P. F. (2012). Genome-wide association study in a Swedish population yields support for greater CNV and MHC involvement in schizophrenia compared with bipolar disorder. *Molecular Psychiatry*, *17*(9), 880–886. https://doi.org/10.1038/mp.2012.73

Braff, D. L., Freedman, R., Schork, N. J., & Gottesman, I. I. (2007). Deconstructing schizophrenia: An overview of the use of endophenotypes in order to understand a complex disorder. *Schizophrenia Bulletin*, *33*(1), 21–32. https://doi.org/10.1093/schbul/sbl049

Calzà, L., Giardino, L., Pozza, M., Bettelli, C., Micera, A., & Aloe, L. (1998). Proliferation and phenotype regulation in the subventricular zone during experimental allergic encephalomyelitis: In vivo evidence of a role for nerve

growth factor. *Proceedings of the National Academy of Sciences of the United States of America*, *95*(6), 3209–3214. https://doi.org/10.1073/pnas.95.6.3209

Deacon, R. M. J. (2006). Assessing nest building in mice. *Nature Protocols*, *1*(3), 1117–1119. https://doi.org/10.1038/nprot.2006.170

Dugan, L. L., Ali, S. S., Shekhtman, G., Roberts, A. J., Lucero, J., Quick, K. L., & Behrens, M. M. (2009). IL-6 mediated degeneration of forebrain GABAergic interneurons and cognitive impairment in aged mice through activation of neuronal NADPH oxidase. *PloS One*, *4*(5), e5518. https://doi.org/10.1371/journal.pone.0005518

Duncan, G., Moy, S., Lieberman, J., & Koller, B. (2006). Effects of haloperidol, clozapine, and quetiapine on sensorimotor gating in a genetic model of reduced NMDA receptor function. *Psychopharmacology*, *184*(2), 190–200. https://doi.org/10.1007/s00213-005-0214-1

Eguchi, M., & Yamaguchi, S. (2009). In vivo and in vitro visualization of gene expression dynamics over extensive areas of the brain. *NeuroImage*, *44*(4), 1274–1283. https://doi.org/10.1016/j.neuroimage.2008.10.046

Etholm, L., Arabadzisz, D., Lipp, H.-P., & Heggelund, P. (2010). Seizure logging: A new approach to synchronized cable-free EEG and video recordings of seizure activity in mice. *Journal of Neuroscience Methods*, *192*(2), 254–260. https://doi.org/10.1016/j.jneumeth.2010.08.003

Flynn, S. W., Lang, D. J., Mackay, A. L., Goghari, V., Vavasour, I. M., Whittall, K. P., Smith, G. N., Arango, V., Mann, J. J., Dwork, A. J., Falkai, P., & Honer, W. G. (2003). Abnormalities of myelination in schizophrenia detected in vivo with MRI, and post-mortem with analysis of oligodendrocyte proteins. *Molecular Psychiatry*, *8*(9), 811–820. https://doi.org/10.1038/sj.mp.4001337

Fourgeaud, L., & Boulanger, L. M. (2007). Synapse remodeling, compliments of the complement system. *Cell*, *131*(6), 1034–1036. https://doi.org/10.1016/j.cell.2007.11.031

Fukuda, S., Yamasaki, Y., Iwaki, T., Kawasaki, H., Akieda, S., Fukuchi, N., Tahira, T., & Hayashi, K. (2002). Characterization of the biological functions of a transcription factor, c-myc intron binding protein 1 (MIBP1). *Journal of*

Biochemistry, *131*(3), 349–357. https://doi.org/10.1093/oxfordjournals.jbchem.a003109

Gallinat, J., Winterer, G., Herrmann, C. S., & Senkowski, D. (2004). Reduced oscillatory gamma-band responses in unmedicated schizophrenic patients indicate impaired frontal network processing. *Clinical Neurophysiology: Official Journal of the International Federation of Clinical Neurophysiology*, *115*(8), 1863–1874. https://doi.org/10.1016/j.clinph.2004.03.013

Giardine, B., Riemer, C., Hardison, R. C., Burhans, R., Elnitski, L., Shah, P., Zhang, Y., Blankenberg, D., Albert, I., Taylor, J., Miller, W., Kent, W. J., & Nekrutenko, A. (2005). Galaxy: A platform for interactive large-scale genome analysis. *Genome Research*, *15*(10), 1451–1455. https://doi.org/10.1101/gr.4086505

Gilbert, P. E., & Kesner, R. P. (2006). The role of the dorsal CA3 hippocampal subregion in spatial working memory and pattern separation. *Behavioural Brain Research*, *169*(1), 142–149. https://doi.org/10.1016/j.bbr.2006.01.002

Goldman-Rakic, P. S. (1995). Cellular basis of working memory. *Neuron*, *14*(3), 477–485. https://doi.org/10.1016/0896-6273(95)90304-6

Goldsmith, H., Wells, A., Sá, M. J. N., Williams, M., Heussler, H., Buckman, M., Pfundt, R., de Vries, B. B. A., & Goel, H. (2019). Expanding the phenotype of intellectual disability caused by HIVEP2 variants. *American Journal of Medical Genetics. Part A, 179*(9), 1872–1877. https://doi.org/10.1002/ajmg.a.61271

Guillozet-Bongaarts, A. L., Hyde, T. M., Dalley, R. A., Hawrylycz, M. J., Henry, A., Hof, P. R., Hohmann, J., Jones, A. R., Kuan, C. L., Royall, J., Shen, E., Swanson, B., Zeng, H., & Kleinman, J. E. (2014). Altered gene expression in the dorsolateral prefrontal cortex of individuals with schizophrenia. *Molecular Psychiatry*, *19*(4), 478–485. https://doi.org/10.1038/mp.2013.30

Gulsuner, S., Walsh, T., Watts, A. C., Lee, M. K., Thornton, A. M., Casadei, S., Rippey, C., Shahin, H., Consortium on the Genetics of Schizophrenia (COGS), PAARTNERS Study Group, Nimgaonkar, V. L., Go, R. C. P., Savage, R. M., Swerdlow, N. R., Gur, R. E., Braff, D. L., King, M.-C., & McClellan, J. M. (2013). Spatial and temporal mapping of de novo mutations in schizophrenia to a fetal prefrontal cortical network. *Cell*, *154*(3), 518–529. https://doi.org/10.1016/j.cell.2013.06.049

Hagihara, H., Shoji, H., Kuroiwa, M., Graef, I. A., Crabtree, G. R., Nishi, A., & Miyakawa, T. (2022). Forebrain-specific conditional calcineurin deficiency induces dentate gyrus immaturity and hyper-dopaminergic signaling in mice. *Molecular Brain*, *15*(1), 94. https://doi.org/10.1186/s13041-022-00981-0

Hagihara, H., Toyama, K., Yamasaki, N., & Miyakawa, T. (2009). Dissection of hippocampal dentate gyrus from adult mouse. *Journal of Visualized Experiments: JoVE*, *33*, 1543. https://doi.org/10.3791/1543

Heyser, C. J., Masliah, E., Samimi, A., Campbell, I. L., & Gold, L. H. (1997). Progressive decline in avoidance learning paralleled by inflammatory neurodegeneration in transgenic mice expressing interleukin 6 in the brain. *Proceedings of the National Academy of Sciences of the United States of America*, *94*(4), 1500–1505. https://doi.org/10.1073/pnas.94.4.1500

Horton, R., Wilming, L., Rand, V., Lovering, R. C., Bruford, E. A., Khodiyar, V. K., Lush, M. J., Povey, S., Talbot, C. C., Wright, M. W., Wain, H. M., Trowsdale, J., Ziegler, A., & Beck, S. (2004). Gene map of the extended human MHC. *Nature Reviews Genetics*, *5*(12), 889–899. https://doi.org/10.1038/nrg1489

Howrigan, D. P., Rose, S. A., Samocha, K. E., Fromer, M., Cerrato, F., Chen, W. J., Churchhouse, C., Chambert, K., Chandler, S. D., Daly, M. J., Dumont, A., Genovese, G., Hwu, H.-G., Laird, N., Kosmicki, J. A., Moran, J. L., Roe, C., Singh, T., Wang, S.-H., … Neale, B. M. (2020). Exome sequencing in schizophrenia-affected parent-offspring trios reveals risk conferred by protein-coding de novo mutations. *Nature Neuroscience*, *23*(2), 185–193. https://doi.org/10.1038/s41593-019-0564-3

Imoto, Y., Segi-Nishida, E., Suzuki, H., & Kobayashi, K. (2017). Rapid and stable changes in maturation-related phenotypes of the adult hippocampal neurons by electroconvulsive treatment. *Molecular Brain*, *10*(1), 8. https://doi.org/10.1186/s13041-017-0288-9

Irizarry, R. A., Hobbs, B., Collin, F., Beazer-Barclay, Y. D., Antonellis, K. J., Scherf, U., & Speed, T. P. (2003). Exploration, normalization, and summaries of high density oligonucleotide array probe level data. *Biostatistics (Oxford, England)*, *4*(2), 249–264. https://doi.org/10.1093/biostatistics/4.2.249

Jain, A., & Atwal, P. S. (2019). Novel HIVEP2 Variant p.Q1248* is Associated with Developmental Delay: A Case Report. *Journal of Pediatric Genetics*, *8*(3), 157–159. https://doi.org/10.1055/s-0039-1683973

Jenkins, T. A., Harte, M. K., Stenson, G., & Reynolds, G. P. (2009). Neonatal lipopolysaccharide induces pathological changes in parvalbumin immunoreactivity in the hippocampus of the rat. *Behavioural Brain Research*, *205*(2), 355–359. https://doi.org/10.1016/j.bbr.2009.07.014

Jones, M. W., & Wilson, M. A. (2005). Theta rhythms coordinate hippocampal-prefrontal interactions in a spatial memory task. *PLoS Biology*, *3*(12), e402. https://doi.org/10.1371/journal.pbio.0030402

Kalkstein, S., Hurford, I., & Gur, R. C. (2010). Neurocognition in schizophrenia. *Current Topics in Behavioral Neurosciences*, *4*, 373–390. https://doi.org/10.1007/7854_2010_42

Karolchik, D. (2004). The UCSC Table Browser data retrieval tool. *Nucleic Acids Research*, *32*(90001), 493D – 496. https://doi.org/10.1093/nar/gkh103

Kataoka, M., Matoba, N., Sawada, T., Kazuno, A.-A., Ishiwata, M., Fujii, K., Matsuo, K., Takata, A., & Kato, T. (2016). Exome sequencing for bipolar disorder points to roles of de novo loss-of-function and protein-altering mutations. *Molecular Psychiatry*, *21*(7), 885–893. https://doi.org/10.1038/mp.2016.69

Kel, A. E., Gößling, E., Reuter, I., Cheremushkin, E., Kel-Margoulis, O. V., & Wingender, E. (2003). MATCHTM: A tool for searching transcription factor binding sites in DNA sequences. *Nucleic Acids Research*, *31*(13), 3576–3579. https://doi.org/10.1093/nar/gkg585

Keshavan, M. S., Morris, D. W., Sweeney, J. A., Pearlson, G., Thaker, G., Seidman, L. J., Eack, S. M., & Tamminga, C. (2011). A dimensional approach to the psychosis spectrum between bipolar disorder and schizophrenia: The Schizo-Bipolar Scale. *Schizophrenia Research*, *133*(1–3), 250–254. https://doi.org/10.1016/j.schres.2011.09.005

Keshavan, M. S., Nasrallah, H. A., & Tandon, R. (2011). Schizophrenia, "Just the Facts" 6. Moving ahead with the schizophrenia concept: From the elephant to

the mouse. *Schizophrenia Research*, *127*(1–3), 3–13. https://doi.org/10.1016/j.schres.2011.01.011

Kimura, M. Y., Hosokawa, H., Yamashita, M., Hasegawa, A., Iwamura, C., Watarai, H., Taniguchi, M., Takagi, T., Ishii, S., & Nakayama, T. (2005). Regulation of T helper type 2 cell differentiation by murine Schnurri-2. *The Journal of Experimental Medicine*, *201*(3), 397–408. https://doi.org/10.1084/jem.20040733

Kimura, M. Y., Iwamura, C., Suzuki, A., Miki, T., Hasegawa, A., Sugaya, K., Yamashita, M., Ishii, S., & Nakayama, T. (2007). Schnurri-2 controls memory Th1 and Th2 cell numbers in vivo. *Journal of Immunology (Baltimore, Md.: 1950)*, *178*(8), 4926–4936. https://doi.org/10.4049/jimmunol.178.8.4926

Kirov, G., Pocklington, A. J., Holmans, P., Ivanov, D., Ikeda, M., Ruderfer, D., Moran, J., Chambert, K., Toncheva, D., Georgieva, L., Grozeva, D., Fjodorova, M., Wollerton, R., Rees, E., Nikolov, I., van de Lagemaat, L. N., Bayés, A., Fernandez, E., Olason, P. I., … Owen, M. J. (2012). De novo CNV analysis implicates specific abnormalities of postsynaptic signalling complexes in the

pathogenesis of schizophrenia. *Molecular Psychiatry*, *17*(2), 142–153. https://doi.org/10.1038/mp.2011.154

Kobayashi, K., Ikeda, Y., Sakai, A., Yamasaki, N., Haneda, E., Miyakawa, T., & Suzuki, H. (2010). Reversal of hippocampal neuronal maturation by serotonergic antidepressants. *Proceedings of the National Academy of Sciences of the United States of America*, *107*(18), 8434–8439. https://doi.org/10.1073/pnas.0912690107

Kobayashi, K., Umeda-Yano, S., Yamamori, H., Takeda, M., Suzuki, H., & Hashimoto, R. (2011). Correlated alterations in serotonergic and dopaminergic modulations at the hippocampal mossy fiber synapse in mice lacking dysbindin. *PloS One*, *6*(3), e18113. https://doi.org/10.1371/journal.pone.0018113

Komada, M., Takao, K., & Miyakawa, T. (2008). Elevated plus maze for mice. *Journal of Visualized Experiments: JoVE*, *22*. https://doi.org/10.3791/1088

Kumar, A., Takada, Y., Boriek, A. M., & Aggarwal, B. B. (2004). Nuclear factor-kappaB: Its role in health and disease. *Journal of Molecular Medicine (Berlin, Germany)*, *82*(7), 434–448. https://doi.org/10.1007/s00109-004-0555-y

Kupershmidt, I., Su, Q. J., Grewal, A., Sundaresh, S., Halperin, I., Flynn, J., Shekar, M., Wang, H., Park, J., Cui, W., Wall, G. D., Wisotzkey, R., Alag, S., Akhtari, S., & Ronaghi, M. (2010). Ontology-based meta-analysis of global collections of high-throughput public data. *PloS One*, *5*(9). https://doi.org/10.1371/journal.pone.0013066

Kvajo, M., McKellar, H., Drew, L. J., Lepagnol-Bestel, A.-M., Xiao, L., Levy, R. J., Blazeski, R., Arguello, P. A., Lacefield, C. O., Mason, C. A., Simonneau, M., O'Donnell, J. M., MacDermott, A. B., Karayiorgou, M., & Gogos, J. A. (2011). Altered axonal targeting and short-term plasticity in the hippocampus of Disc1 mutant mice. *Proceedings of the National Academy of Sciences of the United States of America*, *108*(49), E1349-1358. https://doi.org/10.1073/pnas.1114113108

Li, W., Zhou, Y., Jentsch, J. D., Brown, R. A. M., Tian, X., Ehninger, D., Hennah, W., Peltonen, L., Lönnqvist, J., Huttunen, M. O., Kaprio, J., Trachtenberg, J. T., Silva, A. J., & Cannon, T. D. (2007). Specific developmental disruption of disrupted-in-schizophrenia-1 function results in schizophrenia-related

phenotypes in mice. *Proceedings of the National Academy of Sciences of the United States of America*, *104*(46), 18280–18285. https://doi.org/10.1073/pnas.0706900104

Liu, G. E., Weirauch, M. T., Van Tassell, C. P., Li, R. W., Sonstegard, T. S., Matukumalli, L. K., Connor, E. E., Hanson, R. W., & Yang, J. (2008). Identification of conserved regulatory elements in mammalian promoter regions: A case study using the PCK1 promoter. *Genomics, Proteomics & Bioinformatics*, *6*(3–4), 129–143. https://doi.org/10.1016/S1672-0229(09)60001-2

Manea, A., Manea, S. A., Gafencu, A. V., & Raicu, M. (2007). Regulation of NADPH oxidase subunit p22(phox) by NF-kB in human aortic smooth muscle cells. *Archives of Physiology and Biochemistry*, *113*(4–5), 163–172. https://doi.org/10.1080/13813450701531235

Mansour, A., Meador-Woodruff, J. H., Bunzow, J. R., Civelli, O., Akil, H., & Watson, S. J. (1990). Localization of dopamine D2 receptor mRNA and D1 and D2 receptor binding in the rat brain and pituitary: An in situ hybridization-receptor

autoradiographic analysis. *The Journal of Neuroscience: The Official Journal of the Society for Neuroscience*, *10*(8), 2587–2600. https://doi.org/10.1523/JNEUROSCI.10-08-02587.1990

Matsuo, N., Yamasaki, N., Ohira, K., Takao, K., Toyama, K., Eguchi, M., Yamaguchi, S., & Miyakawa, T. (2009). Neural activity changes underlying the working memory deficit in alpha-CaMKII heterozygous knockout mice. *Frontiers in Behavioral Neuroscience*, *3*, 20. https://doi.org/10.3389/neuro.08.020.2009

Maycox, P. R., Kelly, F., Taylor, A., Bates, S., Reid, J., Logendra, R., Barnes, M. R., Larminie, C., Jones, N., Lennon, M., Davies, C., Hagan, J. J., Scorer, C. A., Angelinetta, C., Akbar, M. T., Akbar, T., Hirsch, S., Mortimer, A. M., Barnes, T. R. E., & de Belleroche, J. (2009). Analysis of gene expression in two large schizophrenia cohorts identifies multiple changes associated with nerve terminal function. *Molecular Psychiatry*, *14*(12), 1083–1094. https://doi.org/10.1038/mp.2009.18

Meyer, K. D., & Morris, J. A. (2008). Immunohistochemical analysis of Disc1 expression in the developing and adult hippocampus. *Gene Expression Patterns: GEP*, *8*(7–8), 494–501. https://doi.org/10.1016/j.gep.2008.06.005

Mirnics, K., Middleton, F. A., Lewis, D. A., & Levitt, P. (2001). Analysis of complex brain disorders with gene expression microarrays: Schizophrenia as a disease of the synapse. *Trends in Neurosciences*, *24*(8), 479–486. https://doi.org/10.1016/s0166-2236(00)01862-2

Miyakawa, T., Leiter, L. M., Gerber, D. J., Gainetdinov, R. R., Sotnikova, T. D., Zeng, H., Caron, M. G., & Tonegawa, S. (2003). Conditional calcineurin knockout mice exhibit multiple abnormal behaviors related to schizophrenia. *Proceedings of the National Academy of Sciences of the United States of America*, *100*(15), 8987–8992. https://doi.org/10.1073/pnas.1432926100

Moran, L. V., & Hong, L. E. (2011). High vs low frequency neural oscillations in schizophrenia. *Schizophrenia Bulletin*, *37*(4), 659–663. https://doi.org/10.1093/schbul/sbr056

Muller, N., & Schwarz, M. (2006). Schizophrenia as an inflammation-mediated dysbalance of glutamatergic neurotransmission. *Neurotoxicity Research*, *10*(2), 131–148. https://doi.org/10.1007/BF03033242

Murphy, C. E., Kondo, Y., Walker, A. K., Rothmond, D. A., Matsumoto, M., & Shannon Weickert, C. (2020). Regional, cellular and species difference of two key neuroinflammatory genes implicated in schizophrenia. *Brain, Behavior, and Immunity*, *88*, 826–839. https://doi.org/10.1016/j.bbi.2020.05.055

Murphy, C. E., Lawther, A. J., Webster, M. J., Asai, M., Kondo, Y., Matsumoto, M., Walker, A. K., & Weickert, C. S. (2020). Nuclear factor kappa B activation appears weaker in schizophrenia patients with high brain cytokines than in non-schizophrenic controls with high brain cytokines. *Journal of Neuroinflammation*, *17*(1), 215. https://doi.org/10.1186/s12974-020-01890-6

Nawa, H., & Takei, N. (2006). Recent progress in animal modeling of immune inflammatory processes in schizophrenia: Implication of specific cytokines. *Neuroscience Research*, *56*(1), 2–13. https://doi.org/10.1016/j.neures.2006.06.002

Nishioka, M., Takayama, J., Sakai, N., Kazuno, A.-A., Ishiwata, M., Ueda, J., Hayama, T., Fujii, K., Someya, T., Kuriyama, S., Tamiya, G., Takata, A., & Kato, T. (2023). Deep exome sequencing identifies enrichment of deleterious mosaic variants in neurodevelopmental disorder genes and mitochondrial tRNA regions in bipolar disorder. *Molecular Psychiatry*. https://doi.org/10.1038/s41380-023-02096-x

Nobrega, J. N., & Seeman, P. (1994). Dopamine D2 receptors mapped in rat brain with [3H](+)PHNO. *Synapse (New York, N.Y.), 17*(3), 167–172. https://doi.org/10.1002/syn.890170305

Ohira, K., Kobayashi, K., Toyama, K., Nakamura, H. K., Shoji, H., Takao, K., Takeuchi, R., Yamaguchi, S., Kataoka, M., Otsuka, S., Takahashi, M., & Miyakawa, T. (2013). Synaptosomal-associated protein 25 mutation induces immaturity of the dentate granule cells of adult mice. *Molecular Brain*, *6*, 12. https://doi.org/10.1186/1756-6606-6-12

Okuno, H., Akashi, K., Ishii, Y., Yagishita-Kyo, N., Suzuki, K., Nonaka, M., Kawashima, T., Fujii, H., Takemoto-Kimura, S., Abe, M., Natsume, R.,

Chowdhury, S., Sakimura, K., Worley, P. F., & Bito, H. (2012). Inverse synaptic tagging of inactive synapses via dynamic interaction of Arc/Arg3.1 with CaMKIIβ. *Cell*, *149*(4), 886–898. https://doi.org/10.1016/j.cell.2012.02.062

Ouagazzal, A. M., Jenck, F., & Moreau, J. L. (2001). Drug-induced potentiation of prepulse inhibition of acoustic startle reflex in mice: A model for detecting antipsychotic activity? *Psychopharmacology*, *156*(2–3), 273–283.

Park, J., Colombo, R., Schäferhoff, K., Janiri, L., Grimmel, M., Sturm, M., Grasshoff, U., Dufke, A., Haack, T. B., & Kehrer, M. (2019). Novel HIVEP2 Variants in Patients with Intellectual Disability. *Molecular Syndromology*, *10*(4), 195–201. https://doi.org/10.1159/000499060

Patterson, P. H. (2009). Immune involvement in schizophrenia and autism: Etiology, pathology and animal models. *Behavioural Brain Research*, *204*(2), 313–321. https://doi.org/10.1016/j.bbr.2008.12.016

Paxinos, G., & Franklin, K. B. J. (2004). *The Mouse Brain in Stereotaxic Coordinates*. Gulf Professional Publishing.

Pierri, J. N., Chaudry, A. S., Woo, T. U., & Lewis, D. A. (1999). Alterations in chandelier neuron axon terminals in the prefrontal cortex of schizophrenic subjects. *The American Journal of Psychiatry*, *156*(11), 1709–1719. https://doi.org/10.1176/ajp.156.11.1709

Powell, C. M., & Miyakawa, T. (2006). Schizophrenia-relevant behavioral testing in rodent models: A uniquely human disorder? *Biological Psychiatry*, *59*(12), 1198–1207. https://doi.org/10.1016/j.biopsych.2006.05.008

Presumey, J., Bialas, A. R., & Carroll, M. C. (2017). Complement System in Neural Synapse Elimination in Development and Disease. *Advances in Immunology*, *135*, 53–79. https://doi.org/10.1016/bs.ai.2017.06.004

Purcell, S. M., Wray, N. R., Stone, J. L., Visscher, P. M., O'Donovan, M. C., Sullivan, P. F., & Sklar, P. (2009). Common polygenic variation contributes to risk of schizophrenia and bipolar disorder. *Nature*, *460*(7256), 748–752. https://doi.org/10.1038/nature08185

Reynolds, G. P., & Beasley, C. L. (2001). GABAergic neuronal subtypes in the human frontal cortex—Development and deficits in schizophrenia. *Journal of Chemical*

Neuroanatomy, *22*(1–2), 95–100. https://doi.org/10.1016/s0891-0618(01)00113-2

Salat, D. H., Buckner, R. L., Snyder, A. Z., Greve, D. N., Desikan, R. S. R., Busa, E., Morris, J. C., Dale, A. M., & Fischl, B. (2004). Thinning of the cerebral cortex in aging. *Cerebral Cortex (New York, N.Y.: 1991)*, *14*(7), 721–730. https://doi.org/10.1093/cercor/bhh032

Schmidt-Hieber, C., Jonas, P., & Bischofberger, J. (2004). Enhanced synaptic plasticity in newly generated granule cells of the adult hippocampus. *Nature*, *429*(6988), 184–187. https://doi.org/10.1038/nature02553

Schneider, C. W., & Chenoweth, M. B. (1970). Effects of hallucinogenic and other drugs on the nest-building behaviour of mice. *Nature*, *225*(5239), 1262–1263. https://doi.org/10.1038/2251262a0

Sekar, A., Bialas, A. R., de Rivera, H., Davis, A., Hammond, T. R., Kamitaki, N., Tooley, K., Presumey, J., Baum, M., Van Doren, V., Genovese, G., Rose, S. A., Handsaker, R. E., Schizophrenia Working Group of the Psychiatric Genomics Consortium, Daly, M. J., Carroll, M. C., Stevens, B., & McCarroll, S. A. (2016).

Schizophrenia risk from complex variation of complement component 4. *Nature*, *530*(7589), 177–183. https://doi.org/10.1038/nature16549

Seok, J., Warren, H. S., Cuenca, A. G., Mindrinos, M. N., Baker, H. V., Xu, W., Richards, D. R., McDonald-Smith, G. P., Gao, H., Hennessy, L., Finnerty, C. C., López, C. M., Honari, S., Moore, E. E., Minei, J. P., Cuschieri, J., Bankey, P. E., Johnson, J. L., Sperry, J., … Inflammation and Host Response to Injury, Large Scale Collaborative Research Program. (2013). Genomic responses in mouse models poorly mimic human inflammatory diseases. *Proceedings of the National Academy of Sciences of the United States of America*, *110*(9), 3507–3512. https://doi.org/10.1073/pnas.1222878110

Shatz, C. J. (2009). MHC class I: An unexpected role in neuronal plasticity. *Neuron*, *64*(1), 40–45. https://doi.org/10.1016/j.neuron.2009.09.044

Shepherd, G. M. G., & Harris, K. M. (1998). Three-Dimensional Structure and Composition of CA3→CA1 Axons in Rat Hippocampal Slices: Implications for Presynaptic Connectivity and Compartmentalization. *The Journal of Neuroscience*, *18*(20), 8300–8310.

Shi, J., Levinson, D. F., Duan, J., Sanders, A. R., Zheng, Y., Pe'er, I., Dudbridge, F., Holmans, P. A., Whittemore, A. S., Mowry, B. J., Olincy, A., Amin, F., Cloninger, C. R., Silverman, J. M., Buccola, N. G., Byerley, W. F., Black, D. W., Crowe, R. R., Oksenberg, J. R., … Gejman, P. V. (2009). Common variants on chromosome 6p22.1 are associated with schizophrenia. *Nature, 460*(7256), 753–757. https://doi.org/10.1038/nature08192

Shi, Y., Li, Z., Xu, Q., Wang, T., Li, T., Shen, J., Zhang, F., Chen, J., Zhou, G., Ji, W., Li, B., Xu, Y., Liu, D., Wang, P., Yang, P., Liu, B., Sun, W., Wan, C., Qin, S., … He, L. (2011). Common variants on 8p12 and 1q24.2 confer risk of schizophrenia. *Nature Genetics*, *43*(12), 1224–1227. https://doi.org/10.1038/ng.980

Shin, R., Kobayashi, K., Hagihara, H., Kogan, J. H., Miyake, S., Tajinda, K., Walton, N. M., Gross, A. K., Heusner, C. L., Chen, Q., Tamura, K., Miyakawa, T., & Matsumoto, M. (2013). The immature dentate gyrus represents a shared phenotype of mouse models of epilepsy and psychiatric disease. *Bipolar Disorders*. https://doi.org/10.1111/bdi.12064

Shoji, H., Hagihara, H., Takao, K., Hattori, S., & Miyakawa, T. (2012). T-maze Forced Alternation and Left-right Discrimination Tasks for Assessing Working and Reference Memory in Mice. *Journal of Visualized Experiments: JoVE*, *60*. https://doi.org/10.3791/3300

Snyder, J. S., Soumier, A., Brewer, M., Pickel, J., & Cameron, H. A. (2011). Adult hippocampal neurogenesis buffers stress responses and depressive behaviour. *Nature*, *476*(7361), 458–461. https://doi.org/10.1038/nature10287

Sponheim, S. R., Clementz, B. A., Iacono, W. G., & Beiser, M. (1994). Resting EEG in first-episode and chronic schizophrenia. *Psychophysiology*, *31*(1), 37–43. https://doi.org/10.1111/j.1469-8986.1994.tb01023.x

Srivastava, S., Engels, H., Schanze, I., Cremer, K., Wieland, T., Menzel, M., Schubach, M., Biskup, S., Kreiß, M., Endele, S., Strom, T. M., Wieczorek, D., Zenker, M., Gupta, S., Cohen, J., Zink, A. M., & Naidu, S. (2016). Loss-of-function variants in HIVEP2 are a cause of intellectual disability. *European Journal of Human Genetics: EJHG*, *24*(4), 556–561. https://doi.org/10.1038/ejhg.2015.151

Stefansson, H., Ophoff, R. A., Steinberg, S., Andreassen, O. A., Cichon, S., Rujescu, D., Werge, T., Pietilainen, O. P. H., Mors, O., Mortensen, P. B., Sigurdsson, E., Gustafsson, O., Nyegaard, M., Tuulio-Henriksson, A., Ingason, A., Hansen, T., Suvisaari, J., Lonnqvist, J., Paunio, T., … Collier, D. A. (2009). Common variants conferring risk of schizophrenia. *Nature*, *460*(7256), 744–747. https://doi.org/10.1038/nature08186

Steinfeld, H., Cho, M. T., Retterer, K., Person, R., Schaefer, G. B., Danylchuk, N., Malik, S., Wechsler, S. B., Wheeler, P. G., van Gassen, K. L. I., Terhal, P. A., Verhoeven, V. J. M., van Slegtenhorst, M. A., Monaghan, K. G., Henderson, L. B., & Chung, W. K. (2016). Mutations in HIVEP2 are associated with developmental delay, intellectual disability, and dysmorphic features. *Neurogenetics*, *17*(3), 159–164. https://doi.org/10.1007/s10048-016-0479-z

Stephan, K. E., Baldeweg, T., & Friston, K. J. (2006). Synaptic plasticity and dysconnection in schizophrenia. *Biological Psychiatry*, *59*(10), 929–939. https://doi.org/10.1016/j.biopsych.2005.10.005

Sung, W.-K., Lu, Y., Lee, C. W. H., Zhang, D., Ronaghi, M., & Lee, C. G. L. (2009). Deregulated direct targets of the hepatitis B virus (HBV) protein, HBx, identified through chromatin immunoprecipitation and expression microarray profiling. *The Journal of Biological Chemistry*, *284*(33), 21941–21954. https://doi.org/10.1074/jbc.M109.014563

Swerdlow, N. R., Light, G. A., Cadenhead, K. S., Sprock, J., Hsieh, M. H., & Braff, D. L. (2006). Startle gating deficits in a large cohort of patients with schizophrenia: Relationship to medications, symptoms, neurocognition, and level of function. *Archives of General Psychiatry*, *63*(12), 1325–1335. https://doi.org/10.1001/archpsyc.63.12.1325

Takagi, T., Harada, J., & Ishii, S. (2001). Murine Schnurri-2 is required for positive selection of thymocytes. *Nature Immunology*, *2*(11), 1048–1053. https://doi.org/10.1038/ni728

Takagi, T., Jin, W., Taya, K., Watanabe, G., Mori, K., & Ishii, S. (2006). Schnurri-2 mutant mice are hypersensitive to stress and hyperactive. *Brain Research*, *1108*(1), 88–97. https://doi.org/10.1016/j.brainres.2006.06.018

Takao, K., Kobayashi, K., Hagihara, H., Ohira, K., Shoji, H., Hattori, S., Koshimizu, H., Umemori, J., Toyama, K., Nakamura, H. K., Kuroiwa, M., Maeda, J., Atsuzawa, K., Esaki, K., Yamaguchi, S., Furuya, S., Takagi, T., Walton, N. M., Hayashi, N., … Miyakawa, T. (2013). Deficiency of Schnurri-2, an MHC Enhancer Binding Protein, Induces Mild Chronic Inflammation in the Brain and Confers Molecular, Neuronal, and Behavioral Phenotypes Related to Schizophrenia. *Neuropsychopharmacology: Official Publication of the American College of Neuropsychopharmacology*. https://doi.org/10.1038/npp.2013.38

Takao, K., & Miyakawa, T. (2015). Genomic responses in mouse models greatly mimic human inflammatory diseases. *Proceedings of the National Academy of Sciences of the United States of America*, *112*(4), 1167–1172. https://doi.org/10.1073/pnas.1401965111

Takao, K., Toyama, K., Nakanishi, K., Hattori, S., Takamura, H., Takeda, M., Miyakawa, T., & Hashimoto, R. (2008). Impaired long-term memory retention and working memory in sdy mutant mice with a deletion in Dtnbp1, a

susceptibility gene for schizophrenia. *Molecular Brain*, *1*, 11. https://doi.org/10.1186/1756-6606-1-11

Takao, K., Yamasaki, N., & Miyakawa, T. (2007). Impact of brain-behavior phenotypying of genetically-engineered mice on research of neuropsychiatric disorders. *Neuroscience Research*, *58*(2), 124–132. https://doi.org/10.1016/j.neures.2007.02.009

Talbot, K., Eidem, W. L., Tinsley, C. L., Benson, M. A., Thompson, E. W., Smith, R. J., Hahn, C.-G., Siegel, S. J., Trojanowski, J. Q., Gur, R. E., Blake, D. J., & Arnold, S. E. (2004). Dysbindin-1 is reduced in intrinsic, glutamatergic terminals of the hippocampal formation in schizophrenia. *The Journal of Clinical Investigation*, *113*(9), 1353–1363. https://doi.org/10.1172/JCI20425

Tamminga, C. A., Stan, A. D., & Wagner, A. D. (2010). The hippocampal formation in schizophrenia. *The American Journal of Psychiatry*, *167*(10), 1178–1193. https://doi.org/10.1176/appi.ajp.2010.09081187

Vann, S. D., Brown, M. W., Erichsen, J. T., & Aggleton, J. P. (2000). Fos imaging reveals differential patterns of hippocampal and parahippocampal subfield

activation in rats in response to different spatial memory tests. *The Journal of Neuroscience: The Official Journal of the Society for Neuroscience*, *20*(7), 2711–2718.

Volk, D. W., Chitrapu, A., Edelson, J. R., Roman, K. M., Moroco, A. E., & Lewis, D. A. (2015). Molecular mechanisms and timing of cortical immune activation in schizophrenia. *The American Journal of Psychiatry*, *172*(11), 1112–1121. https://doi.org/10.1176/appi.ajp.2015.15010019

Volman, V., Behrens, M. M., & Sejnowski, T. J. (2011). Downregulation of parvalbumin at cortical GABA synapses reduces network gamma oscillatory activity. *The Journal of Neuroscience: The Official Journal of the Society for Neuroscience*, *31*(49), 18137–18148. https://doi.org/10.1523/JNEUROSCI.3041-11.2011

Walton, N. M., Zhou, Y., Kogan, J. H., Shin, R., Webster, M., Gross, A. K., Heusner, C. L., Chen, Q., Miyake, S., Tajinda, K., Tamura, K., Miyakawa, T., & Matsumoto, M. (2012). Detection of an immature dentate gyrus feature in

human schizophrenia/bipolar patients. *Translational Psychiatry*, *2*(7), e135. https://doi.org/10.1038/tp.2012.56

Wingender, E., Kel, A. E., Kel, O. V., Karas, H., Heinemeyer, T., Dietze, P., Knüppel, R., Romaschenko, A. G., & Kolchanov, N. A. (1997). TRANSFAC, TRRD and COMPEL: Towards a federated database system on transcriptional regulation. *Nucleic Acids Research*, *25*(1), 265–268. https://doi.org/10.1093/nar/25.1.265

Yamasaki, N., Maekawa, M., Kobayashi, K., Kajii, Y., Maeda, J., Soma, M., Takao, K., Tanda, K., Ohira, K., Toyama, K., Kanzaki, K., Fukunaga, K., Sudo, Y., Ichinose, H., Ikeda, M., Iwata, N., Ozaki, N., Suzuki, H., Higuchi, M., … Miyakawa, T. (2008). Alpha-CaMKII deficiency causes immature dentate gyrus, a novel candidate endophenotype of psychiatric disorders. *Molecular Brain*, *1*(1), 6. https://doi.org/10.1186/1756-6606-1-6

Yue, W.-H., Wang, H.-F., Sun, L.-D., Tang, F.-L., Liu, Z.-H., Zhang, H.-X., Li, W.-Q., Zhang, Y.-L., Zhang, Y., Ma, C.-C., Du, B., Wang, L.-F., Ren, Y.-Q., Yang, Y.-F., Hu, X.-F., Wang, Y., Deng, W., Tan, L.-W., Tan, Y.-L., … Zhang, D. (2011). Genome-wide association study identifies a susceptibility locus for

schizophrenia in Han Chinese at 11p11.2. *Nature Genetics*, *43*(12), 1228–1231. https://doi.org/10.1038/ng.979

Zhang, Z. J., & Reynolds, G. P. (2002). A selective decrease in the relative density of parvalbumin-immunoreactive neurons in the hippocampus in schizophrenia. *Schizophrenia Research*, *55*(1–2), 1–10. https://doi.org/10.1016/s0920-9964(01)00188-8

5. ACKOWLEDGEMENTS

I am thankful to these people for technical supports, collaboration and advice:

Drs. Hideo Hagihara, Koji Ohira, Hirotaka Shoji, Satoko Hattori, Hisatsugu Koshimizu, Juzoh Umemori, Keiko Toyama, Hironori K Nakamura, and Prof Tsuyoshi Miyakawa in Institute for Comprehensive Medical Science, Fujita Health University

Dr. Katsunori Kobayashi and Prof. Hidenori Suzuki in Department of Pharmacology, Graduate School of Medicine, Nippon Medical School

Dr. Mahomi Kuroiwa and Prof. Akinori Nishi in Department of Pharmacology, Kurume University School of Medicine

Drs. Jun Maeda, Makoto Higuchi & Tetsuya Suhara in Molecular Neuroimaging Program, Molecular Imaging Center, National Institute of Radiological Sciences

Dr. Kimie Atsuzawa and Prof. Nobuteru Usuda in Department of Anatomy II, Fujita Health University School of Medicine

Dr. Kayoko Esaki and Prof. Shigeki Furuya in Department of Bioscience and Biotechnology, Graduate School of Bioresource and Bioenvironmental Sciences, Kyushu University

Prof. Shun Yamaguchi in Division of Morphological Neuroscience, Gifu University Graduate School of Medicine

Drs. Tsuyoshi Takagi and Shunsuke Ishii in RIKEN Tsukuba Institute

Drs. Noah M Walton and Mitsuyuki Matsumoto in Astellas Research Institute of America LLC, Skokie, IL, USA

Prof. Nobuhiro Hayashi in Graduate School of Bioscience and Biotechnology, Tokyo Institute of Technology, Tokyo, Japan

Lastly, I like to express my gratitude and respect to Professor Hisashi Mori for assistance in my degree application and for their careful proofreading of my dissertation.